UNIVERSIDADE
BEIRA INTERIOR

Manufacturing and characterisation of a piezoresistive strain sensor based on the rGO@PDMS composite for skin and prosthetic support systems

(Versão Final Após Defesa)

Rodrigo Gonçalves Ferreira

Dissertação para obtenção do Grau de Mestre em
Bioengenharia
(2º ciclo de estudos)

Orientador: Prof. Doutor João Pedro Nunes-Pereira
Co-orientador: Prof. Doutor Abílio Manuel Pereira da Silva

dezembro de 2023

Declaração de Integridade

Eu, Rodrigo Gonçalves Ferreira, que abaixo assino, estudante com o número de inscrição M11340 de Bioengenharia da Faculdade de Engenharias, declaro ter desenvolvido o presente trabalho e elaborado o presente texto em total consonância com o **Código de Integridades da Universidade da Beira Interior**.

Mais concretamente afirmo não ter incorrido em qualquer das variedades de Fraude Académica, e que aqui declaro conhecer, que em particular atendi à exigida referenciação de frases, extratos, imagens e outras formas de trabalho intelectual, e assumindo assim na íntegra as responsabilidades da autoria.

Universidade da Beira Interior, Covilhã 7 /12 /2023

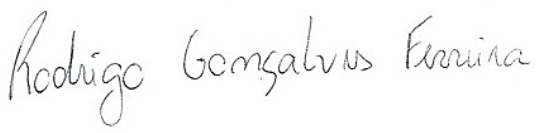

(assinatura conforme Cartão de Cidadão ou preferencialmente

assinatura digital no documento original se naquele mesmo formato

"Think of yourself as dead. You have lived your life. Now, take what is left and live it properly. What does not transmit light creates its own darkness."

-Marcus Aurelius Antoninus, Meditations

Agradecimentos

Com a conclusão de uma das fases mais importantes da minha vida, gostaria de agradecer a todos aqueles que se cruzaram comigo ao longo dos anos e que me ajudaram, de uma maneira ou de outra, a ser a pessoa que sou hoje.

Em primeiro lugar, antes de mais, gostaria de agradecer ao Prof. João Nunes-Pereira e ao Prof. Abílio Silva pela oportunidade de trabalhar num projeto tão desafiante como este, pela exímia orientação, pela integridade, incessante disponibilidade e por me incentivarem a dar e apontar sempre para o máximo.

Gostaria também de agradecer à Eng. Ana Paula Gomes do Centro de Ótica da Universidade da Beira Interior pela disponibilidade para realizar os processos de *sputtering* e adquirir imagens por SEM, bem como ao Natanael pela ajuda durante os ensaios ATR/FTIR.

Ao Prof. João Paulo de Castro Gomes, ao Alexis e à Axelle gostaria de agradecer a ajuda e disponibilidade durante a realização dos ensaios TGA.

Aos meus colegas de laboratório, Diogo, Beatriz e Sérgio, muito obrigado pelo trabalho que fizemos em conjunto e por todas as conversas, ajuda e ideias que partilhamos, foi um prazer aprender coisas novas convosco e fazer parte de uma pequena porção da vossa longa caminhada.

A todos os outros membros do C-MAST, muito obrigado por toda a ajuda e contribuições para a realização deste trabalho.

Aos meus pais, irmã e avós, agradeço-vos do fundo do coração pelos sacrifícios que fizeram para eu perseguir a minha paixão, nunca tendo deixado de acreditar em mim e amando-me incondicionalmente não importando o desfecho. Nada disto seria possível se não fosse por vocês!

Por último, mas não de todo menos importante, quero agradecer à Catarina, por ser o meu rochedo ao longo de toda esta jornada, sendo uma fonte ilimitada de conselhos, companhia, motivação e momentos felizes. Nunca me deixa de admirar a quantidade de coisas que aprendo contigo todos os dias! Também por ti persigo um futuro áureo!

Resumo

A crescente preocupação com os cuidados de saúde pessoais tornou necessária a melhoria dos dispositivos de saúde pessoais, cujo funcionamento se baseia principalmente à volta de procedimentos complexos e trabalhosos que dependem de equipamentos volumosos e pesados. Assim, os pacientes sofrem de constante desconforto e dor causados por métodos invasivos relacionados como a recolha de amostras e a colheita de sangue, bem como outras técnicas tradicionais. A solução passa pelo desenvolvimento de novos sensores flexíveis capazes de detetar e monitorizar temperatura, humidade, deformação, pressão e suor.

Assim, o objetivo desta dissertação foi fabricar, caracterizar e testar possíveis aplicações de um sensor de deformação piezoresistivo à base do compósito de dimetilpolissiloxano (PDMS) nano reforçado com óxido de grafeno reduzido (rGO), com as características físicas e eletromecânicas necessárias para detetar o movimento de articulações e padrões de respiração. As amostras foram preparadas por elementos do *solution casting* e *solvent casting*, seguidas pela caracterização do seu efeito piezoresistivo, as suas propriedades mecânicas (ensaios de flexão em 3 pontos e tração), morfológica por microscópio eletrónico de varrimento (SEM), químicas por espetroscopia de reflexão total atenuada/espetroscopia no infravermelho por transformada de Fourier (ATR/FTIR) e térmicas por análise termogravimétrica (TGA) assim como testes de desempenho em partes do corpo de voluntários.

Assim, foi possível observar a influência da razão elastómero-endurecedor do PDMS utilizado, bem como a temperatura e o tempo de cura, o dispersante escolhido e o teor de rGO no desempenho final do sensor, com a possibilidade de afinar determinadas características do mesmo, para se adequar a aplicações específicas. Além disso, em testes piezoresistivos cíclicos, os *gauge factors* médios obtidos, uma medida da sensibilidade do sensor, variaram entre 7.49-14.85 para 3 wt.%, 9.84-30.8 para 4 wt.%, e 0.56-9.16 para 5 wt.% de rGO, estabelecendo estas amostras como sensores piezoresistivos eficazes para aplicações de bioengenharia.

Concluiu-se também que, para aplicações deste tipo, o rácio elastómero-*crosslinker* mais indicado é 15:1, a cura a 120 ºC durante 20 minutos, o dispersante mais indicado é o álcool isopropílico e o conteúdo de rGO deve-se encontrar entre 3-5 wt.%, dependendo das necessidades de deformação. Os compósitos com concentrações de rGO entre 3% e 5% apresentaram comportamento mecânico com boa linearidade (R^2 = 0.995, 0.999, 0.996) e comportamento piezoresistivo satisfatório entre 1.54 % e 2.87 % de deformação, estabilidade até 100 ciclos de flexão a 3 pontos, resistência mecânica à tração entre 1.05 MPa e 3.084 MPa, temperatura de degradação entre 380 ºC e 410 ºC, bem como a perda reversível da sua componente elétrica antes da rutura da estrutura, quando tracionados, e a capacidade de monitorizar o movimento de articulações e de padrões de respiração.

Palavras-chave:

Bioengenharia, Polímeros Eletroativos, Compósitos Poliméricos, Piezoresistividade, Sensores Flexíveis, Nanomateriais.

Abstract

Due to the ever-increasing amount of the population focusing on their personal health, thanks to rising living standards, nowadays we are facing the need to improve personal healthcare devices, which mostly depend on laborious, time-consuming, and convoluted procedures, relying heavily on cumbersome equipment. Thus, patients repeatedly suffer from discomfort and pain caused by invasive methods related to sample-gathering, blood sampling and other traditional bench-top techniques. With this in mind, the solution lies in the development of new flexible sensors with temperature, humidity, strain, pressure and sweat detection and monitoring capabilities, mimicking some of the skin's sensory capabilities.

Therefore, the aim of this dissertation was manufacturing, characterizing, and testing possible applications of a piezoresistive strain sensor based on a polydimethylsiloxane (PDMS) composite nano reinforced with reduced graphene oxide (rGO), with the physical and electromechanical characteristics required for the effective detection of joint movement and breathing pattern monitoring. The samples were prepared via elements of solution casting and solvent casting, followed by characterization of the piezoresistive effect of the material, its mechanical properties (3-point bending and tensile), morphological (SEM), structural (FTIR), and thermal (TGA) properties, along with performance testing in volunteer's body parts.

Regarding results, it was possible to observe the influence of the used PDMS' elastomer-crosslinker ratio, cure temperature and time, chosen dispersant and rGO content in the final performance of the sensor, with the possibility to tune certain characteristics to be better adjusted to specific applications. Moreover, in cyclic piezoresistive tests, the obtained average gauge factors, a measure of the sensor's sensitivity, ranged from 7.49-14.85 for 3 wt.%, 9.84-30.8 for 4 wt.%, and 0.56-9.16 for 5 wt.% rGO, establishing these samples as effective piezoresistive sensors for bioengineering applications.

Furthermore, it was also concluded that, for this kind of application, the indicated elastomer-crosslinker is 15:1, cured at 120ºC for 20 minutes, with isopropyl alcohol as the dispersant and a rGO content between 3-5 wt.%, depending on the necessities of the application. The composites with a rGO content between 3% and 5% exhibited good mechanical linearity (R^2 = 0.995, 0.999, 0.996) and satisfactory piezoresistive performance, at the 1.54-2.87% strain range, stability in the 100 cycle 3-point bending tests, the tensile strength varied from 1.05 MPa to 3.084 MPa, the degradation temperature ranged from 380 ºC to 410 ºC, as well as composites reversibly losing their electrical component before the structure integrity is lost, when tensile tested, and the ability to detect and monitor joint movement and breathing patterns.

Keywords:

Bioengineering, Electroactive Polymers, Polymer Composites, Piezoresistivity, Flexible Sensors, Nanomaterials.

Index

Figure List

Table List

Nomenclature

General:

% RH	Relative Humidity [%];
Ag	Silver;
Au	Gold;
C	Capacitance [F];
Ca^{2+}	Calcium ion;
Cl^-	Chloride ion;
Cu	Copper;
GF	Gauge Factor;
H_2SO_4	Sulfuric acid;
In_2O_3	Indium oxide;
K^+	Potassium ion;
KCl	Potassium chloride;
$KMnO_4$	Potassium permanganate;
mA	Milliampere;
Na^+	Sodium ion;
NaCl	Sodium chloride;
$NaNO_3$	Sodium nitrate.

Lower Indexes:

A	Effective Plate Area;
d	distance between plates;
E	Young's modulus;
ms	milliseconds;
R_o	Initial Resistance;
R(T)	Resistance at temperature T;
$R(T_o)$	Resistance at temperature T_o;
R^2	Coefficient of determination;
ΔR	Variation of Electrical Resistance.

Greek simbology:

$\Delta\varepsilon$	Induced Mechanical Strain;
ε_o	Free space permittivity;
ε_r	Material permittivity;
σ	Applied stress;

SD Standard deviation.

Acronyms:

AAO	Anodic Aluminum Oxide;
ADC	Analog-Digital Devices;
AgNP	Silver Nanoparticles;
AgNW	Silver Nanowires;
AI	Artificial Intelligence;
ATR	Attenuated Total Reflection;
BFC	Biochemical Fuel Cells;
BLE	Bluetooth Low Energy;
BTO	Barium Titanate;
CB	Carbon Black;
CNC	Carbon Nanocapsule;
CNF	Carbon Nanofibers;
CNM	Carbon Nanomaterial;
CNS	Central Nervous System;
CNT	Carbon Nanotube;
CVD	Chemical Vapor Deposition;
DSC	Differential Scanning Calorimetry;
DTA	Differential Thermal Analysis;
ECG	Eletrocardiogram;
EEG	Eletroencefalogram;
EGaln	Eutectic Gallium Indium;
EMG	Eletromiogram;
EOG	Electrooculogram;
FTIR	Fourier Transform Infrared Spectroscopy;
GF	Gauge Factor;
GO	Graphene Oxide;
GOx	Glucose Oxidase;
IDE	Interdigitated Electrode;
IoT	Internet of Things;
ISE	Ion-Selective Electrode;
ITO	Indium-Tin-Oxide;
LED	Light-emitting diode;
MEMS	Microelectromechanical Systems;
MWCNT	Multi-Walled Carbon Nanotube;
NFC	Near Field Communication;
NP	Nanoparticle;

NTC	Negative Temperature Coeffcient;
NW	Nanowire;
P(VDF-TrFE)	Poly(vinylidene fluoride-*co*-trifluoroethylene);
PANI	Polyaniline;
PBT	Polybutylene terephthalate;
PC	Polycarbonate;
PCB	Printed Circuit Board;
PDMS	Polydimethylsiloxane;
PEDOT:PSS	Poly(3,4-ethylenedioxythiophene) polystyrene sulfonate;
PEN	Polyethylene naphthalate;
PET	Polyethylene Terephthalate;
PI	Polyimide;
POC	Point-of-care;
Ppm	Parts Per Million;
PPy	Polypyrrole;
PTC	Positive Temperature Coefficient;
PU	Polyurethane;
PV cells	Photovoltaic cells;
PVA	Polyvinyl Alcohol;
PVDF	Polyvinylidene fluoride;
PVDF-TrFE	Polyvinylidene fluoride-trifluoroethylene;
PZT	Lead Zirconate Titanate;
RF	Radiofrequency;
RFID	Radio Frequency Identification;
rGO	Reduced Graphene Oxide;
RTD	Resistance Temperature Detector;
SEBS	Styrene-ethylene-butylene-styrene;
SEM	Scanning Electron Microscope;
SWCNT	Single-Walled Carbon Nanotube;
TCR	Temperature Coefficient of Temperature;
TENG	Triboelectric Nanogenerators;
TGA	Thermogravimetric Analysis;
TPU	Thermoplastic Polyurethane;
UV	Ultraviolet;
WPT	Wireless Power Transfer.

Chapter 1

Introduction

1. Introduction

1.1. Framework

An increasing number of people are focusing more on their personal health as a result of rising living standards. Currently, the standard methods for providing personal healthcare mostly rely on antiquated techniques using heavy equipment and convoluted procedures, which are often difficult and time-consuming. Additionally, patients may experience discomfort and pain because of the invasive methods used to gather samples, some of which still call for the need of bulky apparatus, blood sampling, and traditional bench-top testing techniques [1,2]. Despite this, there has been recent advancements in a number of areas, including those that use biological tissue, implanted electronic devices, electronic skin (e-skin), and wearable technology [3].

Looking further at the last two, wearable technology has evolved in recent years from wrist-worn fitness trackers to multipurpose sensors with real-time monitoring of physiological signals like heart rate, blood oxygen levels, hydration, temperature, and sleep patterns [4]. As a result, these new technologies make it easier to detect diseases in their early stages and to monitor their progression and treatment. As an emerging analytical tool, it can be attached to various body parts to collect biochemical and physiological parameters, relying on physical, chemical, and biological information transmitted through the skin. This is made possible by non-invasive techniques, which reveal the condition of the human body in real-time [4]. Tracking the diagnosis, postoperative rehabilitation, and adjuvant treatment of patients with chronic diseases can all be greatly aided by keeping track of these indicators, being especially true for those who live in remote and rural areas with little access to healthcare, who could rely on at-home monitoring for conditions like arthritis, back pain, cardiovascular diseases, asthma, diabetes, and dementia. These sensors can also gather bodily signals for extended periods of time, which is not practical in clinical settings [4].

On the other hand, since the 1970s, touch sensors in prosthetics have been researched, where it has been shown that prosthetic hands can use combined tactile feedback with a touch screen computer. Since then, a wide range of uses for tactile sensors and electronic skins have been discovered in fields such as robotics, artificial intelligence, prosthetics, health monitoring technologies, and human-machine interfaces [5]. The skin, being one of the most amazing human organs, covers our entire body and has several nerve sensors that can concurrently perceive pressure, temperature, and object texture. Human skin possesses exceptional elasticity, stretchability, and self-healing abilities in addition to its superb sense of touch [5].

Knowing this, the focus of rapid development in the research sector has been the e-skin, which employs flexible and elastic electronic devices having skin-like receptor characteristics. Due to the utilization of flexible sensors with pressure, temperature, humidity, and strain detecting capabilities, with devices theoretically nearly resembling the skin's sensory abilities

[3]. Along with that, it can also be conformally adhered to tissue surfaces in close proximity to the sampling site to record thermal, electrical, mechanical, and chemical changes, ensuring the accuracy of the detection and elevating them to the status of one of the most advanced health monitoring technologies [1]. The most popular strain and pressure sensors can be used to detect both types of human movement, including both joint movements and subtle movements brought on by the heartbeat, blood pressure, sound, and breathing.

Wearable sensors must have great stability, specificity, and sensitivity to be effective as a tool for personal healthcare, and their sensing components must have excellent conductivity to convert different impulses into electrical signals. All of these qualities would guarantee that wearable sensors pick up variations in human movements or molecules and ions in bodily fluids [1]. For instance, pressure-sensitive electronics in the medical industry can help amputees and stroke victims regain sensory functions. In addition, they can be used to continuously monitor physiological health [3]. This is accomplished by the action-related information provided by these devices, which includes sticking, slipping, and grabbing motions. Additionally, these devices estimate control parameters such as contact force, depending on the softness/hardness and texture of the items [5]. When multifunctional sensors are used, it is possible to accurately track vital biometrics, including blood pressure, oxygen saturation, temperature, blood sugar level, and level of hydration [5]. In addition to ions and molecules, extensive research has been done in recent years on the detection of physiological traits that can indicate heart activity, such as the electrocardiogram (ECG), electroencephalogram (EEG), electromyogram (EMG), and the gas molecules in exhaled breath [1]. With that in mind, wearable sensors are being extensively researched for their capacity to monitor personal health parameters continuously and accurately, allowing the domestic tracking of patients' recovery after surgeries, avoiding lengthy hospital stays, cutting down on medical costs, and minimizing the exposure to nosocomial infections [1,4].

However, as a result of these factors, there is a significant demand for flexible pressure sensors. For instance, it is important to enlarge the monitoring area, decrease the detection limit, and improve the sensitivity [3]. Thus, the process of making e-skins is difficult due to several aspects, including the rigidity and lack of flexibility of current planar electronics, the very limited responsive range of traditional sensors like strain gauges, and the requirement to integrate multiple types of sensors in the particular circumstance of multifunction monitoring [5].

Hence, the creation of wearable sensors has made use of functional materials, often among them nanomaterials, used due to their high conductivity, rapid electron transfer kinetics, and high aspect ratio [1]. Some of these nanomaterials have outstanding electrical characteristics and are inherently flexible, providing both good tensile properties and sensitivity at the same time [5]. Associated with this rise in interest, wearable sensors have significantly improved over the past ten years as a result, suffering an unprecedented market growth along with scientific advancements in microfabrication of electronics, flexible electronics, nanomaterials, wireless communication, artificial intelligence (AI), and communication

technologies [4,6]. In 2015, wristwear accounted for ≈50% of the wearable sensors market. One of the most important factors is technological innovations and advances, which result in the introduction of new products. Growing demand from consumers and medical applications have also boosted market growth. Apart from that, there's a miniaturization trend, instrumental for the size reduction of sensors and wearables, including wristwear, bodywear, and eyewear, being increasingly influential in healthcare and infotainment market [7].

Figure 1 shows that in 2020 the market for wearable medical devices was forecast to be worth USD 8 billion, and that by 2025, it is expected to be worth USD 19 billion [6], thanks to medical/fitness-related services leading the market for wearable sensing technologies, with demand growing rapidly amid the coronavirus (COVID-19) pandemic. Commercial wearable technology that monitors human body signals continues to be introduced, with researchers worldwide focusing on flexible touch sensors in order to be employed as elements of flexible wearable sensors and electronic skins. Wearable technology for human health has therefore received intense interest because of the crucial part they play in AI and the internet of things (IoT) [6]. Furthermore, due to remarkable changes in worldwide Internet penetration, there's a progressively larger number of Internet-enabled smart devices in developing countries, especially in southeast Asia and Oceania, as shown in Figure 2, a factor that presents itself as an opportunity for further growth [7]. Despite this, a lack of common standards and interoperability issues prevent efficient communication of sensor information and sensor data, harmful for an easy exchange of information between connected devices. Apart from that, technical difficulties related to hardware and software are still prevalent today, including constrained power reserves and small screens and displays, due to the compact sizes of devices or waterproofing issues, because of sweat or washing creating damaging moisture in the electronics [7]. Taking this into account, among the potential wearable technology has, challenges that need to be overcome still exist for the market to truly thrive [7].

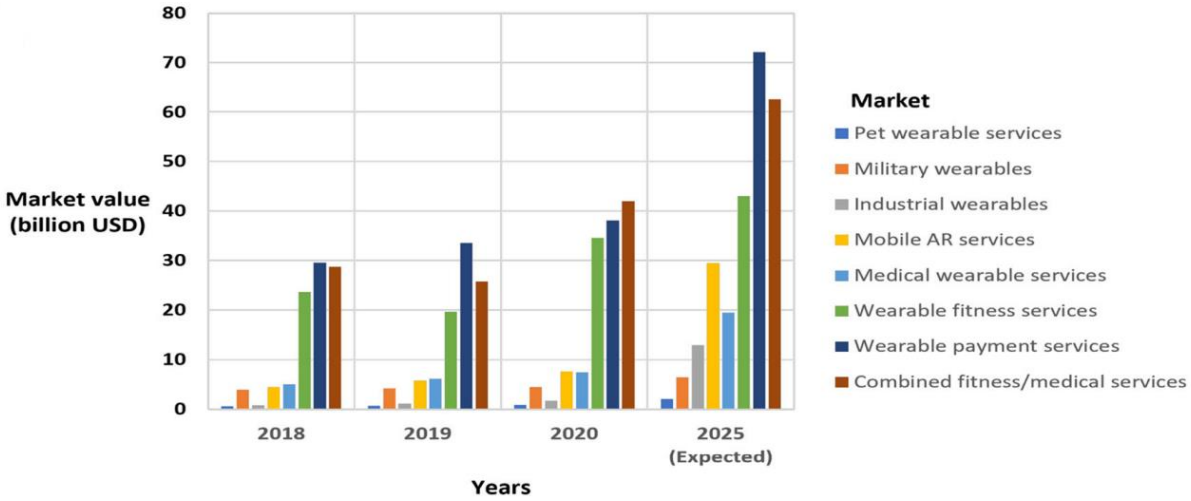

Fig. 1. Market value evolution of various wearable services. (Adapted from [6]).

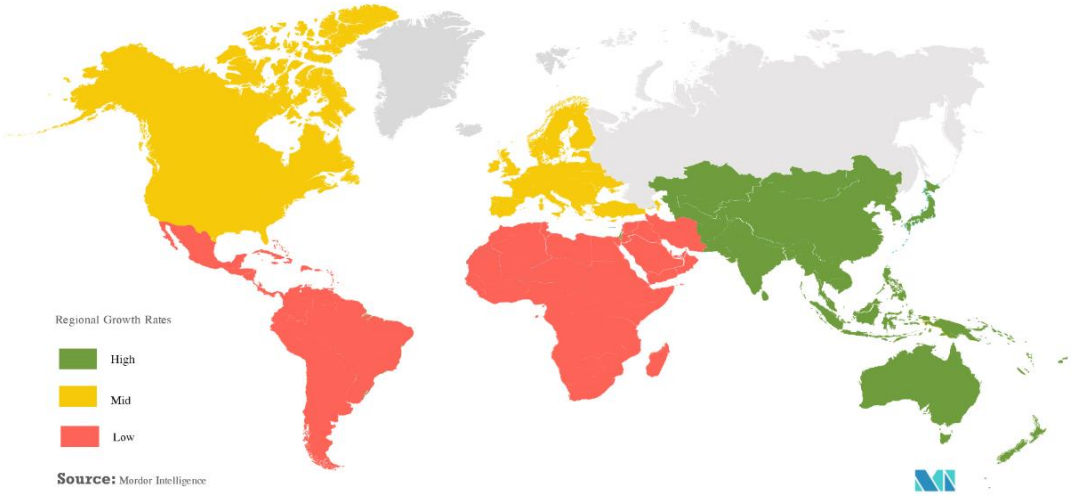

Fig. 2. Wearable sensors market growth rate, by region (2019-2024). (Adapted from mordorintelligence.com)

1.2. The study problems and its relevance

Looking more into the challenges associated with the progress in this field, despite the above-mentioned trends and efforts, many wearable sensors are still a long way from being employed reliably in long term and continuous human activity monitoring applications. Firstly, after learning the relationship between the materials and the properties of the structure they are dependent on, for each type of sensor, further improvement regarding the form factor, mechanical properties and energetic efficiency is necessary [8]. These translate into aspects concerning the user acceptance, data acquisition, validation, transmission, and battery lifetime. Additionally, other technical challenges need to be faced before we can expect wearable devices being used long term. These considerations are mainly related to the lack of standards that exist to this day, limitations in microfabrication technology, stimuli-responsive material demands and selection, along with the debate between human-centred designs or truly personalized models [9-11]. On the other hand, concerns respecting the stretchability, response time, range of detection, linearity, hysteresis and comfortability of sensors need to be addressed [11]. Furthermore, most existing systems are being developed for the fitness market, rather than older adults, seniors, and rehabilitation patients, hindering the progress towards the creation of positive evidence for the effectiveness of this technology in these fields. Moreover, the mix of

researching prototypes, consumer-grade, and clinical-grade systems poses another problem in reaching effective validation and interoperability [9].

In the following subchapter the most pertinent factors for the project at hand will be presented and discussed, with solutions and opportunities being subsequently provided.

Beginning with one of the most opportune and influential aspects, the stretchability of a sensor is a key parameter in the assessment of wearable devices. By definition, this parameter is the maximum strain tolerated by the sensor. It is currently known that, generally, sensors with high stretchability capabilities possess low sensitivity and nonlinear behaviour. Thus, to overcome this, there's an ever-increasing demand for the fabrication of sensors with high stretchability and sensitivity [11]. Looking into the latter, it indicates the accuracy and efficiency of the sensors. Customarily, regarding strain sensors, the gauge factor (GF), the resistance variation under deformation, is used as a measurement of sensitivity. Variations of this value occur depending on the materials and structures employed. Therefore, it is noteworthy that both properties are of core importance for not only strain sensors, but all sensors that deploy detection principles [11].

Furthermore, systems should also aim to reduce the overall effect of artifact sources, being it from motion, electromagnetic or electrostatic origin. Based on the type of noise, several solutions can tackle them, such as tight-fitting garments to mitigate motion artifacts, differential amplification of the acquired signal, filtering or skin-mounted structures [8].

Aside from that, the response time, defined as the time needed for the provision of a stable output under external stimuli, also emerges as an important factor in sensor design, where shorter response times should be considered, especially in real-time monitoring applications. However, issues appear when it is needed to consider that various important factors influence the response time and, due to viscoelastic properties, polymer-based sensors face longer response times, when compared to other materials [11].

Associated with them is the range of detection, the limit of detection and the region between the highest and the lowest amount of stress identifiable by the sensor. This parameter is determined with the support of different methods, including calibration curves, for most sensors. Nevertheless, a challenging issue that still presents itself is making important improvements in the limit of detection [11]. This is the case because both calibration and validation are critical to obtain accurate data from wearable technologies, in a field that is still developing a generally accepted language for measurement and evaluation of the devices' performance, durability and safety. Apart from that, researchers require the access to raw and process data to judge if variations occur due to hardware differences or different post-processing algorithms. Yet, these approaches to calibration don't necessarily grasp the complexity of everyday life or variations in mobility [9].

Another parameter to consider is the linearity, characterized by the percentage of deviation of the output signal from the ideal curve. Therefore, this is a measure of signal stability and is often presented in percentage of nonlinearity, the so-called linearity error. The linearity

can be affected by many parameters, such as humidity, temperature, vibrations and other environmental causes [11].

A distinct obstacle in the field is also the comfortability for human health monitoring, where we should consider the patient's well-being and the sensor's compliance as core parameters, through the selection of the indicated materials and mechanisms, as well as an accurate and comfortable fabrication for the capture of the desired signals, in cases where the sensor is in direct contact with the user's body or skin. Additionally, to increase the overall popularity of these devices worldwide, they should feel comfortable, with its components small and flexible [11].

Inherent with this we have the user acceptance, one of the biggest issues with the current technology, therefore facing many challenges respecting the devices' personalization, design, scalability, data acquisition and transmission. Moreover, a bigger focus should be put on interfaces and designs that feel ergonomic, accessible, intuitive, and simple, due to the need for adaptivity to various settings, while developing and reinforcing engagement and positive behaviour, a very challenging proposition, because of the diversity of user capabilities, motivations, and desired outcomes. However, if researchers manage to implement this properly, we could start witnessing extensive improvement in the overall satisfaction and continued use of wearable technologies past study applications [9,10].

On the contrary, personalized models appear as a way to consider the needs and constraints of specific individuals. Despite having the capability of yielding higher rates of adoption, these personalized systems require the considerations of many variables, mainly the degree of inter-individual variability, privacy concerns, and scalability issues. This has prevented the development of effective and personalized technologies and, consequently, the focus of many of these devices is grasping and promoting positive health behaviours, while also retaining engagement [9].

With everything in mind, in order to design proper wearable devices, a number of considerations should be contemplated: in the first place, it must not disturb regular activities the user does during the daily life, while being comfortable, even after frequent use; secondly, the design should try to be inconspicuous for other people; lastly, the sensors must be close to the body, sensing and transmitting the appropriate measurements accurately [10]. In practice, these changes could bring more adequate healthcare services to users, either by supplying healthcare for the elderly, or empowering sensors via IoT. However, despite giving health systems further accuracy and cost-effectiveness, gathering attention in several fields, its operation is still limited in real-time monitoring of health parameters [11].

This is the case also due to both limitations in techniques and tools for microfabrication or battery life and energy consumption issues. Regarding the first, currently we're facing limitations in the etch of structures at acceptable rates, while employing soft materials, which turns the fabrication of thick films arduous. Furthermore, the usage of biopolymeric materials raises even more problems, since they are not suitable for processing at high temperatures,

leading to more complications amid fabrication. Therefore, the objective should be the production of systems as small as achievable without sacrificing functionality [11].

On the other hand, respecting the battery life complications, these could be circumvented through hardware, software or interface approaches. It should be kept in mind that providing power is a fundamental piece of every device. If the intention is a sensor functioning efficiently for an extended period of time on a battery, the operating voltage employed by device and, therefore, its power consumption, should be reduced [8]. Looking into the hardware, an option would be using energy harvesting technology, obtaining power from kinetic, electromagnetic or solar sources. Additionally, an attempt could be made through the software by reducing the power the system's firmware consumes. Lastly, regarding the interface, the interactions employed to complete tasks should be completed in less than 3 seconds, conserving as much energy as possible. However, some of these approaches are limited by current technology or are simply not feasible, taking into account the size of the devices we have available today [10].

All things considered, with the potential wearable sensors represent, concerning their future, researchers need to target low-cost, biocompatible, and environmentally friendly materials, with simple and cost-effective fabrication processes and superior scalability, resulting in the general acceptance and adoption by society [8]. Regarding the above-mentioned obstacles and challenges, further focus should be put on material development, leveraging specific properties and innovative fabrication processes. As a conclusion, even though numerous and important steps have been taken in the right direction, we still have a long way to go until we reach acceptable performance for long-term and widespread usage [11].

1.3. Dissertation objectives and contribution

In this dissertation, the aim is to develop a synthetic sensorial system, that acts as a skin substitute, through the use of piezoresistive composites, with the intention of making the detection of movements and actions by the user possible, thanks to the development of a highly sensitive strain sensor made of a rGO@PDMS composite material.

This system requires the necessary mechanical properties to be physically compatible with the human skin, while the piezoresistive epidermal sensor could evolve into an entire network and even a medical device prototype, with monitoring capabilities, for rehabilitation and therapy applications. Furthermore, this device must exhibit the required biocompatibility for its function, with a gas-permeable substrate, permitting adequate oxygenation.

Taking this into account, throughout the making of this dissertation, the main categories of sensors, materials and measured parameters will be evaluated, with the appropriate characterisation and justifications for the choice of raw materials and the approaches taken into their transformation. Additionally, the steps required for the manufacturing and operation of the entire system will be addressed, having all fabrication

methods and experimental protocols been thoroughly analysed and characterized, on the basis of the descriptions provided by the literature, focusing on relevant parameters such as the geometry, thickness and flexibility of the entire structure.

After the results are gathered, a meticulous discussion must be made, in order to comprehend the relationship between the various parameters used throughout the experimental tests and the obtained properties, assimilating and describing the associated phenomena and identifying potential limitations.

Regarding the dissertation's contribution, the objective is providing an in-depth analysis of the mechanisms and interactions surrounding electroactive polymers and composite material sensors, in addition to an outright repertoire of the principles respecting material, geometry, architecture and manufacturing methods selection. Additionally, the sensors' performance will be evaluated, according to the variation of the percentage by weight (wt.%) of the elements composing the device.

Lastly, this project also displays the potential to carry out studies on the biocompatibility, long-term usage and user acceptance of flexible, epidermal sensors, for health monitoring applications.

1.4. Dissertation organization and explanation

The development of this work is composed of two main stages, these being designated as the theoretical and the practical components. The first one is comprised of the analysis of the problem at hand, including the entire research process and the establishment of the state-of-the-art surrounding all matters related to sensorial systems and composite materials. The second phase encompasses the procedure where the knowledge gained throughout the first phases of the project is applied in manufacturing, characterizing, testing, and implementing the technology in the real world.

Therefore, this dissertation is divided into six chapters. The present chapter makes the introduction of the challenges at hand, the market trends, as well as the notions regarding sensorial systems, e-skins, physiological parameter monitoring and user experience and acceptance.

Chapter 2 is composed of the state-of-the-art, introducing all the general considerations concerning the phenomena akin to flexible sensors and sensorial systems, including the most commonly employed sensors, along with themes in the field of material science, such as matrices, conductive materials, composite materials, piezoresistivity and sensor manufacturing and trends.

Chapter 3 compiles all materials and experimental methods implemented in sample preparation and characterisation, with fabrication methods, electrode deposition, mechanical characterisation, thermal characterisation, microscopy and spectroscopy being described here.

In chapter 4 are described, presented, analysed, and discussed the obtained results from the characterisation phases of the work, with all results being displayed in the form of tables and graphs, followed by thorough discussions of the achieved outcomes.

Chapter 5 is comprised of the proof of concept, acting as the culmination of all proficiency gained during the work, with the application of the technology in the real world being applied, described and discussed here.

Chapter 6 acts as the conclusion to this work, compiling conclusions, future endeavours and ramifications of the developed study.

Chapter 2

State-of-the-art

2. State-of-the-art

2.1. Introduction

Nowadays, we are witnessing a shift in the healthcare system, where an individual-centred system is being embraced, permitting personalized and accurate medical information to be obtained by monitoring sensors, now deployed on a large scale. Thus, a clinical environment that has the capability to provide superior care for patients and medical personnel alike is unequivocally obtainable [12]. Hence, for a remarkable management of patients, continuous real-time monitoring is vital, especially when dealing with chronic diseases, such as diabetes, cardiovascular, or neurodegenerative disorders, where new strategies for diagnosis are being researched [13]. One of these approaches is healthcare wearable devices, born from the miniaturization of electronics and advancements in nanoelectronics and material selection, opening the door to a new way to process and share acquired data. These can be worn on the body or clothing and several types are being employed today, such as electronic skins (e-skins), tattoos, and implants [13,14].

With the support of this new technology, various biopotentials can now be measured outside traditional clinical environments, in a non-invasive manner, superb for point-of-care (POC) applications. These include the electrooculogram (EOG), which monitors eye movements, EMG, which measures the muscle response to nerve stimulations, ECG, a degree of heart performance, and EEG, the monitoring and analysis of brain activity and performance. Furthermore, flexible substrates that can conform to the human skin could grant accurate measurements of temperature, pulse and other bioelectric signals, reflecting human body's health level. Therefore, real-time monitoring of parameters allows for an increase of correct diagnoses, with the development of flexible devices attracting considerable attention due to its potential in the new generation of sensors and systems [13,14]. Wearable devices are lightweight, soft, flexible, resistant to fatigue and with good sensing performance, having shown promising results due to deformability and compliance properties [12,13].

Additionally, conventional electronic devices, which are heavy, rigid and sometimes difficult to use, are not advisable choices for health wearable devices, prompting improvements in terms of material selection, fabrication techniques and processing circuits. Along these lines, with the emergence of communication modules such as Bluetooth, Near Field Communication (NFC) and Wi-Fi, these electronic devices are not only cheap to produce, but also efficient, regarding its power consumption, while allowing continuous acquisition and transmission of data over long periods of time [13].

Taking this into account, in this chapter, themes surrounding sensorial systems will be addressed, including material-related approaches that make up the devices, general concepts, operation principles of commonly employed sensors, along with their applications. Additionally, there will be discussions surrounding manufacturing and functionalization techniques, concepts

and applications of sensorial systems, finalizing with trends and examples of studies carried out by multiple groups of researchers in the field.

2.2. Flexible Sensors

In the past decade, flexible devices have been advancing, demonstrating immense potential in numerous fields, such as healthcare, robotics and bioengineering, where we can find a need for not only high sensitivity and accuracy, but also flexibility and low cost. One application rises above the rest, flexible electronic skins for pressure sensing, which employ polymer-based flexible biocompatible materials, including a biopolymer made of a blend between recycled PLA and wood, commercially named Ecoflex™, polyethylene terephthalate (PET) and polyethylene naphthalate (PEN), silicone-based polymers, such as polydimethylsiloxane (PDMS) and thin polymers like parylene [13,15,16]. These materials possess good mechanical properties, Young's Modulus similar to human skin and great elongation limits, of up to 900% and 400 %, for Ecoflex™ and PDMS, respectively [13,15,16].

For these reasons, wearable sensors can be placed in multiple parts of the body, including the head, eyes, chest, arms and wrists, through flexible, textile-based and epidermal-based wearables. Because of this, physiological parameters and bodily fluids, such as saliva, urine, sweat and blood, are monitored and correlated in order to diagnose and even treat different diseases, where its drug delivery capabilities could be harnessed, since it retains a more controlled and efficient manner of delivery, relatively to traditional approaches [13].

Moreover, there's an underlying demand for both mechanically compliant and highly sensitive sensors, capable of mimicking the human skin's properties, including multifunctional sensing, while maintaining non-invasive, fast response to temperature and pressure, high resolution ratio, softness, low power consumption and biocompatibility, despite all the challenges inherent to healthcare monitoring and robotics applications [14-16].

Early sensors and biosensors were originally employed as invasive devices focused on the monitoring of physiological signals, such as respiration rate, muscle activity, temperature, and heart rate, in controlled lab settings [12,13]. However, a considerable volume of the materials used could not meet the breathability and comfort standards we have today. Presently, efforts have led to the development of nanomaterials and flexible polymers, applied in high-performance sensors, leading to the establishment of new smart materials, which integrate IoT technology, with outstanding electrical and mechanical properties. These, when combined with elastomer substrates, form composites that have a wide range of functions, attracting the attention of researchers from all over the globe [12,13,15]. Nowadays, the main focus of research are smart wearable devices with seamless integration and self-powering capabilities, empowering robots with fast sensing and response capabilities, human-machine interfaces,

highly sensitive e-skins for diagnosis, physics, chemistry, mechanical engineering, biomedicine and clothing technology [12,15,16].

Despite the above-mentioned criteria, limitations regarding the manufacturing and widespread use of these materials still exist, especially when dealing with domestic testing, due to high costs and difficult methods of production, where it is important to realize that factors like shape, surface area, porosity, wettability, air and moisture permeability, conductivity and mechanical properties all influence the final performance of the sensors [12].

In the following subchapter, general concepts surrounding sensors and their flexible counterparts will be presented, succeeded by required properties by today's standards and by the most commonly used types of flexible sensors, finalizing with the most frequent mechanisms involved in the operation of flexible sensors found in literature.

2.2.1. General considerations

Currently, the development of flexible sensors involves strategies that target cost-effective processes, with nontoxic and non-irritating properties, while retaining flexible and soft form factors, carefully taking into consideration the strict demands regarding enhanced physiological monitoring of the human body [17]. By analysing its biochemistry and electrical signs, the bodily health status and reaction to stimuli can be extracted and properly evaluated [18]. To accomplish this, flexible sensors must be placed on the necessary surfaces with durability, compatibility and abrasion resistance [19]. Commercially, the majority of sensors consist of encapsulated integrated circuits on solid substrates, mechanically incompatible with the morphology of the human body, which leads to inaccurate measurements due to insufficient skin contact or shifts in the data acquisition position [19].

Therefore, flexible electronics hold a critical role in the aforementioned applications, since they possess the necessary adaptability to be positioned in all types of substrates, either curved, flat, rigid or soft. These particular characteristics are made possible by functionalizing sensors on soft substrates, achieving low cost, exemplary stretchability, excellent conformability, and low weight, which allows a more effective capture of analytes and consequent production of high-quality signals, in opposition to conventional sensors, unable to capture good quality signals due to rigidity limitations. This has brought interest and research to the field, where, apart from sensors, flexible light-emitting diodes (LEDs), batteries and antennas have been developed [19,20]. Recently, with the construction of ultrathin, flexible, and stretchable sensors, came the necessity to respond more quickly and accurately to parameters in the detection range of the device, followed by the transmission and display of the processed data. Additionally, this kind of sensing technology demands rather complex systems, which can carry out data acquisition and processing, operation control, and data display [19]. Thus, towards bringing this technology from laboratories to widespread use, some pivotal elements, such as manufacturing, theoretical modelling, and system design must be refined, while questions, regarding the effects and potential of additive manufacturing, need to be researched [20].

Regarding the suitability and performance of a sensor, it can be estimated considering several variables, all required for the design of flexible sensors, including electrical, biocompatibility, stability, durability, sensitivity, working range, hysteresis, response time, mechanical, physicochemical, and device-level properties. However, there are limitations respecting the implementations of these parameters, due to existing strict accepted function values, critical for a high-performance and reliable design [17].

The importance of all these properties will be discussed further in this subchapter.

Classification

According to Lim *et al.* [17], wearable technology can be defined as "network-enabled devices that can be worn on or in the body, which are integrated with the user's everyday life and movements.". Likewise, flexible sensors should closely monitor human-related data without sacrificing their motion, enabled by the use of robust, flexible, lightweight and easily operated components. Along these lines, we can conceive a classification taking into account the location they are placed on the body, leading us to two different fields: implantable devices, which are positioned inside the body, near or on inner organs, and epidermal devices, worn onto the skin [17]. In both cases, these systems, sensors included, must show similar properties to the surfaces they are positioned on, granting the needed compliance and robustness. For these reasons, the term "epidermal" is on some occasions synonym with "skin-like" [17]. However, implantable electronics require polymeric or ceramic encapsulation, that functions as a barrier against bodily fluid penetration and tissue invasion of the circuits and batteries. Apart from that, mechanical hardness, hermeticity, resistance to corrosion, and biocompatibility are indispensable [17,21].

Flexible sensors can also be grouped in accordance with its configuration, being it textile-based or electrodes on soft substrates, where textiles demand some properties that are completely different from the others, such as natural warmth and fashion features, among others [17]. On the other hand, electrodes show motion artifact minimization capabilities, whilst being protected from chemical and electrical disturbances, thanks to the substrate. Focusing on the latter, functional materials are obtained by compositing it with nanomaterials or employing materials with useful intrinsic properties, achieving transparency, waterproofness, permeability to gases and electrical conductivity. Thus, these approaches render sensors nonobtrusive, adoptable to daily life and comfortable [17,22].

On the other hand, Dias and Cunha [18] claim that sensors and wearable devices can also be classified according to the scenario of use, either domestic or clinical, type of monitoring, online or offline, and the nature of the user, healthy or diseased. Therefore, according to them [18], we can divide wearable devices in two main areas, the medical area, divided in three sub-categories, and activity monitoring area. While activity monitoring focuses on fitness and non-medical applications, with some self-monitoring and rehabilitation included, the medical area is

divided into prediction, anomaly detection and diagnosis support: the first aims to identify events that have yet not occurred, mainly providing prevention of chronic problems and diagnosis support; the second is responsible for the identification of unusual patterns, based on classification methods, distinguishing outliers from regular data and raising alarms; lastly, the diagnosis support retrieves information from vital signs, health records and anomaly detection data, making clinical decisions based on the retrieved conclusions [18].

Despite this classification giving us a better understanding of the main areas of application, it also shows the limitations of these systems, where the capabilities are bounded by the number of capturable signals [18].

Human Skin

The human skin is the largest organ of our integumentary system, functioning as an interface rich in biological signs incoming from blood vessels, muscles, inner organs, and the internal layers of the skin. Figure 3 shows the main biological sources of the skin anatomy, along with the information we can obtain from them. For instance, we can extract important biopotentials from major nerves of the muscle layer, action potentials from nerve endings or elastic moduli from the *stratum corneum,* the outermost layer of the epidermis [17]. Knowing that continuous body motion gives rise to motion artifacts, flexible sensors need to maintain conformal contact with the skin for more accurate signal detection, opening the possibility for oxygenation mapping of skin grafts, multipoint measurement of oxygen concentration and even sweat monitoring [17,23]. The latter is one of the most easily accessible biofluids, with Na^+, Cl^-, Ca^{2+}, and K^+ ions, hormones, metabolites, peptides, and small proteins providing vital information and insight regarding our inner organism, since its composition is heavily correlated with the blood and dependent on metabolic activities, such as exercise and stress [17].

For on-skin applications, flexible sensors should present values of Young's modulus between 0.1 - 2 MPa and stretchability higher than 70-100% [17,24,25]. Considering that properties of both skin and electronics are similar and may change over time, if we want to keep recording signals with high-fidelity, it is critical to reduce all possible artifacts, mainly motion-induced ones. In this fashion, sensors should also be permeable to gases and sweat, airy, and stickable yet detachable without leaving macerations [17].

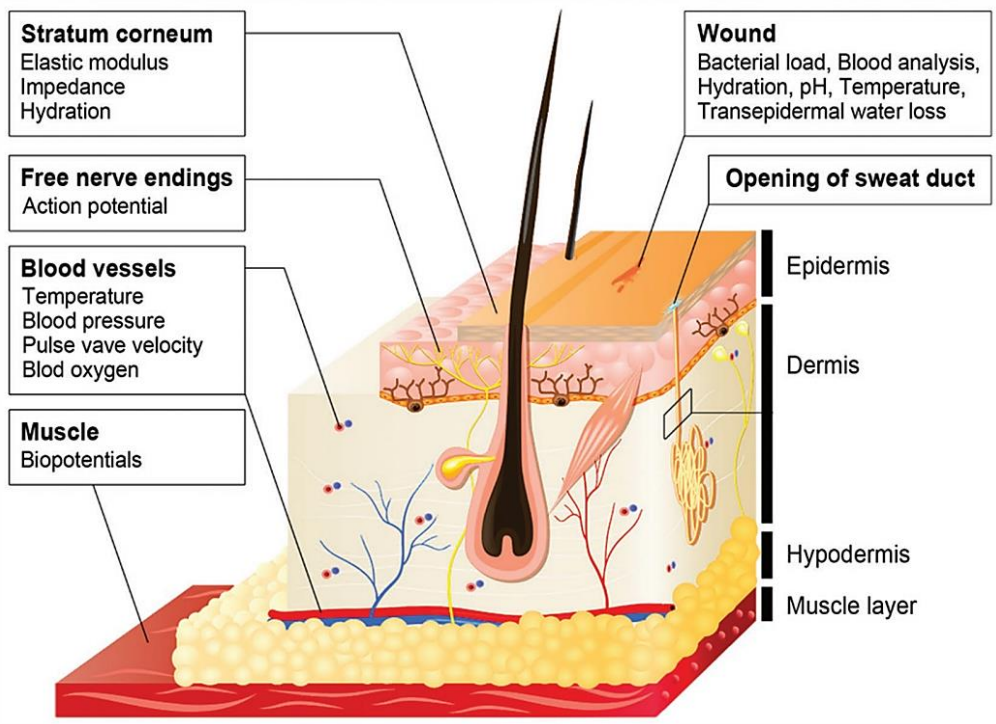

Fig. 3. Model of the skin as a sensing platform for detecting multiple physiological signals. (Adapted from [17])

Amputations

Throughout times, limb amputations have impaired physical mobility and functions of people all over the world, with leading causes varying from region to region. Currently, diabetes and peripheral vascular disease are responsible for the majority of amputations in developed nations, while trauma is the main cause of amputations in developing nations, being considered, by some experts [26], a broadly overlooked epidemic, appealing for concern on both prevention and treatment of this matter. Moreover, the extent of this phenomenon in low-income countries is unknown, due to a lack of tracking and publishing of epidemiologic data on limb amputation, contrarily to high-income ones, such as England, Sweden, Scotland, and Australia [26].

Due to this, while national limb amputation incidence, new cases of limb amputation in a given time period, is relatively simple to access in some cases, prevalence data, consisting of the number of people living with the condition, especially for traumatic amputations, are difficult to find in literature. Therefore, better comprehending global and regional variation in traumatic limb amputation prevalence would lead to optimized prosthetic service needs and planning, benefiting prosthetists all over the world [26].

According to McDonald *et al.* [26], who estimated global prevalence rates, in 2017, around 57.7 million people were living the aftermath of a limb amputation due to a traumatic event, 31.7%, 28.9 million, of which had unilateral lower limb amputations, 19.6%, 11.3 million, had unilateral upper limb amputations, while 19.1%, 11.0 million, had bilateral upper limb

amputations and 11.1%, 6.4 million, had bilateral lower limb amputations. Furthermore, the leading cause of traumatic amputation was, for all levels, falls, accounting for 52.2% of bilateral lower limb, 38.1% of bilateral upper limb, 36.9% of unilateral upper limb, and 31.7% of unilateral lower limb amputations. Additionally, other causes of traumatic amputations mainly depended on the amputation level: while mechanical forces were the second leading cause of bilateral upper limb amputations (15.1%), road injuries were the second leading cause for all others, with 18.6%, 13.9%, and 13.8% for unilateral lower limb, bilateral lower limb, and unilateral upper limb amputations, respectively [26].

Regarding regional prevalence of traumatic amputation, the highest number was observed in East Asia, with 11.2 million, followed by South Asia, with 9.7 million. However, by looking at prevalence rates per 100 000 inhabitants, these regions have 757 and 544, respectively, which could suggest prevalence rates may be mitigated by higher population counts, notably when compared to other regions of the globe, such as Central Europe (2478 per 100 000), Australasia (2220 per 100 000), and Eastern Europe (2096 per 100 000) [26].

Stretchable Substrates

Substrates play a prominent part in the configuration of a flexible sensor. Many polymer films have been developed as substrates for flexible sensors and soft electrodes, such as polycarbonate (PC), thermoplastic polyurethane (TPU), polypyrrole (PPy), polyethylene terephthalate (PET), polyethylene naphthalate (PEN), and polyimide (PI) [19], due to their excellent flexibility, thermal stability, good chemical resistance, and overall great versatility, with some conductive polymers, such as PPy being employed in energy storage applications due to its excellent conductivity and electrochemical activity [12,32]. Furthermore, in recent years, stretchability also arose as a feature of interest for flexible electronics, with PDMS being the most basic and popular candidate, yet still the best choice for a stretchable substrate. Nonetheless, depending on the application, other substrates, such as polyurethane (PU), could be advantageous, thanks to proven compatibility with stretchable printed circuit boards (PCB), with ordinary textile materials and electrospun elastic fibres also proving to be favourable prospects [19, 27].

Despite these substrates not showing electrical conductivity, they have acceptable permeability to gases and biocompatibility. When reinforced with conductive materials, the complete acquisition of signals is allowed, from the target of interest to signal conversion and transmission [12]. Additionally, a lightweight and thin substrate allows for a soft and curved surface that can be continuously used for long periods of time without causing discomfort to the user, while increasing the conductivity helps improve the sensitivity [12,19]. This is also supported by the adhesion, an important factor for both on-skin conformability and attaching components to the substrate, usually achieved through surface treatment procedures, shifting from hydrophobic nature to hydrophilic, thanks to operations of chemical functionalization, ultraviolet (UV) exposure, and oxygen plasma [19].

Despite polymeric thin films being widely employed as substrates, some challenges still need to be overcome: the fabrication and treatment temperature of electrodes has been limited by the lower thermal stability of polymers, which usually endure temperatures lower than 200 ºC; long-term stability of polymer substrates can only be achieved through high permeability; intrinsic poor adhesion of many of these polymers significantly limits applications and commercialization [19]. Figure 4 shows the mechanical flexibility of elastomeric materials such as PDMS.

Fig. 4. PDMS elastomer manipulation. (Withdrawn from ufluidix.com)

Stretchable Conductors

Conductive materials represent one of the most important factors in flexible electronics, considering they connect all the components of the device. Optimal flexible conductors should show high conductivity and strong robustness under all types of mechanical deformation, relevant characteristics for applications that require not only good flexibility and generally adequate mechanical performance, but also for the use of advanced materials and smart designs, greatly improving the wearability of the sensors [12,19]. Thus, the development of stretchable conductors is imperative for their use as interconnect components, electrodes, and wireless antennas. According to Lou *et al.* [19] and Dickey [28], three strategies can be generally considered to make stretchable conductors: intrinsically stretchable conductors, deterministic geometries, and composites.

Due to limitations regarding traditional metallic and semiconductor-based sensors, polymer composites have risen as the best alternative material, with the required stretchability for flexible applications [32]. Thus, stretchable conductors are usually introduced in the form of conductive fillers, such as nanoparticles (NPs), nanowires (NWs), graphene, conducting

polymers, metals, and metal alloys, functionalized in stretchable polymer matrices, where the first provides the sensing features and the latter work as a flexible support structure. These allow for low percolation thresholds with great electrical properties and anisotropic packing, considered superior, at low filler concentrations. However, encapsulation and functionalization reduce the overall air permeability, breathability, and comfort of the composite sensor [19, 32].

Directed toward acquiring outstanding electromechanical stability under stretches above 100%, several geometrical designs have been reported, with wavy or serpentine-shaped structures [4], network patterns [30], 3D porous patterns and crumpled structures [29,31], providing great stretchability to otherwise rigid metal films and conductive nanomaterials, whilst minimizing strain on the conducting materials and maintaining conductivity during reversible elongation cycles [1,19]. On a similar note, material selection is a factor of major importance for improvements in response time and recovery properties, made largely possible by advancements in manufacturing methods, which will be discussed further in this subchapter [19]. In recent years, regularly employed fillers are carbon nanotubes (CNTs), MXene, graphene, including graphene oxide (GO) and reduced graphene oxide (rGO), aluminium, silver, or zinc oxide metal nanowires, particles, 2D semiconductors, organic polymers, along with others. Carbon-based nanomaterials, such as carbon nanofibers (CNFs), CNTs and graphene have intrigued the scientific community thanks to their exemplary electromechanical properties and chemical stability, along with well-known and researched synthesis techniques and scalability [4,19,30,31]. This allows for fillers with high performance and low-cost production, greatly sought after characteristics in today's market [19,32]. Figure 5 shows a scanning electron microscopy image of silver nanowires, used as stretchable electrically conductive nanomaterials.

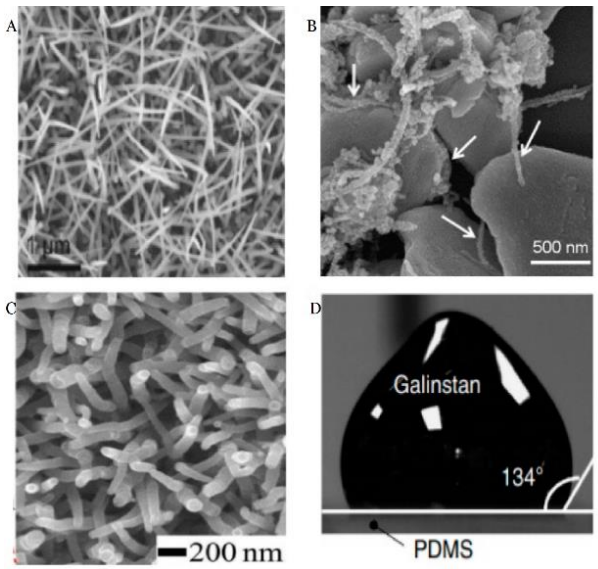

Fig. 5. (A) Scanning electron microscopy (SEM) image of silver nanowires (scale bar of 1μm); (B) SEM image of Ag flakes anchored with Ag nanoparticles and multi-walled CNT; (C) SEM image of PPy nanowires; (D) High surface tension and conductivity of Galistan. (Adapted from [59])

2.2.2. Required properties for sensors

In the context of flexible sensors, these devices are expected to mimic the functions of the human skin, where external physical and chemical stimuli react with the sensing elements of the sensor, changing their configuration and generating electrical signals, in the form of current or voltage [19,32]. These electrical signals can be then processed and converted through an analog-digital converter (ADC), being sent afterwards to a display terminal. Therefore, attention needs to be paid to all elements and roles of the data acquisition chain, including their interactions and how these affect overall performance [19].

On the same note, research and development surrounding flexible sensors require attention to interactions, in the form of interdisciplinary expertise, such as bioengineering, robotics, material science, electronics, and mechanical engineering, due to the requirements this technology possesses. Despite the strategy changing depending on the application at hand, several key parameters need to always be met: use of sensing materials, high sensitivity and working range, highly flexible/stretchable substrates and conductors, wireless communication and display capabilities, low hysteresis, linearity, permeability, biocompatibility, stability and durability, and response time [19, 32]. This allows for systems, such as artificial skins, to detect multiple stimuli, while also being able to differentiate between them, at all times and applications [32]. Figure 6 illustrates a typical data acquisition chain. Something to take into account is that depending on the sensor and its application, the represented data acquisition chain may suffer changes of variable magnitude. Thus, the figure represents the most logical approach to data acquisition and processing.

In the following section, information regarding the key factors for flexible sensor design will be discussed.

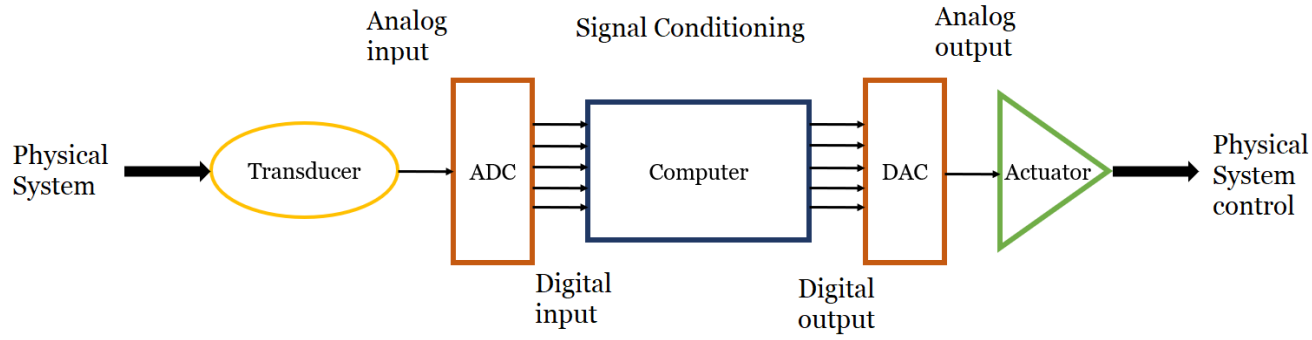

Fig. 6. Data acquisition chain represented through a block diagram.

Sensitivity and working range

According to Huang *et al.* [20] and Sharma *et al.* [32], sensitivity can be defined as the ratio of change in the conversion of the imposed stimuli into quantitative output signals, reflecting the conversion performance of sensors. However, the approaches chosen to define sensitivity can change depending on the application, because sensing mechanisms and the type of measured quantity can create a very wide range of values, being influenced by the active materials employed and the structure of the sensor itself [32].

In order to improve the sensing performance, shape, size and microstructures can be optimized. Furthermore, microstructures can be combined with porous structures, providing high structural deformations and synergistic sensing performance, due to the increase in the number of conductive pathways [32].

On the other hand, working range can be defined as the minimum and maximum value of the measured parameter through the sensor. Generally speaking, sensors with a wide sensing range have low sensitivity, because these factors exhibit an inverse relationship. Thus, research is now focusing on reaching higher sensitivity over a wider range, since human behaviour and motion involves both subtle and large joint movements. Therefore, we should expect sensors to detect these motions with high sensitivity. One approach that could make this possible is designing modifications to the structure of the flexible sensor [32].

Linearity

The linearity of a sensor is another important and desirable property, where a linear relationship between the input and output is expected, for easier data processing. However, the focus normally lies in the calculation of the non-linearity, the deviation between the sensor output and the chosen calibration curve, determined by the linear regression of the coefficient of determination (R^2), where if the value of R^2 is large, the sensor performance should be linear [20,32]. Nevertheless, it is difficult achieving high sensitivity over broad linearity ranges, being preferable having a single linear region with good sensing performance. However, since many flexible sensors have mechanisms that depend on the deformation of its structure or conductive networks, we should expect multiple, non-homogeneous, linearity zones, with different sensitivities [32].

Taking this into account, we can conclude there is a compromise between sensitivity and linearity and working range, where highly sensitive sensors generally show low working ranges and non-linear behaviour over multiple zones and vice-versa [32].

Hysteresis and response time

Hysteresis is a crucial parameter for flexible sensors, showing the tendency of a system to preserve the characteristics created by a stimulus, after it is removed, without restoring the original value in time. In other words, it can be calculated by the maximum difference in the

output between loading-unloading cycles, at any measurement point [20,32]. This property is generally influenced by the viscoelasticity and intrinsic properties of the active materials and electrodes [20].

On the other hand, the response time is defined as the time needed to reach 90% of the stable output, being a measure of the speed in which a sensor responds to inputs. While also being related to the properties of the active materials, it depends on the contact conditions between the materials and the electrodes [20].

With the aim to reduce the effects of hysteresis and response time, porous structures and surface-level modifications are able to improve both effects [20]. Figure 7 shows the principle behind hysteresis, along with its effects on the sensor's performance.

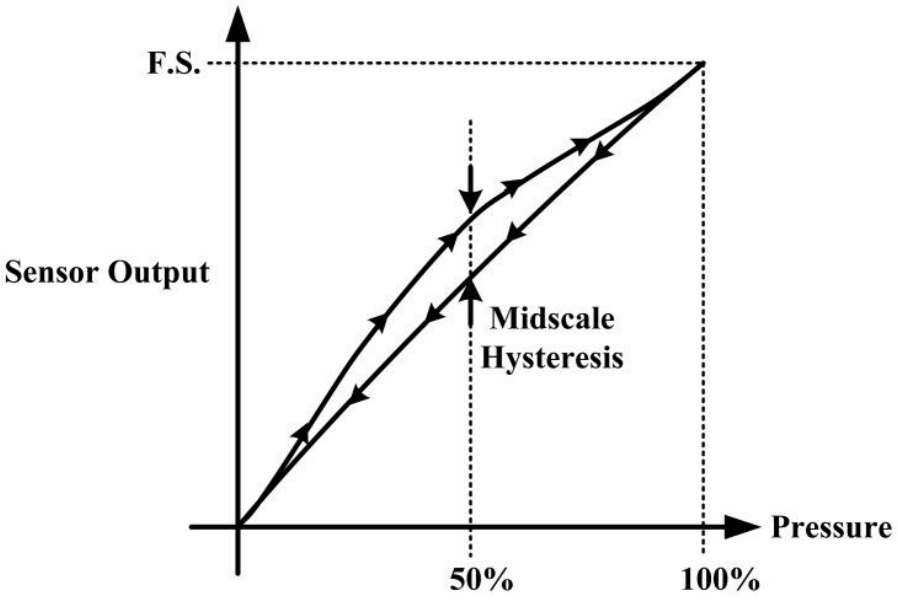

Fig. 7. Hysteresis effect caused by repetitive loading-unloading cycles of a pressure sensor. (Adapted from [51])

Stability and durability

Stability and reliability for long periods of time is another key factor in sensor design. By making continuous loading-unloading cycles, we can track the variations in sensor response. This factor translates into the device's lifetime, since the output degradation usually originates from the deterioration of the active materials. Thus, research regarding the degradation mechanisms could lead to sensors with higher stability in the future [20].

Along these lines, durability is a parameter that measures sensor performance over long term usage. Over time, flexible sensors will experience bending and stretching, as well as various weather and sweaty skin conditions, which could induce the degradation of the sensing elements and layers, resulting in eventual malfunctions [32]. Therefore, achieving high durability is a challenge that all sensors need to complete before widespread use on daily life applications.

Despite a standard not existing, durability is commonly observed during 2500-3000 cycle tests [32]. On the same note, one way to improve durability is encapsulating the sensor in a protective layer, sacrificing to some extent, however, the physicochemical properties [32].

Stretchability

Stretchability has been upheld as a distinct property of flexible sensors, since it directly reflects the capacity to accommodate not only the strain induced by the movements produced by the human body, but also the deformation of the skin, which displays complex and ever-changing topography and stretchability, that can reach as much as 100% [17]. In Sharma *et al.* [32], this parameter is defined as the maximum value of strain/pressure applied to the sensor, without sacrificing the performance's stability and the structural integrity in the process. Stretchability mainly depends on the materials used as substrates and conductors, their interactions, the manufacturing process, and the filler material's aspect ratio [32]. The usage of high aspect ratio fillers embedded in soft or elastomer substrates can provide stretchability to sensors when bent, wrinkled or crumpled. In this situation, the filler materials are allowed to slide against each other, adjusting strain [17]. Graphene is an excellent filler, thanks to the electrical properties, efficient carrier capabilities and low cost it provides [17].

Some approaches to achieve high stretchability include the creation of structures in wave, spatial helical, and fractal design. Another way of achieving this is creating porous structures, providing additional compressibility, compared with dense elastomer layers [32]. Therefore, we can also conclude there is an inverse relationship between stretchability and sensitivity, as the first requires large strains without damage and the latter demands detection of even the smallest strains [32].

Biocompatibility and adhesion

Focusing on flexible sensors that directly contact the skin, the importance of nontoxic, non-irritant, and nonallergenic features should be emphasized, characteristics that lead to the biocompatibility of the device. This parameter can be defined, according to Lim *et al.* [17], as the ability a material has to appropriately perform its desired functions, without negative host response. However, the meaning of biocompatibility, when referring to humans, needs to be expanded to the comfortability the devices provide. To comply with biocompatibility requirements, sensors cannot harm users in any way, while employing materials useful for this purpose, such as stainless steel, titanium alloys, gold, platinum, ceramics, including zirconia and alumina, and stable polymers, from polyacrylates and silicone elastomer groups [17]. One strategy to bestow biocompatibility is covering the material in question with a biocompatible one, allowing for functionality and biocompatibility at the same time [17].

On the other hand, when two different structures come into contact, it is only natural that at some point, either by design or accident, they will come apart. This is mediated by the sensor's adhesion, essential to capture highly accurate signals. Despite being present in all sorts

of medical equipment, including adhesives, dressings, tapes, ECG electrodes, and patches, some important drawbacks are the possibility of allergic contact and maceration on the skin, due to difficulty removing these equipments [17]. This may lead to skin losing some of its barrier function, causing irritations from the substances, or even potential infections. Therefore, recent studies shifted the focus to dry adhesives, investing in interfacial adhesion, the formation of a dry and continuous contact through Van der Waals interactions or electrostatic forces, which completely negates sticky residues and irritations [17]. Other approaches include adding a surfactant to the substrate, which is the case with Triton X being added to PDMS [17].

Permeability

The applications in which flexible sensors are employed are generally abundant in liquids, gases, and foreign molecules. This may lead to penetration of chemical species into the sensor, deteriorating the capabilities of the device over time. Therefore, the environment presents itself as a key obstacle to long-term sensing performance [17]. Aside from the vulnerability electronics have towards water, continuous moisturization of the skin can lead to damage, pain, infections, and delayed rehabilitation. Consequently, devices should selectively permeate gases, especially from the environment, and liquids with salts and other small molecules present, mainly from the body [17]. In spite of this, synthesizing stretchable polymers that are effectively impermeable to water and gases is impossible, due to the large length of the chains, with pores bigger than the molecules it tries to repel. One solution to this problem is employing an encapsulating layer that is less permeable or water repellent, protecting the sensor. However, if the operational timescale is small enough, this approach can be somewhat disregarded, in favour of capturing the target analyte [17].

Another important aspect to consider is the long-term wearing and strong adhesion provided by a breathable flexible sensor, during perspiration. In this case, substrates permeable to water and gases have the advantage, since they do not block sweat glands, reducing the probability of skin inflammation [17].

As a conclusion, despite selective permeability being the key to long-term success of wearable sensors, it relies on materials with high surface-to-volume ratios, prone to accumulating unwanted molecules, turning ineffective over time. Therefore, the key to this challenge is employing ion-selective, permeable membranes, which act as barriers towards undesirable molecules and preserving the necessary ones [17].

Conductivity

All the previous parameters were aimed at improving the sensing capabilities and performance of the sensors. Regarding the conductivity, the same is expected, where this parameter should be stable under high strain, over long periods of time, without suffering

degradation from the environment [17]. Having this in mind, some materials rise above the others, in terms of conductive performance. Silver (Ag) is one of the best choices, being relatively cheap and possessing well-known behaviour, along with copper (Cu), more cost-effective but still highly conductive. However, these present high levels of hysteresis and non-linearity. Carbon-based composites, such as CNTs, CNFs, and CB possess exceptional electrical properties and stability, but are more expensive and its manufacturing is more complex. On the other hand, graphene appears as a material with unique properties, excellent conductivity and relatively low cost, while showing high sensitivity only in very specific ranges. Lastly, conductive polymers, like PPy, are also a choice, being flexible, but retaining an overall lower intrinsic conductivity [17].

Scalability

One parameter that is usually ignored in many studies is the scalability potential of a design. According to Lim *et al.* [17], the ultimate goal in the field of wearable flexible sensors should be the practical implementation and widespread use of the technology in daily life. However, most manufacturing processes are complex and expensive, employing high-cost materials, a challenge the industry needs to overcome in order to accomplish its objective. Thus, progress could be made in the form of solution-synthesized materials or printing methods, as a way to decrease the costs, when compared to the conventional systems, where functional substrates and nanomaterials could be synthesized, with the desired properties [17].

Wireless Communication and display

After capturing the signals of interest, the framework of a sensing systems demands the data to be transferred to a remote system that collects, records, and displays data. Recently, this has been enhanced due to the rise of wireless communication, used by and large in remote monitoring and controlling [19].

Therefore, communication is a key factor in wearable devices, with extended use in biomedical research, human-computer interfaces and monitoring of internal zones of our bodies. Thanks to improvements in communication technology, in the form of near-field communication (NFC), Bluetooth low energy (BLE) and the proliferation of 2.4 GHz Wi-Fi, the development of new wireless sensor systems is being greatly promoted, with many new models being produced every year [19]. Figure 8 shows a wearable health monitoring device, widely used today.

Fig. 8. Wearable health monitoring device, with wireless communication capabilities. (Withdrawn from devicelab.com)

2.2.3. Employed sensors

Broadly speaking, we can compare the operating principle of an electromechanical sensor to a human brain, in the way that the latter works through filtering and differentiating important information from irrelevant one, where thoroughly designed body elements collect signals for processing in the brain, preceding muscle responses. Similarly, circuits with sensing capabilities will capture data as a function of time, with later transmission to the processor and activation of programmed responses, to the assigned condition [33].

Nowadays, research on physical sensing is responsible for the biggest contributions to the wearable sensor field, where an unprecedented growth in use is taking place, with sensors being woven and adhered onto attires or simply inserted on the skin [34]. This kind of sensor fits in a wide range of applications, being it outdoors or indoors, including on-body measurements, biomedical settings, agriculture, room and environmental monitoring, among many other settings [35]. On the other hand, non-physical sensors, such as sweat sensors, provide the highest potential for continuous monitoring of biochemical parameters on and of the body, reflecting its physiological state and the environment surrounding it. These biosensors capture biomarkers, allowing them to distinguish if they are naturally secreted by the body or a consequence of chemical hazard exposure, depending on the analyte's nature [34].

Considering these applications, data of interest will be amassed in a vast set of information, where selectivity through data filtration is becoming more and more important, as crucial data measured from one parameter of the body must be exclusive to it and not impact nor mislead data regarding other parameters, safeguarding the overall accuracy and quality of the measured signals [33].

Taking this into consideration, material selection presents itself as one of the most vital fundamentals of sensor design. Silver is employed in the majority of designs, despite its shortcomings, mostly for electrode patterning, while humidity sensors mainly use the substrate

as the sensing layer, strain and pressure sensors rely on polymer composites to achieve the required mechanical properties, temperature sensors incorporate conductive polymers with optical transparency, plasticity and biocompatibility, and sweat sensors primarily achieve their objectives through electrochemical sensing of biomarkers, via biosensors [35, 37].

In Barmpakos and Kaltsas [35], the most employed sensors in literature from 2013 to 2020 were presented, as presented in Figure 9, through graphic representation, from a sample of 4462 publications. Along these lines, Table 1 presents a summary of the sensing approaches that will be discussed further in this section, with the appropriate sensing positions and physiological relevance.

Therefore, in this section, the main physical sensing platforms, strain/pressure, temperature and humidity, will be categorized, together with sweat sensing, a non-physical approach. Furthermore, the operating principles, most common materials used, challenges and applications of these technologies will also be discussed.

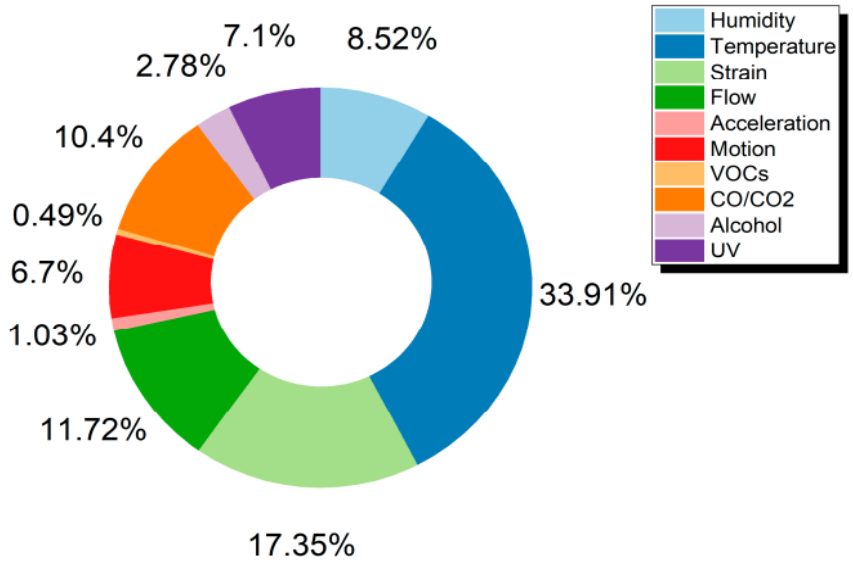

Fig. 9. Percentage of most employed sensors, of 4462 publications, ranged from 2013 to 2020. (Adapted from [35])

Table 1. General summary of physical and non-physical sensing parameters and positions [33,34,35,37,41].

Sensing parameters	Sensing positions	Physiological relevance
Strain	Hands; Fingers; Limbs; Face; Thorax; Wrists; Throat	Body motion; Phonation; Face expression; Finger flexibility; Hand gesture; Respiration; Pulse monitoring.
Pressure	Hands; Feet; Wrists; Neck; Throat; Hips; Legs;	Tactile sensing; Hepatic sensing; Diabetic foot; Gait analysis; Pulse monitoring; Pressure ulcers; Pressure control.
Temperature	Skin	Body temperature; Blood flow; Hydration
Humidity	Nose; Mouth; Skin;	Respiration; Dehydration; Breathing patterns; Respiratory conditions diagnosis
Sweat	Skin	Physicochemical health monitoring; Dehydration; Cystic fibrosis diagnosis; Diabetes and kidney conditions monitoring;

Temperature sensors

Body temperature is an elementary yet vital parameter to monitor, since it allows an insight into a person's physical condition, metabolism, and vital activity, since irregular variations of this parameter are indicators of specific diseases that may cause intense fevers or hypothermia. Because of this, a viable, portable, continuous, and precise measurement device is convenient, with real time high sensitivity, high resolution, high precision, and accuracy [37, 38].

Flexible temperature sensors allow for these measurements at the skin level, acting like a thermometer, where changes in electrical resistance reflect the body's temperature and its variations, after thorough calibration. Apart from measuring temperature, these devices can be employed to determine blood flow and hydration. With a good performing sensor, we could timely prevent diseases, make screenings and diagnoses, globally revolutionizing conventional medical treatments. To make that possible, a constant monitoring of temperature and its regulation must be done by the sensor, in order to prevent abnormal physiological conditions, including infections that lead to hyperthermia [33,34,38]. On the other hand, wearable temperature sensors attached to the patient's skin must be biocompatible and adaptable to variable skin environments, especially regarding contact with sweat, enabling satisfactory long-term usage. Presently, these sensors use a wide variety of materials, such as CNTs, nickel, silver, copper nanoparticles and nanowires, graphene, along with conductive polymers as the thermal-sensing elements [37].

The great majority of these devices have integrated in its circuits resistance temperature detectors (RTD) or thermistors, with either positive temperature coefficients (PTC) or negative temperature coefficients (NTC), with the main difference between the two being that the first has a faster response to temperature variations and endures higher values, but exhibits a smaller sensing range, while the latter works best when a specific temperature, usually within 50ºC of ambient, needs to be maintained [35]. Thermistor behaviour is represented in Figure 10.

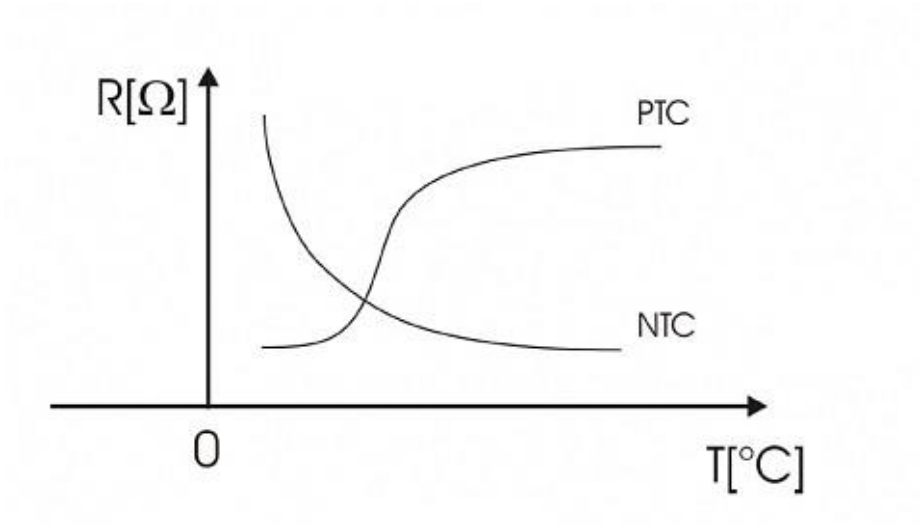

Fig. 10. Graphic representation of the behaviour of PTC and NTC thermistors. (Adapted from cobocards.com)

Focusing on wearable applications, flexible substrates are the optimum choice for mounting the sensor onto the human skin, in which the sensing element is functionalized. Capitalizing on the substrate's flexibility, the temperature detection is usually performed on the rear-facing side of the sensor, as close to the skin as possible [35]. Figure 11 exemplifies the general setup of a temperature sensor being developed today. According to Barmpakos and Kaltsas [35], composites containing poly(3,4-ethylenedioxythiophene) polystyrene sulfonate

(PEDOT:PSS) and CNTs or graphene are temperature sensitive organic materials used for the development of temperature sensors, with the added option of being printable. The introduction of graphene as a temperature sensing material is due to its excellent in-plane thermal conductivity. Furthermore, Ismail *et al.* [33] asserted that polymer/graphene composites are mechanically robust, not easily cracked or scratched with use and highly sensitive towards temperature, when graphene coatings are used. Apart from these materials, silver-based temperature sensors are also popular, due to the fact that silver is compatible with a wide array of substrates. Additionally, Kapton™, a commercial PI film, is a good candidate for Ag-based sensors, with its properties already well-known and proven [35].

However, some challenges still arise in the development of temperature sensors. Ismail *et al.* [33] reported that the majority of temperature sensors work well in the range between 10ºC and 80 ºC, with lack of reports of temperature sensing above 120ºC being caused by limitations in the substrate's thermal properties, since PET, PU, and even cellulose are also widely used. Additionally, the effects mechanical stimuli have on the sensor's performance need to be further researched, since the resistance of a flexible temperature sensor may be impacted by human-induced strain and stress, decreasing their reliability [39]. While they must be precise and reliable, skin-like conformability and stretchability are significant features that cannot be ignored, where conformity to curved and irregular surfaces should always be achieved [39]. The solution conceived for this is the usage of highly deformable thermoplastic and elastomer polymers, such as PET, PDMS, Ecoflex™, and PU. Furthermore, structural arrangements can improve the degree of stretchability, including serpentine designs, net-shaped, fractal, and noncoplanar designs, preventing the influence of body motions on the performance of the sensor, while improving sensitivity under fixed strains. Also, the reliability of the sensor can be monitored subjecting it to cycles of temperature changes and searching for variations in the resulting resistance/current peaks [33, 39].

Other challenges include achieving humidity stability, due to wearable sensors being inevitably subjected to ambient humidity, resistance to washing, where it is important to prevent the degradation of the sensor after several washing cycles, and breathability, where porous, low thickness and good substrate elongation must be achieved for the sensor to be breathable when applied [39].

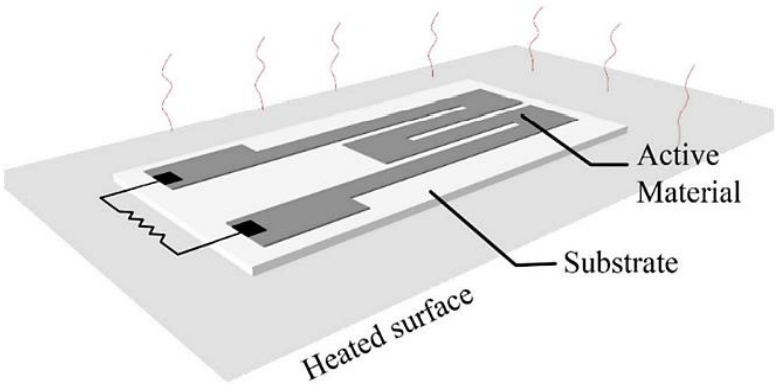

Fig. 11. Typical setup for a flexible temperature sensor. (Adapted from [35])

Humidity sensors

Humidity is another physical parameter considered indispensable for the survival of life on the planet. Despite the humidity requirements often varying over different environments, there is always a suitable humidity range required for the promotion of survival and development. This is also true with humans, where too high or too low humidity may impact negatively our comfort, industry or agricultural production [40].

Humidity is defined as the physical quantity of water vapor in the atmosphere, being normally expressed as absolute humidity, relative humidity or dew point, with the second being the most used in industrial and environmental applications, as the standard for expressing humidity values. Relative humidity refers to the ratio of current absolute humidity to the highest possible absolute humidity or, in other words, the difference of relative percentage between water and air concentration, at a determined temperature, commonly expressed as % RH [40]. When attached to the human body, it is possible to measure and observe the skin dryness, sweating and breathing rate [33].

This sensor works by absorbing and diffusing water molecules from either the substrate, negatively impacting performance, or active films, inducing changes in the electrical properties of the sensing layer [35]. This is useful when monitoring the nature of objects in tactile medical devices or observing the composition of the air exhaled through the nose, that contain more moisture that when inhaled, allowing for the analysis of breathing patterns and diagnosis of respiratory diseases, such as lung cancer, chronic obstructive pulmonary disease, and asthma [34,37]. Not only is the performance of humidity sensors important for the medical field, but also in industrial and agricultural production, meteorology, environmental protection, and food and fuel storage, where there's an ever-increasing need for more information regarding the impacts of this parameter on the cost, safety, comfort, and quality of human health [40].

Therefore, the ideal humidity sensor should be easy to manufacture, low cost, mass produced, reproducible, stable, highly sensitive, linear, exhibiting small temperature drift and hysteresis, along with fast response and recovery times [40]. For a sustainable development and

production, electronic biomaterials are attracting attention from the research field, where material selection is crucial for performance. Because of the high skin contact requirements and constant cycles of swelling and deswelling of the active materials, the choice of substrate and reinforcement are equally relevant, where biocompatibility with the human skin, without allergic reactions, and high sensitivity to water moisture are paramount, taking into account that humidity influences the conducting mechanisms of the materials [33,35].

In Barmpakos and Kaltsas [35], humidity composite sensors can employ silver and PEDOT: PSS with substrates made of PI, PET, polyester, paper, or even ceramics and glass, depending on the manufacturing approach taken, where the electrodes can be patterned and the sensing layer is printed on top. An array of possible setups is presented in Figure 12.

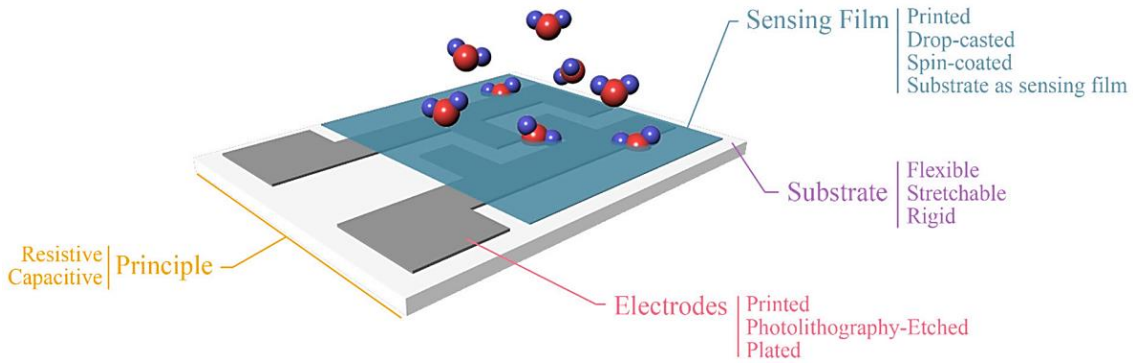

Fig. 12. Possible humidity sensor setups currently employed in the field. (Adapted from [35])

Regarding challenges, one is the difficulty to desorb previously captured water molecules, due to the nature of the active materials used, especially multi-walled carbon nanotubes (MWCNT), which offer high water absorption, high surface area to volume ratio, but lead to difficult desorption of water without external assistance [35]. To approach this difficulty, there's a need for planning and material combination selection that favour fast and repeatable absorption-desorption cycles, along with active materials that serve as heaters, which assist in humidity desorption [35]. Another challenge is manufacturing limitations due to temperature, such as paper, which cannot be heated above certain temperatures, prohibiting annealing approaches, for example. One way to circumvent this is utilizing drop-cast or spin coating methods for material deposition [35].

Also, according to Ma *et al.* [40], a great number of works have been developed for measuring techniques over wide relative humidity ranges (10-90% RH), due to generally low accuracy requirements. However, detection at low humidity (<10% RH) and high humidity (>90% RH) ranges is still demanding, especially at low humidity conditions. This happens due to limitations that also plague conventional humidity sensors, where the sensitive layer cannot absorb a great deal of water molecules, making the detection of changes in the electrical signal

very difficult, to the point where the sensor's minimum detection threshold of the device is not reached by the water vapor concentration in the air [40].

In conclusion, low-cost humidity sensors, with reliability and accuracy in high and low humidity environments are in high demand today in multiple sectors of the industry, in order to improve productivity and safety. These include semiconductor manufacturing, petrochemical processing, atmospheric research, aerospace technology, food packaging, seed storage, lithium-ion batteries, air filters and purifier manufacturing [40].

Strain/pressure sensors

With the advancement of microelectronics, nanotechnology, and manufacturing methods, in recent times, we are witnessing never before seen miniaturization, high integration and multi-functionalization of wearable devices and electronics. This has led to demands involving the enhancement of strain sensors, with better operation and material flexibility, since they are the perfect candidates for human health monitoring in on-skin applications [41]. These stretchable, flexible sensors are the key to superior human motion monitoring, quantifying variations in electrical signals correspondent to physical deformations induced in the active material, useful tools to supervise joint movements of fingers, elbows, knees, and wrists, among other applications, discussed further below [41]. Allied to fast response times, high sensitivity, and good pressure/strain mapping, these sensors pose an interesting and promising prospect for research and future widespread use [41].

Tracking the user's habitual physical activity can provide handy information regarding gait and breathing patterns, posture, pulse, sound vibration, and hand movements, for example. If abnormalities in these parameters are detected, such as sudden tremors or/and atypical gait patterns, we could be observing precursors of diabetes or Parkinson's and Alzheimer's disease, allowing for an early diagnosis and treatment [37, 41]. Having this in mind, flexible strain sensors opened applications in all kinds of fields, including human-machine interfaces, rehabilitation enhancement, smart prosthetics, and sports training [37]. Along these lines, with the explosive growth of smartphones, IoT, and wearable technology, other fields can also benefit from these devices, including the automotive industry, minimally invasive surgeries, and robotics, where exoskeletons could acquire sensing capabilities and execute even more complex tasks [35, 41].

One thing to consider is that depending on the installation and application, this type of sensor can also detect changes in pressure, bending, and touch, where the same sensor could both sense pressure and strain, whenever deformation is applied to it [35]. Figure 13 illustrates the mechanical forces usually applied on these sensors, in order to observe the behaviour under tensile and compressive stress.

According to Gong *et al.* [41], many studies have been conducted on highly sensitive and even multifunctional sensors, able to simultaneously detect stretching, pressure or touch. Since most commercial metal strain sensors limit the detection of human motion, researchers have turned their eyes to flexible sensors with high performance and stretchable characteristics. Worn on the skin, the sensor must be conformal enough to capture the entire range of the skin's strain, in various positions throughout the body, in order to perfectly reflect the physiological condition [34]. Thus, most studies conducted employed materials such as metal nanomaterials, graphene and GO, CNTs, and carbon black (CB) [41].

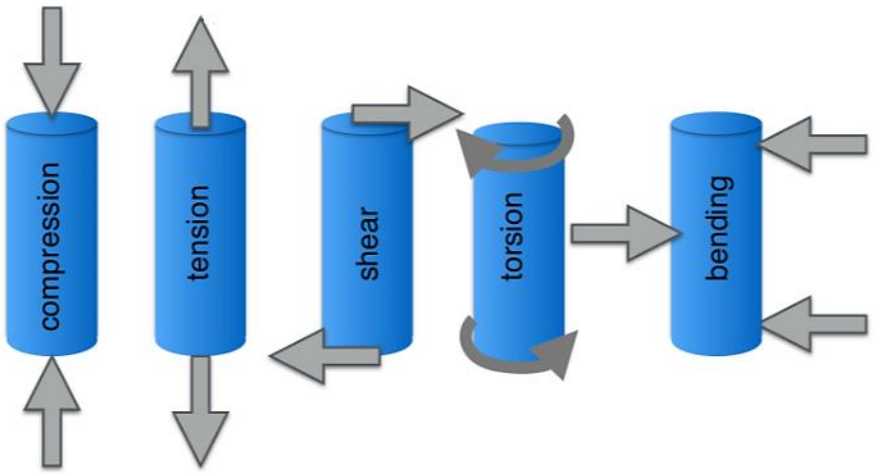

Fig. 13. Different types of mechanical deformation that can be induced on a sample. (Withdrawn from linearmotiontips.com)

Regarding motion monitoring, we are faced with two categories: large-scale movements, where finger, hand, and knee bending are included, and small-scale movements, including subtle throat and chest activity during deglutition and breathing [37]. In Wang *et al.* [37], it is affirmed that if sufficient reliability and validity is reached, activity monitoring has broad prospects in many clinical environments, not only regarding limb-related complications, such as stroke and amputation rehabilitation, but also enhanced postoperative recovery of heart and lung diseases and continuous counselling of diabetic or chemotherapy patients [37]. However, to achieve this, pressure sensors must accomplish great sensitivity ultra-low detection thresholds, fast response/recovery times, along with wide pressure range [42].

Several other applications, apart from the above-mentioned ones, include identifying abnormal strain level of fingers, due to hand related disorders or unsatisfying rehabilitation from it, sport-related monitoring of elbow and knee's joint movement, capturing shifts in strain induced by emotional expressions on the face, which could help paralyzed patients better

interface with auxiliary apparatuses, breathing pattern and physiological process examination, through minute changes in the volume of body parts, and smart gloves and prosthetics, where the softness or roughness of objects can be deduced and perceived by the user when touched, benefitting prosthetic's learning time and rehabilitation by amputees [34,42]. Additionally, pressure could also be monitored around other areas, to manage pressure sores, helping patients confined to beds and wheelchairs, along with evaluations of vocal cord disorders, by attaching pressure and strain sensors on the skin that covers the throat and evaluating the ensuing vibrations [34]. On the other hand, human-machine interfaces could be improved to better suit the interaction with robots, where due to its properties, flexible pressure sensors are the most promising candidates, enabling users to better obtain the output signals throughout the operation of these machines, either in their smartphone or dedicated consoles [42]. Figure 14 shows the mechanical robustness of a pressure sensor that can be worn on the throat.

Despite all the attraction and research conducted in this area, we are still facing significant challenges meeting the requirements of some applications, mostly due to critical parameters like response time, sensitivity, detection thresholds, and stability [42]. In practice, this can be adjusted and even solved through the selection of active and passive materials, fabrication methods and better assembly of the system and consequent gauge factor (GF), defined as the ratio of relative change in electrical resistance to mechanical strain, achieved. GF is expressed as Equation (1) below [33]:

$$GF=\frac{\Delta R/R0}{\varepsilon} \quad (1)$$

Where ΔR is the variation in electrical resistance, R_o is the initial electrical resistance and ε is the induced mechanical strain [33].

Along these lines, graphene-based strain sensors have risen due to their favourable sensing properties, such as high sensitivity, low detection thresholds, low response time, and durability to long-cycles of use. This allows this kind of sensor to detect all kinds of physiological motions, including vocal cords induced vibrations [41]. Since these parameters, together with GF, are considered to be major criteria for flexible strain sensors, graphene-based sensing manages to associate both, with, according to Ismail *et al.* [33], stretchability of at least 100% and GF in the 5-100+ range.

However, skin-like pressure sensors face other difficulties, in the shape of airtight membranes without gas permeability, that induce skin inflammation and allergies after prolonged use. To solve this, breathable layers, with sensing capabilities, are crucial for this type of electronics [41].

Fig. 14. Mechanical robustness of a throat-worn pressure sensor being evaluated. (Adapted from [33])

Sweat monitoring sensors

With the above-mentioned development of microelectronics and IoT, people are exploring new options in regards to devices related to health status monitoring and exercise in daily life. Despite blood tests being already effective at showing most of the information needed to make an assessment about our health, this procedure is moderately invasive and may cause discomfort to the subject. On the opposite side, sweat is rich in chemical information, which contains biomarkers that reflect the biomolecular state and fitness level of the individual [37,41]. During perspiration, between 500 and 700 mL of hypotonic fluid is secreted by the sweat glands of the average adult human, per day, under most climate conditions. This is the main manner our bodies thermoregulate, and during this process a whole myriad of biomolecules, hormones, proteins, amino acids, peptides, ions, and metabolites are excreted, mainly consisting of lactate, glucose, uric acid, ascorbic acid and cortisol. Depending on the concentrations of these elements, researchers can draw conclusions regarding the biomolecular state of the body, including continuous physical health monitoring, through metabolite concentration, such as lactate, or looking into the pH values and concentration of Na^+, K^+ and Cl^- ions, which are very similar to the blood and can reflect its health [36,37,41].

This straightforward access is what makes sweat an especially useful biofluid, since it can be retrieved via non-invasive methods, contrary to blood, while providing information related to diet, drug use, health condition and dehydration [37,41]. For example, normally, increases in chloride ion concentration mean dehydration, while abnormal levels of it could indicate cystic fibrosis or other genetic conditions [36,37,41]. On the other hand, abnormal losses in sodium ion levels are monitored to detect diseases associated with cystic fibrosis. Additionally, researchers can establish correlations between the glucose-level in sweat and blood, which could further benefit diabetes monitoring and diagnosis, while levels of lactate can

be monitored to detect Ischemia [36,37]. Furthermore, high urea levels in the sweat are linked to impending kidney failure, a condition also visible through white crusts on the patient's skin. However, both lactate and urea still lack the necessary blood-sweat correlation for accurate diagnoses [36,37].

The analysis of sweat has been mostly achieved by methods of electrochemical sensing using biosensors, with real-time data monitoring of multiple analytes in the same sample. However, since we are focusing on flexible sensor applications, it also needs to respond, conform, and respond quickly enough to adapt to the skin's deformation, while advancements in sweat collection methods are crucial for the overall progress of sweat sensing, especially in the case of commercial applications [36,37,41]. Nowadays, these biosensors are commonly employed in PoC, helping the diagnosis of diseases in a less invasive manner than conventional methods.

Therefore, a good analytical performance in the fields of healthcare and fitness is dependent on the sensor's composition, layer configuration, and wearable nature. Regarding materials, according to Gong *et al.* [41], CB has some valuable advantages over other options, including distinguished electrochemical properties, easy preparation of stable dispersants, and relatively simple fabrication. On the other hand, not only biosensors are employed in sweat sensors, but also nanostructured metal oxides, which have a prominent role in electrochemical sensing, where printing or functionalization of these materials on flexible substrates could lead to engaging new prospects for monitoring via sensors [41].

However, despite sweat offering large amounts of physiological information for disease detection, many obstacles still lie in the way for proper wearable use of this technology. These include poor sweat collection methods, the absence of simultaneous multiple analyte monitoring, and separate collection and analysis stages. Allied to this, as mentioned above, there is still a lack of correlation between sweat and blood for many of the former's elements, with ethanol being the only confirmed analyte in recurrent *vivo* validation tests. Furthermore, despite measured analytes being well-documented, with steroid hormones and drugs exhibiting strong correlations with blood, the clinical significance of some is still unproven. This issue occurs due to the very complex composition of this biofluid, where detecting multiple biomarkers with a single wearable device poses a great challenge to accurate real-time signal processing. To overcome this problem, more research has to be done towards blood-sweat concentration correlation in *vivo* trials, for a better understanding of biomarker pathways, before the full potential of wearable sweat sensing is unlocked [36,37,44].

Other major challenge involved in this field is the lack of appropriate active materials with acceptable mechanical properties. Since conventional electrochemical sensors are rigid, heavy, and dependent on bulky electronic support systems, which are incompatible with wearable applications, researchers turned to softer, more flexible and miniaturized devices, that in theory could achieve better conformation with the epidermis and resist cyclic multiaxial mechanical deformations. However, proper flexibility, stretchability, and transparency, essential characteristics of wearable chemical sensors, are still difficult to attain [37].

Lastly, having in mind that the majority of the perspiration is originated from the eccrine sweat glands, and that sweat is carried to the skin's surface by dermal ducts, helps concluding that the required ultra-sensitivity and selectivity might be compromised for some analytes, due to the sheer number of cellular barriers that need to be overtaken, even with thorough sweat collection systems. This is particularly true for larger biomarkers, where the level of filtration by tighter junctions is increased, leading to their higher dilution. The most outstanding example of this is glucose, which is transported through paracellular pathways and is roughly 100 times more diluted than the glucose found in blood plasma or interstitial fluid, providing an even greater challenge for wearable sensing [36]. A representation of this process is presented in Figure 15.

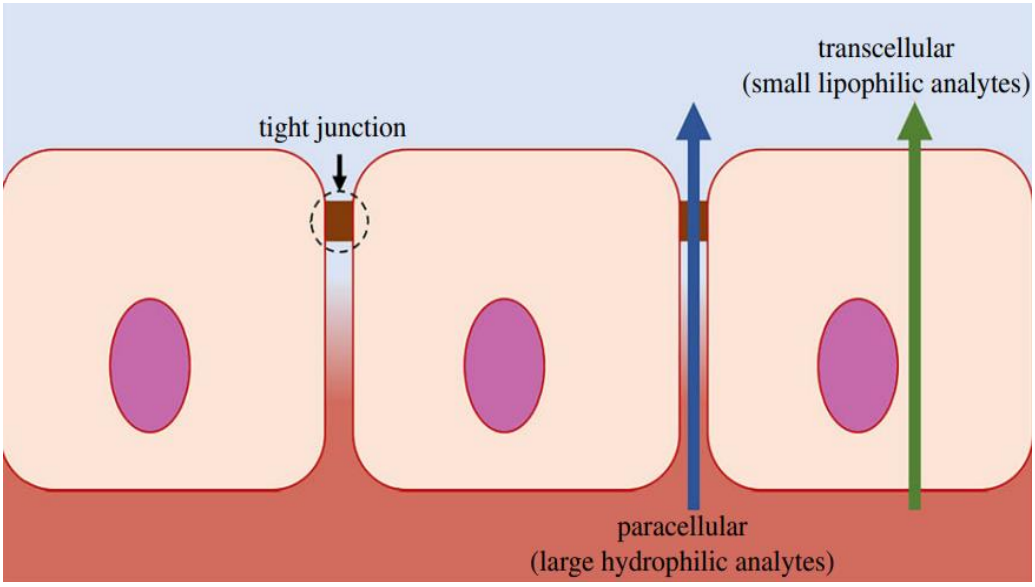

Fig. 15. Representation of analyte pathways from interstitial fluid and blood to sweat through lipophilic cell membranes. (Adapted from [36])

Thus, to combat this, for proper collection of physiological data, sensors must be in close contact with the skin, allowing *in situ* sweat collection and analysis, while enduring dynamic cycles of deformation by non-planar skin and remaining wearable, followed by signal processing. This can be done either by a component integrated in the circuit or by a computer or smart device, after wireless transmission via Bluetooth and NFC, less expensive but still compatible, or other network protocols, such as Wi-Fi or ZigBee, more complex but also hardware-demanding [36,37].

Multiplexed sensors

In the sensor field, multiplexing can be defined as the practice of detecting and measuring multiple parameters simultaneously, where sensor systems, inspired by the features

of the human skin, acquire ample information regarding the environment the user is contacting with, thanks to the assistance of various sensing modules, including pressure/strain, temperature, humidity, and sweat sensors, all discussed above. This is the case because focusing on a single parameter is normally insufficient information for early clinical diagnoses and accurate disease tracking, since some diseases can only be identified via multiple criteria monitoring, where parameters fluctuate differently depending on the stage the condition is in, or behave in a distinctive way, in the case of tumours, allowing the correct identification of benign and cancerous cases [43].

Multiplexed technology work by analysing the electrical output differences in physicochemical signals, generated by the variation of specific biomarkers and analytes, being better suited for PoC applications, personal health monitoring and on-site diagnosis [43]. By having this approach, powerful tools are granted for healthcare treatments, which focus on both chemical contents and physical properties of patients, such as forecasting dehydration during exercise by concurrently measuring the variation of the pH level in the skin's surface and its temperature [43,44]. Not only this, but many other parameters can be obtained with a single device, including heart rate, oxygen saturation, respiratory rhythm, among others [44]. Figure 16 shows a schematic representation of a ion-sensitive field-effect transistor (ISFET) with pH and temperature sensing capabilities.

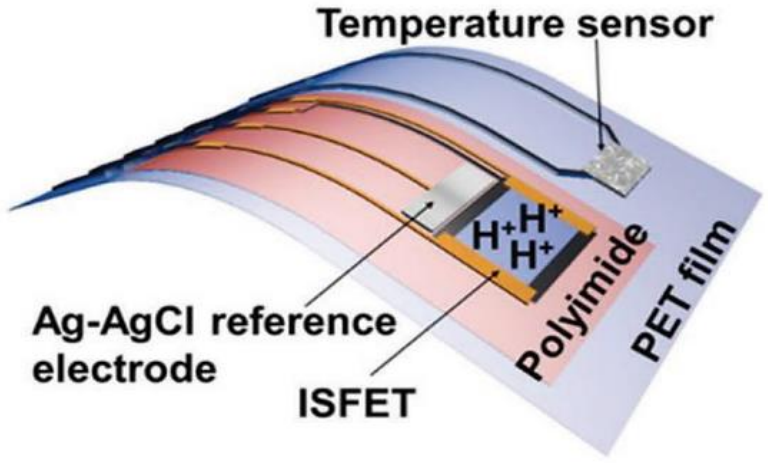

Fig. 16. Multiplexed sensor schematic, with flexible temperature and pH sensing capabilities. ISFET means ion-sensitive field-effect transistor. (Adapted from [44])

In recent years, efforts have been dedicated to new materials, electronic configurations, and fabrication approaches, contributing to better integrated multiplexed sensors and versatile human-machine interfaces by mimicking skin-like functions, such as tactile, temperature or humidity sensing, while being able to distinguish between stimuli, amid the complex environment that is the human body [44]. Thus, another application that has risen recently is building devices that support prosthetic operation, allowing users to perceive touch and object

morphology, while capturing physicochemical signals produced and secreted by the organism, evaluating the health condition [44].

However, in spite of these advancements, a big demand for more advanced and practical medical solutions still exist, with special focus on better diagnosis and treatment in locations with less resources, factors that turn multiplexed sensors into obvious candidates for this kind of approaches. Additionally, diagnoses should provide as much information as possible, from the smallest sample available [43]. With sweat, for example, sensors can obtain information regarding glucose, potassium, metal ions and calcium concentration, along with pH values and taking into account the influence of skin temperature variation [44].

Regarding challenges, after many attempts, one of the most inconvenient concerns is the cross-coupling effect originated from the simultaneous generation of multiple signals, by the active layers functionalized in the sensor. Apart from this, the outputs of these flexible sensors tend to always be influenced by other physiological information captured. Unfortunately, according to Xu *et al.* [44], alternative approaches, such as the transduction of multiple stimuli into a single signal, are plagued with interferences and artifacts. Thus, these reasons, allied with complex fabrication procedures and other requirements, today limit the integration of more than three sensors into a chip, in order to retain high mechanical flexibility, signal selectivity and wearing comfort [30,44]. Another challenge is the limited number of repeated uses, which results in a less than adequate service life and long-term high costs. This can be addressed by developing a sensor with one expensive layer with components that can be used for long periods of time, paired with cost-effective layers that are fabricated for disposable use [44]. Lastly, the integration of more active layers, signal processing capabilities, and power supply components lead to thicker films, due to the manner fabrication works, where ease of manufacturing is preferred. However, low thickness is favoured, since skin temperature measurements need to be as accurate as possible. Taking this into account, more research needs to be put into developing ultrathin films, with thickness of a few micrometres, if it is desirable to keep moving in the direction of more reliable sensing and wearability, according to Xu *et al.* [44].

In conclusion, the biggest challenge that needs to be overcome is achieving multiple signal measurement without cross-coupling effects, through innovations regarding the configuration of multiple active layers or creating others able to capture multiple parameters at the same time [44]. After tackling this issue, without a doubt, multiplexed sensors could be employed and improved for electronic skin applications, aiding the growth of various fields, including humanoid robotics, smart prosthetics, and a new generation of health monitoring technology [44].

2.2.4. Sensor operation

Having looked into the most popular sensors in the field of flexible sensors, the functionality of these devices should now be considered, where the aim should be integrating

sensing platforms into the human skin, for physical and chemical target monitoring. These targets can be physical forces, such as strain, pressure, shear, torque and vibration, physical chemistry parameters, including temperature and humidity, or biochemistry parameters, where glucose, lactate, sodium, chlorine, and potassium are included. If we combine the readings from these individual targets, we can accurately obtain relevant physiological information about our bodies, which facilitates the detection of anomalies in the body and around the environment. Figure 17 shows the demands and sheer potential of wearable sensors for the human body [34].

Among these devices, the most popular working principles are based on the change of resistance, where physical stimuli create shifts in the sensor's resistance and conductance. These are usually employed to measure strain, pressure, humidity, and temperature of the human body. However, besides this approach, many other sensors operate based on the variation of its capacitance or by piezoelectric and triboelectric mechanisms. While resistive and capacitive sensors require external power sources to function, the last two can generate their own power, due to the manner their mechanisms are organized [34].

Therefore, in this section, various working principles for temperature, humidity, strain, and sweat sensors will be thoroughly discussed, where the parameters they capture are taken into account and the most popular mechanisms for each one are analysed.

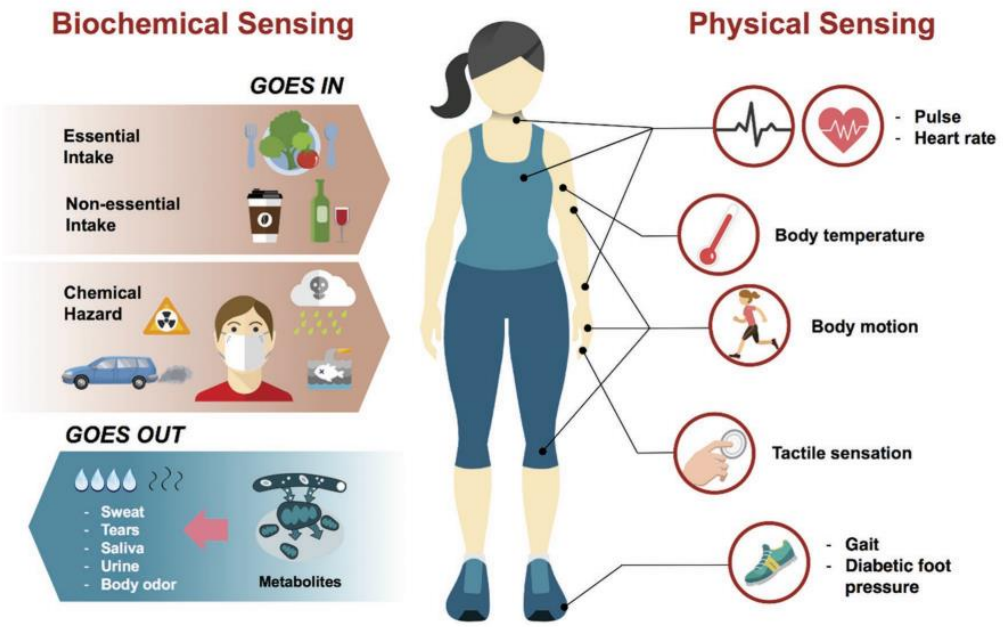

Fig. 17. A schematic illustrating the demands of a wearable sensor physiological signal monitoring. (Adapted from [34])

Temperature sensors

Beginning with temperature sensors, these usually exploit the active material's thermal properties, especially its thermal coefficient of resistance (TCR). In the research field, many works employ screen-printed silver, PEDOT: PSS, pristine or combined with graphene or CNT, platinum, gold, and other materials that exhibit either positive or negative TCR. For flexible

sensor applications, this type of sensors can provide piezoresistive and pyroelectric, piezoelectric and capacitive outputs, while being functionalized with an elastomer, such as PDMS, due to the high demand of temperature detection in sensorial systems, which make the use of flexible sensors almost mandatory [35,46]. Figure 18 shows an example of a flexible temperature sensor.

These mechanisms are decisive for the measurement of many phenomena, since volumetric expansion, vapor pressure, and most biological processes are temperature dependent. Thus, physical stimuli associated with temperature are the aim of the development of these devices. The output, i.e. temperature value, is obtained by measurement models based on the measurement principles of RTD, thermocouples and thermistors [40].

Beginning with the resistive working principle, the most basic configuration of a wearable temperature sensor can be achieved with a mesh-shaped metal circuit whose resistance changes with the variation of temperature [34]. Monitoring temperature by observing changes in the resistance of the active materials is the most popular method for on-skin devices. Therefore, the TCR is a valuable indicator of the sensor's sensitivity, being defined as the relative variation of resistance when temperature changes by 1ºC. This is a critical parameter for RTD applications, defined by Equation (2) [40]:

$$TCR = \frac{1}{R(T_0)} \frac{R(T) - R(T_0)}{T - T_0} \quad (2)$$

where R(T) is the resistance at temperature T, $R(T_o)$ is the initial resistance measured at the initial temperature T_o, with higher TCR values implying higher precision. For human body applications, the sensing materials should have high TCR on an interval between room temperature and 42ºC [40].

Regarding materials, according to Gu *et al.* [46], this type of sensor can use pure metal elements, such as platinum, gold, and copper, metal oxide particles, CNT polymer composites, and graphene as sensitive materials. The good thermal and non-oxidation properties of platinum, despite its low TCR, make it a preferable option, while nickel is chosen due to its TCR value, low cost and high endurance [40]. On the other hand, to achieve high sensitivity, metals are the preferred option, due to rises in temperature enhancing the thermal vibration of the structure, scattering the electron wave and increasing the resistivity. However, metal-based temperature sensors provide very limited stretchability and flexibility, where the maximum values of the former are located between 25-30%, according to Kuzubasoglu and Bahadir [46]. Therefore, the usage of inherently stretchable materials is needed to overcome the tensile limits of current technology.

Considering the mechanisms surrounding TCR, RTD use the material's electrical resistance dependence on temperature to determine it, where temperature increments cause a rise in resistance, due to higher electron vibrations preventing their free flow in the conductive

material. A higher degree of accuracy, linearity and quicker responses make RTD more preferable than other options, such as thermocouples [40]. Similarly to all sensors, focusing the RTD design to specific applications is not an easy task, since several aspects, including material selection, size, chosen configuration, precision, durability, and temperature coefficients need to be considered in order to achieve the required performance. Along these lines, the final design can also be affected by issues such as cost, oxidation resistance and manufacturing requirements [40].

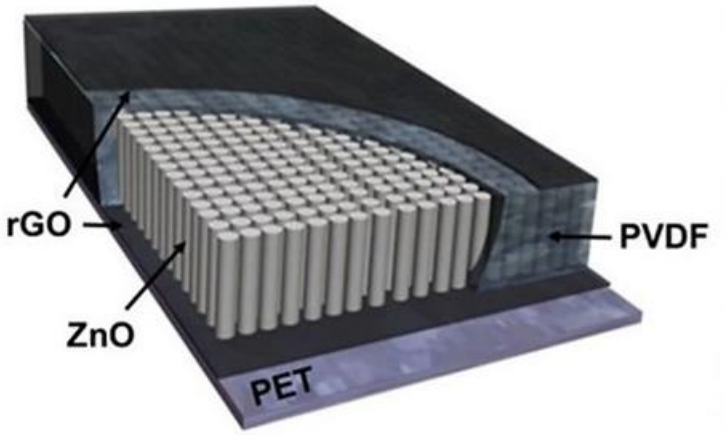

Fig. 18. Schematic diagram of a flexible temperature sensor, based on a zinc oxide (ZnO)/ polyvinylidene fluoride (PVDF) composite film and rGO electrodes. (Adapted from [47])

Carrying on to pyroelectric temperature sensors, the operation depends on the variation of temperature that induces polarization shifts of the pyroelectrical materials, generating opposite bound charges on the surface of the crystal. Despite many pyroelectric devices witnessing widespread use in fire alarms and missile detection, among other fields, these are fabricated on rigid substrates and, thus, flexible options need to be explored, especially poly(vinylidene fluoride-*co*-trifluoroethylene) (P(VDF-TrFE)), ideal for this kind of sensing applications [46]. In Gu *et al.* [46], it is said that the remnant polarization in the interior of this material changes with temperature, leading to a shift in the density accumulated by the holes located at the interface between the semiconductor channel and the material. Thus, when temperature rises, the source-drain current does the same. Allied to this, the linear response of the device over a favourable temperature range and its simple fabrication display the potential of this mechanism in flexible temperature sensors [46].

Regarding the response and recovery time of this type of sensor, there is no issue with the response time being a few milliseconds, but a problem rises when the recovery time is too long. Shortening the time difference between response and recovery time is the key to higher efficiency and capability. Furthermore, avoiding the interference of multiple signals so that individual stimuli can be accurately studied has become an urgent issue in the field, since these

challenges need to be overcome in order to achieve the flexible temperature sensors of the future [47].

Moving on to thermocouples, this type of sensor consists of two different thermoelements, either semiconductors, conductors, or a combination of both, allowing for the generation of voltage by the thermoelectric phenomenon, also known as Seebeck [40]. According to this effect, if heat is applied to one conductor end, an electromotive force occurs between the end points, causing the electrons to move from the hot end to the cold one. Despite having cost-effective, self-powered properties and stable reference temperature, they are less stable than RTD, nonlinear, with difficult recalibration, limiting their use as wearable sensors [40].

On the other hand, thermistors are ideal for detecting small temperature changes, being manufactured with materials that significantly change their electrical resistance with temperature variation. These devices are thermally sensitive resistors that can have NTC or PTC behaviours, with semiconductor-based thermistors exhibiting NTC, contrarily to thermocouples based on the Seebeck effect [40]. Most thermistors are manufactured in disc, rod, or bead shape, being the latter the smallest in size, with a diameter between 0.15 and 1.25 mm, with glass or plastic encapsulations. The circuit thermistors used to measure temperature must retain their accuracy throughout their expected lifetime, depending on the thermistor's resistance tolerance, as well as reference accuracy [40].

Humidity sensors

For low-complexity devices that employ humidity sensors, a general approach in the design is the deposition of a single active material on the substrate, followed by the exploitation of both materials' physical properties for better sensing capabilities. On the other hand, another approach, usually chosen in traditional sensors, is functionalizing conductive electrodes on a substrate, measuring the response of the active layer/material, usually deposited onto the electrodes [35]. Figure 19 illustrates the inner workings of a capacitance humidity sensor.

The working principle of humidity sensing is simple and intuitive, where higher water content, measured in relative humidity, equates to higher conductance. Taking this into account, researchers can monitor, for example, the breathing patterns of a patient during physical exercise of variable intensity, since breathing in and out correlates with decreasing and increasing conductivity, respectively [34].

However, when faced with low relative humidity environments or harsh environments with chemical hazards, the sensing capabilities are restrained, caused by poor sensitivity, slow response time, hysteresis, non-linearity, and instrument failure, among others. Thus, a great demand for more reliable measurement methods is being witnessed, with better sensitivity and accurate detection in more severe conditions [41]. Nonetheless, there is no single method that can meet all requirements, with all of them having certain advantages and limitations in terms

of the before-mentioned properties [41]. Hence, in this section, a discussion regarding the operation of capacitive and resistive humidity sensors will take place, with a discussion of their potential prospects in terms of portability, flexibility, and mass production cost [41].

Beginning with capacitive humidity sensors, these are one of the first choices for humidity detection, thanks to its easy fabrication, low power consumption, high sensitivity, quasi-linear response, and compatibility with modern technology [41]. Therefore, despite capacitance mechanisms being considered more complex, regarding reliable measurement and acquisition of data, its notable performance compensates for the drawbacks [35].

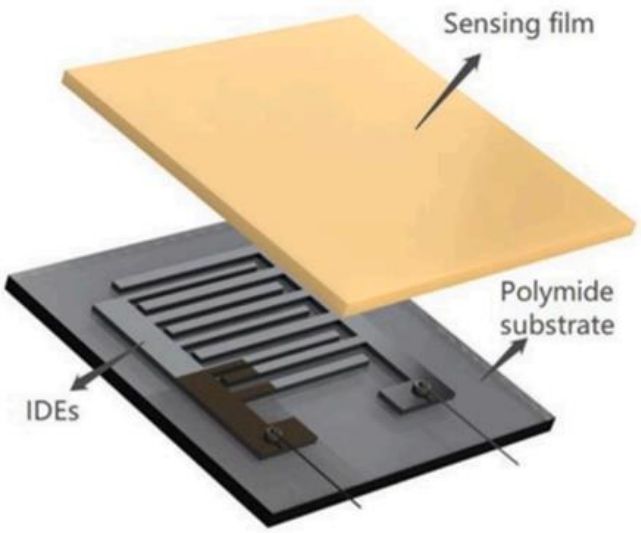

Fig. 19. Illustration of capacitance humidity sensor, made of a PI substrate, active layer, and an interdigitated electrode (IDE). (Adapted from [40])

This kind of humidity sensors uses capacitance changes in the signal frequency and effective dielectric constant of ceramic or polymer dielectrics caused by losses or presence of moisture, respectively. Its operation is made possible by the deposition of electrodes patterned onto a substrate of variable thickness. Depending on the thickness of the film, sensors can be divided into thin film-type and thick-film type. Thin films allow for smaller sizes and more sensitivity, while thicker films have more durability, cost-effectiveness, and reliable interfacing with other electronic circuits [41]. Regarding electrodes, these can also be divided into two categories, interdigital electrodes (IDE) and parallel plates. While, according to Ma *et al.* [41], the majority of humidity sensors reported in the literature employ IDE structures, parallel plate electrodes, with equal device size, could obtain higher sensitivity, due to a larger sensing area [41]. This structure consists of two metal electrodes and a porous dielectric layer between them, where the thin, porous, dielectric layer is the most important element for humidity detection. Thus, the shape and size of the electrodes and the thickness and quality of the films arbitrate the final performance of the parallel electrode and, consequently, of the capacitive sensor [41]. Figure 20 shows a capacitive humidity sensor employing a parallel plate electrode structure.

Despite this, the fabrication of the ideal commercial thin film, parallel plate, sensor is a difficult process, due to potential short circuits causing the entire sensor to fail [41].

Taking what was mentioned above into account, researchers employ a myriad of sensing materials, such as porous alumina and silicon, zeolites, metal-organic frameworks, polyimides, polyvinyl alcohol, among others, with the research on porous alumina being very prevalent nowadays [41]. However, with developments in materials science and microelectronics, polymers are also growing in interest. Polyimide, despite its poor sensitivity at lower relative humidity, is a popular choice when it comes to tailoring a flexible substrate for standard acquisition and processing techniques.

Fig. 20. Capacitive flexible humidity sensor with a parallel plate electrode mechanism. (Adapted from [41])

On the other hand, polyvinyl alcohol (PVA) adheres well to PI, since the latter accepts PVA quickly and easily. Therefore, PVA can be employed as the sensing material of the humidity sensor, as long as the water content in the polymers is less than 200 parts per million (ppm), to avoid the degradation of the polymer's properties by hydrolysis, according to Ma *et al.* [41].

Passing on to resistive humidity sensors, or sometimes called impedance humidity sensors, these resistive output sensors provide straightforward interface with measurement electronics, having the advantages of simple fabrication, high sensitivity, low cost, fast response times and easy integration into integrated systems. This type of sensor can either incorporate a set of electrodes and a sensing film deposited on top, or work with the substrate's intrinsic electrical behaviour to humidity variations for humidity detection [35,41]. Resistive humidity sensors operate by relying on the resistance change caused by the absorption of water molecules on the active layer, leading to ionic conduction, which generally functions well over the most of the relative humidity's range, even in low humidity situations, albeit with some limitations, due to trace moisture not being able to reach the required threshold of regular circuit designs [41].

To ensure adequate sensitivity, the high impedance created by low relative humidity needs to be reduced. Therefore, designing a humidity sensor with hydrophilicity and high conductance sensing materials is required for all applications, especially the above-mentioned

ones. Conductive polymers, such as polyaniline and polypyrrole, have been studied recently due to their inherent high electrical conductivity, since the addition of conductive polymers is an efficient way to enable accurate and reliable humidity measurements [41]. Additionally, these materials can be functionalized with other highly conductive materials, including carbon nanotubes, carbon black, and graphene. Regarding composite materials, the conduction mechanisms can be categorized as ionic conduction or electronic conduction, with impedance spectroscopy being an invaluable asset to analyse and understand their contributions to humidity sensing capabilities [41].

In conclusion, despite many works reporting the use of porous alumina as a way to improve sensitivity, other materials can be employed to reach the same performance. Similarly, compared with capacitive mechanisms, there is a huge opportunity for development of other, and even novel, sensing materials and technologies, since the arrival of nanometre-sized materials brought inevitable trends of development, going towards higher sensitivity, compactness and smaller size, favourable characteristics for the integration of novel sensing platforms with existing integrated circuits [41]. Furthermore, fully understanding how different low humidity mechanisms work and improving them is very important for the overall design of humidity sensors, considering that perceiving the aspects surrounding materials, structures and device principles, and their interactions, can revolutionize the way we see these devices [41].

Strain/pressure sensors

Force sensors are devices that can detect mechanical forces, such as stress, torque, stress, and pressure, followed by their conversion into electrical signals. Among these, pressure and strain sensors rise above the rest, due to their capabilities for physiological activity monitoring, for instance, of pulse and heart rate, breathing patterns, muscle movements, and blood pressure. Since traditional force sensors are generally heavy and bulky because of their mostly metal and semiconductor composition, they are not the best option for vital sign capturing via wearable electronics, due to severe portability and flexibility limitations [46]. Comparatively, flexible force sensors use plastic and elastomeric substrates, achieving a series of advantages, including better stretchability, transparency, wearability, biocompatibility, and more capable continuous detection [46].

To better understand the sensing devices and the capabilities they should have, the pressure below 100 kPa can be categorized into 4 categories. According to Bijender and Kumar [44], these could be: ultra-low pressure, at < 1 Pa, subtle pressure, at 1 Pa – 1 kPa, low pressure, at 1 kPa - 10 kPa, and medium pressure regime, at 10 kPa -100 kPa. The ultra-low-pressure regime rarely occurs in our daily lives, with sound pressure being an example of this kind of pressure. Pressure sensors play an important role in the development of microphones, hearing aids, and micromechanical systems (MEMS). The subtle pressure regime is the indicated for the development of highly sensitive sensorial systems and touch display devices of mobile phones. The low-pressure regime is a very notorious range for covering the human body's internal pressures, being widely used in human health monitoring and medical diagnostic systems [44].

Thus, understanding this categorization helps researchers develop the desired wearable devices, with the indicated characteristics for the application in mind [44]. In this section, the main transduction mechanisms, principles, and characteristics of pressure and strain sensors will be discussed, focusing on piezoresistive, capacitive, piezoelectric and triboelectric mechanisms. Figure 21 illustrates the first three mechanisms, while Figure 22 does the same for the triboelectric.

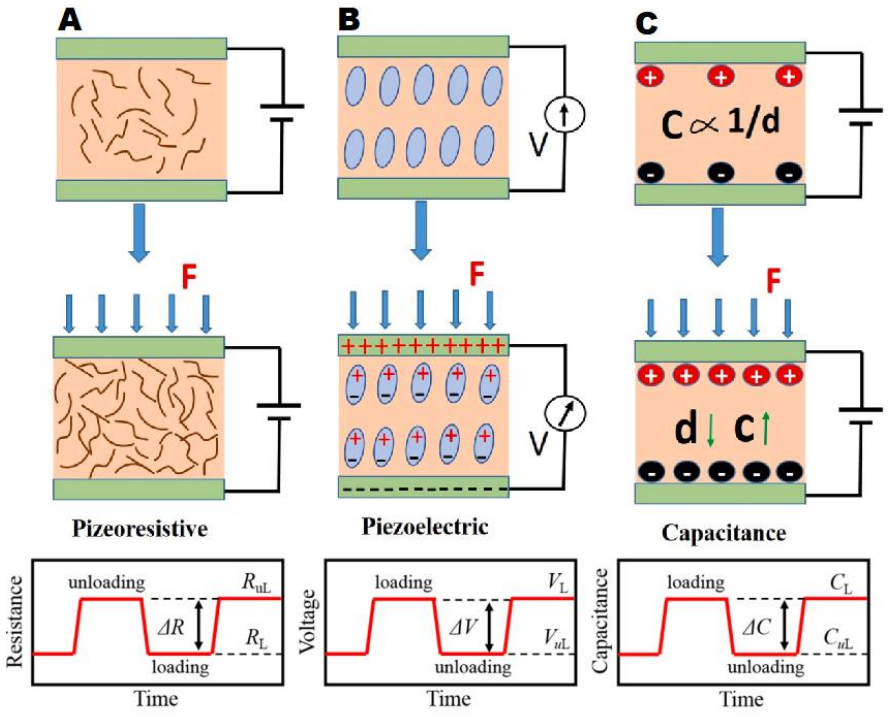

Fig. 21. Diagram of strain/pressure sensing mechanisms, with the correspondent resistance, voltage, and capacitance variation over time graphs: (A) piezoresisistive; (B) Piezoelectric; (C) Capacitance. (Adapted from [44,48])

Beginning with piezoresistive sensors, this mechanism is defined by the variation of the sensor's internal resistance, when external stimuli are applied, followed by its conversion to an electrical output [44,46]. In other words, every time the composite is deformed by mechanical forces, the contact area and disposition of the conductive materials, within the matrix, changes, leading to a variation in conductance and, therefore, resistance [44,46,49]. Depending on the input signals, resistive sensors can be divided into pressure and strain sensors, which monitor pressure and strain, respectively. Furthermore, considering biocompatibility and stability questions, the majority of piezoresistive sensors employed for health monitoring are wearable devices [44], with many of these flexible sensors employing elastomers, such as PU and PDMS [46], reinforced with conductive materials, including CNT, CB and CNF, metal nanowires and

nanoparticles, conductive polymers, thin metallic films, along with graphene and its derivates [46,47].

According to Gu *et al.* [46], these resistance variations can be explained through three factors, these being changes in contact resistance between different layers of materials, changes in the gaps between nanowires or nanoparticles, or changes in the sensitive material's geometry. For these reasons, piezoresistive sensors have received substantial attention thanks to their simple fabrication processes and structure, low power consumption and cost, easy integration and signal acquisition, with broad operating pressure range and quick response time, while possessing a great number of potential applications, especially medical diagnostic systems [44], human body motion monitoring, rehabilitation [46], and smart heartbeat monitoring, averting heart-related diseases [49]. However, issues regarding the sensor's stability and power consumption still need to be assessed [49].

Focusing further into piezoresistive sensing, traditional strain gauges employ piezoresistive metals or semiconductors as the sensing element. In spite of its high sensitivity and low cost, these commercial strain sensors are directionally fixed and able to measure only very small strains, of less than 5%. Therefore, this approach is not advisable for flexible and wearable sensors, since multidirectional, high sensitivity, wide pressure range, and even multifunctional characteristics may be required. Taking this into account, meeting these requirements will involve novel sensing elements based on nanomaterials [48]. Additionally, embedding conductive materials into elastomer matrices, with porous structures, is a great way to achieve two- and three-dimensional conductive networks capable of providing high performance to piezoresistive sensors, with potential ultra-high sensitivity to applied strain or pressure [46]. Therefore, remarkable progress has been made in improving the flexibility, stretchability, sensitivity, frequency response, and durability of this new generation of sensors [48].

Passing on to capacitance-based strain/pressure sensors, capacitive sensing mainly relies on capacitance changes of the dielectric layer between two plates, converting applied pressure or strain deformations into capacitance changes. In the case of a parallel plate capacitance sensor, the output value will change when the distance between the two plates is shortened under external forces [48,49]. Thus, capacitance-based sensors also witness widespread use due to their high sensitivity over wide pressure ranges, low-pressure detection thresholds, fast response time, durability, and applications in the wearable and health monitoring fields [44].

When external forces are applied to the sensor, causing deformation, the total volume of air voids in the dielectric layer decreases, while its permittivity increases. Therefore, the rise in the capacitance value can be caused by two factors, this increase of permittivity or the reduction in the plate spacing [46]. This has led researchers to improve their sensor's sensitivity by modifying the dielectric layer structure through microstructure modifications, either by tilted micropillar arrays or by employing porous pyramid PDMS layers [44]. Microstructures and their modifications will be addressed further down this chapter.

If we compare capacitive with piezoresistive sensors, the first retains higher sensitivity and lower detection thresholds, while, however, possessing poorer linearity and susceptiveness to not only parasitic and fringing capacitance, but also electromagnetic interferences that could lead to limitations in its practical applications. Nevertheless, capacitive sensors are effective at detecting small deflections, having good frequency response, large dynamic range, low power consumption, high spatial resolution, and sensitivity [46,49].

Mathematically, the capacitance of a capacitor can be defined by Equation (3) [44]:

$$C = (\varepsilon_r . \varepsilon_o . A)/d \quad (3)$$

where capacitance is denoted by C, ε_r and ε_o are the permittivity of materials and free space, respectively, while A and d represent the effective area of the plates and the distance between both plates of the capacitor. According to this equation, the capacitance value has an inverse relationship with the dielectric layer's thickness and directly with the effective area [44].

Considering a capacitive flexible force sensor, the structure of its elastomeric dielectric layer is vital to the final performance. Nowadays, these layers employ surface microstructures or 3D porous structures, contrarily to traditional approaches, where the dielectric layer was made of solid elastomers, which suffered from low sensitivity and high values of hysteresis thanks to the elastomers' viscoelastic properties [48]. With new approaches, the existence of voids in the microstructures enables the dielectric layer to reversibly deform when external forces are applied to it, significantly improving the sensitivity and hysteresis values [48]. Additionally, there is also a need for stretchable electrodes for capacitive flexible sensors, in the form of various carbon nanomaterials, usually CNT, metal nanoparticles, silver nanowires, and conductive ionic materials, providing excellent electrical conductivity and mechanical properties. If the combination of multiple microstructured and porous dielectric layers with these electrodes is possible, the overall sensing performance of capacitive force sensors can be greatly enhanced. On the other hand, low Young's Modulus stretchable materials, such as PDMS, Ecoflex™ and styrene-ethylene-butylene-styrene (SEBS) are good candidates for the dielectric layer [46, 48].

Regarding piezoelectric strain and pressure sensors, its working principle is based on the piezoelectric effect, a widely used mechanism in the fabrication of sensors, where physical quantities, such as acceleration, force, strain, and pressure, when applied in a certain direction, are converted into measurable electrical quantities, due to the deformation of the anisotropic crystalline materials, leading to the polarization of internal dipoles and the generation of a potential difference between the two opposing surfaces of the crystal [46,48,49].

Devices based on this sensing mechanism show great potential for dynamic pressure applications, benefit from rapid response times, low manufacturing cost, simple fabrication methods, and high sensitivity, being capable of efficiently measuring high-frequency dynamic signals, despite existing challenges, mainly regarding static pressure monitoring, since voltage is

only generated by these materials when pressure is applied or withdrawn [44,46,49]. Furthermore, these sensors consume a small amount of energy, even achieving, in some cases, energetic self-sufficiency. However, due to also possessing pyroelectric properties, the polarizations are massively affected by temperature, leading to output signal drifts [49].

Traditionally, single crystals, piezoelectric ceramics, and ceramic/polymer composites were employed as sensing materials. Yet, inorganic ceramics are brittle and not suitable for flexible sensor applications. Thus, polymer-based piezoelectric materials, including polyvinylidene fluoride (PVDF), copolymerized polyvinylidene fluoride-trifluoroethylene (PVDF-TrFE), zinc oxide, and lead titanite ($PbTiO_3$) have gained attention and are employed in flexible strain and pressure sensors, with PVDF-TrFE being considered, according to Gu *et al.* [46], one of the favourite materials, due to its flexibility, high stability, large piezoelectric coefficient, and simple fabrication process [46, 48]. Additionally, a great deal of new hybrid nanocomposites were developed, such as $PbTiO_3$/graphene heterostructures and composite films of alkaline niobate powders functionalized in a PDMS matrix. Nevertheless, available piezoelectric polymer materials face limited usage, while other materials, with the required stretchability and good piezoelectric properties, demand more research and development [48].

Lastly, triboelectric sensing, despite being an emerging technology, is facing rapid developments in the wearable electronics field, due to its broad application prospects, allowed by its low cost and high energy conversion rate, perfect for wearable and implantable devices [34,49].

Triboelectric-based sensing relies on the contact electrification principle, the generation of voltage when physical contact occurs between two different materials with opposite tendencies to acquire charges, such as friction or contact under pressure, with the generated values depending on the interaction properties of each material. After release, the materials are separated from each other, generating a charge transfer between them and, consequently, a measurable potential difference or alternating current [34,44,49].

For these reasons, sensors based on this effect are capable of converting mechanical forces into electrical signals, with the former's magnitude being correlated with the force applied on the sensor, without requiring any external power supply [34,44]. When the sensor is stretched, the contact electrification induces charge transfers between the layer and the ground, with the generated electrical current, voltage and charge density being all linked to the experienced strain [34]. Furthermore, similarly to piezoelectric sensors, triboelectric sensors produce electrical signals only when they experience contact followed by separation, thus, also being more suitable for dynamic force sensing [49]. Hence, these sensors are indicated for human motion detection, body thrust measurement, and object weighing [34].

Triboelectric nanogenerators (TENG), presented in Figure 22, are a key element of triboelectric sensors, where both triboelectricity and electrostatic induction are combined, with promising studies in the areas of low-powered or self-powered force sensors [49].

However, TENG-based sensors face issues regarding its biocompatibility, biodegradability, miniaturization, integration, and service life, while regular triboelectric

sensors show low detection thresholds, but at the cost of unstable output signals, since this mechanism's intrinsic generation of kinetic energy negatively affects the sensing device's performance [44,49].

Mainly due to these reasons, triboelectric sensors are staying behind piezoresistive, capacitive and piezoelectric sensing mechanisms, when speaking of medical applications such as human body monitoring and blood pressure-related measurements [44].

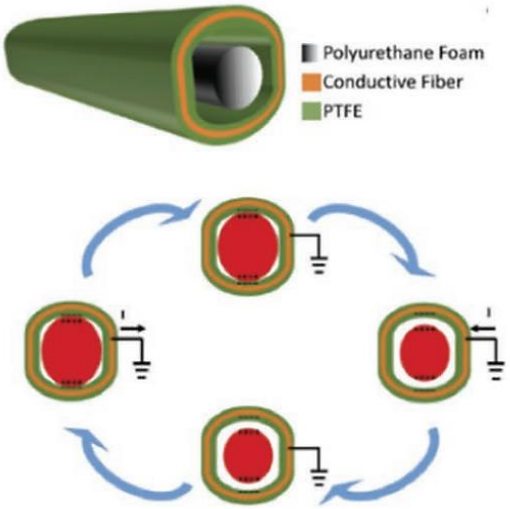

Fig. 22. Schematic and working principle of an auxetic triboelectric generator with strain sensing capabilites. (Adapted from [34])

Sweat monitoring sensors

Chemical sensors are devices that typically contain two key elements, a signal transducer, usually a physicochemical detector element, that extracts useful biological information from the sample, such as individual concentrations, in the form of a detectable signal, and the receptor, containing a biorecognition element, which is responsible for the specific recognition of analytes through ion and electron exchange or transfer, depending on the analyte's concentration. Electrochemical sensing is a well-established technique, beneficial when implemented in the fabrication of sweat sensing devices, thanks to the high sensitivity, low cost, and easy miniaturization it provides [36,50]. Therefore, the biological component chosen for the biosensor's recognition system must be dependent on the desired analyte, in the addition of being able to output its concentration as an identifiable and measurable physicochemical signal. In the same manner, the transducer has to be chosen depending on the bioreceptor and measurement technique [36]. Figure 23 illustrates the main components and general working principle of a biosensor.

Multiple sweat-based biosensors have been employed to monitor physiologically relevant analytes and other elements of interest, with electrochemical sensing being the primary

approach for low cost, high performance, and portable health monitoring applications. Currently, the most crucial analytes for this method are electrolytes and metabolites, while the most used detection methods being enzymatic amperometric and potentiometric ion-selective electrode sensors [36].

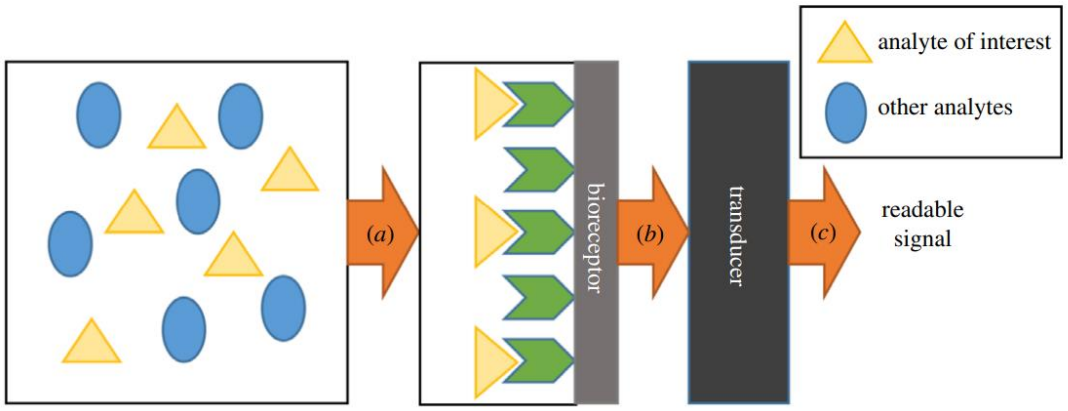

Fig. 23. Main components of a biosensor: (a) The analyte interacts with its specific receptor; (b) The bioreceptor outputs a physicochemical signal, depending on a defined sensitivity; (c) The transducer transforms the output into a readable signal, ready for amplification and processing. (Adapted from [36])

Starting with enzymatic amperometric sensors, amperometry is a dynamic approach to interfacial sensing methods, where direct or indirect responses can be observed, in the presence of a specific analyte on an electrode surface, leading to the generation of a measurable electrical signal disturbance. Thus, the electron transfer between the electrode and the analyte, during its oxidation or reduction, creates a current, proportional to the electroactive product's concentration [50].

These electrochemical sweat sensors commonly employ three or four electrodes, the working electrode, the reference electrode, counter electrode, and cathode, all deposited on a flexible substrate. The reference electrode has a known and stable electrical potential, being used to determine the electrical potential of the working electrode. The most used reference electrode is based on silver/silver chloride (Ag/AgCl), with potentials ranging from +0.2 V to +0.25 V, according to Chung *et al.* [36]. For the metabolite sensing, researchers employ enzyme recognition elements in their biosensors, where the enzyme is immobilized in the working electrode, by various possible mechanisms, including covalent cross-linking, covalent bonding, and entrapment [36].

In the case of amperometric-based sweat sensors, a three-electrode setup is used, with a working electrode, a reference electrode, and a counter electrode. While redox reactions take place on the working electrode's interface, where receptors are modified in response to the target analyte, with transduction of a catalysed redox reaction into a current signal, the reference electrode is used to maintain stability and is not sensitive to the analytes, and, on the other hand, the counter electrode is used to close the circuit during amperometry [36].

This type of sensor employs insoluble materials, supported by natural polymers, including chitosan, synthetic polymers, or inorganic materials, such as glass, while the most commonly used enzymes are glucose oxidase, for glucose sensing, alcohol oxidase, for ethanol measuring, and lactate oxidase, for lactate sensing [36]. One factor to keep in mind is that the product concentration, caused by the enzymatic reaction, can be read through amperometry, only if the substances are electroactive [36].

More recently, to allow for more efficient electron transfers, a redox mediator can be incorporated in the sensor, with ferric materials such as Prussian blue and ferrocene witnessing widespread use as mediators [36]. An illustration of this process can be observed in Figure 24, with this mechanism applied to glucose monitoring.

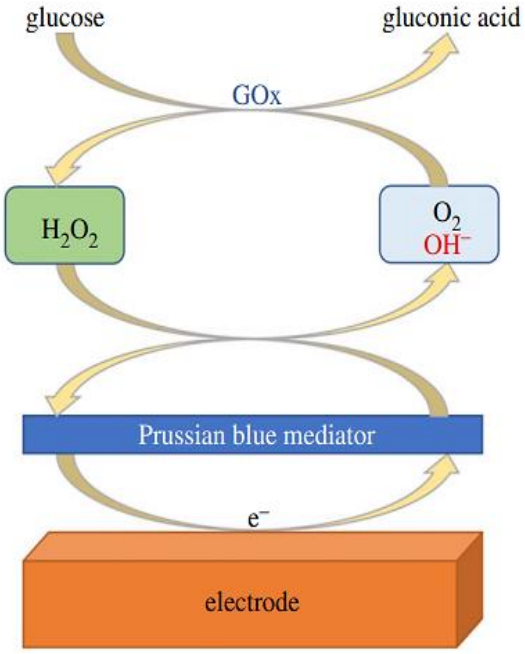

Fig. 24. Schematic of enzymatic amperometric biosensor, with a prussian blue mediator, for glucose detection, using glucose oxidase (Gox). (Adapted from [36])

In relation to ion-selective electrode sensors, or ISEs, these are transducers with the capability of converting specific ion activities into readable electrical signals [36]. Traditional ISEs employ liquid contacts, also known as inner filling solutions, that separate the sensing membrane from the inner reference element. If the Nernst equation is considered, the logarithm of the ion activity can be correlated to the generated voltage, which achieves the target selectivity through direct potentiometry. In ISE sensors, the ISE functions as the working electrode, with a reference electrode being required, similarly to the above-mentioned amperometric sensors. According to Chung *et al.* [36], ISEs can be classified into three categories: liquid membranes, which employ mobile ion exchanges, solid-state membranes, with

fixed ion exchanges, by the use of glass or crystals, and membranes in special electrodes, notably employed for gas-sensing.

The use of solid-state sensors has aided the development of wearable potentiometric sensors, because eliminating the liquid contact has allowed for more accessibility in terms of miniaturization, storage, and processability. The most widespread used sensors of this type detect ions such as Na^{+}, K^{+}, NH^{4+}, thanks to a polymer-based sensing membrane doped with lipophilic ion-exchangers and highly selective ionophores, a lipidsoluble chemical species usually synthetized for carrying ions through the cellular membrane, permitting the attraction of a fixed concentration of the target analyte, followed by selective binding and carry process by the ionophore [36,50]. Additionally, the activity of the ionophore induces ionic activity, which also leads to the generation of specific electrical potentials. The most commonly used ionophores employed in ISE sensors are monensin, for sodium ions, and valinomycin, for potassium ions [36].

However, apart from its sensitivity to sample temperature and pressure, these ISE sensors also require delicate fabrication methods and maintenance processes, posing a challenge for miniaturization. Furthermore, it has been observed that the potential on the interface between the membrane and the metal contact is unstable, caused by the transition from ionic conduction in the membrane to electronic one in the metal. Along these lines, the formation of a water layer in the polymeric membrane is possible, due to the uptake and diffusion of water molecules, leading to the failure of the whole device. Therefore, more research is needed regarding ion to electron transduction mechanisms and layers, between the sensing membrane and electron-conducting substrate, in order to achieve stable responses from the sensor [50].

2.3. Sensorial Systems

The skin is considered our largest organ, weighing, on average, 16% of our body weight. This essential element of the integumentary system carries out a multitude of functions, acting as an important barrier between the organism and the external environment, regulating in a highly efficient manner temperature and hydro-electrolytic balance, while allowing for the housing of bones, internal organs, muscles, and bodily fluids. Apart from that, skin is also considered the primary interface between our central nervous system (CNS) and the external environment, providing important pain, thermal, and tactile-related information. Furthermore, this exceptional multi-functional organ presents unique elasticity and healing abilities [52].

If we tried to create an analogy between the biological capabilities of the skin and an electronic device, the latter would be a giant array of sensors with high sensing performance and negative feedback loops, with the capability to process remarkable amounts of data in a real-time fashion, to further control the balance of the human functions, to replicate homeostasis [52]. Following this line of thought, that is how sensorial systems, also known as electronic-skins (e-skins), came about, a device that works as an artificial skin, consisting of a group of

sensors distributed either over a large area of interest or stacked together in the same place. With the potential to mimic some of the features of the human skin, devices like this could bestow robots and prosthetics with the sense of touch [53].

On the other hand, e-skins can also function as a second skin for humans, sticking to the body's surface and augmenting the natural sensory capacity through sensors that measure numerous body parameters, including heartbeat, body temperature, and blood pressure, among others, such as environment-related parameters, such as radiation, gases, and chemical hazards [53]. Thus, sensorial systems hold the key to the development of high-performance prosthetic devices, enhanced robotics, medical monitoring, and biocompatible implants, thanks to thorough interdisciplinary research, combining bioengineering, materials science, biotechnology, micro/nanoelectronics, data acquisition, processing and transmission, as mentioned before in this work [52]. Along these lines, e-skins also require the integration and synergic behaviour of a large group of sensing components, deposited on flexible and conformal surfaces, such as sensing medical patches, force sensitive artificial skins for robots/prosthetics, and active-matrices for touch screens, leading to power-related demands, requiring energy-dense harvesting and storage devices. Accomplishing this means obtaining sensorial systems with energetic autonomy, which would improve the overall acceptance of flexible wearable devices that employ this technology [53].

Having this in mind, the potential of epidermal electronics functioning as biomimetic sensors is very high, since these can improve the capabilities of soft neural probes and other skin-inspired devices, in addition to the ones mentioned above. Despite this, the attainability mostly relies on already discussed characteristics of flexible devices, including stretchability, flexibility, biocompatibility, and biodegradability, but also others, such as self-healing, self-powering properties, scalability, and large-scale manufacturing processes [52]. However, especially regarding the power supply, currently there is a lack of solutions, despite conducted efforts to develop solutions such as lighter e-skins, wearable energy harvesters, using many transducer mechanisms and miniaturized energy storage devices, including supercapacitators and flexible batteries [53]. Considering all energy sources, thermal, mechanical, and light-source energies have demonstrated superior performance for powering sensorial systems, according to Núñez *et al.* [53]. Thus, progresses in the field of energy-harvesting mainly include the creation of flexible and stretchable thermocouple energy generators, triboelectric energy nanogenerators, and photovoltaic cells (PV cells).

Nevertheless, the performance of this technology is still not enough to reach the requirements of fully autonomous e-skins, where the device needs to work in a continuous, stable and reliable manner for a period of 24 hours, also according to Núñez *et al.* [53]. The main issues regarding this matter are the low power conversion efficiency of flexible technology and the impacts of discontinued energy supply. Because of this, current challenges do not only focus on energy-autonomous sensorial systems, where there is a search for other power supply

approaches, such as chemical, electrochemical energy, and highly efficient energy harvesters, but also the integration of these components in a portable pack [53].

In this section, questions regarding e-skin development, recent trends in component development, and research tendencies will be addressed, with general concepts, power supply approaches and applications also being discussed.

2.3.1. General concepts

Today's accepted and implemented design in research is presented in Figure 25 and Figure 26, providing the crucial building blocks of a sensorial system. The sensing block, the first one in the chain, picks up the parameter of interest, being it temperature, strain, pressure, humidity, pulse rate, transducing it into measurable and readable electrical signals. This component is followed by the data processing and transmission unit, which includes amplifiers, filters, and a radiofrequency (RF) front end, that can be directly placed into the e-skin. This unit is responsible for collecting all the analogue signals from the sensor and performing the first steps of signal processing, with its output being usually connected to an antenna for wireless data transmission, due to the RF front-end generating RF signals [52]. After this step, the received data is relayed to a dedicated receiver, such as a cloud or smartphone, through Bluetooth, NFC communication or Wi-Fi. All of these blocks but the external unit receive power from the power supply and management module, which should use rechargeable/exchangeable batteries, perform energy harvesting, or transfer power wirelessly [52].

Despite the building blocks for sensorial systems being well-known, similarly to flexible wearable sensors, developing mechanically flexible, stretchable, and conformal materials similar to the human epidermis is a challenging task, with complicated fabrication processes, in order to achieve high performance devices, since the chosen materials must allow and maintain intimate contact, while dynamically conform to the complexities of the human skin and the machines integrated in the circuits, if we consider robotic applications [52]. Moreover, to build better stretchable electronic systems, the development of microfabrication technologies is imperative, where existing techniques for rigid materials should be modified, in order to obtain electronic devices capable of withstanding elongations, compressions, and torsions, while preserving its electrical functions [52].

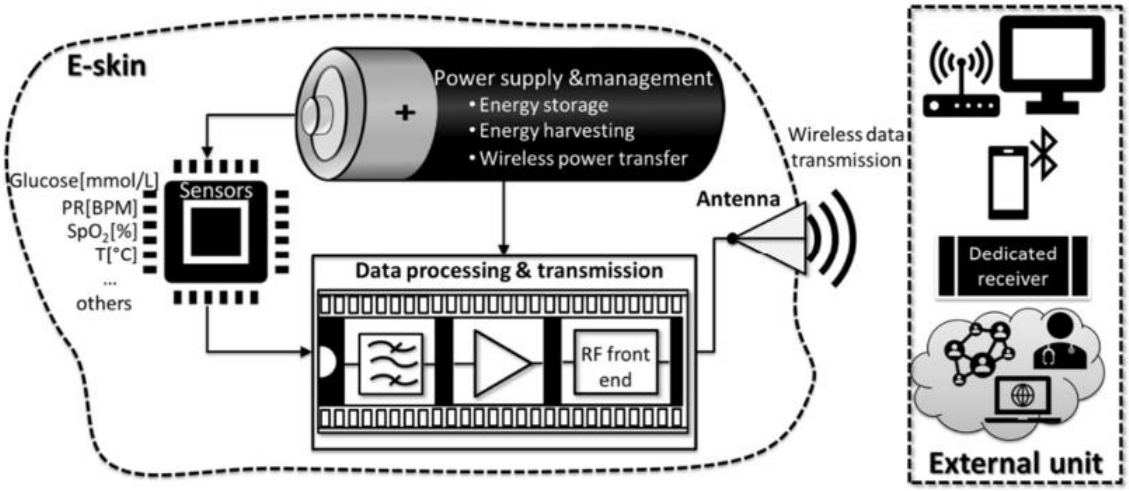

Fig. 25. Blocks diagram illustrating the working principle of a sensorial system, with all the necessary elements. (Adapted from [52])

As discussed before, monitoring biological parameters is a vital element of any sensorial system used for medical, rehabilitation, and even fitness applications. For these reasons, biocompatibility and wearability are the essential properties to focus on, since the sensing elements must not cause discomfort, irritation, allergies, or sweating over the targeted portion of skin. According to Bunea *et al.* [52], thinner and softer sensors, that present smaller contact pressure between the epidermis and the substrate are more comfortable to use. Hence, in recent research, soft, ultra-thin elastomeric materials have shown sufficient performance for conformal contact with the skin's surface, only employing Van der Waals interactions to adhere to the skin, which may lead to increased contact area and fewer motion-related artifacts [52].

For the above-mentioned reasons, components such as the substrate, conductors, semiconductors, and dielectrics must meet the mechanical requirements without sacrificing or modifying the electronic and functional properties during operation [52]. The usage of self-healing materials could provide the means to increase the device's lifetime, due to their capability of mending and preventing the formation of microcracks in the material, avoiding major structural damage that could render the device inoperable. These are formed due to extensive wearing, which leads to fatigue and, consequently, damages to the composite's surface, substrate, conductors, or dielectric [52]. On the other hand, since the sensors are in close contact with the skin, these should be especially comfortable and biocompatible, with long-term usage. Thus, according to Bunea *et al.* [52], materials with interconnected pores can be employed as substrates for permeable and wearable skin-mimicking electronics. One of these materials could be PVDF, which with the correct modification processes, could achieve remarkable hydrophobicity and breathability, allied to porosity, flexibility, and smoothness, perfect for incorporation in light, breathable, and printable electronic systems [52].

Regarding the fabrication process, the application defines the chosen substrate, sensors, transistors, resistors, and all other required electronic components, while the manufacturing techniques can be divided into two groups, also according to Bunea *et al.* [52]: classical techniques based on conventional microfabrication processes, where photolithography, vacuum based-deposition technology, and etching, and printing techniques, where additive manufacturing is included. All techniques will be further presented and discussed in the following subchapters. However, it can be said that printing techniques has attracted some attention, since it can produce devices in a low-cost and large-scale manner, with the possibility to explore novel materials for sensors and substrates, with enough conformity to adhere to non-planar surfaces. With the production of 3D surfaces with specific curvatures, or the attachment of other structures and sensors to the substrate, 3D printed antennas, sensing elements, and conductive layers could prove advantageous for future devices [52].

When compared with other flexible sensor fabrication methods, additive manufacturing has promising prospects due to its system's simplicity, low cost, customization features, and scalability, which has progressed into an approach that allows the production of strikingly customized parts. This has made the fabrication of flexible sensors obtainable at a competitive cost, while retaining huge scalability potential, without losing any of its desired configurations [54]. Despite the huge progress made in the past few years, the main challenge now is establishing adequate techniques for large-scale applications, due to the limiting number of material characteristics, which the majority of materials and methods are not fit for [54].

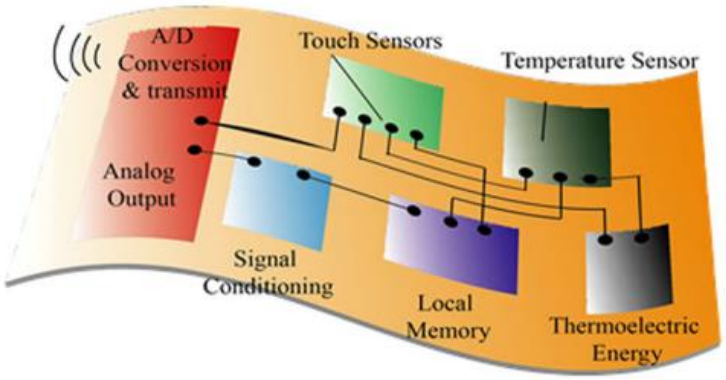

Fig. 26. Multi-sensing and flexible electronic skin for robots and humans. (Adapted from [53])

Elements of a sensorial system

The sensors nowadays made for e-skin applications can measure physiological parameters such as the heart rate, blood oxygen saturation, sweat composition, temperature, humidity, chemical hazards, respiration and gait patterns, sound vibration, and a wide range of movements, followed by readable displays [52]. Therefore, an efficient analysis of stimuli and biomarkers must occur in a network of sensors, each with a different target parameter, in order to precisely make diagnostics and monitoring treatments, based on the feedback the system gives. This multifunctionality can only be achieved through a large array of biomaterials, and

conventional or hybrid polymers deposited on flexible substrates [51]. Furthermore, thin-film materials deposition or additive material deposition could be chosen for some substrates, enabling precise sensing functions or monitoring changing skin morphology and surface temperature [52].

The most popular groups of sensors employed in sensing systems were already discussed in previous subchapters, which included temperature, humidity, strain/pressure, and sweat sensors, the best candidates for evaluating a myriad of physiological information from our organism [52]. Temperature sensors are designed to monitor the skin's surface temperature on a local level and, in order to achieve that, similarly to the other types of sensors discussed in this section, it should have flexibility, conformability, high sensitivity, biocompatibility, and low mass. Relevant classes of temperature sensors, based on their transduction mechanisms, are RTDs, PTC and NTC thermistors, and thermocouples [52]. Lastly, thermoelectric temperature sensors are flexible and accurate, resolution-wise, being suited for e-skin applications. This sensor had the added value of having the possibility of being tuned to a narrower temperature range, in order to better appropriate the applications in hand. Furthermore, the thermoelectric effect could supply energy to the other sensors in the network [52].

Regarding flexible pressure/strain sensors which, as discussed before, convert external mechanical stimuli into electrical signals, several working principles can be taken into account, when choosing an approach for sensorial systems. Among them we have piezoresistive, piezoelectric, capacitive, and triboelectric mechanisms [52]. Something to have in mind is that this type of sensor will be used in multiple different applications and places in the body's surface, leading to the conclusion that each transducing mechanism has its advantages and disadvantages, mostly stemming from the technological complexity, linearity, sensitivity, durability, and fabrication costs. On another note, according to Bunea *et al.* [52], multilayer structures lead to sensors with higher sensitivity and linearity, where the measuring mechanism depending mainly on the application in mind [52].

Lastly, sweat analysis is considered a viable alternative to blood analysis, thanks to its non-invasiveness, convenient collection of samples and possibility of real-time monitoring of several body biochemical parameters. This approach allows the evaluation of a significant number of physiological parameters, either directly or indirectly, while being performed on variable e-skin platforms, that can analyse single or multiple analytes simultaneously [52]. These characteristics make the use of this type of sensor possible in the evaluation of sports performance and metabolic disorder evaluation, since sensorial systems, as a multifunctional device, need the capacity to detect concomitantly simple or complex molecules. Additionally, analyte partitioning is a valuable mechanism that can be integrated in more complex systems, for easy and non-invasive analysis of analytes [52]. In the case all these properties and characteristics are integrated in a single system, the diagnostic value for some diseases would skyrocket, with cystic fibrosis and diabetes mellitus being such examples. Furthermore, another characteristic of sweat that attracted major interest from researchers was the ability to secrete

generated analytes that are not natural to the organism, such as alcohol, drugs, or related to specific pathologies, such as heavy metals. Hence, non-invasive and continuous monitoring of chemical changes in bodily fluids could be one of the keys to identify pathologies that negatively affect the organism, at deeper levels [52].

Power Supply Approaches

Regarding the power supply, the implementation of e-skin technology requires the examination of the entire system, including not only the sensors, but also the actuators and the pathways for signal extraction, processing, and transmission. In the case of wearable devices, portability is one of the main factors to be achieved and maintained throughout the design's evolution. For this reason, today's tendency is to consider other options apart from interchangeable batteries, such as self-powering elements for long-term continuous use, and wireless power transfer (WPT) systems for on-demand data acquisition and transmission [52].

Energy autonomous sensorial systems can employ energy harvesting schemes based on natural phenomena of our daily lives, such as heat, movement, light, or biochemical elements harvested by specific transducers. Additionally, produced excess energy can be stored in a supercapacitor or a battery, facilitating a continuous operation for long periods of time [51]. Thus, harvesting from these renewable energy sources is the key to develop self-powered systems, with suitable schemes for energy storage in flexible, rechargeable batteries being a very promising and intensive subject of investigation [53].

On the other hand, flexible photovoltaic cells have demonstrated very high values of power conversion efficiency, with, according to Bunea *et al.* [52], InGaP-GaAs tandem solar cells can achieve values up to 30.8%, while other flexible films show values of around 20%, such as $Cu(In,Ga)Se_2$ solar cells, deposited on polymeric substrates, and perovskites on plastic substrates [52]. In spite of its incredible promise, challenges have emerged, such as large area requirements and limitations in light availability, which impede the applicability of flexible photovoltaic cells in e-skins or make their use as support energy sources mandatory. Other materials have been also considered, where flexible thermoelectric materials based on carbon and polymers showed promising prospects, despite regular issues being the difficult integration with other components and the low amount of power harvested directly from the human body [52]. Another well-known approach is converting mechanical energy into electrical energy, where piezoelectric and triboelectric effects are the only mechanisms with self-powering properties. The most popular choices for piezoelectricity-based generators were lead zirconate titanate (PZT) films, composite films with barium titanate (BTO) nanoparticles, and ZnO nanostructures, while TENGs have been implemented with success in sensorial systems, combining pressure and strain sensing mechanisms with the self-powering [52].

Regarding the skin's biochemistry and the fluids secreted by it, another possible self-powering approach are biochemical fuel cells (BFC), where the production and energy harvesting from bacteria and enzymes can be witnessed. Starting with bacteria-based BFCs, these microorganisms are employed as metabolic biocatalysts, converting the chemical energy of

fluids like tears and sweat into electricity. Although some concerns exist, regarding cytotoxicity, this type of BFCs could achieve self-assembly, self-maintenance, and even self-repair properties. Recent works utilized not only Gram-positive bacteria that exist naturally in the skin, such as *Micrococcus luteus*, *Staphylococcus capitis*, and *Staphylococcus epidermidis*, but also Gram-negative species, including *Nitrosomonas europaea*, relatively uncommon in the skin, but with ammonia-oxidizing properties [52]. On another note, enzymatic BFCs utilize enzymes as its biocatalyst for power generation, with lactate BFCs having the capability to simultaneously monitor multiple target metabolic biomarkers and physiological parameters [52].

Lastly, the final approach relies on flexible batteries, where recent research mainly concentrates on the now common lithium-based batteries, with flexible electrodes, materials based on carbon derivates, and supercapacitors. If we consider a complete and complex e-skin system, the development of novel batteries with focus on material research, mechanical properties, cycling reliability, energy density, and self-healing properties is crucial for the success of the design. Thus, batteries with high stretchability have also been reported, using zig-zag-shaped patterns to achieve superior mechanical behaviour without losing function [52].

However, one of the crucial issues with the portable energy storage devices we use today is the high dependence on cumbersome and heavy wires for energy transfer, further hindering the system's autonomy and portability. In the wearable health monitoring field, tools like e-skins for prosthetics and robots, along with electronic patches must quickly have a radical reduction of its wires' size and density, with wireless power transfer emerging as a good candidate for substitution. Apart from the before-mentioned tools, many other electronic devices would benefit from more flexible, lightweight, and even wire-free energy storage and transfer technologies [53].

After discussing power generation and harvesting, data transferring design choices will now be discussed, since nowadays, data transfer mainly depends on standard communication protocols, such as radio frequency identification (RFID), NFC, BLE, and Wi-Fi, depending on the target range of transmission our application will have [52].

2.3.2. Applications

As we have seen before in this work, the active and real-time monitoring of the health condition is an insistent and continuous priority. Furthermore, the focus of the research field on the development of novel technologies has led to the creation of new devices with the capabilities to support diagnosis, prevent medical conditions, and aid in therapy and rehabilitation. These advances allowed for more patient-friendly, reliable, and efficient measurement mechanisms of physiological, biochemical, and physical parameters, being used in real-time health monitoring or personalized interventions, but especially in the case of patients with chronic diseases, who fell the necessity of continuous long-term monitoring of their vital signals [52,54].

Additionally, 3D printing of stretchable and flexible sensors is establishing new opportunities in the wearable electronics field, where we are witnessing the birth of a new generation of soft robotics, human-machine interfaces, epidermal electronic systems, biomedical devices, and education support systems, among many others. In the case of epidermal electronics, which this work focuses on, the developed sensors have now the ability to improve the application regarding the detection and analysis of gait patterns, facial expression recognition, voice and speech monitoring, sign language translation, swallowing and blinking patterns analysis, posture and body gesture identification, along with chronic disease diagnosis, for diseases such as Parkinson's [54]. Moreover, these sensors can also achieve positive results, with high sensitivity, in the sensing range of <10 kPa, by detecting subtle pressure variations in the wrist, caused by the pulse, while a wireless, 3D printed, multifunctional pressure and temperature sensor could, for example, be embedded into a shoe insole as a platform for continuous monitoring of gait patterns and posture monitoring [54]. Figure 27 shows a sensorial system integrated into a robotic hand, enabling sensory feedback from the device.

As the IoT becomes more prevalent with time, fitness and rehabilitation fields will also demand new tracking devices to better maintain a health record. For these applications, according to Kumar *et al.* [54], a carbon fibre-filled conductive silicon composite could be developed as a strain sensor, through printing methods, used to analyse the wrist motion, while sensors of the same kind, placed in compression clothing, could provide important information regarding pressure and strain information to the legs and core regions of our body, since human motion analysis is one of the most advantageous applications for personalized rehabilitative therapy, for patients who suffer from disabilities, were victims of traumatic injuries, or have to deal with neurodegenerative conditions [54].

On the other hand, in the field of interfaces and robotics, flexible sensors can be employed in haptic interfaces, object identification, soft robotics, conveying commands, robotic arms control, and texture recognition. Along these lines, in the biomedical field, flexible sensing elements are taking part in functional electronic skin systems for prosthetics, while attempts are also being made to implant these monitorization elements during the post-operative period, as is the case with smart sensors that could be implanted during knee replacement interventions, in order to monitor the kinematic performance and load distribution in the area. However, customizing the sensor for each patient is essential to prevent interference with the different critical geometries in our bodies. Thus, with the aid of artificial intelligence algorithms, in the near future, it could be possible to reduce the creation of motion artifacts and improve the interface between the epidermis and the e-skin, reaching an unheard level of accurate feedback and comfort [52,54].

With this in mind, in recent years researchers have mostly focused on designs with cost-efficient manufacturing methods and products, while maintaining an appropriate level of material quality, with stretchability, transparency, and flexibility, along with ultra-thin, high precision, and lightweight sensing elements, also converging in new, more sensitive techniques for analyte detection [52]. This precise collection of biomarkers, allied to the more conventional

collection of large sets of information on physicochemical homeostatic parameters could capture meaningful health status patterns and variations, allowing for more immediate interventions, which would lead to a more efficient prevention process [52]. However, considering the main limitation of today's biosensors, the capability to only sense a single analyte at a time and a non-existent on-site signal processing unit, this is being addressed with priority, through new flexible platforms which can house multiple sensors simultaneously, further contributing to the potential e-skin systems exhibit in providing real-time, multi-parameter monitoring, with little to no discomfort to users [52].

In conclusion, progress in the IoT field, allied to demands for more personalized medicine, have induced consistent improvements and manufacturing of ever-more reliable and stable systems, with multi-functional sensing mechanisms. On the other hand, despite the complexity tied to the necessary multidisciplinary work in improving sensorial systems, the collaboration between academia and various industrial fields is being strengthened, opening the doors to long-term stability of devices capable of timely detection of conditions, in an accessible manner [52].

Therefore, this technology will certainly, in the future, cement the usage of smarter, user-friendly, multifunctional, and low-cost products, kickstarting an era with non-invasive investigation at the molecular level, data collection at unprecedent rates and illness prediction before the onset of symptoms [52].

Fig. 27. Sensorial system integrated into a robotic hand. (Adapted from [53])

2.4. Materials

As previously stated, efforts have been made into nanotechnology and materials science, where sensors are designed with more miniaturization potential, conformation and skin-attachability. This is being made possible by controlling nano and micro-scale morphologies of inorganic, organic, and even hybrid materials, which allows for the improvement of certain characteristics of the material, including lighter weight, flexibility, and ultra-thinness, enhancing the overall performance and functionality of the sensor [55,56]. Due to their inherent mechanical extensibility, these materials can be manufactured into many types of membranes for on-skin applications, being employed in a large number of wearable sensors. These can not only provide a base for the sensor, but also act as a vital structural element in the mechanisms of signal transduction [12]. Figure 28 illustrates the mechanical stimuli a flexible wearable sensor might experience throughout its service life. Despite this, a challenge still presents itself when we need to develop skin-attachable healthcare devices that employ flexible and stretchable interconnections, multifunctional sensors, and wireless communication, while retaining a viable power supply [55].

When considering the indispensable components of a flexible electronic device, we should mainly focus on the substrate, active layer, and interface between them. The first one acts as the base to build the entire device, the second uses electrical circuits or materials to add

the necessary functionalities, and the last is critical in the cases where the active layer must stay on or inside the substrate [56]. Regarding the active layer, both organic and inorganic options have been considered. While organic materials have gathered attention mainly because of their flexibility, the latter presents good physicochemical properties, chemical durability and mechanical strain, along with high electron mobility [56]. On the other hand, composite materials, such as CNT-silver nanoparticle (AgNP) composites, are also functionalized as the active conductive layer in many flexible substrates, where the interface is also an important matter to discuss [56].

Additionally, taking into account wearable sensors based on polymeric composites, carbonaceous materials, where graphene, CNF, and CNT are included, and metal fillers, such as silver nanowires and nanoparticles, are the most commonly used materials to act as the active layer. Nevertheless, metal fillers tend to have relatively high cost, poor surface modification, non-linearity, and poor acid and alkali resistance, which limits their durability and application in the physiological signal monitoring field. Thus, developing metal fillers with optimal properties is, nowadays, the main focus of research, while also keeping a rational electrode design and structural optimization, important requirements to improve the detection efficiency and versatility in various detection environments [12].

With major developments in nanotechnology, novel nanomaterials with special functional and structural characteristics are being ever-more researched for sensor-related applications. These nanomaterials can be divided into zero-dimensional (0D), one-dimensional (1D), two-dimensional (2D), and three-dimensional (3D) materials, with at least one of their dimensions having <100 nm. Therefore, most properties of nanomaterials can be correlated with their morphology and dimensionality. Typical 0D nanomaterials exist in the form of nanoparticles. These have ultra-small dimensions, good biocompatibility, along with high surface-to-volume ratio and abundant active sites, which is advantageous when used as receptors, but lack in their transducer function and are not suitable for sensor manufacturing. However, when deposited in 1D or 2D structures, they can be excellent selectivity agents [12]. Thanks to the great number of existing structures, morphologies, and sizes of nanoparticles, unique physicochemical properties can be achieved. This, allied to future improvements in the stability of these nanomaterials, could broaden their applications in the human signal detection [12]. Taking into account what was previously stated, 0D materials are normally deposited without agglomerations on the surface of 1D and 2D conductive materials, improving their charge storage performance, while filling the gaps present in 1D materials, leading to the improvement of its role as electrodes in sensor applications [12].

Considering 1D nanomaterials, these can be found in a variety of morphologies, including nanotubes, nanowires, nanofibers, and nanocolumns. Due to their particular advantages in electronic sensor development, improvements in 1D nanomaterials are of vital importance to the industry, since the combination of these materials with other dimensionalities can lead to enhanced mechanical flexibility and biocompatibility, reducing any cytotoxicity that

otherwise would occur. These characteristics have led to these materials experiencing widespread use in applications ranging from medicine to heat conduction materials, among others [12]. Regarding materials, carbon is widely used, especially in the form of CNT, due to their high specific surface area, high electrical conductivity, high carrier mobility, optical transparency, and flexibility, along with abundant availability of carbon sources, a favourable factor for large-scale production. Additionally, their unique structure also provides great electromechanical properties, good thermal stability, and excellent chemical stability [12].

In view of 2D nanomaterials, typical structures include nanomembranes, nanoplates, nanosheets, and nanoflakes, among others. 2D nanomaterials are employed due to their high surface-to-volume ratio, good compatibility with integration in other devices, and good optical transparency. Additionally, 2D nanomaterials show excellent mechanical properties, including flexibility and extensibility, making them the perfect candidates for usage in flexible sensors. Carbon-based materials, especially graphene, are widely used in a great number of sensors, thanks to its electromechanical characteristics [12]. Furthermore, when used as a substrate for the deposition of 1D nanomaterials, their mechanical flexibility provides some mechanical flexibility for the composite, advantageous for the production of new flexible devices. However, mixed structures of 1D and 2D materials are still in the early stages, requiring more research into harnessing more effectively the mechanical properties of 2D nanomaterials, improving biocompatibility and service life [12].

Lastly, looking into 3D nanomaterials, these are composed of one or more 0D, 1D, or 2D materials. 3D structures on the nanometre or micron scale are able to significantly improve ion and electron transport performance, while having a larger degree of freedom and a variety of special functions, with broad potential applications in the fields of biomedicine and mechanics [12]. Research efforts have led to conductive networks being developed for physiological signal acquisition by depositing 0D, 1D, or 2D nanostructures, usually carbon derivates or metals, on the surface of elastomers. Despite the dimensionality of the material influencing different characteristics and roles that can be obtained, some problems remain throughout the research efforts, including deeper investigations on the interactions that nanomaterials with different dimensionalities have with each other, and its influence on the structure, along with environment-friendly materials and fabrication processes, since the materials' sustainability and degradability need to be taken into account in these times of major population growth [12].

Therefore, in this section, a summary of the main materials employed in the substrates and active layers of flexible and wearable sensors will take place, along with the geometries and architectures used to boost the signal capture and monitoring performance of the produced sensors, with Figure 29 showing the variety of material dimensionality available nowadays.

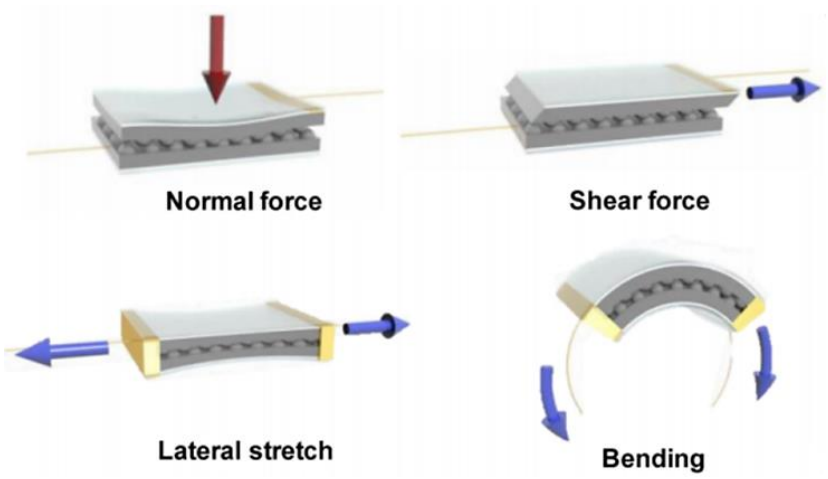

Fig. 28. Schematic illustration of multiple mechanical stimuli that a flexible sensor might experience. (Adapted from [57])

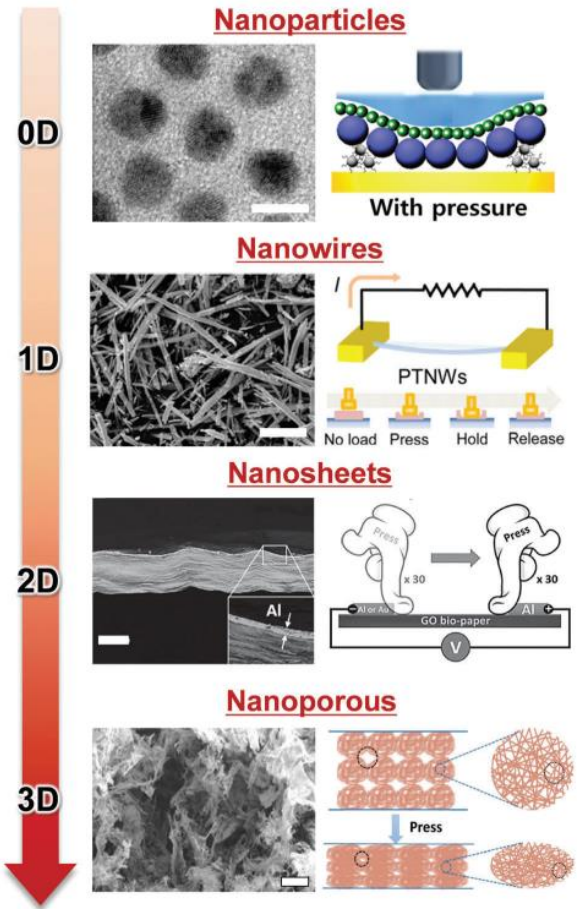

Fig. 29. Variety of material dimensionalities, from 0D to 3D. (Adapted from [55])

2.4.1. Substrates

Most substrates only have the function of supporting tensions experienced by the entire device, such as bending and stretching, where the main requirement is a low Young's modulus and high resistance to cracks. Therefore, the first choices for the substrate or matrix, in the case of composites, consist of inherently stretchable materials, especially elastomers, due to their large-scale deformation, endurance to dynamic strains, of more than 100% of their original size, and durability, with unchanged characteristics after thousands of loading-unloading cycles. Thus, with these characteristics in mind, most substrate materials are polyurethane or silicone-based [57]. Additionally, these materials also exhibit characteristics such as low cost of production, lightweight, good compatibility with other materials, and great flexibility, providing the desired properties that other materials cannot achieve [58].

Presently, the most used elastomer as a flexible substrate is PDMS, a material already discussed in this work, because of its high elasticity, transparency, acceptable thermal stability, chemical inertness, non-toxicity, biocompatibility, low cost, customizable mechanical properties, and simple processing, along with an elastic modulus of around 0.4-3.5 MPa [52], providing superior flexibility, when compared to other polymers [57,58]. Other commonly employed polymers for substrates are PU, PVA, PI, PET, and Ecoflex™. PI also receives attention in the sensor field due to its high flexibility, low creep, high tensile strength, but mainly due to its enormous thermal stability, when compared to other polymers, being able to maintain its properties and conformation up to 450-470 ºC [58]. However, PI has a yellow colour, making it less transparent and limiting its application in more discreet wearable devices [58]. Regarding PU, this material has excellent flexibility and elasticity, with great performance observed, when employed as a substrate or matrix of a composite. Additionally, when employed, PET is used as the substrate of conductive materials, such as nanofibers, graphene derivates, and thin-tin-oxide (ITO), but tends to experience significant damages when bent above its limits [52].

Taking these factors into consideration, researchers today mainly focus on PDMS as a substrate when developing skin-like stretchable sensors, with surface modifications being used as a way to control the adhesion and interactions between the substrate and the conductive materials. However, some thermoplastic elastomers, such as TPU, are employed as well, functioning as the matrix/substrate of systems that require higher stretchability than PDMS, usually in the 120-160% strain range [57]. On the other hand, though, the sensitivity of these materials may be affected by temperature variation, material fatigue, and creep [57].

On the same note, attention has also been gathered around thermoplastics, including PVDF, PP, parylene, and epoxy, for high strength-requiring applications, with some of these, such as parylene, being well-known for its biocompatibility, chemical inertness, and low permeability to moisture, being already employed in implantable and MEMS devices at a large scale [52]. In spite of this, after functionalization with conductive fillers, some toughness and ductility are usually sacrificed, leading to smaller elastic regions and narrower strain sensing ranges, with the application of too much strain causing irreversible changes in the

substrate/matrix and the active layer. Thus, thermoplastics tend to be employed mainly in structural health monitoring applications [57]. Along with these, not only paper and silk fibre, but also low-cost and even recyclable materials have been used to some extent by researchers, due to its flexibility, comfortableness, and biocompatibility [45,52]. These materials support stackable architectures, providing high conformability and deformability to the device, with applications ranging from monitoring temperature, through heart rate and blood pressure signal capture, to skin hydration monitoring [52].

To experience success in daily life applications, researchers need to developed ways to reach acceptable sensitivity over a wide range of strain. According to Duan *et al.* [57], increasing the Young's modulus of a material leads to enhanced sensing performance, since mechanical-induced hysteresis leads to non-linearity and imperfect sensing performance, with long response and recovery times. Hence, low-hysteretic substrates and matrices are preferable for strain sensor fabrication [57]. However, according to Bunea *et al.* [52], decreasing the Young's modulus of the substrate may lead to increased comfort levels when wearing on-skin devices, with attention being given to substrates made of materials with native or induced flexibility and stability, allowing for conformal integration of the needed electronic components on the skin, while avoiding mechanical degradation of the sensor during operation [52].

Considering the majority of sensing mechanisms, researchers could functionalize an insulated polymer with conductive fillers, such as the previously mentioned carbon black, CNT, metal nanoparticles, and graphene, along with others that will be discussed further below, including MXenes, in order to obtain a composite material with an internal conductive network [58].

Despite all the positive factors, detachment of the device, caused by skin sweat or moisture is a likely possibility, while mismatches, although small, between the human skin and PDMS may bring some drawbacks regarding comfort and long-term usability. Nonetheless, despite other silicon elastomers being considered, including Ecoflex™, and even Dragon Skin™, composed of overlapped high tensile strength silicon carbide ceramic discs, and Silbione™, a platinum catalyzed silicone gel elastomer. Despite all of them being considered biocompatible and some with elongations at break of around 1000%, PDMS, due to its unique properties and easy access, has remained the main choice of researchers all over the world [52].

2.4.2. Conductive fillers

For flexible sensor applications, it is vital we pursue the development of stretchable conductors, with high performance, stretchability, and stable electrical conductivity in order to create better electrodes for sensing elements, wireless antennas, and interconnect components, for the new generation of wearable devices [55]. Figure 30 illustrates the typical material approaches taken by researchers, where inherently stretchable elastomeric polymers are combined with conductive nanomaterials of diverse dimensionalities, including metal

nanoparticles and nanowires, carbon derivates, conducting polymers, and liquid metals. In this case, some of the methods used to obtain the conductive material are, according to Ha *et al.* [55]: 1) simply depositing the conductive nanomaterials on the surface of the polymeric substrate; 2) embedding conductive nanomaterials in the stretchable polymers, through multiple layers of it; 3) fabricating composite materials, where the polymeric matrix presents flexibility and stretchability, while the above-mentioned nanofillers give the desired electrical conductivity to the final material.

Throughout the years, metal nanoparticles have been considered inappropriate as active fillers for stretchable matrices, due to the high values of percolation concentration required, which is needed to create a fully conductive network inside the matrix, where stimuli are met with the maximum variation of conductivity, achieving the best possible sensitivity. Allied to this, contact resistance observed in a great number of inter-particle junctions is also a major problem for researchers. Therefore, attention shifted towards metal nanowires, CNT, and graphene, which allow for highly sensitive conductive networks with unique morphologies at low percolation concentrations, while being able to achieve and maintain electrical conductivity throughout its operation [55].

Additionally, it has also been reported that, compared to the direct methods of conductive material deposition, embedding conductive layers instead provides added robustness to the entire structure, without the delamination of the conductive material, even after repeated loading-unloading cycles. Along these lines, hybridizing conductive materials is also an option, where hybridized graphene and CNT films are a very popular choice since graphene 2D nanostructures have attracted tremendous attention as an excellent electrical conductor and mechanically strong option for functionalization with flexible substrates. This hybridization is able to suppress the delamination of CNT from the substrate during its operation cycles, which in turn leads to a reliable and continuous electrical conductivity, along with enhanced mechanical properties. All of this can be obtained with a percolation concentration lower than that of single nanowires or CNT, proving its great potential for future endeavours [55].

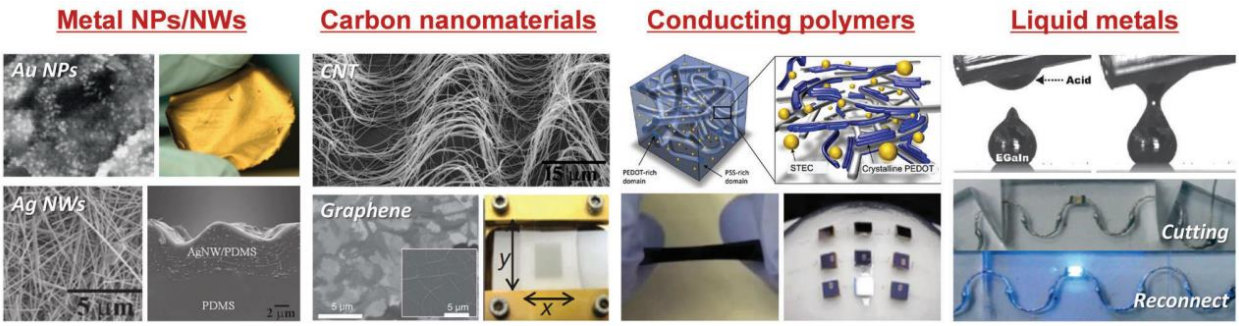

Fig. 30. Stretchable hybrid materials employed as active materials in composite wearable sensors. (Adapted from [55])

Passing on to the discussion of specific groups of materials employed as conductive fillers, as previously mentioned, metals are most employed as 1D nanoparticles mixed with other

dimensionalities, along with nanoflakes and nanowires for the fabrication of flexible composite materials. Contrarily to carbon-based materials, where their properties are influenced by the fabrication process, while also facing possible agglomerations, metal-based nanowires provide high conductivity, large surface area, and large aspect ratio. However, these nanowires are also known for their non-linearity, difficult adhesion to the substrate, and tendency to oxidate when exposed for long periods of time, factors that sacrifice the service life of the device [58]. Furthermore, inducing high strains in composites may lead to irreversible gaps and cracks between nanoparticles, which leads to devices having a very limited strain range [57]. The most commonly used metal nanowires are based on silver, copper, gold, and platinum, with silver being the most widely employed today [58]. In conclusion, despite its excellent electromechanical properties, which make the fabrication of stretchable, flexible, and transparent sensors possible, when functionalized with polymers, issues regarding stability, durability, high cost, low abundance, and roughness hinder the scalability of metal-based nanoparticles and nanowires in this field [57].

Regarding another group of nanomaterials, graphene is one of the most widely employed nanomaterials nowadays, made of a single layer of carbon atoms arranged in strongly bound hexagon rings, providing superior flexibility, excellent electromechanical properties, lightweight, and adjustable 2D structure, along with an optical transmittance of ≈98% and a Young's modulus of around 1000 GPa, perfect for flexible sensor development. Graphene can be used in sensors in multiple dimensionalities, such as 1D fiber-shaped sensors, 2D films, and 3D monoliths. Additionally, other forms of regular graphene, such as GO, rGO, graphene ribbon, graphene sheets, and nanoparticles can be employed as a building block for other materials required to achieve higher performance in flexible sensors, where PVA, PU, PDMS, and MXene can be included. Among these, GO and rGO stand out, where while GO has a semiconductor behaviour, rGO is highly conductive, almost at the same level of pristine graphene [58]. In this fashion, 2D graphene films are popular mainly due to their high flexibility, lightweight, conformability, and simple fabrication processes, being able to achieve a large contact area with the human skin, capturing physiological signals more reliably. As will be discussed in the next section, graphene films can be obtained from GO solutions by vacuum filtration, spin coating, spray coating, wet spinning, dip coating, and self-assembly methods, followed by reduction through physical or chemical methods, in order to harness the high conductivity of rGO [58]. Lastly, 3D graphene structures are a new research topic, with potential to replace 2D nanostructures. 3D graphene structures consist of monoliths, which are foams or sponges with high porosity, large surface area, and good structural stability. These can be built by electrospinning, 3D printing or template-directed methods [58].

Passing on to other carbon derivates, carbon nanotubes, also known as CNT, are one of the most used forms of carbon in flexible sensor applications, composed of a graphene sheet forming a cylindrical shell, with lengths up to hundreds of nanometers and diameters of a few nanometers, thus achieving high aspect ratios and often being considered a 1D structure.

Presently, CNT is employed in the fabrication of CNT/polymer composites, allowing for materials with superior electromechanical properties, relative to both individual elements and other fillers [58]. Furthermore, percolation thresholds can be reached relatively quickly with low concentrations, when considering polymer-based composites. Comparatively, carbon black nanofillers, which have a lower aspect ratio because of higher diameters, only reach percolation at higher concentrations. Apart from this, CNTs have superior mechanical flexibility, along with acceptable stretchability, high carrier mobility, and good sensitivity, making them one of the best options for conductive fillers. Therefore, in flexible sensor application, this filler is functionalized with elastomers such as Ecoflex™, PET, PI, and PDMS [58]. Additionally, CNT can be put in two categories, depending on the number of carbon atom layers, these being single-walled CNT (SWCNT) and multi-walled CNT (MWCNT), as illustrated in Figure 31. While SWCNT exhibits overall better thermal conductivity, flexibility, and aspect ratio, MWCNT has higher mechanical resistance and electrical conductivity. Despite the advantages, composite fabrication with CNT faces agglomerations of the material, caused by electrostatic interactions, negatively affecting the final performance of the device [58].

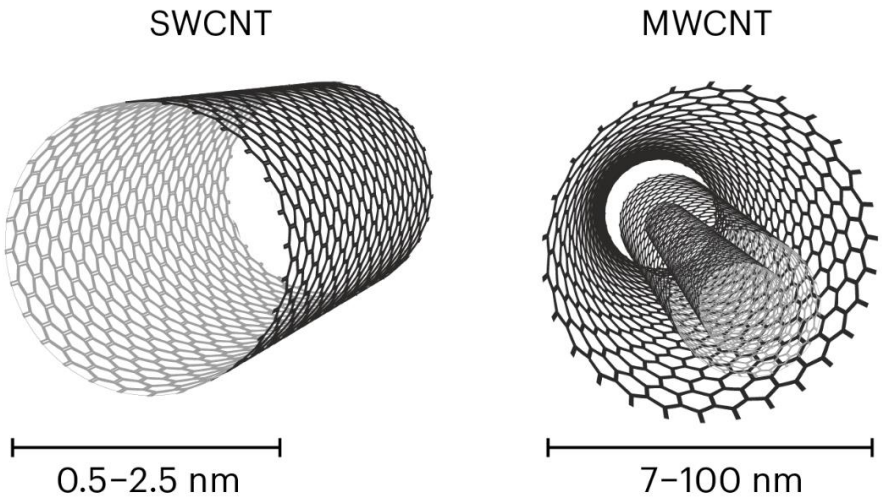

Fig. 31. Illustration of single-walled carbon nanotubes (SWCNT) and multi-walled carbon nanotubes (MWCNT). (Taken from tuball.com)

Another candidate as the conductive filler of choice are conductive polymers, with their main asset being their tuneable conductivity, allied to great flexibility. Before 2000, polymers were used mainly as insulators, but with the discovery of conductive polymers, nowadays we can see them in a myriad of applications, including conductive polymer composites, with electrical properties and behaviour similar to metals and semiconductors [58]. These composites are composed of an insulating polymer matrix functionalized with conductive fillers, in which the latter provides the necessary carriers. This approach is one of the more popular among sensors with piezoresistive mechanisms. As stated in previous sections, insulated polymers, such as PI and PDMS, can be functionalized with conductive fillers, such as graphene, metals, and CNT, with the filler, overall geometry and the resulting interface influencing the sensor performance

[58]. The main asset of this type of material is the adjustment of their conductivity via doping, changing the chemical structure, or by switching fillers. However, inherently conductive polymers also exist, as is the case with polypyrrole, PEDOT:PSS, and polyaniline (PANI), which can be used in conjunction with substrate polymers such as PDMS and PET [58]. Thus, conductive polymers can help researchers achieve the so-desired compromise between flexibility and electrical properties/sensitivity. However, despite meeting the required flexibility for sensorial systems, these materials present lower electrical conductivity than the above-mentioned metals. Hence, the main focus of research in this field is developing simpler fabrication processes that achieve mechanically robust devices with larger areas of contact with the skin. On the same note, PEDOT:PSS is a good candidate to improvements over the stretchability of conductive polymer composites, upon the addition of fluorosurfactants and non-ionic plasticizers, according to Bunea *et al.* [52].

Another family of employed materials are MXenes, 2D nanomaterials with distinguished electrical conductivity, unique layered structures, hydrophilicity, large specific surface areas, thickness in the 1-100 nm range, and abundant terminal groups, presenting themselves as potential candidates for applications related to wearable sensing devices [58]. Despite MXenes being employed plenty of times as matrices for composites, due to its excellent compatibility with other materials, combining or complementing the properties of the final material, with a great deal of work being put on production at the lab-scale. However, combining MXenes with polymers has also shown exceptional results and properties, mainly regarding electrical conductivity and durability, with valuable outcomes in the detection of respiratory biomarkers, among other advantages in signal capture and monitoring [12,58]. Nonetheless, MXenes also have some disadvantages associated with them, mainly mechanical properties and instability under oxygen atmosphere, which limits the utilization of pristine MXenes in wearable sensing devices [12].

Lastly, liquid metals are also witnessing some usage in the research field, due to their inherent flexibility, stretchability, and excellent conductivity, being expected to thrive when applied to prosthetic, robotics, and wearable devices that operate in especially curved or soft surfaces. The most commonly employed metals of this kind are Galinstan, an alloy composed of gallium, indium, and tin, along with eutectic gallium indium (EGaln), prolific in electrode and sensor operation [56]. Considering that both liquid metals and conductive polymers, such as the mentioned PEDOT:PSS films, display similar characteristics, with the addition of fluidic behaviours, various stretchable conductors with different patterns and microchannels have been designed to guide liquid metals effectively, such as PMDS and Galinstan composites. Furthermore, this fluidic characteristic also may lead to self-healing properties, in reusable devices [55]. Contrarily to other materials, where extreme or prolonged stretching, bending, and twisting leads to cracks and disconnections, liquid metals have the ability to self-heal the damages and maintain good and, most importantly, continuous electrical performance [56].

2.4.3. Geometries

In spite of all the advancements in wearable device technology, these still face various challenges, mainly long-term reliability and sensing functionality, due to the mechanical discrepancies with human skin. Taking this into account, in order to overcome this mismatch, additional research towards the structure of the sensor is required to achieve the necessary conformity and endurance to stretching and bending cycles, intrinsic to body motion [59].

Therefore, in this section, we will discuss geometric designs used to improve sensor performance, including serpentine/wavy, rigid-soft, ultrathin, mesh, three-dimensional, and biomimetic approaches. Effectively controlling these geometric designs enables the more rigid metal films and conductive materials more stretchability, minimizing the direct strain on these. For this reason, according to Ha *et al.* [55], many works report the usage of serpentine, wavy, and buckled geometries in the development of stretchable devices, integrating hard materials onto soft electronics. Controlling the topology of lines and meshes, along with the adjustment of sizes, achieved success in epidermal adhesion [55], since the introduction of the nanostructures enables better control of stress transmission and concentration to the sensing elements of the sensor, leading to maximal electrical variation to applied stimuli. Apart from improved mechanical behaviour, other properties, such as hydrophobicity, wettability, and optical transmittance can be adjusted [55]. Figure 32 illustrates the main geometries chosen in flexible sensor fabrication.

Starting with serpentine and wavy geometries (Figure 32a), without considering the internal chemistry of the materials, this geometry is one of the novel approaches used to achieve interconnects with enhanced flexibility and stretchability, positively affecting the accommodation of strain by on-skin sensors. A serpentine geometry is a design with a determined curved shape that is periodically repeated [59]. Serpentine and fractal designs are being employed in research to enable elastic but also reversible responses against large deformations, since strain energy is released when properly conformed to the skin [34,59]. Another very important characteristic in this geometry is the capability to minimize the mechanical behaviour discrepancies between sensors and actuators [59]. On the other hand, serpentine geometries can also lead to more stable electrical conduction and minimization of electromagnetic disturbances, along with better conformity, factors that contribute to higher performance in mechanical robustness and physiological signal recording [34,59]. Another approach that grants constant conductive performance is using out-of-plane geometries (Figure 32b), where in prestretched substrates are deposited conductive materials, leading to wavy geometries that can avoid material fractures under strain, while maintaining high conductive performance [34,59]. The most commonly employed materials in these geometries are metals, dielectrics, such as polyimide and epoxy, along with patterned combinations of both [34].

Regarding rigid-soft designs, this is a geometry where reinforced islands are embedded in an elastic layer, also being known as hybrid designs. In this approach, both the islands and

the elastic layers are composed of two different materials with different elastic moduli. Therefore, when the entire structure suffers deformations, the more rigid and reinforces islands support the active elements of the sensor with minimum deformation, while the elastic layers disperse the rest of the strain [59]. These characteristics are allied to high rates of transparency, around 93%, and low haze, of ≈2% in the visible spectrum, according to Yun *et al.* [59], perfect for soft contact lenses applications [59].

Another approach are ultrathin structures, where the main objective is achieving a linear and proportional relationship between the induced strains and the overall thickness of the electronics. Taking this into account, researchers diminish the thickness of the flexible sensor in the hopes of reducing the induced strains and maintaining some mechanical stability. These ultrathin structures can also be crumpled in order to reach higher percentages of deformation, in order to enable enhanced conformation to softer and curvilinear surfaces, such as human skin [59].

Furthermore, mesh designs (Figure 32c) are made to allow devices to exhibit higher stretchability. In this geometry, when an external strain is applied, each mesh and empty hole play a role in enabling stretching and bending motions. Thus, mesh geometries enable highly stretchable, conformal attachments to the human skin, with uniform heat transfers during body movements, with articular thermotherapy being a potential application for this approach [59].
Three-dimensional 3D structures (Figure 32d), including 3D coiled and 3D sponge structures exhibit many advantages. Regarding the first, deformations of the coil alleviate the strain induced to it, enabling superior stretchability, even when compared to 2D serpentine geometries, and 20 times higher than conventional CNT yarns, while operating without electromechanical instability, according to Yun *et al.* [59]. Considering the latter, 3D porous and interconnected scaffolds are able to maintain conductivity and stretchability throughout shape deformation cycles, without changing the electrical conductivity [59].

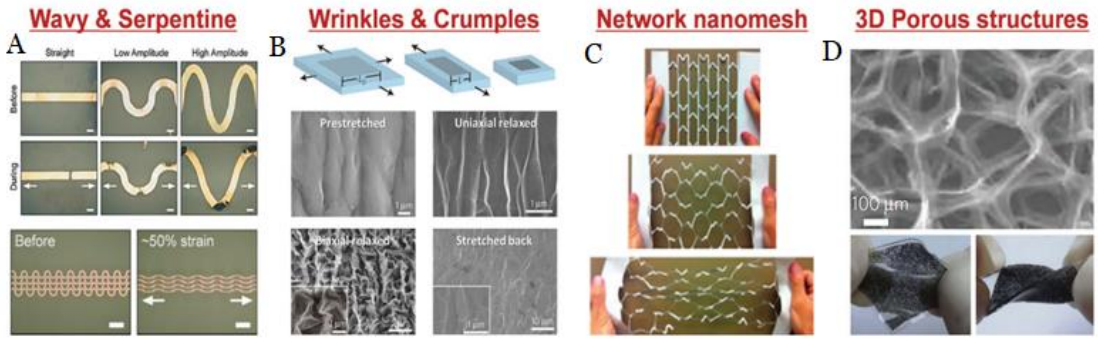

Fig. 32. Main geometries employed to achieve higher stretchability and overall superior mechanical performance: (A) Wavy and serpentine; (B) Wrinkles and crumples; (C) Network nanomesh; (D) 3D porous structures. (Adapted from [55])

Lastly, structures that mimic biological structures are also employed in research, a novel way to enhance detection range, sensitivity, selectivity, and response time, mainly in the case of pressure and strain sensors. Mimicked biological structures allow for wearable sensors with ease of deformation, larger contact area, enhancing sensitivity, and directionality of the sensing materials. Figure 33 shows some of the structures mimicked from nature. Considering the figure, a strain sensor inspired by mammalian whiskers (Figure 33a) would exhibit high aspect ratios, with superior sensitivity and directionality, able to detect subtle variations in air flows. Additionally, nanoscale cracks, inspired by the well-known spider's slit (Figure 33b), allow for reversible connections and disconnections of these structures, leading to a physical sensor with ultrahigh sensitivity, able to detect vibrations in the environment [55]. Moreover, tactile sensors inspired by the functions of the human fingertip (Figure 33c) inspire devices with the ability to grasp the surface texture of the material and object it contacts with. Lastly, hierarchical structures inspired by biological systems (Figure 33d), which will be discussed further below, provide extraordinarily large contact area and effective stress transmission, used in the development of hypersensitive physical sensors [55].

In conclusion, sensing materials that are structurally modified show outstanding responses to external physical stimuli, with great signal transduction and conversion capabilities [55].

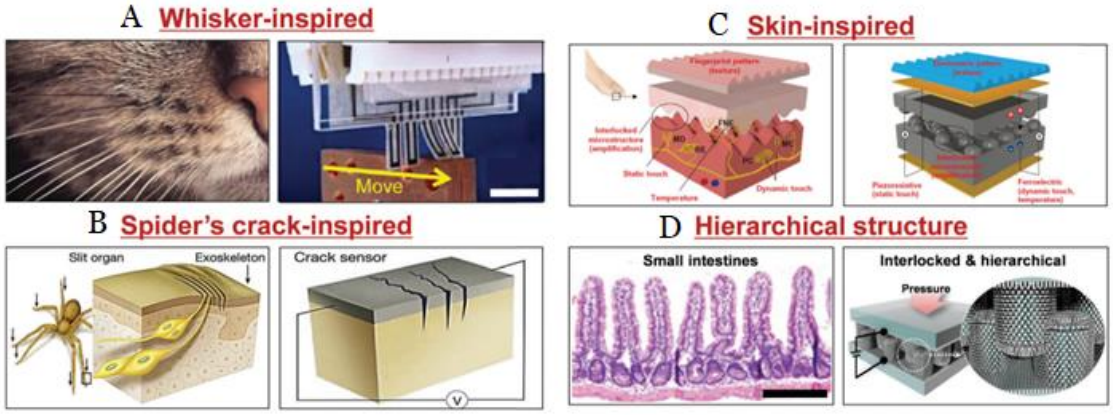

Fig. 33. Biomimetic geometries inspired by life, including mammalian's whiskers (A), spider's sensory system (B), human skin (C), and intestinal vilosities (D). (Adapted from [55])

2.4.4. Architectures

Following what was discussed in the previous section, where geometry-related approaches were taken in order to achieve higher sensitivity and improved mechanical behaviour, other structures and architecture approaches could amplify mechanical loading effects, while the resulting conductivity and resistance changes in the system could be augmented, leading to better sensitivity. Nowadays, most employed architectures can be categorized in three major groups: nature-inspired, periodic, and hierarchical architectures, which will be covered in this section [60].

Regarding nature-inspired architectures, throughout the eons, living organisms have developed very delicate biological systems to sense environmental stimuli. As stated above, mammals have cochlear hairs that can be distorted due to small vibrations, being able to detect subtle sounds, along with changes in air flow. Inspired by these, researchers are able to develop devices with elastomeric substrates and opposite-facing arrays of conductive nanofibers that contact and change resistance when a stimulus is applied and the geometry changes, with low response times [60]. One such example of interlocked nanofibers can be found in Figure 34. Another example, also previously covered, are the interlocked epidermis/dermis-inspired structures that are located beneath our fingertips, providing the necessary recognition of objects and surfaces through contact force. As such, according to Li *et al.* [60], interlocked microdome arrays of PDMS-CNT composite can be used with this architecture, where external stimuli enlarge the contact area between the microdomes, along with tunneling currents, leading to variations in electron movements and conductivity changes, also with very low response times. This architecture is also capable of distinguishing between shear and bending motions [60]. Apart from human skin or cochlear hair, chameleon skin-like capabilities can be combined with pressure/strain, temperature, and humidity sensors in sensorial systems, where variations of

these parameters are correlated with specific colours, making the visualization easier for the untrained eye and all possible users of the technology [60].

However, fabricating these architectures, with the use of nanofibers and other microstructures can prove a very costly, complex, and laborious process. Considering this, living creatures and their systems should be taken as inspiration or even molds, whereas our products should be able to simplify the process. As stated by Li *et al.* [60], rose metals can work as molds for PDMS films, due to their micropapillae on the surface, whose structure is similar to the human epidermis. This structure, functionalized with nanowires, could enable interesting new perspectives, performance-wise [60].

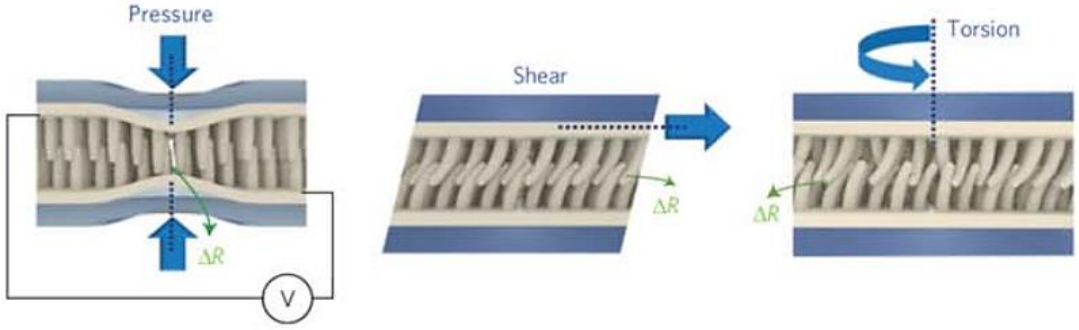

Fig. 34. Operation of a piezoresistive sensor, with cochlear hair-inspired nanofiber arrays, depending on the experienced mechanical stimuli, namely, pressure shear and torsion. (Adapted from [60])

Other than nature-inspired architectures, periodic structures, such as pyramidal micro arrays have been used in capacitive sensors due to the high values of sensitivity achieved by the sharp tips. Therefore, sensors that employ this kind of structure are especially good at ranges around <100 Pa, where good sensitivity, along with ultra-fast response times, of around 0.2 ms, can be achieved. Furthermore, previously mentioned composites, such as PDMS-CNT, can be modified to prepare interlocked micropyramidal structures, allowing for multiple direction sensing [60]. Apart from pyramidal architectures, other approaches, like pillars and domes are being developed and studied presently. Some examples include micropillar arrays covered in gold, where the sensitivity can be tuned by varying their diameter, along with semi-cylindrical and dome-shaped 3D fiber networks, capable of changing their resistivity when pressure is applied, since changes in the cylinder morphologies and two opposing dome networks making contact with each other, respectively, result in conductivity variations [60].

Comparing these structure designs, microdomes, micropyramids, and micropillars, according to Li *et al.* [60], microdomes have the best sensitivity for tensile and bending loads, while micropillar arrays are best to sense shear loadings. Beyond these additive architectures, subtractive hollow-pillar structures can also perform in strain sensing applications, with enhanced sensitivity. Thus, both “positive” and “negative” micropillar arrays can operate in multiple forms of mechanical loads [60].

Lastly, based on our knowledge of above-mentioned geometries and architectures, we can develop hierarchical combinations of various architectures and additives, a very favorable design approach to obtain high-performance sensors, mainly for those based on piezoresistive mechanisms. The most straightforward method is depositing additional nanowires or over fabricated microstructures, such as platinum or nickel coating in PDMS-ZnO micropillars, or ZnO coating of PDMS-silver nanowires (AgNW), in order to fill the gaps between the conductive network [60]. The main asset of these architectures is providing good sensitivity, of around 6.8 kPa^{-1}, along with ultrafast response times, of <5 ms, and better directional sensing performance [60].

Additionally, textiles are also considered as hierarchical structures, due to its fibrous nature. Fibers, the most basic unit, which exhibit significant ratios of length to diameter, are interlaced with each other, in order to obtain thread, the first integration. Followed by this we have the second level of integration, where threads are twisted into yarns. Lastly, we reach the third level of integration we can form textiles by multiple techniques, such as weaving and knitting, among others [60]. Taking this into account, the hierarchical level of textiles enables researchers to achieve various degrees of functionality, by functionalizing different materials and composites onto these structures. Carbon derivates, such as graphene and CNT, polymer-graphene composites, among other composite materials, can also be incorporated into textile structures. Hence, textile sensors have potential for wearable devices in human motion sensing, monitoring hand gestures, physiological signals in real-time, and diagnosis of arthritis and spine conditions, among many others [60]. Graphene is a notable material in these applications, since its usage enables significant gauge factors, of around 26, remarkable conformity, along with long-term durability [60].

2.5. Sensor manufacturing

As previously stated, the overall capability and quality of wearable flexible sensors can be estimated by a myriad of parameters, already discussed in other sections. In the biomedical field, despite the operation of these sensors being done, for the most part, in laboratory settings, to determine physiological and anatomical changes in the human body, their behaviour and potential have opened possible applications all over the healthcare sector and beyond. Thus, the composition these devices should have is currently being debated in the research community [61].

Since wearable models are advantageous over their stationary counterparts, due to enhanced productivity and higher convenience, the biomedical and bioengineering field have harnessed the great potential of these devices to capture and monitor physicochemical parameters and anomalies in human beings [61]. Therefore, as stated in previous sections, polymers such as PDMS and Ecoflex™ are employed as substrates and matrices, in the form of

porous films, foams, and modified with microstructures, increasing sensitivity and general performance. Typically, the process to fabricate a patterned substrate or matrix is simple, where in a previously fabricated micro-patterned mould is poured PDMS, followed by curing and peeling processes [58].

However, regarding other materials and their fabrication, depending on the approach, the structure and dimensions of resultant sensors can greatly vary, where both parameters are of great importance, depending on the sensor's application. To achieve the required properties, a wide selection of materials is available today, with material science developments providing new options and innovative processing methods periodically [61].

In flexible sensor fabrication, especially regarding composite materials, the substrate/matrix works as the flexible support, providing the required stretchability and mechanical flexibility, while active layers or conductive fillers are responsible for the transduction mechanisms and complementing the matrix's properties and characteristics. Regarding conductive materials, many have been employed in flexible sensor applications, in order to obtain composites with enhanced sensing range, stability, and sensitivity, including carbon-based materials, such as graphene, CNT, CB, and CNF, along with metallic nanowires and nanoparticles, made of silver, gold, and zinc oxide, among other materials [61,62].

Regarding carbon-based materials, these have been employed due to their superior electrical conductivity and mechanical behaviour, exhibiting outstanding development potential. Among them, graphene is a good candidate for various sensing applications, notably strain and pressure sensing, due to its excellent electromechanical characteristics and the ability to be mixed with an elastomeric matrix, providing excellent long-term stability, high gauge factor values and appropriate strain ranges [61].

On the other hand, metal nanowires and nanoparticles can also be employed as the conductive filler of composite materials. One example is AgNW, which have gathered great attention due to its excellent rigidity and electrical conductivity properties, and potential in smart textiles, e-skin, and structural health monitoring applications. Nonetheless, oxidation-related issues still need to be solved in order to overcome possible sensor limitations created by these materials [61].

In this section, subjects regarding conductive filler manufacturing will receive particular focus, especially in the case of carbon-based and metallic nanomaterials synthesis processes, along with functionalization methods and its influence in the performance of sensors.

2.5.1. Conductive filler manufacturing

In order to meet the huge flexible electronic demands we are witnessing today, researchers are discovering and establishing new nanomaterials for sensing applications. Among them, as discussed before, carbon-based nanomaterials are an attractive alternative to silicon-based materials, due to their known unique morphologies, allied to their electromechanical properties, chemical versatility, and ease of manipulation [63]. However,

their structure and nanoscale significantly hinder attempts to achieve uniform diffusions and control assembly structures in polymer matrices and substrates, making some of the fabrication steps complex tasks [63].

Presently, researchers have developed various manufacturing processes able to improve nanomaterial functionalization and overall better sensing performance, including the usage of more efficient uniform mixing methods along with ordered structures, such as nanofibers, films, yarns, fabrics, and foams, among others, with the sensor's properties shifting depending on the assembly method [62]. Despite composite material-based flexible sensors generally exhibiting lower sensitivities than sensors manufactured from pure nanomaterial sources, polymeric matrices achieve superior stability, sensing range, and linearity. Thus, obtaining stable interactions between the matrix and the conductive nanomaterial reinforcement is crucial for overall sensing performance [62].

Furthermore, with an inherent size range of <100nm, the properties of these nanomaterials mainly depend on their atomic structures. Hence, nanomaterials in general, but especially carbon-based nanomaterials, have emerged and are being marketed as one of the most studied nanomaterials, due to their great potential in applications with electrical conduction, high flexibility, along with sensitivity, such as physical and electrochemical sensing, electromagnetic shielding, supercapacitors, strain and pressure sensing, and anticorrosion coating, among others. This happens due to precise structural arrangements of carbon and sensitivity tuning through surface functionalization of functional groups, which enable high carrier mobility and outstanding crystal structures [63].

In this section, the structure, synthesis methods and properties of carbon-based nanomaterials, including graphene, CNT, CB, and CNF, along with metal nanomaterials, will be presented and discussed.

Starting with graphene, this nanomaterial is considered the building block of carbon-based nanomaterials, with its usage to develop flexible sensors being attributed to its extraordinary electromechanical properties, such as Young's modulus of 1 TPa, high surface-to-volume ratio, along with excellent carrier mobility of 25 $m^2/(V.s)$ and thermal conductivity of 5000 W/(m.K) [63]. Comparable to CNT, graphene can also be employed in sensor manufacturing through covalent and non-covalent functionalization. On the other hand, in order to synthesize graphene, various methods are available today, such as top-down approaches, where chemical and mechanical exfoliation, along with chemical synthesis are included, bottom-up approaches, with available methods being epitaxial growth, chemical vapor deposition (CVD), pyrolysis, among others, along with reduction of graphene oxide, successive intercalation, and CNT zipping [63].

Considering some of these approaches, mechanical exfoliation of graphene is made by repeatedly stripping off graphite fragments with adhesive tape until graphene layers are extracted. Despite this method entrapping graphene layers, it is not favorable to the required mass-scale production, due to its labor-intensive nature [63]. On the other hand, chemical

exfoliation involves the addition of oxygen-containing moieties, a portion of a molecule common to other species, into graphite sheets, employing strongly acidic solutions of potassium permanganate ($KMnO_4$), sulfuric acid (H_2SO_4), or sodium nitrate ($NaNO_3$), in order to obtain GO, also known as the Hummer's method. Regarding the reduction of GO to obtain rGO, this can be done by dispersing GO into aqueous solutions of hydrazine, ascorbic acid, pyrrole, and hydroxyamine, which act as reducing agents. Nevertheless, without proper process quality control, the resulting rGO will present many structural defects, when compared to pristine graphene [63].

Regarding epitaxial growth of graphene, this process requires heating hexagonal silicon carbide substrate to a temperature higher than 1000 ºC to form graphene. Despite being suitable for large scale production of continuous graphene layers, this technique incurs high costs and energy consumption. Therefore, and lastly, chemical vapor deposition has been developed as a way to produce large areas of high-quality graphene sheets with low costs. This method allows the growth of graphene on copper, nickel, and other metal substrates from hydrocarbon gases at temperatures between 600º and 1200ºC [63]. Figure 35 illustrates some of the available graphene synthesis methods employed today.

Passing on to CNT, these are graphitic nanomaterials with cylindrical structures and surface consisting of carbon atoms arranged in a hexagonal-shaped network, with attractive characteristics including great tensile strength, high electrical conductivity and surface area of 50-1350 m^2/g, and an aspect ratio, in this case, the ratio between length and diameter, greater than 1000. Similarly to graphene, CNT presents entirely sp^2 hybridized carbon atoms, with strong covalent bonding occurring between neighboring carbon atoms in the hexagonal structures, while weak Van Der Waals forces occur between different graphene layers [63]. Something to take into account is that these bonds are even stronger than sp^3 bonds, providing CNTs with uniquely high mechanical strength [63]. However, these strong bonds are limited by subpar chemical reactivity with the physical environment, requiring covalent and non-covalent functionalization to promote the dispersion of CNT and minimize agglomerations, in order to achieve superior interfacial interactions between CNT and the matrix [63].

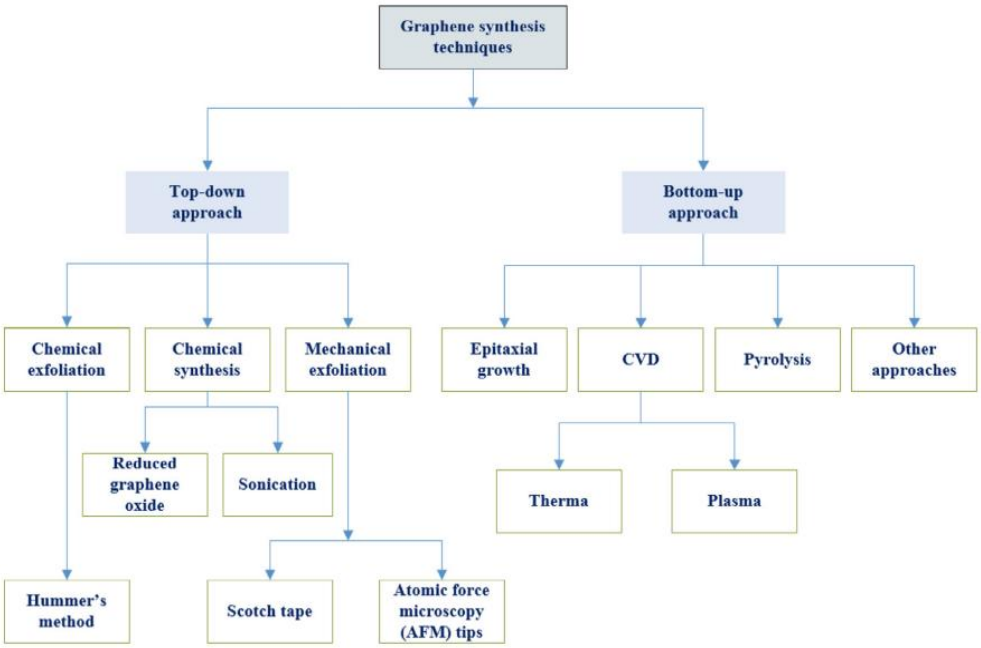

Fig. 35. Process flow diagram of graphene synthesis methods. (Adapted from [63])

When speaking of CNT, we can categorize it as single-walled carbon nanotubes (SWCNT) or multi-walled carbon nanotubes (MWCNT). Beginning with SWCNT, these are formed by rolling a single layer of graphene sheets into a hollow cylinder, with its curvature naturally forming by the rolling movement of the sheet. SWCNT can be further classified with basis on the chiral angle and tube diameter [63]. While diameter typically ranges between 0.5mm and 1.5mm, chiralities are known as zigzag or armchair, depending on the orientation of the carbon atoms around the cylinder. When $\theta = 0^{o}$, the chirality is zigzag type, while $\theta = 30^{o}$ is an armchair type. These characteristics significantly influences the electrical properties of SWCNT, making the operate either as conductors or semi-conductors, depending on the chirality, diameter and manner of rolling [63].

On the other hand, MWCNT are formed by rolling multiple graphene sheets or rolling a single layer of graphene into concentric cylinders, with typical diameters of above 100 nm. Structurally, MWCNT can be categorized depending on the arrangement of graphene layers, with Russian Doll and Parchment models being such examples. Figure 36 illustrates these models. In the former, graphene sheets are arranged in concentric cylinders, while in the latter a single layer of graphene is rolled into the shape of a scroll [63].

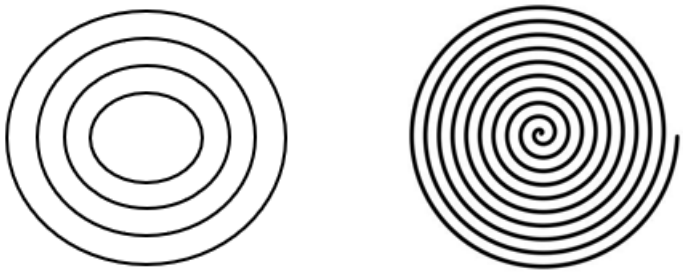

Fig. 36. 2D representation of (A) Russian doll model and (B) Parchment model MWCNT.

Comparing both MWCNT and SWCNT, according to Yee *et al.* [63], the mechanical properties of the first are superior, attracting more attention as a conductive material in strain sensing applications, for example. However, both types can be synthesized by the same techniques, them being laser ablation, CVD, and arc discharge. Considering the laser ablation process, primarily used for SWCNT synthesis, a graphite target material is vaporized by a focused laser beam in an inert gas environment, such as Helium and Argon, with yields of around 70%, also according to Yee *et al.* [63]. Furthermore, CVD method involves the thermal decomposition of hydrocarbon vapor in a quartz tube, at temperatures above between 600 and 1200°C, accompanied by a metal catalyst, generally made of nickel, iron, or cobalt, that coats a substrate. With increased temperature, hydrocarbons such as acetylene, ethylene and methane are broken down into pure carbon, which diffuses towards a heated substrate. Due to high temperatures, the carbon-containing gas gradually grow CNT in the metal catalyst's surface [63]. Therefore, the CVD method is commonly used in the scaling up process of CNT production due to lower cost and energy requirements, along with high yield and process parameters ease of control. Generally speaking, lower temperature-CVD (600°C-900°C) synthesizes MWCNT, while higher temperature-CVD (900°C-1200°C) yields SWCNT [63].

Lastly, in the arc discharge technique, CNT are produced by striking electric arc between two graphite electrodes, acting as a negative cathode and a positive anode, in an inert atmosphere. This electric arc vaporizes carbon in the cathode at a temperature greater than 3000°C, in order to grow CNT. To support this process, inert atmospheres of Argon or Helium are commonly employed, with good quality yields of around 90% [63].

In conclusion, despite both laser ablation and arc discharge approaches being able to synthesize high quality CNT with yields up to 70% and 90%, respectively, these methods have inherent limitations, such as the high cost of the target graphite materials and high energy consumption, especially in the case of laser ablation, where the creation of a high-power laser beam is needed, along with impurity issues in the resulting CNT. In order to solve these challenges, researchers developed the CVD method, an approach that has a lower cost and energy consumption, with high yields of CNT [63]. A brief summary of these methods is available in Table 2.

Table 2. Comparison of laser ablation, arc-discharge and CVD methods, for CNT synthesis [63].

Variables	Arc Discharge	Laser Ablation	CVD Method
Growth Temperature	>3000 °C	1200°C	600-1200°C
Availability of Carbon Source	Low	Low	High
Energy Requirement	High	High	Low
Process parameter control	Difficult	Difficult	Easy
Yield of CNTs	Up to 90%	Up to 70%	95%-99%

Another employed nanomaterial is carbon black (CB), which consists of colloidal particles of pure elemental carbon, mass-produced by incomplete combustion and vapor-phase pyrolysis of liquid hydrocarbons or heavy gaseous, under controlled conditions. Carbon black is different, at the physical level, from black carbon, presenting higher elemental carbon content as well as well-controlled properties, being an asset in numerous applications, including tires, pigments, vehicle parts, plastics, batteries, sensors, and supercapacitors [63]. Regarding the physical appearance, CB is a spherical-shaped, fine powder of carbon particles, with particle size lesser than 50 nm but superb surface area, greater than 1000 m^2/g, along with density of 2.25 g/cm^3 [63]. Considering composite materials, employing CB as filler enables enhanced mechanical strength, better light absorbency, along with UV resistance. According to Afsarimanesh *et al.* [61], strain sensors which employed composites with this composition achieved stretchability of up to 500%, with superb durability, since 10000 loading-unloading cycles produced negligible variation in operation.

Commercially, manufacturing CB can be categorized in 4 main types of processes, them being gas furnace process, oil furnace process, thermal process, and channel process [ae].

Furnace processes are used mainly to synthesize microscopic CB particles through the introduction of heavy petroleum, in the form of oil and coal, as feedstock into a hot gas stream for partial combustion. While released residual gases, such as carbon monoxide and hydrogen, can be used to produce electric power or heat, this method is suitable as a mass production approach, thanks to its high yield and control of particle size [63].

Lastly, carbon nanofibers (CNF) are cylindrical nanostructures with graphene layers arranged in stacked cones. CNF have high aspect ratio, enabling the formation of effective conductive networks at extremely low percolation concentrations. Along with this, this nanomaterial also exhibits superior mechanical properties, high chemical stability, and good electrical conductivity, ideal for nanocomposite and sensor applications [63]. According to Yee *et al.* [63], generally, CNF have a typical diameter of 50-200nm, larger than CNT, thermal conductivity of 1950 W/ (m.K), electrical resistivity of 1 x 10^{-4} Ω.cm, aspect ratio of between 250 and 2000, along with tensile strength of 2.92 GPa and tensile modulus of 240 GPa.

Since the overall structure and properties of CNF depend on the way graphene layers are stacked together, electrospinning and CVD are the two main options for the synthesis of this nanomaterial. Regarding electrospinning, CNF are obtained by spinning a polymeric solution under high voltage, leading to the polymer solution's ejection from a syringe tip onto a rotating collector. Due to the high values of voltage, a Taylor cone tip is formed in the polymer solution droplet. With a further increase to the electric field, a charged polymer jet is ejected from the Taylor cone tip, being chaotically attracted by the collector due to electrostatic forces, producing randomly ordered CNF [63]. This process is followed by a carbonization step, performed in an atmosphere without oxygen, in order to fully form CNF. On the other hand, in the CVD method, as previously explained, CNF are typically produced via pyrolysis of methane, acetylene, among other hydrocarbons, in a metal catalyst, at high temperatures. Similarly, to CNT synthesis, in this case, CVD method is a reliable and auspicious technique for CNF mass production, with the advantage of achieving well-defined diameters, at relatively low cost [63].

Shifting the focus from carbon-based nanomaterials, metal nanomaterials, metal precursors, and organometallic compounds can also be employed as conductive fillers or conductive ink in sensing applications. Presently, nanomaterials such as silver, gold, and copper, among others, are used thanks to their good electric conductivity, with potential for commercial applications. Additionally, mixing or creating hybrid materials from two or more of these nanomaterials can provide improved electric conductivity and stability, useful for functionalization with different substrates and matrices, for numerous applications [64].

Presently, a myriad of manufacturing processes for metal nanomaterials exists, including physical, photochemical, and biological methods, along with CVD, microemulsion, and ultrasonic approaches. Starting with the physical method, metal nanomaterials are prepared by heating reactants in a furnace tube at high temperature, via solid phase reactions, where molecules are covalently bound on a solid support material, with the final product being synthesized in the reaction vessel. Thus, reactants are placed in a crucible and vaporized into carrier gas, in order to prepare silver, gold, copper nanoparticles, as reported by Shrivas *et al.*

[64]. Despite the results, this method has some disadvantages, namely consuming large amounts of energy and taking large spaces. Furthermore, to reach thermal stability, more precursor material is consumed than necessary, along with several kilowatts of power being spent to reach the desired operating temperature [64].

Regarding the photochemical method, metal nanomaterials are synthesized by photocatalytic or photoinduced reductions, clean processes that obtain nanomaterials in different mediums, including micelles and emulsion. These photoreductions are carried out at room temperature, in the presence of a capping agent, responsible for binding molecules, at different light sources, including orange, green, cyan, blue, white, and UV. According to Shrivas *et al.* [64], if well-controlled, this method is able to synthesize nanoparticles with long-term stability.

Respecting the biological method, this is one of the greener approaches for metal nanomaterial synthesis, involving natural reduction processes of metal precursors to nanoscale metals. This approach can be divided into two main groups: bio reduction and biosorption. The former involves the use of enzymes and microorganisms to reduce metal ions and obtain stable nanostructured materials, easily removable from such enzymes and microorganisms. On the other hand, the biosorption method works by binding metal ions to cell walls, creating stable complexes, without any energy input for the synthesis of nanomaterials. This can be done with modified cell walls of certain fungi, plants, and bacteria [64].

Furthermore, CVD is a straightforward method used for nanomaterial synthesis, with various controlled shapes and sizes. However, despite its simplicity, the choice of solvent, capping agent, pressure, heating temperature, and reducing agent are crucial for the morphology control of nanomaterials. Some reducing agents presently employed are sodium citrate, sodium borohydride, ascorbic acid, hydrazine, and ethylene glycol. Additionally, the choice of capping agent influences the solubility, reactivity, stability, and dispersibility, along with the size and shape of nanomaterials [64].

Shifting towards microemulsion processes, these are used to synthesize many types of nanomaterials, including metal-based ones. Microemulsion consists of stable dispersions of two immiscible liquids with certain amounts of surfactant. Nowadays, there are two types of microemulsion methods: oil-in-water and water-in-oil. The first forms micelles in the presence of surfactants, with the hydrophilic polar head pointing outwards and the hydrophobic tail pointing inwards. Contrarily, the water-in-oil method forms reverse micelles. According to Shrivas *et al.* [64], most nanomaterials are fabricated through reverse micelle techniques, with the addition of capping agents.

Lastly, synthesizing metal nanomaterials through ultrasound-based methods is a possibility, despite requiring long periods of time. This approach uses ultrasound waves to generate microbubbles in the synthesizing system. Whenever the ultrasound's intensity is higher than the threshold, microbubbles collapse due to the created shockwaves, leading to the decrease in thickness of the diffusion layer, which increases reaction rates, due to improved

reactant transport. In recent times, sonochemistry-related methods have attracted great interest for the synthesis of metal nanomaterials [64].

2.5.2. Sensorial element manufacturing

After developing the topic related to the synthesis of the most commonly used conductive fillers in wearable and flexible sensors today, in this section, the functionalization methods of 2D and 3D sensing structures will be summarized, with additional focus on strain and pressure sensing, due to different requirements needing different functionalization approaches, when compared to other flexible sensors.

Sensing systems based on 2D active films consist of a substrate patterned with nanomaterials with 0D or 1D dimensionalities, on a single or multi-layered periodic structure. Regarding multiple layers, the same procedure can be executed two or more times, in the same substrate, but in different directions. The functionalization methods employed in active film preparation can be classified into coating, electrospinning, assembly, transfer printing, and orientated growth approaches [65].

Beginning with coating methods, due to its simplicity, many researchers employ these techniques in the preparation of active films at large scales. In this approach, nanomaterials such as nanowires, nanotubes, and nanorods, with 1D dimensionalities, are dispersed in coating solutions and deposited in the desired substrate. With the application of a shearing force, nanomaterials that would otherwise show random orientations can assume the desired ones [65]. One of these coating methods is direct coating, where a dispersion of 1D nanomaterials is deposited dropwise on a substrate. During this process, a brush, Mayer bar, or other tool is dragged through the dispersion at a constant speed, aligning the nanomaterials parallelly to the dragging direction, due to the resulting shearing forces created by these tools [65]. Direct coating is a facile method for 2D micro/nanostructure preparation due to the alignment being directly influenced by the solvent viscosity, aspect ratio of the chosen nanomaterials, along with the dragging speed. Despite this, limitations in coating tool technology may limit the entire process, since the regularity of the obtained structures is very poor, with needed nanomaterial realignments post-procedure being common [65].

Another coating method is dip-coating, a process where the desired substrate is dipped into a dispersion of the conductive nanomaterial, followed by their alignment whilst the obtained structure is lifted out of the dispersion, due to gravity. In this method the alignment of the conductive nanomaterials can be facilitated by the flowing solution, depending on the lifting rate of the substrate, the solution's viscosity, and the evaporation rate. Considering the wide range of applications, potential candidate substrates, along with low consumption of conductive nanomaterials, dip-coating has gathered plenty of attention in the research community as an effective approach to fabricate films based on 1D nanomaterials. However, one issue that may arise is the lack of alignment control in this method, since the conductive nanomaterials attach themselves to the substrate's surface in a random manner [65].

Passing on to electrospinning, this is a promising method that mainly focuses on the preparation of nanofibers with ultra-high aspect ratios. As previously stated, when a strong electrical field is applied between the metal needle and the collector, the solution containing the desired nanomaterial is dragged towards the collector via electrostatic forces, creating nanofibers. Unfortunately, due to the instability inherent to this process, the produced nanofibers are not aligned and show completely random arrangements. Hence, multiple approaches have been tried in order to align nanofibers produced via electrospinning, including collector modifications, or the application of a magnetic field [65].

Regarding collectors, two types have been employed to prepare nanofiber-based active films. The first approach is making the collector rotate at high speeds, by using a collector with a drum-like shape, which induces the alignment of the nanofibers in one direction, due to the created high shearing forces. However, the rotating speed needs to be carefully calculated, since low rotating speeds lead to poorly aligned nanofiber yields, while too high rotating speeds may break the nanofibers [65].

On the other hand, according to Lin *et al.* [64], to the collector can be added two parallel electrodes, creating two parallel electric fields, which straighten the nanofibers, making them exhibit an alignment angle of between 60º and 90º, relatively to the electrodes.

Regarding assembly functionalization methods, these work by inducing arrangements and aggregations of previously randomly oriented nanomaterials by applying external forces, such as electric fields, tensile stress, and shearing forces, among others, or creating attractive and repulsive interactions between the conductive nanomaterials, producing a yield of well-aligned films with regular patterns [65].

Contrarily to above-mentioned methods, especially coating methods, which exhibit films with conductive nanomaterials poorly aligned, without regularity, in this method, their orientation can be directly controlled through external forces, with significantly higher regularity. Furthermore, the application of electromagnetic fields have the ability to assemble conductive or semiconductive nanowires, generally made of gold, silver, silicon, or zinc oxide, and other nanomaterial dimensionalities into aligned and organized structures [65].

Another approach is transfer printing, where previously synthesized conductive nanomaterials, usually with random orientations, are detached from a donor substrate, reorganized, and placed onto a receiver substrate, yielding aligned nanomaterial patterns. Transfer method can work by directly contacting the receiver and donor substrates, or by using a stamp as an intermediary.

According to Lin *et al.* [65], ideally, any transfer printing process should meet two key requirements: achieving the desired nanomaterial alignment on the receiver substrate's surface and making sure the nanomaterials readily detach from the donor and adhere to the receiver. Regarding the first requirement, a manufacturing design that employs external forces, such as friction or capillary forces, as a support mechanism can enhance the nanomaterials' overall

alignment. In order to accomplish the second requirement, the entire process depends on the following expression [65]:

$$G_{material/receiver} > G_{material/stamp} > G_{material/donor} \quad (4)$$

where G is the adhesion strength of the nanomaterial to each one of the elements of the process. Only by respecting this expression can we achieve defect-free transfer of the nanomaterials to the receiver substrate. Despite finding materials that fit this requirement being a difficult task, some physical strategies may ease the entire process, namely the usage of blade-shaped stamps and gecko-inspired structures. Due to increased contact area between the nanomaterial and the blade, there is an observable higher adhesion to the blade, when compared to regular stamps, which press nanomaterials perpendicularly. Moreover, nanomaterials had the tendency to detach from the blade-like structure when it retracted, according to Lin *et al.* [65].

In conclusion, active films prepared via transfer printing exhibit well-aligned conductive nanomaterials, despite complications regarding size limitations of the stamp, receiver, and donor substrates, along with structural modifications on the stamps and donor substrates [65].

Figure 37 illustrates the previously mentioned functionalization methods, which enable the production of active sensing 2D films.

Shifting the focus towards 3D sensing structures, these can be fabricated from 3D micro/nanomaterials, such as domes, spheres, pyramids, walls, rods, pillars, sheets, among others. Additionally, hierarchical structures can be obtained by surface modifying the nanomaterials. The main methods employed to manufacture 3D sensing structures are epitaxial growth, template methods, carved templates, and bionic approaches [65].

Starting with epitaxial growth, nanomaterial synthesis can be achieved through hydrothermal methods, where the substrate is immersed into a solution of the desired nanomaterial, until seeds are formed on it. This is followed by continuous *in situ* growth and calcination or annealing treatments, leading to the formation of 3D nanomaterial structures [65]. Considering this approach, the *in situ* growth is mainly influenced by the reaction's time and temperature, along with the nanomaterial of choice, parameters that control the general morphology of the structure [65]. In order to obtain hierarchical structures, epitaxial growth can be executed twice.

In conclusion, epitaxial growth is a relatively simple method for the synthesis of 3D active structures, due to the low number of required steps, being a suitable candidate for large-scale production and applications. Despite this, to achieve desired growths, long reaction times and a large amount of reactants are needed. Furthermore, manufacturing highly uniform structures may prove a difficult task via epitaxial growth [65].

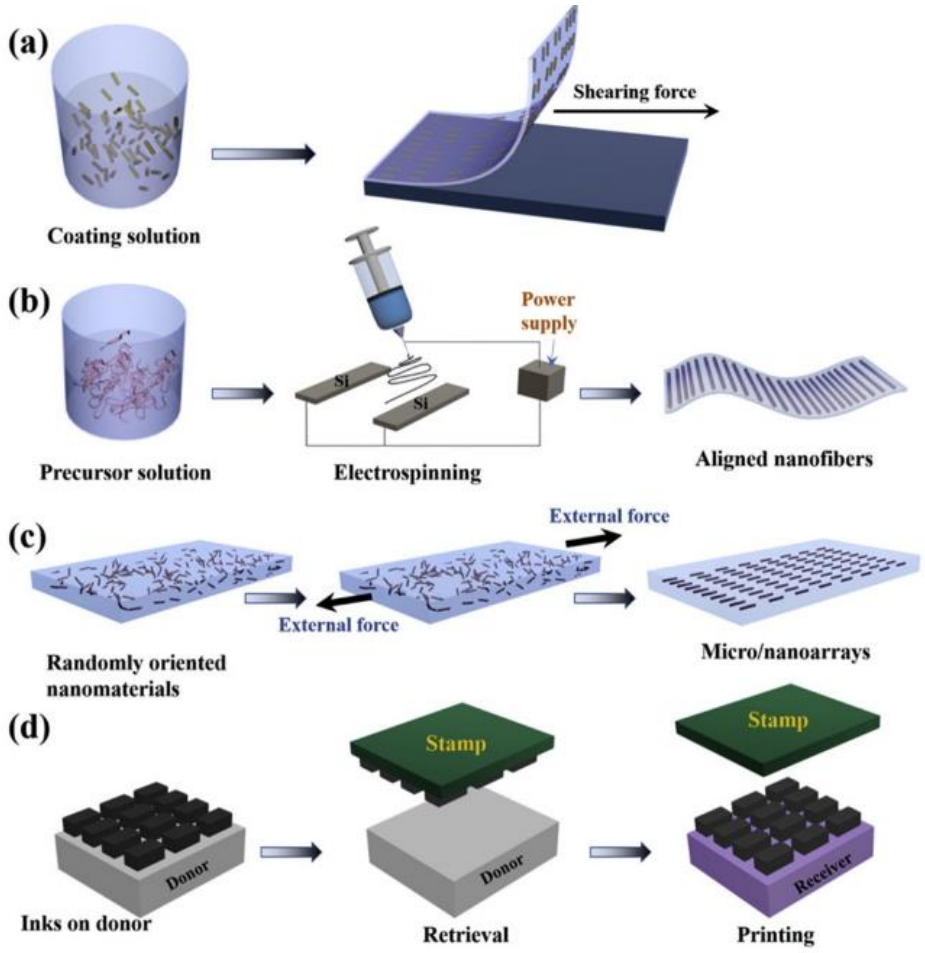

Fig. 37. Preparation of 2D active sensing films, by functionalization through various methods: a) coating; (b) electrospinning; (c) assembling; (d) transfer printing. (Adapted from [65])

Regarding template-based methods, the support given by a template enables the deposition and growth of nanomaterials along the same direction, forming desired patterns, followed the template's removal when the process is concluded. Anodic aluminum oxide (AAO) is the most used template in this method, especially for the preparation of pillar-shaped structures. This is the case due to the post-modification-friendly pore size of the templates, usually between 10-400 nm, along with rigid pores, which are densely packed, allowing for the formation of well-defined nanostructures. Furthermore, the high thermal stability of AAO grants physicochemical processes to take place at high temperatures, while the AAO's hydroxylated pore walls allow for an adequate infiltration of polymer solutions [65].

Whenever a polymer solution is cast onto an AAO template, the solution quickly permeates and yields solid polymer nanopillars, after the solvent's evaporation. Thus, this approach has exceptional potential for self-powered sensor applications [65].

Furthermore, we can also manufacture templates with complex nanostructures, including nanopillars and pyramids, through carving technologies such as photolithography.

However, due to the inherent high cost and complex nature of this process, simpler methods are being researched, including drilling holes on hard substrates to prepare templates, according to Lin *et al.* [65].

On the other hand, bionic templates use structures found in nature, such as leaves and petals, due to their versatile and aligned nanostructures, optimal candidates as natural templates. Some examples of this are the surface of lotus leaves, which present a great number of micro papilla-like structures on their surface, along with *Acacia mill.* leaves, which have needle-like microstructures with high aspect ratio, since the diameter is around 25mm and the length is ≈300mm. According to Lin *et al.* [65], after lotus leaves are dried to a certain point, their inner structure and surface morphology can be retained, in order to be used as templates for dielectric layer manufacturing, for sensorial system applications [65].

Changing the subject to strain and pressure sensing, where some of the functionalization approaches are different, common methods to achieve flexibility and stretchability with proper sensing performance involve the dispersion of conductive fillers inside an elastomeric matrix. These include shear mixing, *in situ* polymerization, and solution mixing. Regarding the last, researchers choose surface functionalization and the addition of surfactants to achieve more uniform dispersions. However, and naturally, all methods have their own advantages and disadvantages [57].

Depending on the composite's desired morphology and shape, there is the possibility of further processing it, through spinning, compression molding, extrusion, and film casting methods. Something to take into account is that the transduction mechanisms of these composite materials can be adjusted by variating the conductive filler's concentration in the matrix, which leads to different interactions between the two and resulting in different conductive network morphologies. Thus, researchers need to make a compromise between sensitivity and conductivity with stability and mechanical stretchability, in order to achieve good performance and optimization in both fields [57].

Additionally, this type of sensor can also be produced by assembling entire conductive layers on top or inside flexible substrates and matrices. Regarding their deposition, this can be achieved through already discussed methods, but also others are included, such as drop-casting, dip-coating, bar coating, spray coating, Meyer rod coating, spin coating, printing, and infiltration [57]. On the other hand, strain and pressure sensors with embedded conductive layers in flexible substrates, are much better suited for flexible electronic applications, despite limitations regarding the environment-friendliness of some methods, complications in controlling the film's uniformity, and bonding interaction-related issues between the conductive filler and the matrix still existing, which could lead to the conductive layer's delamination [57].

In this second category, where conductive materials are encapsulated in the flexible matrix, there are two possible functionalization approaches: the first mainly depends on the blending of two or more elements, including processes like coating, infiltration, transfer and filling, or more complex multi-step approaches, which involve these and other processes, in order to obtain specific structural designs, for enhanced electrical conductivity or mechanical

behaviour [57]. The most important factor to take into account is that there is always a compromise between complexity and obtained results, where more complex methods are time-consuming, but may yield sensors with high sensitivity and low hysteresis, while simpler fabrication approaches are quicker but may exhibit poorer sensing performance [57].

Therefore, in conclusion, despite the proper selection of matrix and conductive filler being imperative to achieve optimum performance, the functionalization and manufacturing methods are the ones responsible for the strongest impact in the sensor's final performance. For these reasons, researchers today are investigating more cost-effective, mass-producible, and practical methods, while retaining some simplicity and not being time-consuming, in order to produce the next generation of flexible sensors, with higher degrees of stretchability, sensitivity, durability, stability, and low hysteresis [57]. Figure 38 illustrates the methods used to produce carbon-based nanomaterials, mentioned and discussed throughout this subchapter.

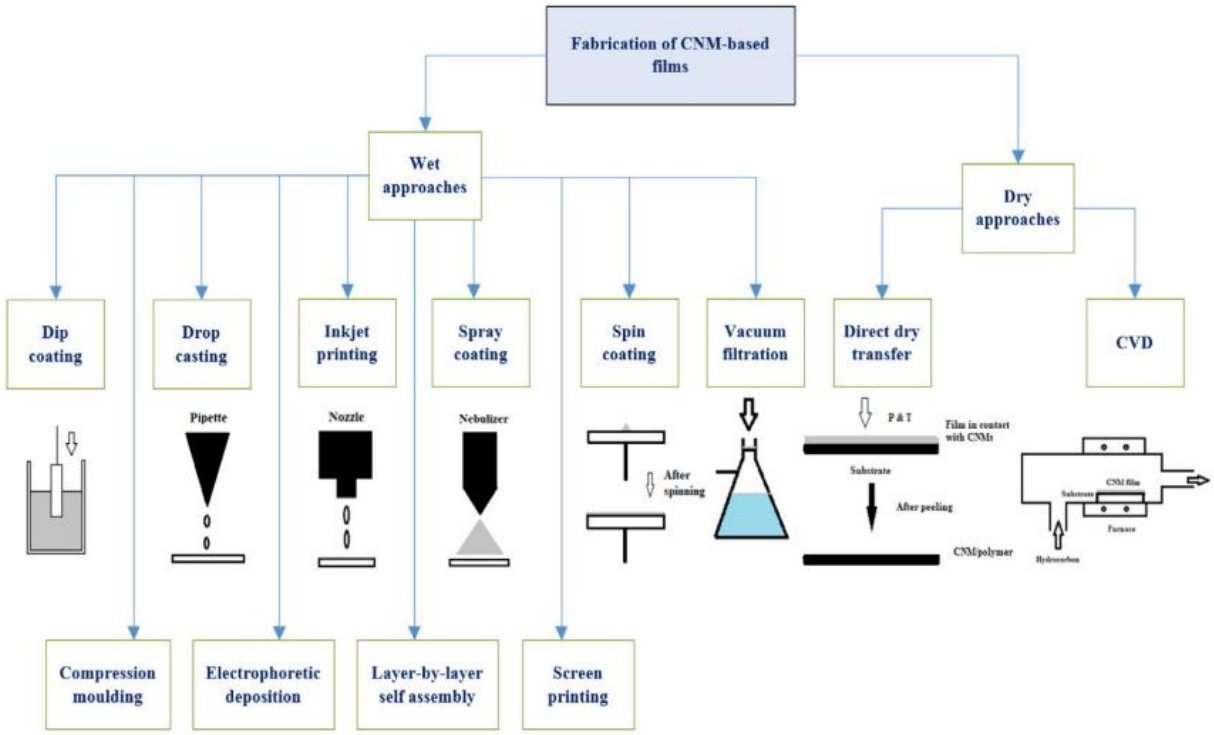

Fig. 38. Fabrication methods for carbon-based nanomaterials (CNMs). (Adapted from [63])

2.6. Experimental studies

After discussing, throughout this chapter, the main types of employed sensors in sensing and sensorial system applications, along with the working principles and manufacturing approaches which receive most attention by the research community. In this subchapter, an updated compilation, gathering published works in the last five years, is available, where only

publications regarding the usage of temperature, humidity, strain/pressure, and sweat sensing, for sensorial system applications, were considered.

This is the case in order to better comprehend researchers' preferences considering various factors, namely chosen materials, preferred working principles, fabrication and functionalization approaches, along with the desired application for the produced sensor.

Additionally, this subchapter will also summarize each sensor's resulting performance, to better *visualise* the correlation between the chosen parameters/characteristics and the achieved results.

Starting with temperature sensors, Ben-Shimon and Ya'akobovitz [66] developed a flexible and biocompatible temperature sensor based on a PDMS@CNT composite, for body temperature monitoring. In this work, these researchers demonstrated the potential of these on-skin applications by using a CNT forest design to sense thermal variations between the matrix and the reinforcement, inducing changes in electrical resistance. Additionally, the chosen working principle leads to a simpler fabrication process and sensing scheme, along with excellent performance, biocompatibility, and stability and reproducibility during long-term operation. Furthermore, the sensor showed high recoverability for both mechanical loads and sequential thermal loads. The produced sensor exhibited a sensitivity up to 0.01 Ω/ºC and a stable Young's modulus of ≈0.1MPa at 100ºC. Compared to other sensors, this one has higher sensitivity, compared to the average ≈1 Ω/ºC presented by other works, with 35ºC and 38ºC showing electrical resistances of 101.1 Ω and 99.6 Ω, respectively.

In Chen *et al.* [67], a fast-response flexible temperature sensor was fabricated by drop-coating based on laser-reduced GO, for contactless human-machine interfaces. This work sought to study the influence of both processes, along with GO concentration, in the final sensitivity and response times. Hence, the produced sensors showed good linearity, stability, small hysteresis, good repeatability, and response times of 0.196s and 0.274s, for sudden temperature rises and drops, respectively, shorter than most rGO-based temperature sensors, according to the researchers. Additionally, the sensor was able to monitor human breathing, detect blowing and human fingertips, along with contactless unlocking a phone's code lock. Results showed that a GO concentration of 4mg/mL exhibits the highest sensitivity, 0.37%/ºC, between 30ºC and 100ºC, and superior linearity, R^2 = 0.996, relatively to other parameter combinations. Additionally, the produced device has a recovery time of ≈9.7s and good temperature response characteristics, in heating-cooling cycles, in the 30ºC-50ºC range.

In Zhu *et al.* [68], a flexible temperature sensor based on a TPU@SWCNT composite was developed by solution blending and thermal annealing, for respiration monitoring, distinguishing between deep breathing and normal breathing, along with non-contact temperature detection applications. The prepared sensor exhibits a relatively linear NTC effect in the temperature range of 30ºC-100ºC. Additionally, it has excellent reproducibility, high reliability, and an accuracy of ±0.1ºC, without its thermal response being influenced by deformation and heating rate, after at least 200 bending cycles. Regarding composite manufacturing, it was observed that the electrical conductivity is increased and stabilizes after 2

hours of thermal annealing. Moreover, relative resistance variation decreases linearly with temperature increments, exhibiting an NTC effect, with SWCNT contents of 0.25wt.% and 0.5wt.% showing more dependance of relative resistance variation on temperature, exhibiting higher sensitivity than other SWCNT contents. Lastly, the sensor also possesses electrical resistance to infrared radiation, due to the excellent thermal effect of SWCNT.

In Wang *et al.* [69], a wearable and flexible temperature sensor was developed by integrating polybutylene terephthalate (PBT) with rGO and CNT, via ultrasonication, hydrothermal reduction, and dip-coating, for human body and environment temperature monitoring applications. The produced sensor was able to detect the body's temperature while placed in the forehead, palm, and back of hand, along with temperature variations caused by blown air, cementing its potential in human medical field and daily temperature monitoring. By using these methods, both rGO and CNT were uniformly loaded onto the PBT's surface, forming a continuous and stable conductive network with high sensitivity, -0.737% / ºC, linearity, R^2 = 0.98, and accuracy, 0.1 ºC, between 25 – 45 ºC. Moreover, a response time of 31 s, stability within 300 s and good repeatability were also observed, while monitoring human body temperature from 37 ºC and 38 ºC, respiratory rate, and detecting ambient temperature in the 25 – 45 ºC range. Compared to pristine PBT, the mechanical properties of the sensor were improved, along with long-term stability, a signal of good circularity.

In Geng *et al.* [70], a wearable and tunable temperature sensor was produced through the integration, by solution blending, of acrylate copolymer, fabricated by radical polymerization, with CB, for smart, wearable and adjustable temperature sensors applications. The assembled sensor has an accuracy of 0.5 ºC, high sensitivity, with relative resistance variation of 12.5% per 0.5 ºC, fast response times, with a cold and hot cycle taking 20 s, stability throughout 200 heating cycles, and resistance changes by nearly 3 orders of magnitude, when the temperature changed from 33 ºC to 40 ºC. Apart from this, the sensor is highly sensitive to temperature variations in a wide range of values, with a resistance change of more than 4 orders of magnitude at temperature changes from 25 ºC to 40 ºC. Since these characteristics enable temperature monitoring in real-time, researchers also integrated a LED bulb on the device, which turns on or off according to increased or decreased temperature.

Shifting to humidity sensors, Zhao *et al.* [71] produced a single-sided, flexible, non-toxic, and breathable humidity sensor based on a PVDF@PANI composite, for breathing and speaking monitoring applications. PANI was unilaterally deposited on a PVDF microporous matrix by *in situ* polymerization, showing good humidity sensing properties at room temperature, including small hysteresis (≈5%RH), detection range of 11-98%RH, relative resistance variation up to 226%, along with a reversible, fast and stable response, even under bending deformation. The unilateral deposition of PANI minimizes the contact between the material and human skin, preserving the humidity sensing characteristic of the former, while averting harm to the latter. Furthermore, the functionalization method avoids the need to further integrate a patterned interdigital metal electrode in the structure. The prepared 0.01

mol/L-PANI/PVDF humidity sensor, when compared to other sensors, shows hysteresis and response times comparable or superior to other reported flexible sensors, while showing stable responses during deformation, rarely found characteristic in flexible humidity sensors.

In Yoshida *et al.* [72], a printed, flexible humidity sensor, based on a dry-blended cellulose nanofiber/graphene nanoplatelet (GNP) composite ink, screen-printed on a PEN substrate, was produced for human respiration and skin moisture monitoring applications. This sensor exhibited showed a high resistive response of 240% over the relative humidity range of 30-90%RH, with response and recovery times of 17s and 22s, respectively, along with good mechanical flexibility. Due to the abundancy of cellulose and GNP in nature, this work aimed to manufacture a cost-effective, eco-friendly, degradable, and biocompatible humidity, with high performance. Regarding the composite ink's production, GNP was easily dispersed in the cellulose nanofibers using a planetary centrifugal mixer, without sonication or other complex surface modifications, in order to preserve the composite's ability to be screen-printed. Furthermore, the need for electrode integration was eliminated, since the composite ink was used as both sensing layer and electrodes, eliminating the need for gold and silver. Due to these factors, allied to a relative resistance variation of 2.4 along the 30-90%RH range, these researchers concluded that the produced sensor is a promising candidate in the new generation of IoT technologies.

In Guo *et al.* [73], a self-powered flexible humidity sensor based on a unique sandwich structure of PVA/nanocarbon powder (NCP)/$MgCl_2$, produced through solution casting, for human respiration monitoring applications. The sandwich structure allowed this sensor to readily adsorb and diffuse water molecules from the environment, achieving a response linearity of R^2 = 0.9978, response and recovery times of 6s and 11s, respectively, sensing range of 11-98%RH, stability for over 30 days, along with high voltage and current outputs, of ≈0,6V and ≈2.3 μA, and a calculated power of ≈1.38 μW, at RH 98%. Additionally, due to the good water solubility properties of PVA and $MgCl_2$, the sensor can be recycled and reused with up to 90.31% of the original response voltage value, dramatically minimizing material waste and reducing overall manufacturing costs. Along with this, researchers also managed to integrate the sensor in a mask for human respiration monitoring, distinguishing between different breathing rates and patterns, along with human speech and coughing detection.

In Liang *et al.* [74], a flexible humidity sensor, based on a pre-stretched PDMS substrate integrated with rGO has been developed for breathing patterns and respiration monitoring applications. The sensor was produced with rGO in a wrinkled structure, which improves both response and recovery times, while also preventing water aggregation and condensation, along with shortened water adsorption and desorption times. Additionally, this structure gives flexibility whilst maintaining the sensor's characteristics during deformation. Thus, this sensor is suitable for on-skin monitoring applications. Regarding results, researchers have concluded that rGO thickness is correlated with response and recovery times, where response and recovery times can be further sped up by reducing the thickness of rGO. Thicker rGO exhibited response and recovery times of 6 s and 7.5 s, respectively, while thinner rGO had response and recovery

times of 2.4 s and 1.7 s, respectively. Moreover, stability and repeatability were achieved for more than 30 cycles, along with high sensitivity in the 11 – 95 % RH range. Furthermore, maximum wet hysteresis was observed at 85% RH, with the maximum value being 3% RH, proving the capabilities of wrinkled structures.

In Li *et al.* [75], a capacitive humidity sensor, based on a indium oxide (In_2O_3) and GO film integrated on an epoxy substrate, was developed for breathing pattern and respiratory disease, including asthma and other complications, monitoring applications. This device exhibits portability, accuracy, instantaneity, and low power consumption, along with other characteristics that were improved, when compared to pristine In_2O_3 or GO, including high stability, repeatability, lower response and recovery times, and higher sensitivity. Regarding results, humidity sensing capabilities were investigated over a 11 – 97% RH range, at 20 ºC. As RH increases, researchers observed a real-time significant increase in the sensor's capacitance response, with especially high sensitivity and capacitance value changes at lower RH values, between 11% and 23%. Along with this, the response and recovery time of the composite film was shorter than single materials, at 15s and 2.5s, respectively. Lastly, the maximum hysteresis value was 0.054% RH, observed at 85% RH.

Considering strain and pressure sensing, Du *et al.* [76] proposed a systematic study on piezoresistivity, electromechanical behaviour, impedance, conductivity, morphology, and Young's modulus, of PDMS@MWCNT composite materials, with crescent MWCNT weight ratios (1 to 10wt.%), produced by dry blending followed by mold casting, with the aim of monitoring human motion, such as finger, foot, and arm movement, with large strain, up to 40%. Study results showed that the composite's piezoresistive sensitivity had an inverse relationship with weight ratio increments of the conductive reinforcement, with MWCNT at 8wt.% showing the best sensitivity and linearity at 40% strain. Thus, this was the chosen weight ratio for further tests, regarding body movement measurements. Additionally, by employing the dry blending method, the percolation threshold was reached at ≈2wt.%. For this reason, 3wt.% PDMS@MWCNT composite had the highest sensitivity to strain, whilst, however, also exhibiting a narrowed linear range (15%-25%) and high amounts of background noise, limiting the application of this parameter combination. With the increase of MWCNT weight ratio, both linear range and mechanical properties were dramatically improved. Thus, researchers concluded that 8wt.% PDMS@MWCNT composite shows the widest piezoresistive linear range, between 0% and 40%, while exhibiting a gauge factor of 1.21, suitable characteristics for strain sensing.

In He *et al.* [77], a breathable, durable, sensitive and wearable piezoresistive strain sensor based on a hierarchical microporous PU@CNT composite film was produced by NIPS method followed by dip-coating, for deglutition, speech, and human motion monitoring applications. The produced sensors were approximately 8 times more permeable to both air and moisture, the hysteresis related to the operation of these sensors was optimized up to 67.8%, while the structure was stable and durable for more than 8000 cycles. On the other hand, the

fabrication method is relatively simple, controllable and requires low amounts of energy. Regarding specific parameter combinations, the air permeability of 10%PU@CNT composite film was 867.76% higher than pristine, non-porous, PU films, while its moisture permeability was 801.48% higher than the non-porous film. Something to take into account is that moisture permeability does not affect the sensor's piezoresistive response. Furthermore, with PU concentration increments, the overall electrical resistance of the composite film decreased, with maximum sensitivity reaching a value of 51.53 kPa^{-1}, at 3kPa. Lastly, to test the sensor's performance in long-term e-skin applications, the sensor was successfully applied in the detection of pulse vibration, throat movements during vocalization and deglutition, along with finger movements, including bending, pressing, and gripping.

According to Wang *et al.* [78], a novel flexible strain sensor based on a PDMS@rGO conductive elastomeric composite was manufactured by latex film forming for the first time, when this work was released. They achieved the formation of a 3D conductive network with a ultra-low amount of rGO, 0.44vol%, allowing for more mechanically robust and flexible composites. Furthermore, due to the matrix's elastic behaviour, the enhanced destruction and reconstruction process of the conductive network under stimuli granted the sensor with excellent sensitivity. Regarding results, the achieved gauge factor was 6.52 for strain range within 100%, 14.67 for 100-180%, 24.64 for 180-230%, reaching a peak value of 44.01 at 230-300% strain. Additionally, the sensor also exhibited good stability for 2500 loading-unloading cycles. Furthermore, the resistance changes, under strain, at a frequency of 0.025 Hz, with cyclic stretching and releasing the sensor under 10-120% strain led to proportional and linear increments of the relative resistance variation, an indicator that the sensor has the ability to distinguish different applied strain. Moreover, the sensor exhibited a response and recovery time of 165ms and 248ms, respectively, at 100% strain, along with successful physiological signal monitoring from the human body, detecting delicate human motions, such as bending fingers, facial expression changes, vocal cord vibration, pulse and speaking. Lastly, the chosen fabrication method is generic, scalable, eco-friendly, and cost-effective, contributing to its commercialization potential in the near future.

In Herren *et al.* [79], a strain/pressure sensor was fabricated by dispersing CNT in a PDMS matrix, allied to a novel microwave-based porogen removal technique, which is capable of obtaining porous sensors with tailorable porosity, piezoresistivity, and electromechanical properties, for human motion monitoring applications. Despite all CNT loadings demonstrating similar piezoresistive performance, sensors with CNT at 3 wt.% exhibited the highest average sensitivity, along with a gauge factor of 4.8 and a minimum compressive strain detection of 2%, the highest among the samples. This CNT loading displayed the most extensive conductive network, an essential factor that contributes for more reliable connection with the electrodes. On the other hand, lower porosity sensors exhibit long-term durability and minimal strain rate influence, while displaying greater energy absorption and recovery than more porous sensors, in the 5 – 50% strain range. Moreover, in the 10 – 15% strain range, the reported gauge factor was comparable to other nanocomposite-based sensors. Taking this into account, researchers

concluded that highly sensitive and low porosity sensors exhibit the necessary characteristics for skin-attachable sensors in dynamic human motion detection and monitoring applications. Thus, both step-sensing detection and compression measurements were conducted in a prosthetic hand, along with sensors being attached to elbows, knees, and chest, for breathing, walking, running, joint bending, and throwing motion monitoring, with successful outcomes.

In Mu *et al.* [80], a strain/pressure sensor was fabricated with basis on a PDMS@Carbon nanocapsules (CNC) composite material, through a NaCl-based template method, with the aim of combining high sensitivity with a broad detection range, due to the production of a multi-level porous structure, for human motion monitoring and intruder detection applications. By combining the excellent electromechanical properties of CNC with the flexibility and toughness of PDMS, the developed sensor exhibits a positive resistance change under a pressure detection range from 0 – 450 kPa, a maximum gauge factor of 150.7, stability for at least 2000 loading-unloading cycles, along with detection occurring in the 0 – 20% strain range. Additionally, the sensor is able to operate without compromising the human body's regular daily activities. Considering results, the flexible composite film displays excellent mechanical response to bending, stretching, and twisting motions, along with high elongation at break in the 82 – 124 % range and Young's modulus of up to 110 kPa. Moreover, by adjusting the ratio of CNC and NaCl template, the film's conductivity and sensitivity can be tuned, since the hollow structure, inherent to CNC, provides superior mechanical behaviour, acting as a stress absorbing structure. Hence, the produced sensor could detect finger and wrist bending motion without disturbing the user's activities. Along with this, its structural design allows for a flexible sensor with broader range, while retaining high sensitivity.

Changing the subject to sweat sensing, in Parlak *et al.* [81] an electrochemical transistor was integrated in a synthetic and biomimetic SEBS@PEDOT:PSS polymeric membrane, by laser patterning and spin-coating methods, acting as a molecular memory layer for stable and selective recognition of cortisol levels, the human stress hormone. The device was fabricated on a SEBS elastomer substrate, allowing for a wearable sensor with superior flexibility and stretchability, which enables more precise sample acquisition and delivery to the sensor's interface. The produced device was successfully used in both *ex-situ* skin-like microfluidics and human subjects with real-sample analysis. The molecularly selective device showed high physicochemical stability at body temperature, along with resistance to induced physical deformation, when applied over the expected and tolerated conditions, which were similar to the ones found in the normal motion range of the human epidermis. Furthermore, laser-patterned sweat channels and reservoirs were able to absorb and collect sweat, providing stable and reliable readings, while also preventing direct mechanical contact between the skin and the sensor.

In Payne *et al.* [82], this work reports the development, optimization, and characterisation of a amperometric enzymatic-based sensor, for lactate-level monitoring applications. Therefore, researchers chose lactate oxidase as the sensing mechanism while TTF

operated as the mediator, reaching optimized results for sporting applications. The sensor showed linear range up to 24 mM lactate, and a sensitivity of 68μA.cm^{-2}/mM, when accounting for the sensor's surface area. Regarding results, researchers observed that sodium chloride (NaCl) and potassium chloride (KCl) concentrations decreased enzyme activity and resulting electrical current, consequently affecting the sensor's performance. Moreover, increments in $CaCl_2$ concentration induced nonlinear variations in sensor performance and enzyme activity. In the produced sensor, lactate concentration variation corresponded to a current change of approximately 10μA. Additionally, when measuring current changes induced by salt interference, they observed the values were lower than the necessary threshold to distinguish between aerobic and anaerobic metabolism. For these reasons, while the advantages this sensor are relevant, the accuracy of blood and spectroscopic sweat testing cannot be overtaken by the device. Nevertheless, with only variations in lactate concentration influencing the enzyme activity in the sensor, the sensor manages to circumvent possible interferences caused by other electrochemical reactions, functioning as a good indicator of the transition between aerobic and anaerobic metabolism. Hence, according to the researchers, it is unlikely that enzymatic lactate sensors will be able to operate in continuous health monitoring applications.

In Hartel *et al.* [83], a fully screen-printed ion-selective electrode and electrochromic self-powered sweat sensor was reported, for sweat lactate monitoring applications. The produced sensor exhibited reversible and vigorous colour changes, over ten cycles, depending on concentration and time profiles. Further results showed that the device has potential for on-skin continuous lactate-level monitoring with readily reversibility, ease of fabrication, and simple colourimetric read-outs. Moreover, the sensor operated and adapted to different analyte concentrations, covering the entire physiological range, with power generation up to 13 μW/cm^2, double the amount to successfully bleach the electrochromic display within two minutes. These results, including self-generation of power by sweat, ease of data read-out, mass-production potential, and stable reversible electrochromic performance demonstrated the device's potential for practical applications, according to the researchers, with possible expansion to other enzymatic sensing systems, such as ethanol monitoring, to promote safer driving, or glucose monitoring for diabetic patients.

In Zheng *et al.* [84], a flexible and wearable cloth-based sweat sensor was developed by multi-level screen-printing and drop-coating, for glucose-level analysis applications. The produced sensor exhibits excellent sweat collection and transport channels, actuated by a microchannel network equipped on the sensor's bottom side, helpful to collect flowing sweat on the skin's surface, along with shortened sweat collection times, due to the use of capillary forces in order to efficiently absorb the biofluid, a simple and cost-effective approach achieved by today's screen-printing technology. In optimal conditions, the sweat sensor can measure the concentration of sweat glucose in the 0.05 – 1 mM range, with a sensitivity of 105.93 μA/ mM/ cm, for up to 9 hours, along with excellent selectivity, reproducibility and stability. Additionally, the sensor's output is consistent with the results given by glucose kits. In conclusion, researchers concluded that the sweat collection and transport channels could allow for durable

and stable detection of glucose in sweat, screen-printing and drop-coating methods could easily manufacture sensors at a low cost, and the sensor was skin-friendly and durable thanks to the working electrode avoiding direct contact with the skin. Moreover, under optimal conditions, the sensor exhibited acceptable detection range, sensitivity, reproducibility, stability, and selectivity.

In Xu *et al.* [85], a wearable microfluidic-based amperometric sweat sensor was developed by incorporating PEDOT: PSS and copper in a PDMS matrix, for uric acid-level monitoring applications. According to researchers, the microfluidic device, made of PDMS, is responsible for capturing sweat in real-time, while the conducting and large area PEDOT: PSS enhances the overall flexibility, detects uric acid levels and stores electrolytes. Furthermore, the sensor achieved an ultrahigh sensitivity of 0.875 μA/ μM/ cm and low limit of detection of 1.2 μM. When compared with other uric acid sensors, the produced sensor displayed considerably lower low limit detection and a suitable linear range, in the 2 – 250 μM for uric acid detection in human sweat, between 30 – 80 μM. Thus, it was believed that this sensor had potential for high performance monitoring of biomarkers, metabolites and nutrients. Regarding other obtained results and taken conclusions, the porous structure and large specific surface area of PEDOT: PSS endowed the composite material with excellent electrochemical behaviour, with the largest recorded response to uric acid levels being observed at an applied potential of 0.4 V, along with acceptable levels of background noise. Furthermore, the output signal remained consistent for 50 cycles, demonstrating electrochemical stability, along with long-term stability, since the sensor was also tested across 25 days, retaining more than 95% of the initial signal response to uric acid. Additionally, the sensor's performance was not influenced by the presence of other substances, such as ascorbic acid, lactic acid, glucose, or ethanol, whose concentrations are commonly significant in sweat, displaying the selectivity of the device. Lastly, it takes 166 s to fully fill the microfluidic sweat reservoir, while repeated induced deformations did not significantly influence the sensor's electrochemical performance, both of which are promising characteristics for wearable sensors that can adapt to the user's daily life.

2.7. Overview

Considering the themes and factors surrounding wearable and flexible sensors, namely their key characteristics, essential properties, and working principles, along with the most commonly used sensors in sensorial systems, which employed functionalized matrices and substrates with electrically conductive nanomaterial reinforcements, previous sections and subchapters proceeded with the discussion of the main manufacturing approaches today in use. These mainly focused on conductive nanomaterials and their functionalization with the remaining structure, in order to produce composite materials, with synergic interactions between their elements, or active layers, equally effective in sensing applications.

Taking everything into account, a compilation gathering some published works was made, whose objectives and main characteristics coincide with the aim of this dissertation. Thus, in this section, a table will be constructed, congregating all the discussed works in a more organized and visualizable manner. This table, Table 3, will consider the year the work was published, the employed sensor and key materials, working principle, fabrication approach, desired application and overall final performance. Followed by this, several conclusions will be taken, based on their listed results and collected considerations throughout the state-of-the-art chapter.

Table 3. Featured published works and descriptions in the experimental studies chapter, in flexible and wearable sensors.

Reference	Year	Key Materials	Working Principle	Fabrication Method	Application	Performance
[66]	2020	PDMS@CNT	RTD (Temperature sensing)	CVD + Moulding	Body temperature monitoring	Sensitivity up to 0.01Ω/°C and a stable Young's modulus of ≈0.1MPa at 100°C; The sensor has higher sensitivity, compared to the average ≈1 Ω/°C, with 35°C and 38°C showing electrical resistances of 101.1 Ω and 99.6 Ω, respectively.
[67]	2021	PET@rGO	RTD (Temperature sensing)	Laser-Reduction + Drop-coating	Contactless human-machine interface	Good linearity, stability, small hysteresis, good repeatability, and response times of 0.196s and 0.274s; A GO concentration of 4mg/mL exhibited a sensitivity of 0.37%/°C, between 30°C and 100°C, and superior linearity, relatively to other parameter combinations; Recovery time of

						≈9.7s and good temperature response characteristics.
[68]	2021	TPU@SWCNT	NTC effect (Temperature sensing)	Solution blending + thermal annealing	Respiration monitoring and non-contact temperature detection	Linear NTC effect in the temperature range of 30°C-100°C; Excellent reproducibility, high reliability, and an accuracy of ±0.1°C; SWCNT contents of 0.25wt.% and 0.5wt.% showed higher sensitivity.
[69]	2022	PBT@rGO/CNT	RTD (Temperature sensing)	Ultrasonication + Hydrothermal reduction + dip-coating	Human body and environment temperature monitoring	High sensitivity of -0.737% / °C, linearity of R^2 = 0.98, and accuracy of 0.1 °C, between 25 – 45 °C; response time of 31 s, along with achieved stability within 300 s; good repeatability in the 25 – 45 °C range; overall mechanical properties of the sensor were improved.

[70]	2022	Acrylate copolymer@CB	RTD (Temperature sensing)	Radical polymerization + Solution melting	Smart wearable and adjustable temperature sensors	The assembled sensor had an accuracy of 0.5 ºC, high sensitivity, with relative resistance variation of 12.5% per 0.5 ºC, along with fast response times; stability was observed throughout 200 heating cycles; resistance changes rose by nearly 3 orders of magnitude, when temperature changed from 33 ºC to 40 ºC.
[71]	2021	PVDF@PANI	Capacitive (Humidity sensing)	*in situ* Polymerization	Breathing and speech monitoring	Good humidity sensing properties at room temperature, including small hysteresis, detection range of 11-98%RH, relative resistance variation up to 226%, along with a reversible, fast and stable response; When compared to other sensors, the hysteresis and response times were comparable or superior to other reported flexible

						sensors.
[72]	2022	PEN@Cellulose nanofiber/GNP	Capacitive (Humidity sensing)	Dry blending+ Screen-printing	Human respiration and skin moisture monitoring	High resistive response of 240% over the relative humidity range of 30-90%RH, with response and recovery times of 17s and 22s, along with good mechanical flexibility; Relative resistance variation of 2.4 along the 30-90%RH range.
[73]	2022	PVA@CNP/$MgCl_2$	Capacitive (Humidity sensing)	Solution casting	Human respiration monitoring	Response linearity of R^2 = 0.9978, response and recovery times of 6s and 11s, respectively, sensing range of 11-98%RH, stability for over 30 days, along with high voltage and current outputs, of ≈0,6V and ≈2.3 μA; Recycling and reusing with up to 90.31% of the original response voltage value.

[74]	2022	PDMS@rGO	Capacitive (Humidity sensing)	Hummer's method	Breathing patterns and respiratory monitoring	rGO in a wrinkled structure, improved both response and recovery times, while also preventing water aggregation and condensation; thinner rGO had response and recovery times of 2.4 s and 1.7 s, respectively; stability and repeatability were achieved for more than 30 cycles, along with high sensitivity in the 11 – 95 % RH range; maximum wet hysteresis was observed at 85% RH, with the maximum value being 3% RH.
[75]	2019	Epoxy@Indium oxide (In_2O_3) /GO	Capacitive (Humidity sensing)	Hydrothermal method	Breathing patterns and respiratory diseases monitoring	As RH increases, a real-time significant increase in the sensor's capacitance response was observed, especially between 11% and 23% RH; the response and recovery time of the composite film was 15s and 2.5s, respectively; the maximum hysteresis value was

						0.054% RH, observed at 85% RH.
[76]	2020	PDMS@MWCNT	Piezoresistive (Strain/pressure sensing)	Dry blending+ Mould casting	Human motion monitoring	MWCNT at 8wt.% showed the best sensitivity and linearity at 40% strain; The percolation threshold was reached at ≈2wt.%, with 3wt.% PDMS@MWCNT composite having the highest sensitivity to strain; 8wt.% PDMS@MWCNT composite showed the widest piezoresistive linear range, between 0-40%, while exhibiting a gauge factor of 1.21.
[77]	2020	PU@CNT	Piezoresistive (Strain/pressure sensing)	NIPS + Dip-coating	Deglutition, vocalization and finger motion monitoring	Hysteresis optimized up to 67.8%, stable and durable for more than 8000 cycles, air permeability 867.76% higher than non-porous, PU films, while moisture

						permeability was 801.48% higher than the non-porous film; Maximum sensitivity of 51.53 kPa^{-1}; Detection of pulse vibration, throat movements during vocalization and deglutition, along with finger movements.
[78]	2022	PDMS@rGO	Piezoresistive (Strain/pressure sensing)	Latex film forming	Human motion, speech and deglutition monitoring	Ultra-low amount of rGO, 0.44vol% was formed; Gauge factor reached a peak value of 44.01 at 230-300% strain, with stability during 2500 loading-unloading cycles. Response and recovery times were 165ms and 248ms; Detection delicate human motions, such as bending fingers, facial expression changes, vocal cord vibration, pulse and speaking.
[79]	2021	PDMS@CNT	Piezoresistive	Solvent-based	Human motion	Sensors with CNT at 3 wt.%

			(Strain/pressure sensing)	sonication method	detection	exhibited the highest average sensitivity, along with a gauge factor of 4.8 and a minimum compressive strain detection of 2%, the highest among the samples; lower porosity sensors exhibited greater energy absorption and recovery than more porous sensors, in the 5 – 50% strain range; at 10 – 15% strain, the reported gauge factor was comparable to other nanocomposite-based sensors.
[80]	2022	PDMS@NaCl@Carbon nanocapsules (CNC)	Piezoresistive (Strain/pressure sensing)	Template method	Human motion monitoring and intruder detection	Positive resistance change under a pressure detection range from 0 – 450 kPa, a maximum gauge factor of 150.7, stability for at least 2000 loading-unloading cycles, along with detection occurring in the 0 – 20% strain range; excellent

						mechanical response to bending, stretching, and twisting motions, along with high elongation at break in the 82 – 124 % range.
[81]	2018	SEBS@PEDOT: PSS +Ag/AgCl	Organic electrochemical transistor (Sweat sensing)	Laser-patterning+ Spin-coating	Cortisol-level monitoring	SEBS elastomer substrate allowed for a wearable sensor with superior flexibility and stretchability; The molecularly selective device showed high physicochemical stability at body temperature and in the normal motion range of the human epidermis; Stable and reliable readings were achieved.
[82]	2019	Lactate oxidase+ TTF+ chitosan/CNT; Ag/AgCl; Gold	Amperometric (Sweat sensing)	Inkjet printing + Screen-printing	Lactate-level monitoring	Linear range up to 24 mM lactate, and a sensitivity of 68µA.cm^{-2}/mM. NaCl and KCl concentrations decreased enzyme activity, affecting the sensor's performance; Lactate

						concentration variation corresponded to a current change of approximately 10μA.
[83]	2022	PET@Carbon Ink; Lactate oxidase; TTF+MWCNT; Prussian Blue mediator	ISE + Electrochromism (Sweat sensing)	Screen-printing	Biofuel cells and lactate-level monitoring	Achieved reversible and vigorous colour changes, over ten cycles; potential for on-skin continuous lactate-level monitoring with readily reversibility, ease of fabrication, and simple colourimetric read-outs; Operation and adaptation to different analyte concentrations; Power generation up to 13 μW/cm^2.
[84]	2021	Cloth/Paper@Carbon Ink; GOx; Prussian Blue + MWCNT mediator	Amperometric (Sweat sensing)	Screen printing + Drop-coating	Glucose-level monitoring	Concentration of sweat glucose could be measured in the 0.05 – 1 mM range, with a sensitivity of 105.93 μA/mM/cm, for up to 9 hours, along with excellent selectivity, reproducibility and

						stability; the sensor's output is consistent with the results given by glucose kits; under optimal conditions, the sensor exhibited acceptable detection range, sensitivity, reproducibility, stability, and selectivity.
[85]	2021	PDMS@PEDOT:PSS+Cu	Amperometric (Sweat sensing)	Etching+ Electrodeposition + Spin-coating	Uric acid-level monitoring	Ultrahigh sensitivity of 0.875 μA/μM/cm was achieved, along with a low limit of detection of 1.2 μM; when compared with other uric acid sensors, the produced sensor displayed considerably lower low limit detection and a suitable linear range, in the 2 – 250 μM range; the output signal remained consistent for 50 cycles; more than 95% of the initial signal

						response remained, after 25 days of testing; filling the microfluidic sweat reservoir took 166 s; repeated induced deformations did not significantly influence the sensor's electrochemical performance.

Throughout the state-of-the-art chapter, the most commonly employed flexible and wearable sensors were described in-depth, with added focus on their operating mechanisms and required properties, along with the most chosen materials, composites, and the interactions between their elements. Furthermore, requirements for material selection, geometries, and architectures were also addressed, denoting their importance and influence in the sensor's overall performance. Additionally, questions surrounding biocompatibility, long-term usage and patient acceptance rates were discussed.

With everything taken into account, developing a sensorial system is a very complex task, which requires interdisciplinary efforts and the combination of different types of sensors, in order to achieve desired and competitive sensing performance. Regarding the addressed sensors in this work, the desired characteristics and properties are all the same, namely high flexibility, competitive sensitivity on a wide sensing range, low hysteresis, linearity, durability, stability, along with low response and recovery times. On the other hand, the produced sensors must achieve the necessary mechanical compliance with the human skin, in other to better adhere and mimic its functions.

For these reasons, composite materials based on carbon are popular among researchers, due to their electromechanical stability, low cost, high variety, and known behaviour, while graphene, despite being a relatively new material, has attracted great interest, since it has excellent electromechanical behaviour, high Young's modulus, exceptional specific superficial area, and extraordinary electrical conductivity.

Despite this, available and employed manufacturing methods for each kind of sensor differ significantly, as well as the commonly chosen materials. Moreover, both the functionalization and fabrication method, allied to the used weight ratio between the matrix and the electrically conductive reinforcement, significantly influence the achieved results at the end of the process, since nowadays a great number of possible composite combinations exist for the same application in sensorial systems. Lastly, researchers are focusing their efforts on manufacturing methods, which lead to more simplified, cost-effective, scalable, and eco-friendly, crucial characteristics for the potentiation of the technology's commercialization.

Passing on to the analyzed experimental studies found in subchapter 2.6., temperature sensors mainly relied on RTD operation mechanism, with coating and blending being the most commonly employed fabrication methods for the development of composite materials capable of performing in human body temperature and environment temperature monitoring. Regarding their performance, the overviewed sensors displayed linearity, stability, low hysteresis, repeatability, sensitivity between 0.37%/ºC and 12,5%/0.5 ºC, accuracy in the 0.1 – 0.5 ºC range, along with response and recovery times in 0.196 s – 31 s and 0,274 s – 300 s ranges, respectively.

Looking at humidity sensors, the most popular working principle is, by far, the capacitive, while fabrication methods, on the other hand, don't show any tendency or preference, despite all sharing the same applications, human respiration and breathing pattern monitoring. Considering performance, the sensing range was in the majority of observed works

11 – 98% RH, with relative resistance variation up to 240%, response times between 2.4 s and 17 s, along with recovery times between 17 s and 22 s. Furthermore, hysteresis ranged from 0.054% RH and 3% RH.

Regarding strain and pressure sensors, the majority of developed devices employed piezoresistive working principle, with the most popular applications were human motion detection and monitoring. Focusing on fabrication methods, a great diversity of approaches can be taken, including latex film forming, dry blending and dip-coating, observed in most of the studied works. Moving on to performance, developed sensors displayed gauge factors between 1.21 and 440.1, strain range up to 300% with one of the works showing a compressive strain detection of 2%, another with pressure detection up to 450 kPa, while other displayed response and recovery times of 165 ms and 248 ms, respectively.

Lastly, after observing some of the updated works published in the sweat sensor development field, we can infer that a great number of them employ amperometric working mechanisms, with others choose to employ organic electrochemical transistors or ISE. This correlates with the huge number of possible applications, that range from cortisol, lactate, glucose, and uric acid detection and monitoring, among many other analytes, along with biofuel cell development. However, regarding fabrication methods, most researchers prefer to use either screen printing techniques or spin coating. Looking at performances, sensitivity varied between 0.875 and 105,93 μA/cm/mM, showed stability of up to 50 cycles, while one work included a 25 day-long test with up to 95% of the initial response remaining, along with another work showing power generation of 13 $\mu W/cm^2$ and sensing range from 2 μM to 250 μM.

In conclusion, the study and advancements in this field is vital for improvements regarding devices' efficiency and conformity, boosting the potential of this new generation of more individualized approaches and faster rehabilitation processes.

Chapter 3

Materials and Methods

3. Materials and Methods

After establishing, in the previous chapter, the standards related to sensorial system development, namely, the employed sensors and their applications, along with the most prominent composite materials, architectures and geometries for each approach, this chapter will address the themes associated with the sensor manufacturing processes chosen for this dissertation. A thorough characterisation of the selected raw materials will take place, in addition to a comprehensive description of the implemented techniques and their respective equipment. Moreover, the following sections will also discuss how the electromechanical characterisation of the produced samples will take place, including the employed devices and instruments to better comprehend the relevant properties of the system. This chapter will also feature an experimental protocol, where a meticulous explanation of the manufacturing and testing processes will be present. All the decisions made in this chapter follow the current trends observed in sensorial systems and on-skin sensor production.

Therefore, chapter 3 is partitioned in multiple sections, where the employed materials, the methodologies and fabrication approaches chosen are presented in a sequential manner, concluding with the chosen experimental protocols and characterisation techniques.

3.1. Materials and equipment

For this work, rGO (average particle size ≈43.95 μm; purity 98.2 wt.%) was purchased from Shenzhen Gauss Scientific Instruments (Guangdong, China), PDMS (Sylgard 184/Dow Corning 184) was purchased from Shenzhen Huazhisheng New Material Technology (Guangdong, China), 1,4-dioxane was purchased from Fisher Scientific (New Hampshire, EUA), and Isopropyl Alcohol from LabChem (Zelienople, PA, USA). Regarding the sensor's electrodes, silver paste was acquired from RS Components (Corby, UK) and copper wires were obtained locally, as well as distilled water.

Considering the key materials, rGO was chosen due to its great electromechanical behaviour, high surface area and good sensing properties, all very similar to pristine graphene, while easily allowing functionalization with other materials, namely elastomers and other polymers, leading to composites with superior characteristics [86]. Considering the elastomers, PDMS was selected in view of its outstanding properties, including high thermal stability, optical transparency, isotropy, high elasticity, and conformability, along with cost-effectiveness, ease of access and popularity among researchers [86,87]. On the other hand, regarding solvents, while distilled water, isopropyl alcohol and 1,4-dioxane will be compared, the last will also be used as a mean to observe a possible reduction of the rGO's overall disorder and defects in the composite's crystal lattice, leading to a material with superior crystallinity, higher uniformity, and lesser deficiencies [88].

On the other hand, regarding machinery, an AU-65 ultrasonic cleaning machine from Argo Lab, a VA/WA series analytical balance from Oertling, an OS20 digital overhead stirrer from LBX Instruments, a vacuum chamber from Baco Engineering, a 34461A digital multimeter from Keysight Technologies, a Nikon SMZ-2T stereomicroscope with ×20 amplification, and two Shimadzu AGS-X universal testing machines, with 10kN and 50kN load cells, were employed for this work, TGA was run on a TA instruments® Q50 thermogravimetric analyser, ATR/FTIR was performed in a Nicolet™ iS 10 FTIR spectrometer, while SEM was done employing a Hitachi S-3400N scanning electron microscope (SEM) (Hitachi Manufacturing Co., Ltd., Tokyo, Japan).

3.2. Methods

After stating all materials employed during this stage of the work, in this section, descriptions of all matrix and composite manufacturing procedures, along with the electrode deposition technique by sputtering, direct silver paste deposition, mechanical characterisation by tensile tests, piezoresistive characterisation by 3-point bending tests, average gauge factor calculations and cyclic stability testing will be made.

Moreover, the courses of action taken to thermally characterize the samples of interest, together with sample morphology observations by SEM, thermal characterisation by TGA, and spectroscopy tests by ATR/FTIR will also be compiled here.

3.2.1. Fabrication of pristine PDMS films

The fabrication of flexible PDMS films followed the general guidelines provided by the manufacturer [89]. Firstly, the desired elastomer mass was poured and weighted in a container, followed by the crosslinker, according to the selected ratio. Despite the manufacturer recommending a 10:1 ratio, others were tested, including 15:1 and 20:1, with the aim of observing how a significant variation in crosslinker concentration would affect the mechanical properties of the polymer. Afterwards, the mixture was manually stirred for 5 minutes and placed in a vacuum chamber for 10 minutes, in order to remove all air bubbles created by the stirring process. Additionally, the mixture was poured into previously built cardboard moulds, measuring 50 mm × 50 mm × 1 mm. These were built by cutting a square shaped cardboard piece of the desired area and thickness of 3 mm, which acted as the substrate, followed by an acetate layer and a second layer of cardboard 1mm thick, both with the same area. To the last one a square orifice was cut in the middle, creating the region where the PDMS would be poured. Furthermore, Flashbreaker® 1 tape, a polyimide carrier film coated with silicone adhesive, was also added to the inner edges, sealing it off and preventing any capillary action of the crosslinker, a phenomenon that would lead to its absorption by the cardboard and render all

samples unusable. The last step consisted of gluing all 3 layers with double sided tape. Moreover, before pouring the mixture, all moulds were cleansed with ethanol 70%, which prevented sample tainting by cardboard particles. Figure 39 shows a mould with the obtained film, at a ratio of 10:1 and cure temperature of 120°C.

Additionally, multiple curing times and temperatures were tested, for the sake of observing differences in mechanical behaviour between samples. Table 4 displays all 12 configurations tested, with a thickness of 1 mm, labelled according to the chosen cure temperature and elastomer-crosslinker ratio, respectively.

Table 4. Elastomer-Crosslinker ratio configurations tested during the fabrication of PDMS 1 mm thickness films.

		Temperature		
		20°C	**65°C**	**120°C**
Elastomer-Crosslinker ratio	10:1	PDMS@20/10	PDMS@65/10	PDMS@120/10
	15:1	PDMS@20/15	PDMS@65/15	PDMS@120/15
	20:1	PDMS@20/20	PDMS@65/20	PDMS@120/20

Regarding the values related to temperature and curing times, the datasheet provided by the manufacturer was considered for 120°C and ambient temperature, while other samples were cured at 65°C for 70-80 minutes. It should be noted that some curing times were slightly adjusted for some configurations, in order to obtain a fully cured film. Table 5 summarizes the curing temperatures and times used during the sample fabrication process.

Table 5. Curing temperatures and times for the fabrication of 1 mm thick PDMS films.

		Temperature		
		20°C	**65°C**	**120°C**
Elastomer-Crosslinker ratio	10:1	48h	80 min	20 min
	15:1	48h	80 min	20 min
	20:1	48h	80 min	20 min

Some preliminary conclusions, observed macroscopically, were quickly taken during the fabrication process: samples with higher elastomer-crosslinker ratios, especially at 20:1, required higher curing times at the same temperature, while having a bigger tendency to lose crosslinker through capillary action and higher stickiness, whenever the films were touched. Furthermore, the sample with a ratio of 15:1 deflected under self-weight the best, followed by the 20:1 ratio sample and lastly the 10:1 ratio one. Regarding samples cured at ambient temperature, major capillary action of the crosslinker was observed, leading to a strenuous demoulding process and film rupture in the 15:1 ratio sample. Figure 40 shows the deflection under self-weight of different elastomer-crosslinker ratios.

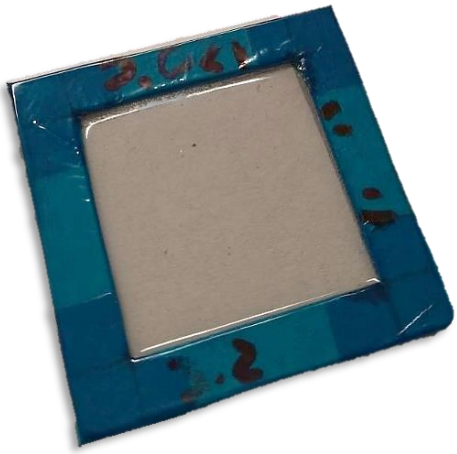

Fig. 39. Mould with a PDMS film with an elastomer-crosslinker ratio of 10:1, cured at 120ºC for 20 minutes.

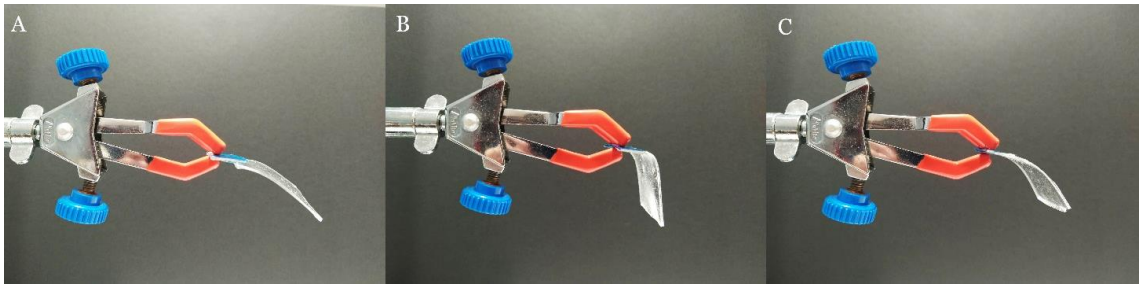

Fig. 40. Self-deflection, under own weight, of different configurations of PDMS elastomer: (A) PDMS@10:1 ratio; (B) PDMS@15:1 ratio; (C) PDMS@20:1 ratio.

3.2.2. Fabrication of rGO@PDMS composites

During the fabrication of the flexible rGO@PDMS composites, several samples were produced, where the percentage by weight was varied in order to better understand the effects of the rGO conductive activity in the matrix, to measure the percolation threshold and to achieve an adequate conductive network. Therefore, after consulting multiple works developed in the field [78, 88, 90-92], it was decided that the composites would be manufactured until the necessary conductivity requirements were met for piezoresistive tests, starting from the lowest rGO content upwards, leading to the production of samples with percentages by weight of rGO of 0.25 wt.%, 0.5 wt.%, 0.75 wt.%, 1 wt.%, 1.5 wt.%, 2 wt.%, 3 wt.%, 4 wt.%, and 5 wt.%.

While many of the taken fabrication steps were similar to the ones used to obtain pristine PDMS films, such as the chosen moulds, others were changed or added to improve the entire process or to later compare the results, namely the used substances to disperse the rGO in.

With this in mind, in this subchapter all experimental procedures regarding the composite's fabrication will be described, focusing mainly on the employed dispersant, namely, distilled water, 1,4-dioxane and isopropyl alcohol, since the other steps are common to all approaches. Figure 41 shows a schematic illustration of the fabrication technique, which uses elements of solvent casting and drop casting, and is referred in this work as solution casting. Moreover, this process can take from 4h30m, when isopropyl alcohol is used, to 6h, when distilled water is used, due to the different times it takes to evaporate the dispersants in the oven.

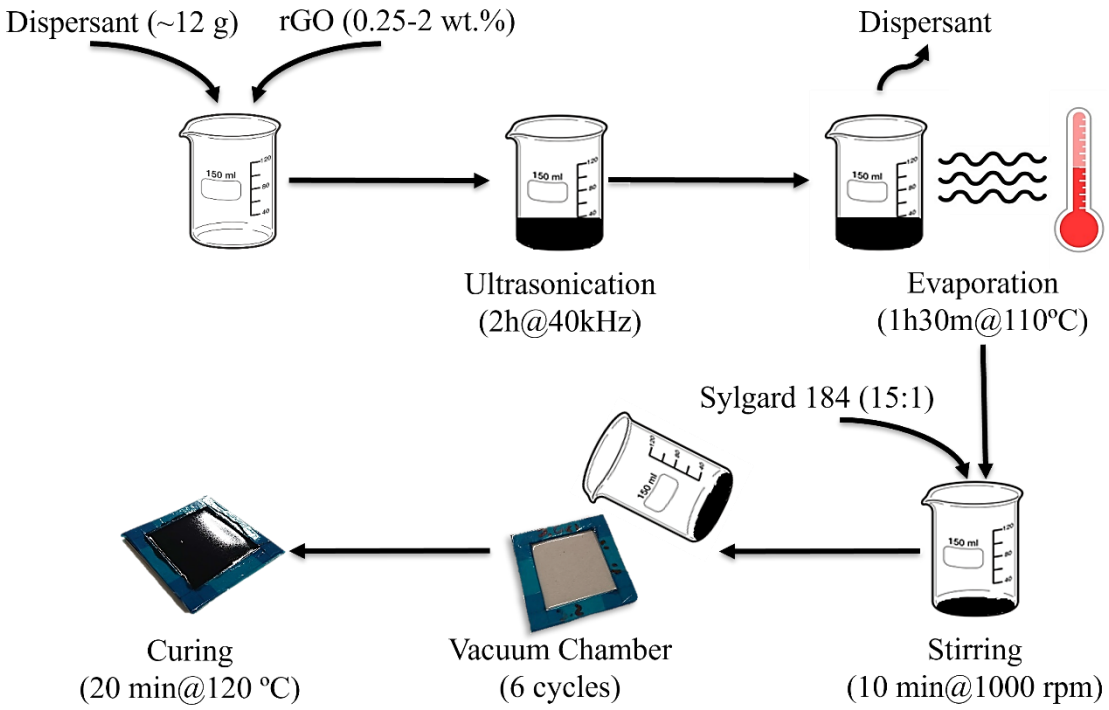

Fig. 41. Schematic illustration of the solution casting technique used to fabricate the rGO@PDMS composite film.

Fabrication of composites with distilled water as a dispersant

In this approach, the desired amount of rGO, depending on the percentage by weight, was measured inside a beaker put in an analytical balance, followed by the addition of ≈15 g of distilled water. Although the amount of distilled water was never exactly the same because some of it was used to disaggregate rGO from the used utensils, to reduce rGO losses, this factor is unimportant, since all the water would be evaporated in the following steps. After this, the

mixture was put in an AU-65 ultrasonic cleaning machine for 2 hours, at 30 ºC, 180 W and 40 kHz, with the objective of dispersing the rGO by reducing any existent agglomerations.

With the ultrasonication concluded, the resulting dispersion was put in an oven at 110 ºC for 2h45m hours, which evaporated the dispersant and left thin rGO flakes at the bottom of the beaker. To these were added 15 parts of PDMS elastomer followed by 1 part of PDMS crosslinker and the mixture was mixed at 1000 rpm for 10 minutes.

Once this process was concluded, the mixture was poured into a mould and its air bubbles removed by applying six vacuum chamber cycles to it. Lastly, the final step was curing the composite at 120 ºC for 20 minutes in the oven. Figure 42 shows the difference between a pristine PDMS film and a rGO@PDMS composite.

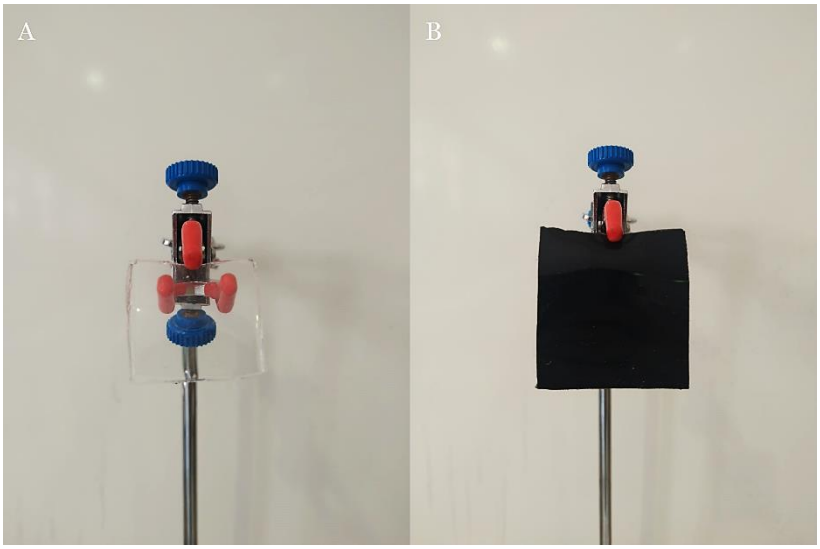

Fig. 42. Macroscopical view of PDMS films: (A) Pristine PDMS film; (B) rGO@PDMS film.

Fabrication of composites with 1,4-dioxane as a dispersant

For fabrication of composites with 1,4-dioxane as a dispersant, most of the taken steps were similar to those for distilled water, with ≈10 g of 1,4-dioxane being used. However, the time it took to evaporate the dispersant in this situation was shorter, around 2 hours at 110 ºC, while also showing better dispersion of rGO nanoparticles, both before and after ultrasonication, as well as after the curing process, where the obtained film showed greater opacity. With the use of this dispersant, the objective was observing the possible stabilization effects that 1,4-dioxane had in the rGO's crystal lattice, which could supposedly lead to a lower number of defects and therefore higher overall performance [88].

Fabrication of composites with isopropyl alcohol as a dispersant

In the case of the fabrication process with isopropyl alcohol as a dispersant, the taken steps were also the same, with ≈12 g of it being poured into the dispersion. Furthermore, the use of isopropyl alcohol led to the least amount of time inside the oven, 1h30m at 110 ºC, while also providing the best macroscopic dispersion, before and after ultrasonication, as well as after the curing process. Moreover, the produced films showed great quality, with high opacity, signs of superior rGO dispersion in the PDMS matrix. For these reasons, isopropyl alcohol is most likely the best option out of the three, if the assumption regarding the stabilization effect of 1,4-dioxane does not come into fruition, mainly due to the time it takes to evaporate, allied to a great rGO dispersion, one of the factors which give composites superior characteristics. Figure 43 shows three different macroscopic views of composites, where the used dispersant was varied. The images were acquired with a Nikon SMZ-2T stereomicroscope with a magnification of x10.

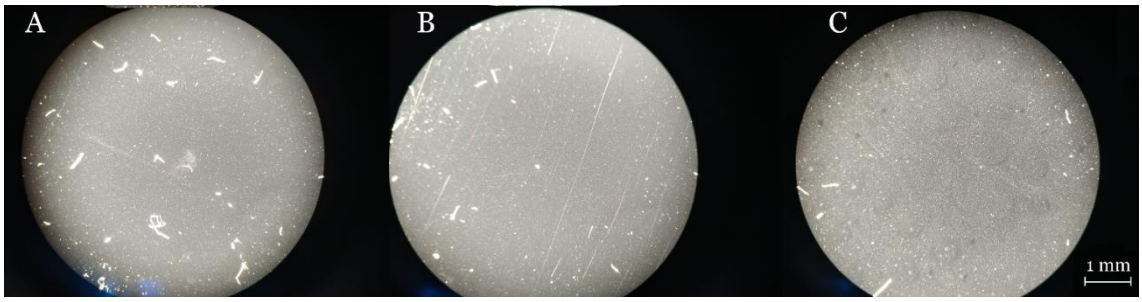

Fig. 43. Macroscopical view of rGO@PDMS composites (0.5 wt.%), with different dispersants used, achieved through a Nikon SMZ-2T stereomicroscope (×10 amplification): (A) Distilled water; (B) Isopropyl alcohol; (C) 1,4-dioxane. The white-coloured features in the images are cloth and paper fibers adhered to the films resulted from their cleaning processes.

By observing the images, it is possible to conclude that only a small amount of air bubbles can be detected macroscopically, with no significant difference between dispersants, while other defects are impossible to be detected at this scale. Therefore, macroscopically speaking, composites fabricated using these dispersants may behave differently during the fabrication process, but no long-lasting differences can be observed in the final product, if all steps are followed properly.

3.2.3. Electrode deposition by sputtering

With the successful fabrication of rGO@PDMS composite thin films, this step in the sample preparation had the aim of getting them ready for piezoresistive and other electromechanical tests. However, in order to accurately measure resistances and better grasp the electromechanical behaviour of each sample, gold electrodes were deposited by sputtering in the surface of some samples, thanks to an electrode mask. Otherwise, without electrodes,

resistance values would be too high to be measured, thanks to the insulator nature of the PDMS matrix.

Concisely, sputtering, one of the most prominent bottom-up approaches, consists of a system that includes an evacuated chamber, a vacuum pump, a gas supply, a sputtering source, a substrate holder and an electrode [93]. In this technique, nanomaterials and nanoparticles are deposited on the surface of a substrate by ejecting particles from the target material with high-energy ions. Thus, this process enables surface coating, thin layer deposition, and surface etching of samples [93]. Regarding this type of deposition, the core idea is inputting high energy on a pristine solid material, to generate a vapor that solidifies on the substrate, due to the presence of very high energy gases such as argon, hydrogen, oxygen, and nitrogen, as well as high vacuum environment conditions [94].

By varying the chamber's pressure and electric current between the electrodes, different results and deposition times can be achieved, due to the acceleration of the electrons and their collision with the gas atoms, creating plasma [93]. Afterwards, these strike the target material, in this case gold, sputtering atoms from its surface, which travel towards the substrate and grow a film, whose thickness depends on the time inside the chamber [94]. Figure 44 shows a schematic diagram of the sputtering chamber and technique. Argon is commonly employed by these devices due to being an inert gas which does not interact with the substrate, including the Q150R ES rotary pumped coater, produced by Quorum, which was used in this work.

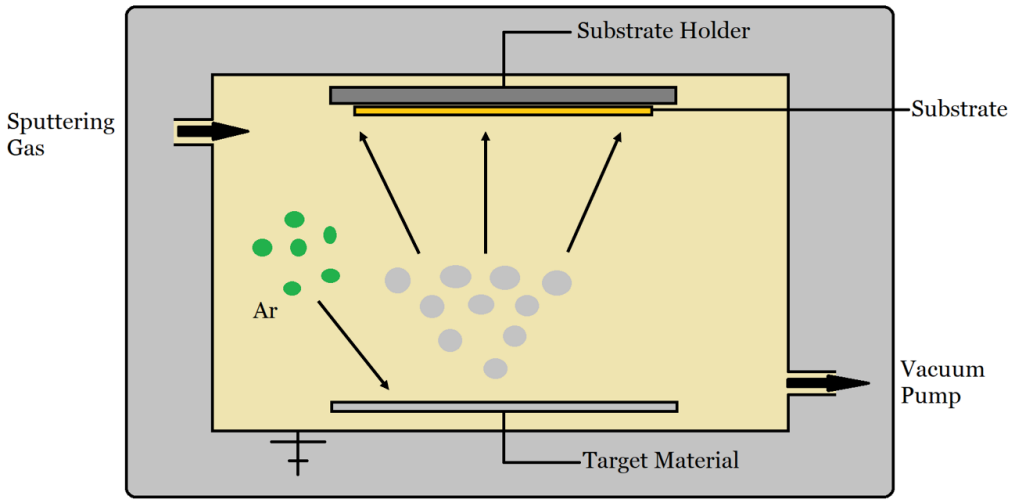

Fig. 44. Schematic diagram of the sputtering technique, with argon being used as the sputtering gas.

Therefore, for the sake of growing electrodes of uniform size and equal distance between each other, and to better calculate surface and volume resistivity measurements, two metal electrode masks were designed in SolidWorks® and built by a waterjet cutting machine, shown in Figure 45. By building two masks, the samples could be placed in the middle and electrodes

deposited on both sides. In order to fasten the masks to each other, one M4 screw and a nut was placed on each quadrant.

The chosen dimensions are as follows: the rectangular orifices measured 4 mm × 8 mm, with the longitudinal distance between them being 2mm and the transversal one 4 mm; the circular orifices measured 8 mm in diameter and were separated by 30 mm transversally and 48.50 mm longitudinally; as a whole, the piece had a diameter of 100 mm and a thickness of ≈1mm. While the circular configuration had the aim of volumetric resistance measurements, the rectangular configuration was made for superficial resistance ones. Figure 46 shows a 2D drawing, with all these measurements put in place.

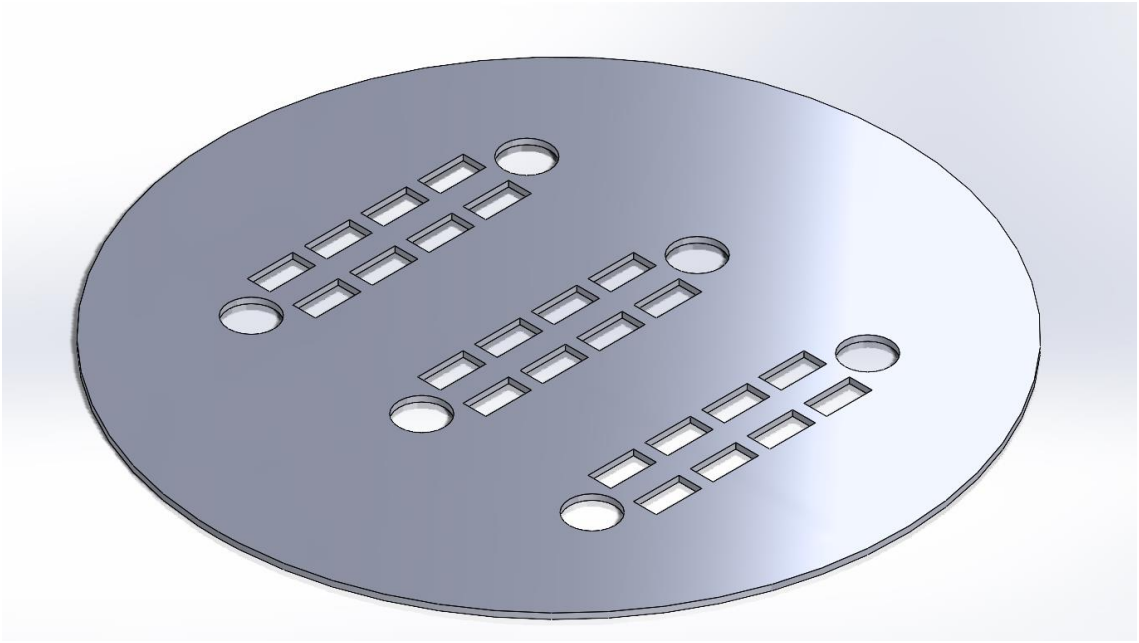

Fig. 45. Electrode mask, as designed in SolidWorks®.

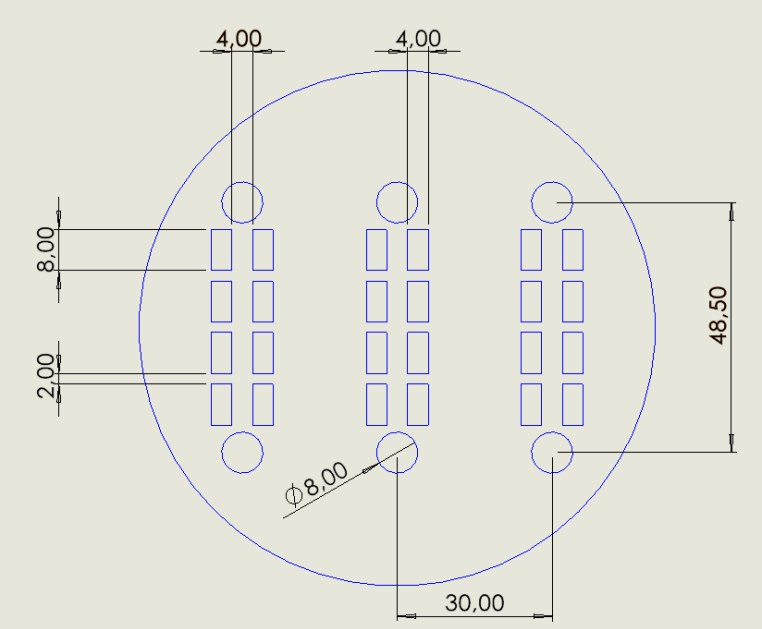

Fig. 46. 2D drawing of the electrode mask design, made in SolidWorks®, with all the relevant measurements, in millimeters, available.

Lastly, regarding the chosen samples for deposition, samples fabricated with a rGO content of 0.5 wt.% and 1 wt.% dispersed in distilled water went through this process. Therefore, with this design, it would be possible to comprehend the effects of different percentage by weight of rGO, among other variables, on the piezoresistive behaviour of the samples during testing.

Concerning the process itself, each side of the sample was sputtered with gold two times for 1 minute, with the chosen plasma intensity current being 50 mA. However, the Q150R ES does not support changes in the chamber's pressure, so only the plasma intensity current and time inside the chamber was varied. Figure 47 shows the final result on two samples, along with the electrode mask, after the sputtering process.

With this process finished, two copper cables were secured to the films with conductive silver paste, to facilitate electrical measurements from the experimental setup during piezoresistive testing.

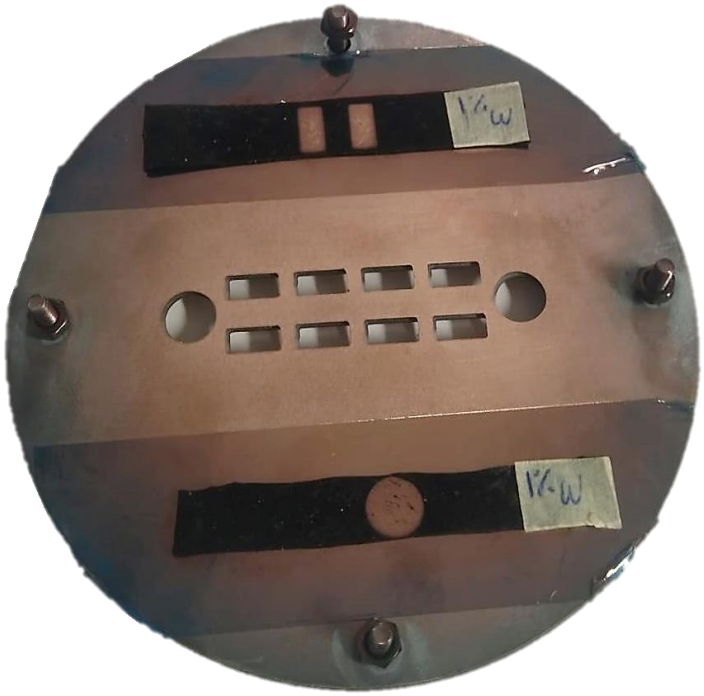

Fig. 47. Deposited electrodes on two rGO@PDMS composite samples, along with the electrode mask, after two-1 minute sessions in a Q15OR ES rotary pumped coater, at 50 mA of plasma intensity current.

3.3. Characterisation techniques

3.3.1. Mechanical characterisation

Due to many materials undergoing the application of mechanical forces or loads when used in a myriad of fields, a design requirement is knowing the characteristics and limits of the compound that is being employed, to better project a device that will not suffer excessive deformations or even break under stress [95].

Thus, by taking into account that the mechanical behavior of a material is dependent on the relationship between a force/load and its response, mechanical characterisation techniques are carefully performed on samples with the aim of replicating, to some extent, service conditions. Moreover, a necessity in these tests is consistency when performing measurements and interpreting results, which is met with the introduction of test standards periodically and coordinately published by professional societies and entities [95], some of which will be used throughout this work.

Knowing this, after concluding the fabrication of all 9 configurations of pristine PDMS films, the mechanical tests phase was proceeded, where the main objective was determining the Young's modulus along with the maximum tensile stress and strain during testing, for all configurations, following Equation (4) [95]:

$$E = \frac{\sigma}{\varepsilon} \quad (4)$$

where E is the Young's modulus, σ is the applied stress, and ε is the observed strain. Thus, it would be possible to better understand how the variation of cure temperature and elastomer-crosslinker ratio parameters would influence the film's final mechanical performance.

Taking this into account, from the fabricated 50mm × 50mm × 1mm PDMS films, 5 strips were cut, measuring 50mm × 8mm × 1mm. All measurements, including the test conditions explained further, are based on the ASTM D882 – 10 test standard, but were adapted to better serve the purpose of this work [96]. Figure 48 shows the initial film and one of the strips, after the cuts were done.

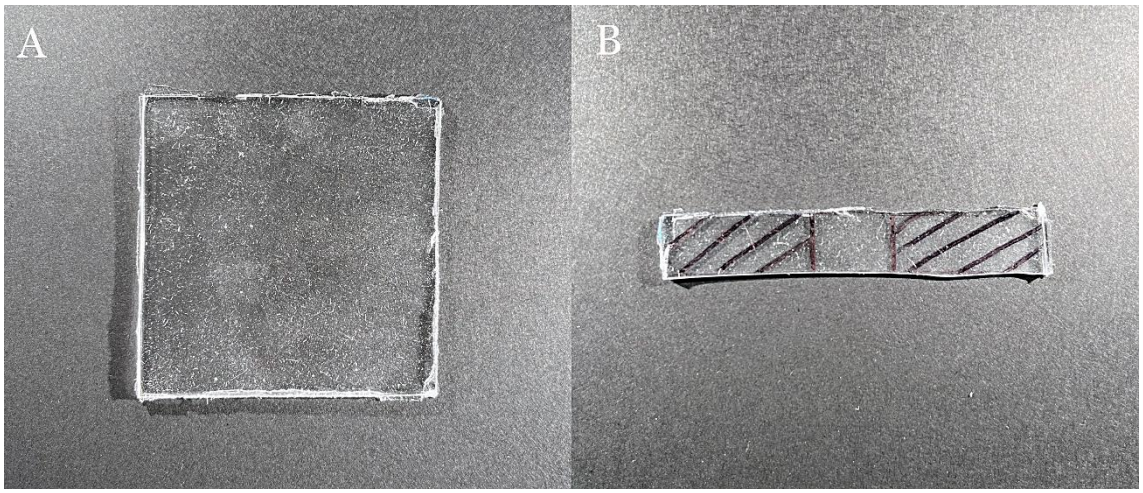

Fig. 48. (A) Original pristine PDMS film, measuring 50 mm × 50 mm × 1 mm; (B) One of the cut strips, with the oblique lines showing the area gripped by the universal testing machine's grips. The central zone is the area between grips and will suffer the bulk of all applied strain.

Regarding the mechanical tests, all configurations were tested in the Shimadzu AGS-X universal testing machine where, following the test standard, the chosen distance between grips was 12 mm, while the gripping area measured being 19 mm × 8 mm. Along these lines, the chosen speed of testing was 5 mm/min while the sampling frequency was 2 Hz. Furthermore, all samples were tested until full rupture was achieved. Figure 49 shows how the samples were placed in the universal testing machine.

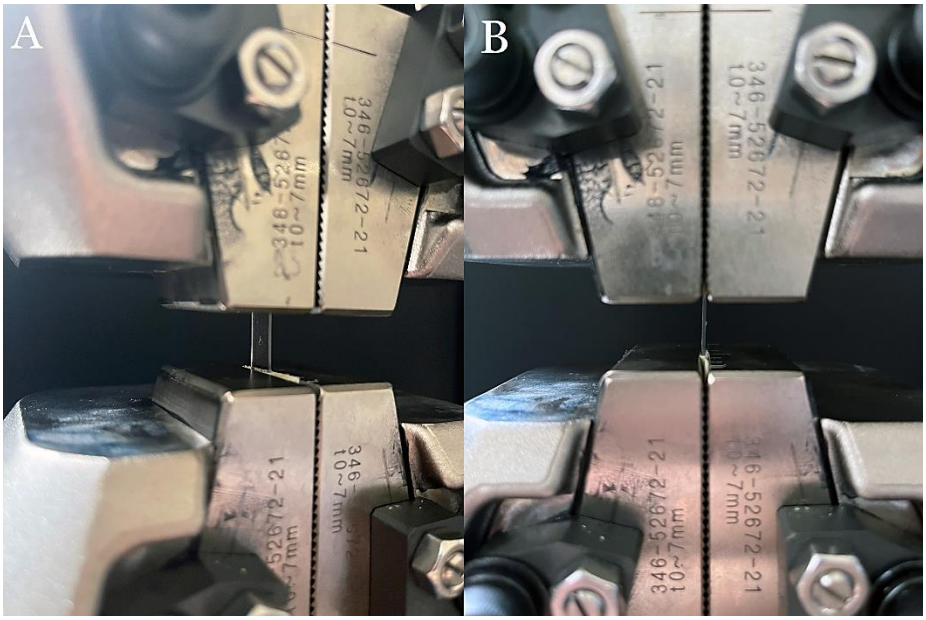

Fig. 49. Placement of PDMS strip samples in the Shimadzu AGS-X universal testing machine: (A) Oblique view; (B) Front view.

3.3.2. Electromechanical characterisation- Piezoresistive tests

Taking into account that a strain sensor such as this requires a measurable piezoresistive behaviour, where it is possible to observe changes in resistance when geometrical parameters are changed due to an external stimulus, such as mechanical deformation, performing an electromechanical characterisation allows for the direct quantification of certain parameters, including sensitivity, linearity, resolution, and hysteresis, among others [97].

In the case of semiconductors, such as the composite developed in this work, this phenomenon is very important up to its manifestation at the atomic level, where changes in electrical resistance are associated with the variation in free electrons and their mobility by the crystal lattice's deformation [97].

With this in mind, in this subchapter, all characterisation techniques employed to explore the electromechanical performance of the produced composite samples will be presented and discussed. Moreover, the average gauge factors were calculated in the ascendent portion of the curve in each cycle, following the previously mentioned Equation (1):

$$GF=\frac{\Delta R/_{R0}}{\varepsilon} \quad (1)$$

Where ΔR is the electrical resistance variation, R_0 is the initial electrical resistance, and ε is the strain observed in the samples.

3-point bending tests

In order to characterize the piezoresistive behaviour of the produced rGO@PDMS composite films, the first step was measuring the resistance between the deposited electrodes, with a Keysight 34461A. By doing this, it was possible to observe which samples manifested conductivity in a range which permitted piezoresistive performance monitoring, typically the ones with semiconductor behaviour. Thus, after the measurements were conducted, only samples with rGO at 3 wt.%, 4 wt.% and 5 wt.% showed measurable resistance values, with the average values being 298.66 Ω (SD = 46.44 Ω), 31.75 Ω (SD = 13.05 Ω) and 4.55 Ω (SD = 0.39 Ω), respectively, while the other samples induced resistance overload in the multimeter, mainly due to the highly insulating nature of the PDMS matrix, allied to lower concentrations of rGO, which meant the percolation threshold was not achieved in them.

Taking this into account, the selected samples were given designations based, firstly, on its rGO content, it being 3, 4 or 5 wt.%, secondly, the employed dispersant in the fabrication method, isopropyl alcohol (A), 1,4-dioxane (D) or distilled water (W), and thirdly, the order in which the samples were cut from the main film. Therefore, it was decided to produce samples with isopropyl alcohol as the dispersant and prepared for piezoresistive testing, with them being referred as 3A1, 3A2, 3A3, 4A1, 4A2, 5A1, 5A2 and 5A3. Regarding this test, it was once again employed the Shimadzu AGS-X universal testing machine with a load cell of 10 kN, responsible for the 3-point bending of the samples, which results in an electrical response, whose magnitude was sampled by the Keysight 34461A digital multimeter. Concerning the sample's placement in the machine, these were secured on a 70 mm × 15 mm polypropylene substrate, with the objective of avoiding the composite's deflection under its own weight.

Lastly, regarding the electrode placement, after a few attempts to secure the electrodes to the sputtered films, where silver paste and copper cables were put on top of the gold, it was observed that they still broke off from the structure. Thus, it was decided to instead proceed with a more default method, where the electrodes were made of carefully painted silver paste directly on the composite's surface, since the sputtering process caused too many time and cost constraints, along with no obvious benefits to the tests. Despite this shortcoming, the electrical behaviour of the samples was perfectly measurable. Figure 50 shows the used setup for piezoresistive testing.

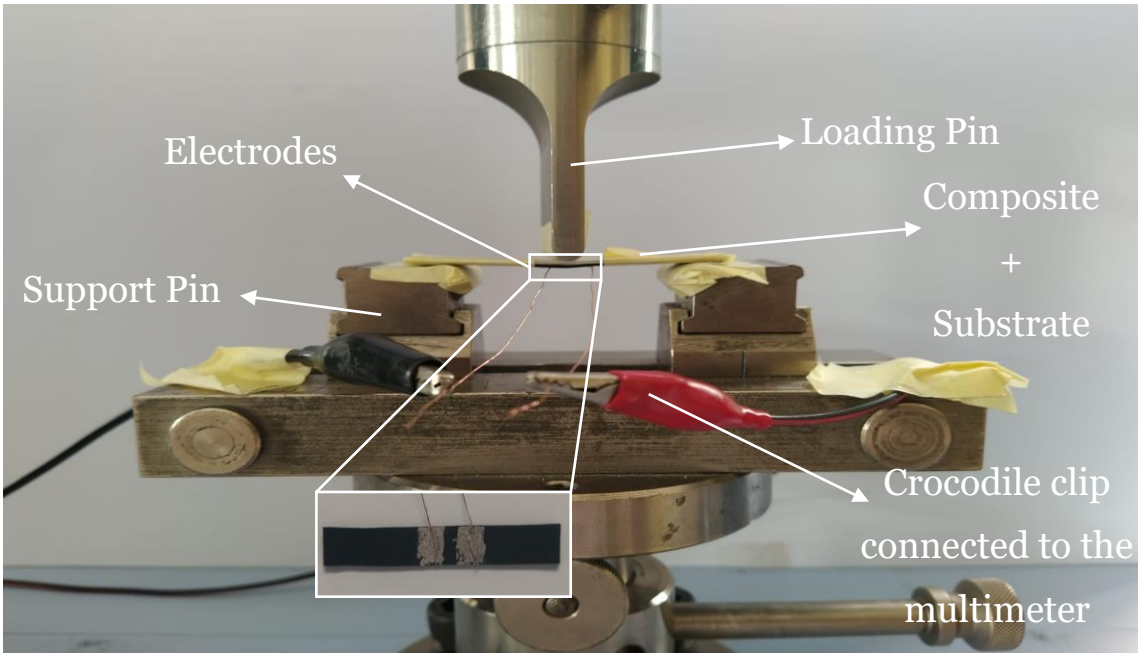

Fig. 50. Piezoresistive testing setup for the rGO@PDMS composites for a 3-point bending test, with a detail of the deposited electrodes. The sample has all possible contact points isolated with masking tape.

Respecting other testing parameters, the composite samples measured ≈60mm × ≈10mm, with variable thicknesses, both because they were fixed to the substrate and because there was no fail-proof method of achieving equal film thickness throughout the entire structure, during the fabrication method. Along these lines, the tests were comprised of four cycles where the samples were mechanically flexed at variable strain values, in this case from 0.22% up to 1.54%, 1.99%, 2.43% and 2.87%, along with a 100-cycle stability test at ε_{max} = 1.54%. These strain rates were calculated using Equation (5), present in the ASTM D790 – 03 standard test method [98]:

$$\varepsilon = \frac{6.d.displacement}{g^2}.100 \quad (5)$$

where ε is the strain induced in the sample, d is the sample thickness, and g is the distance between the support pins. In this work, the chosen distance between support pins was 48 mm. By choosing different strain rates, the aim was observing the composite's electrical behaviour at and simulating, to some extent, how these devices would work in real situations. Speaking of chosen strains, 2.87% was the maximum due to the silver electrodes breaking off from the surface at ε ≈ 3%.

Lastly, the speed at which the loading pin is displaced was also preliminary tested with the 3A1 sample, with the speed rate varying between 1 and 10 mm/min, results of which will be discussed below.

Tensile tests

Regarding the tensile tests, the samples were tested at strains at which the electrical response could be measured without not compromising their structural integrity. Therefore, samples with 3 wt.% rGO were put in a Shimadzu AGS-X universal testing machine with a 50 kN load cell and cycle tested up to ε = 40%, while the ones with 4 wt.% and 5 wt.% where tested up to ε = 20%, due to these exhibiting higher rigidity and brittleness, caused by higher concentrations of rGO in the matrix. Moreover, other tests were also carried out, more specifically, one where samples were stressed until the composite's conductive network stopped functioning and the resistance value overloaded the multimeter. Regarding the electrode placement, silver paste and a copper cable were applied to each extremity of the sample, due to the different nature of this experiment.

In order to achieve the best results possible, a Canon EOS 90D digital camera was also incorporated in the cyclic tests, with the aim of capturing the entire procedure and accurately calculating the strain values achieved, using a third-party software. Figure 51 shows the used setup for the piezoresistive tensile tests.

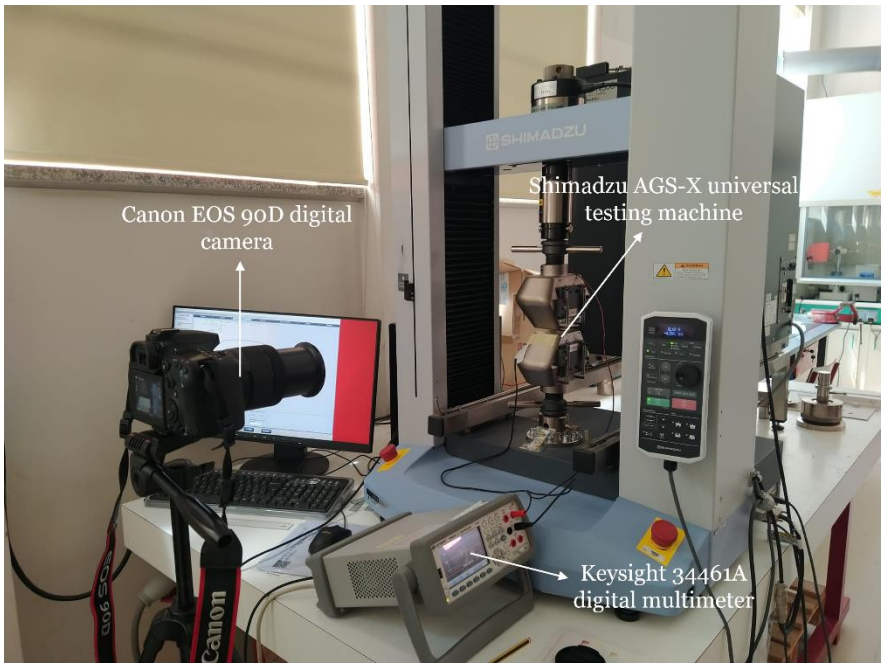

Fig. 51. Setup used for piezoresitive tensile tests, comprised of a Canon EOS 90D digital camera, a Shimadzu AGS-X universal testing machine, a Keysight 34461A digital multimeter and a computer.

3.3.3. Mechanical characterisation of rGO@PDMS composites

With the fabrication and piezoresistive testing of all rGO@PDMS samples concluded, the mechanical tests began, where the aim was comparing the maximum tensile stress and Young's modulus of the composites with the pristine PDMS films, fabricated with an elastomer-crosslinker ratio of 15:1 and cured at 120 ºC for 20 minutes. Therefore, by observing the mechanical behaviour of both films, it is possible to comprehend how the presence of a rGO network inside the matrix affects the film's final mechanical performance.

Taking this into account, all samples previously put through piezoresistive testing were chosen. Similarly to the pristine PDMS films, all measurements, including the test conditions, were based on the ASTM D882 – 10 test standard, but were adapted to better serve the purpose of this work [96].

Regarding these tests, all samples were tested in the Shimadzu AGS-X universal testing machine with a 50 kN load cell, with a chosen distance between grips of 12 mm and a gripping area of 24 mm × 10 mm. Along these lines, the chosen speed of testing was 5 mm/min while the sampling frequency was 2 Hz. Furthermore, all samples were tested until full rupture was achieved. Figure 52 shows on of the samples used in the mechanical tests.

Fig. 52. rGO@PDMS composite sample used during mechanical testing.

3.3.4. Morphological characterisation

Another aspect of the composite's characterisation is observing its morphology and microstructure by Scanning Electron Microscopy (SEM), a powerful characterisation tool in materials science, capable of analysing organic and inorganic materials on a nanometre to micrometre scale and revealing surface structures, surface morphology, microorganisms, and particles by providing high-resolution 3D images at magnifications ranging from 300000x to 1000000x, in some cases [99, 100].

By applying a high-energy beam of electrons, commonly emitted from a thermal source, usually in the 100 eV – 30 keV range, analyses and images can be produced with high precision, consistency, lateral resolution, and depth of focus [100]. Hence, it is possible to characterize samples of variable density and thickness according to their morphology.

Nevertheless, something to consider is that nonconductive samples must be coated with a thin layer of platinum or gold, usually made by sputtering [99]. Furthermore, the possibility exists that, during imaging, the electron beam fired from the device could irreversibly damage the sample, inducing degradation or altering the surface's morphology, a factor that without a doubt changes the obtained results [99].

Regarding the main components of a SEM microscope, it is composed of: an electron gun that acts as the source of high-energy beams of electrons; a column where the electrons travel through, thanks to the existence of a group of electromagnetic lenses, responsible for focusing the beam; two scan coils, part of the deflection system, responsible for deflecting the electron beam, which scans the area of interest; an electron detector that collects secondary and backscattered electrons, producing the topographic image; a chamber where the sample is placed and moved, tilted and rotated, when necessary; and a computer system that controls the entire process, along with displaying the scanned images [100]. Figure 53 shows all the main components of a SEM microscope device.

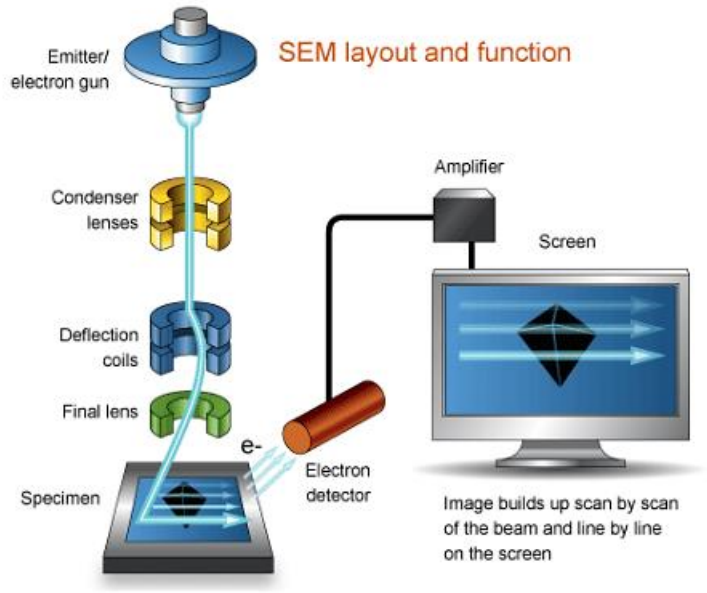

Fig. 53. Main components of a SEM microscope. (Adapted from [100]).

Knowing this, the morphology and structural features of the cross-section of produced pristine PDMS, 3 wt.%, 4 wt.%, and 5 wt.% rGO content rGO@PDMS composites were

characterized using a Hitachi S-3400N scanning electron microscope, by first cutting three small portions from each film, sputtering them in a Q150R ES rotary pumped coater for 65 seconds at a plasma intensity current of 50 mA and a pressure of 0.1 mbar, followed by the SEM observation at magnifications of ×150 and ×500 and an acceleration voltage of 20 kV. Figure 54 shows the SEM device employed in this characterisation technique.

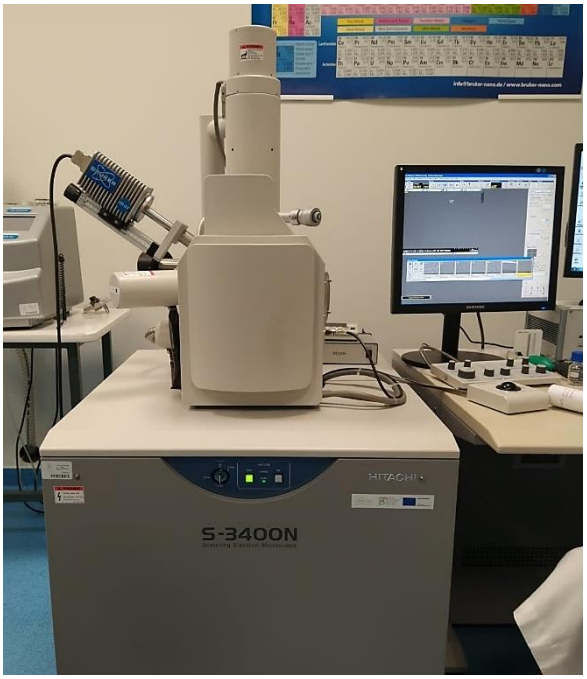

Fig. 54. Hitachi S-3400N Scanning Electron Microscope.

3.3.5. Structural characterisation

One technique used during the composite's structural characterisation is Fourier Transform Infrared Spectroscopy (FTIR), a very popular analytical technique able to perform spectral characterisation of both biological and chemical species in all states of matter, as it passes an infrared beam directly through the test sample [101]. Despite being largely employed in scientific research involving diagnosis and treatment of health-related complications, its easiness of use, allied to cost-effectiveness and rapidity, are very useful advantages in the field of materials science [101].

Due to its non-destructive, simple, and reproduceable properties, a sample of small dimensions is enough to provide valuable information of the arrangement of functional groups and chemical bonds present within the molecules, thanks to FTIR peaks that are intrinsic and specific to each one of them [101]. This is possible due to the focal plane array used by FTIR, instead of the more traditional single element detectors, along with a wide variety of different setups and approaches, enabling a whole new level of structural analysis performed on polymers [102].

However, despite FTIR spectroscopy being a fast data acquisition method, without requiring extensive sample preparation, it exhibits limited sample volume requirements, mainly when measuring aqueous solutions, because of the high absorbance of water, with the thickness limit usually being 6 μm [102]. Nonetheless, it is possible to boost the capabilities of the system by integrating different modules, depending on the necessity, such as macro and micro imaging, attenuated total reflection (ATR) devices, as well as transflection and transmission modes [102].

Keeping this into account, the structural characterisation, via Attenuated Total Reflectance Fourier Transform Infrared (ATR/FTIR), was made to a pristine PDMS film, sample PDMS@120/15, and rGO@PDMS composite samples with 3 wt.%, 4 wt.%, and 5wt.% rGO content. The characterisation was carried out using a Nicolet™ iS 10 FTIR spectrometer, manufactured by ThermoFisher Scientific. The spectra were recorded in the 525-4000 cm^{-1} range at ambient temperature and with a resolution of 4 cm^{-1} (32 scans). The chosen blank was air, at ambient temperature, being recorded with 128 scans. Regarding data management, spectroscopy data was collected, *visualise*d, processed and analysed with the support of the OMNIC™ software, developed by the same enterprise. Figure 55 shows the Nicolet™ iS 10 spectrometer employed for this characterisation technique.

Fig. 55. Nicolet™ iS 10 spectrometer, employed in the ATR/FTIR characterisation of pristine PDMS films and rGO@PDMS composite films.

3.3.6. Thermal characterisation

In order to further characterize the manufactured samples, it was decided to also investigate the composite's thermal properties by implementing thermal characterisation in the form of thermogravimetric analysis (TGA). In the field of materials science, this characterisation

technique is a standard method to study the overall thermal stability of a material, where its thermal degradation, as the temperature is rising, is evaluated and presented in a curve [103]. This curve, or thermogram, is a graphical representation of the sample mass change versus time or temperature, being dependent on a great number of factors, including the compound itself, sample shape, sample mass, heating rate, atmosphere, flow rate [103-105]. Thus, apart from determining weight loss at a certain temperature, it also returns the material's thermal stability, activation energy, kinetic parameters of pyrolysis, oxidative stability, product lifetime, along with volatile and moisture content [103, 104].

Carrying on with other characteristics, TGA tests usually employ an atmosphere of regular air, argon, helium, or nitrogen, at ambient pressure, although some high pressure TGAs being capable of reaching pressures of up to 15 MPa. Furthermore, TGA tests can be coupled with other techniques, such as differential scanning calorimetry (DSC) or differential thermal analysis (DTA), which complement and expand the potential of the characterisation, as will be explained below [104-106].

With this in mind, the thermal properties of samples with 0 wt.%, 3 wt.%, 4 wt.%, and 5 wt.% rGO content were determined using TGA on a TA instruments® Q50 thermogravimetric analyser (TA instruments, New Castle, DE, USA). Small circular samples were cut from the original films, with their weights varying between 28-32 mg, being these heated in a platinum pan from ambient temperature up to 800 ºC at a ramp of 10 ºC/min in a nitrogen environment at a flow rate of 40 mL/min. Figure 56 shows the equipment used for this characterisation technique.

Fig. 56. TA instruments® Q50 thermogravimetric analyser.

Chapter 4

Results

4. Results

With all materials, methods and characterisation techniques described for this work, this chapter will include all the obtained results during the testing phase, which encompasses the mechanical behaviour of both pristine PDMS films and rGO@PDMS composite films, piezoresistive response of rGO@PDMS composite samples, thermal properties by TGA, morphology and microstructure observation by SEM, and structural analysis by ATR/FTIR.

Moreover, all results are supplemented by images and graphs related to the tests carried out, to better grasp the influence of each parameter in the final performance, as well as the interactions that these variables have between each other.

4.1. Mechanical characterisation of pristine PDMS films

Regarding the mechanical behaviour of pristine PDMS films, these were grouped in three strain/stress graphs, depending on the elastomer-crosslinker ratio. For each configuration, 5 samples (45 samples total) were tested, with the best result for each configuration being chosen to integrate the graphs.

Firstly, for the 10:1 ratio samples, the observed maximum stress was the highest among all tests, with PDMS@20/10 configuration samples achieving 0.53 MPa (SD = 0.11 MPa), PDMS@65/10 achieving 1.58 MPa (SD = 0.12 MPa) and PDMS@120/10 achieving 7.52 MPa (SD = 0.71 MPa). On the other hand, the obtained strain was also the highest, being inversely proportional to the cure temperature. PDMS@20/10 configuration samples achieved 204% (SD = 38.6%), PDMS@65/10 achieved 152% (SD = 5.8%) and PDMS@120/10 achieved 157% (SD = 12.7%). This can be explained by the great influence of curing temperature at which crosslinking takes place, where higher temperatures have the tendency to catalyse the process and significantly alter the mechanical properties, leading to a crystal lattice with more crosslinks and an overall stiffer PDMS [107], explaining the higher values of stress obtained. Figure 57 shows the stress/strain graph of the 10:1 ratio pristine PDMS samples.

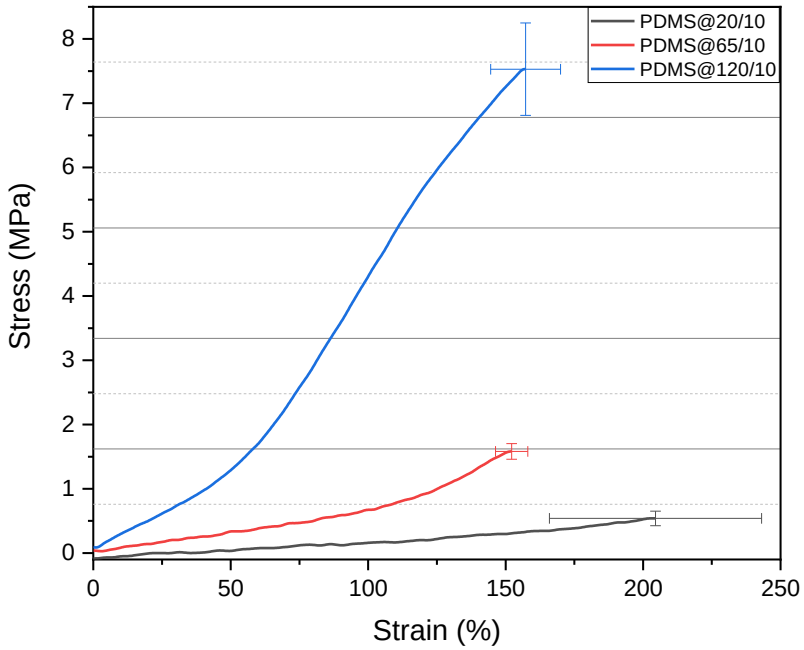

Fig. 57. Strain/stress graph of 10:1 ratio pristine PDMS films.

Passing on to 15:1 ratio sample results, it was immediately observed that the maximum stress achieved by these configurations was lower than those with a 10:1 ratio, due to the lower concentration of crosslinker, which lead to lesser promotion of stiffer crystal lattices [107]. However, temperature was still a big driving factor of film rigidity, where samples cured at 120 ºC achieved higher stress values, namely PDMS@20/15 with 0.17 MPa (SD = 0.04 MPa), PDMS@65/15 with 0.38 MPa (SD = 0.01 MPa) and PDMS@120/15 with 1.92 MPa (SD = 0.38 MPa). Regarding strain values, these diminished slightly, with PDMS@20/15 achieving 194% (SD = 16.9%), PDMS@65/15 achieving 133% (SD = 4.9%) and PDMS@120/15 achieving 151% (SD = 10.0%). Thus, it can be seen that the samples with the lowest strain possesses the highest strain standard deviation, while the sample with the highest stress exhibited the highest stress standard deviation. Figure 58 shows the stress/strain graph of the 15:1 ratio pristine PDMS samples.

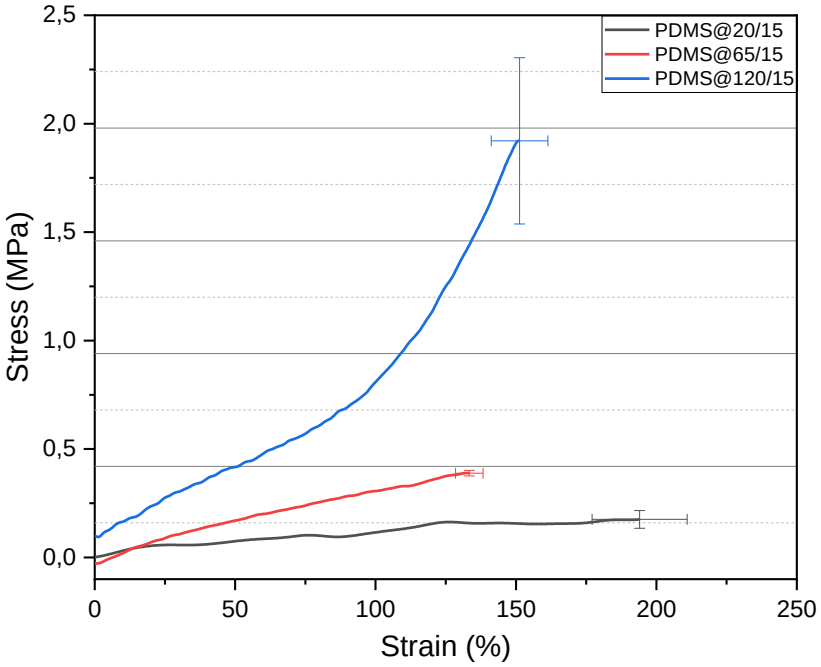

Fig. 58. Strain/stress graph of 15:1 ratio pristine PDMS films.

Finally, regarding samples fabricated with 20:1 ratio, these had the lowest stress values, with PDMS@20/20 achieving 0.18 MPa (SD = 0.01 MPa), PDMS@65/20 achieving 0.26 MPa (SD = 0.06 MPa) and PDMS@120/20 achieving 1.68 MPa (SD = 0.40 MPa). Regarding strain, PDMS@20/20 achieved 160% (SD = 10.1%), PDMS@65/20 achieved 98% (SD = 14.3%) and PDMS@120/20 achieved 169% (SD = 18.4%). Lower stress values can be explained by an even lower concentration of crosslinker than the one recommended by the manufacturer (10:1 ratio), leading to the formation of deficient crystal lattices and the consequent loss of mechanical performance. Figure 59 shows the stress/strain graph of the 20:1 ratio pristine PDMS samples.

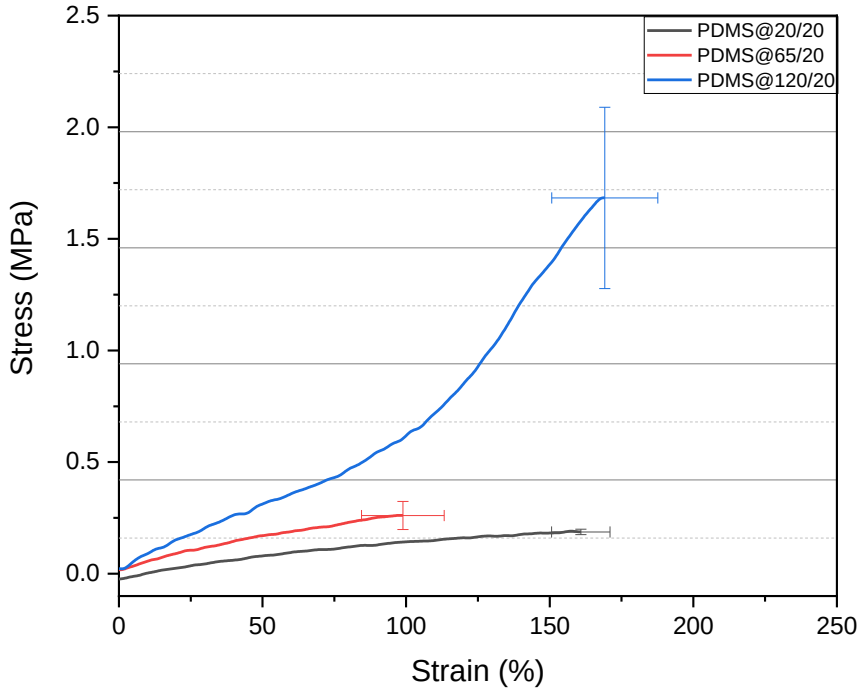

Fig. 59. Strain/stress behaviour graph of 20:1 ratio pristine PDMS films.

After concluding the mechanical tests, all data was analysed with the objective of calculating the Young's modulus for each sample. This was made possible by calculating the slope of the linear regression in the elastic zone or by applying Equation (4), according to [95]. In the case of PDMS, its elastic zone is located after the curve's first inflection point, which separates the conformation zone from the elastic zone, since this behaviour was transversal to all samples. Table 6 shows the calculated Young's modulus for all the tested configurations.

By observing the obtained results throughout the tests, as well as the Young's Modulus of each sample, it is possible to conclude that the cure temperature, along with the crosslinker concentration, are extremely important parameters for the successful fabrication of thin PDMS films. Taking this into account, rising temperatures are accompanied by rising Young's modulus values, in all configurations. On the other hand, when the crosslinker concentration was lowered, the Young's modulus decreases in all configurations but one, PDMS@120/20. To further validate the results, Johnston *et al.* [108] applied and measured stress in PDMS samples, fabricated with a 10:1 ratio, achieving very similar stress values to PDMS@120/10.

Therefore, depending on the mechanical characteristics of the desired body's surface, it is possible to tune the PDMS film's mechanical behaviour, by varying either the cure temperature or the elastomer-crosslinker ratio, in order to achieve the indicated conformity and the best possible comfort, avoiding high Young's modulus values, which also benefits the prosthetics and smart clothing fields.

Table 6. Maximum stress, strain and calculated Young's Modulus for all configurations tested.

Configuration	Maximum Stress (MPa)	Maximum Strain (%)	Young's Modulus (MPa)	R^2
PDMS@20/10	0.53	204	0.21	0.948
PDMS@65/10	1.58	152	0.99	0.972
PDMS@120/10	7.52	157	6.81	0.999
PDMS@20/15	0.17	194	0.19	0.7973
PDMS@65/15	0.38	133	0.28	0.996
PDMS@120/15	1.92	151	1.05	0.964
PDMS@20/20	0.18	160	0.11	0.978
PDMS@65/20	0.26	98	0.19	0.988
PDMS@120/20	1.68	169	1.21	0.966

4.2. Piezoresistive behaviour of rGO@PDMS composites

In this section, all data related with the rGO@PDMS composites piezoresistive testing will be compiled, making a comparison between the responses each sample gave when mechanically deformed. Thus, in this section, the results regarding testing velocity, gauge factor variation depending on applied strain, 3-point bending tests, tensile tests and cyclic stability test will be addressed and discussed. An important factor that will also be focused on is the peak gauge factor, as well as its average and variation when comparing samples with different rGO content.

Gauge factor per test velocity

In order to decide which testing velocity was the best candidate for the 3-point bending tests, ten velocities, between 1 mm/min and 10 mm/min, were tested during a 4-cycle 3-point bending test, done to sample 3A1, followed by the calculation of the average gauge factor. Hence, the optimal velocity is the one that leads to higher average gauge factors, without compromising the electrical data acquisition by the multimeter nor turning the test too time-consuming. Figure 60 shows the graph that compiles the test velocities and the calculated average gauge factors.

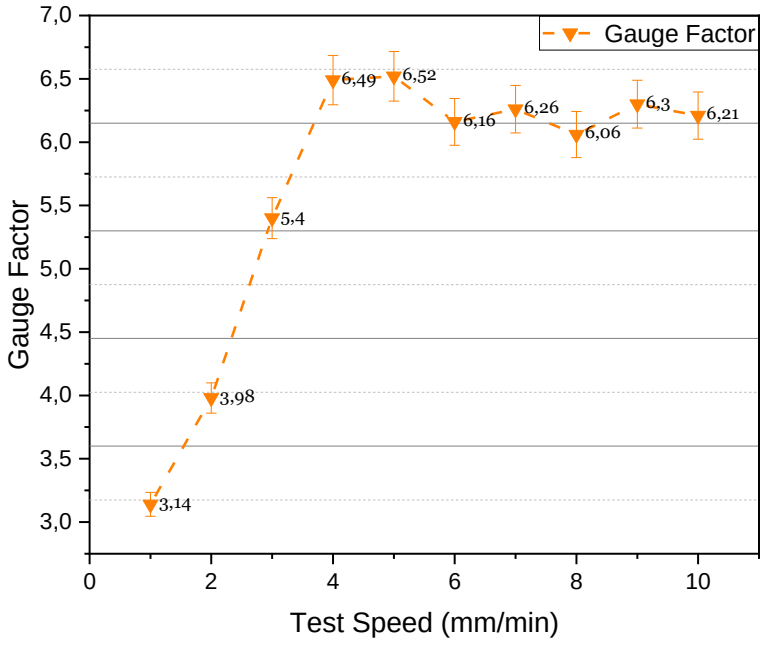

Fig. 60. Average ascending gauge factors calculated from a 4-cycle 3-point bending test, with a maximum strain of 1.54%, for sample 3A1.

Looking at the results, it can be concluded that velocities equal and above 4mm/min show much higher average gauge factors, always above 6, while the ones up to 3mm/min do not. On the other hand, by analysing the electrical response captured by the multimeter, the conclusion was that the highest velocities could have compromised the signal, due to the multimeter's sampling rate of 1Hz not being high enough to detect the resistance peaks when maximum strain was applied. Thus, speeds of 4, 5 and 6 mm/min were indicated for the tests, with 5 mm/min being chosen due to being a common value seen in literature, allied to showing the highest calculated gauge factor.

3-point bending tests

With the test velocity decided, all chosen rGO@PDMS samples were tested as described in the subchapters above, followed by the analysis of their average gauge factor throughout the different strains tested. In this section, samples will be divided by wt.% of rGO and compared between each other, since all percentages by weight above 3 wt.% exhibited responsive piezoresistive behaviour.

Starting with samples produced with 3 wt.% of rGO, these showed some of the highest average gauge factors, only surpassed by samples with 4 wt.% of rGO. Nevertheless, these films had the mechanical characteristics most suited for the aim of this work, being able to endure the manipulation by the user, at all times, withstanding high values of strain and stress, which

makes them the best option for zones of the body with intrinsically high rates of deformation. Figure 61 shows a graph where the average gauge factors are compiled for samples 3A1, 3A2 and 3A3, depending on the induced strain.

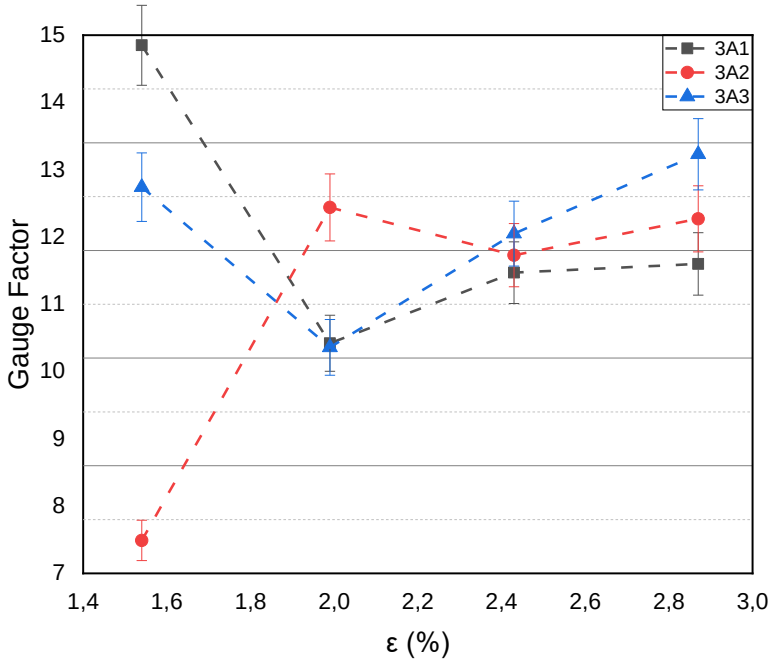

Fig. 61. Compilation of the average gauge factors calculated for each strain rate, for samples 3A1, 3A2 and 3A3.

Taking into account that sample 3A1 had, overall, the highest average gauge factors, with the maximum average gauge factor being 14.85, calculated on the first cycle of the lowest deformation, and the most representative of the typical electromechanical behaviour, graphs consisting of the piezoresistive response, compiling both strain and the variation of relative electrical resistance through time, for ε_{max} = 1,54%, 1.99%, 2.43% and 2.87%, equivalent to a displacement of 3.5 mm, 4.5 mm, 5.5 mm, and 6.5 mm, respectively, are available in Figure 62. The the sampled electrical signal shows great linearity, despite the tendency that the variation of relative electrical resistance has to gradually reduce each bending cycle. One possible explanation could be that mechanical deformations induce morphology changes on the rGO conductive network, leading to ever-present variations on the sampled peak electrical resistance, as well as the hysteresis effect that is to be expected, since these materials tend to preserve some properties and deformation when the stimuli stops being applied [109]. Despite this, the phenomenon is more prevalent at the lowest strain rate, being substantially reduced at higher strains.

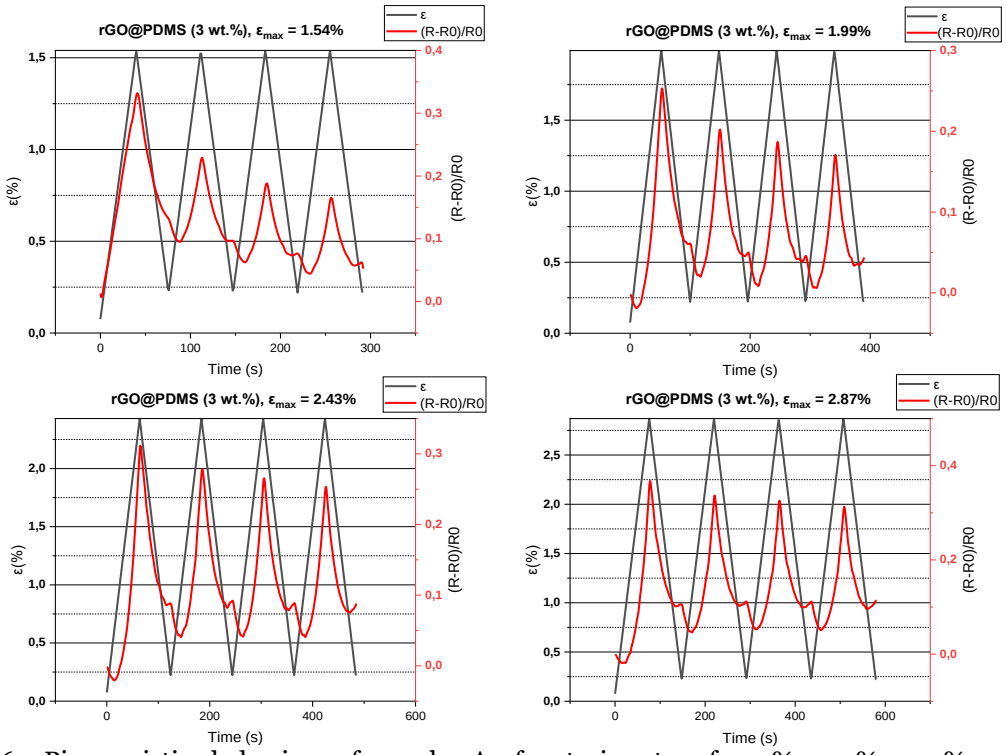

Fig. 62. Piezoresistive behaviour of sample 3A1, for strain rates of 1.54%, 1.99%, 2.34% and 2.87%.

Passing on to samples 4A1 and 4A2, produced with 4 wt.% of rGO, these exhibited the highest recorded values, reaching, in one instance, an average gauge factor of 30.8, calculated on the first cycle of the lowest deformation. Thus, samples produced with this quantity of rGO show great electromechanical behaviour, with the highest sensitivity obtained in this work. However, its mechanical properties leave something to be desired, due to withstanding lower deformations and showing higher brittleness, a product of the interaction between the PDMS matrix and the rGO reinforcement, which, to some extent, negatively influenced the matrix's crystal lattice. Thus, devices employing this composite should focus on zones of the body with lower intrinsic deformations, compared to the previous ones. Figure 63 shows the graph representing the average gauge factors calculated at the same strain rates as above.

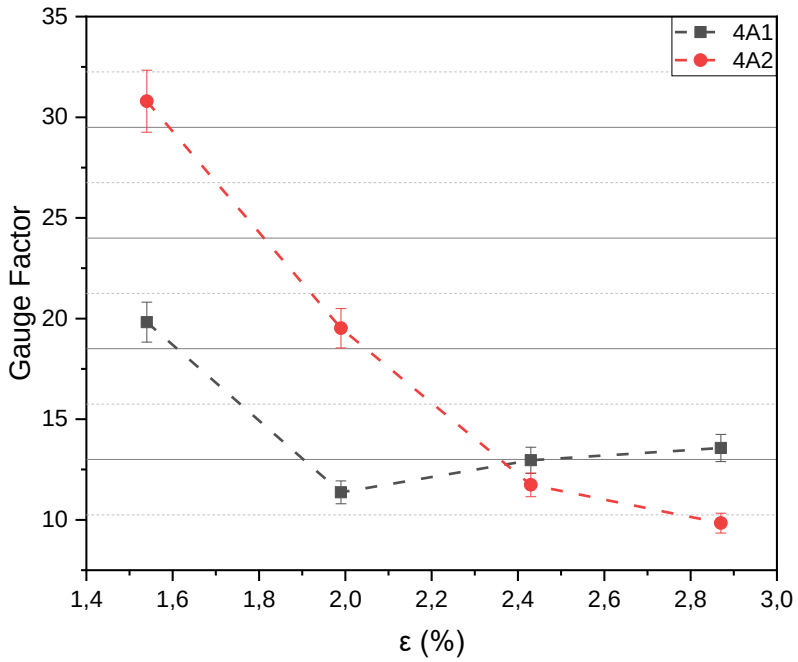

Fig. 63. Average gauge factors calculated for each strain rate, for samples 4A1 and 4A2.

Since sample 4A2 showed very high average gauge factors, compared to sample 4A1, graphs compiling strain and relative electrical resistance variation through time were also presented, as shown in Figure 64.

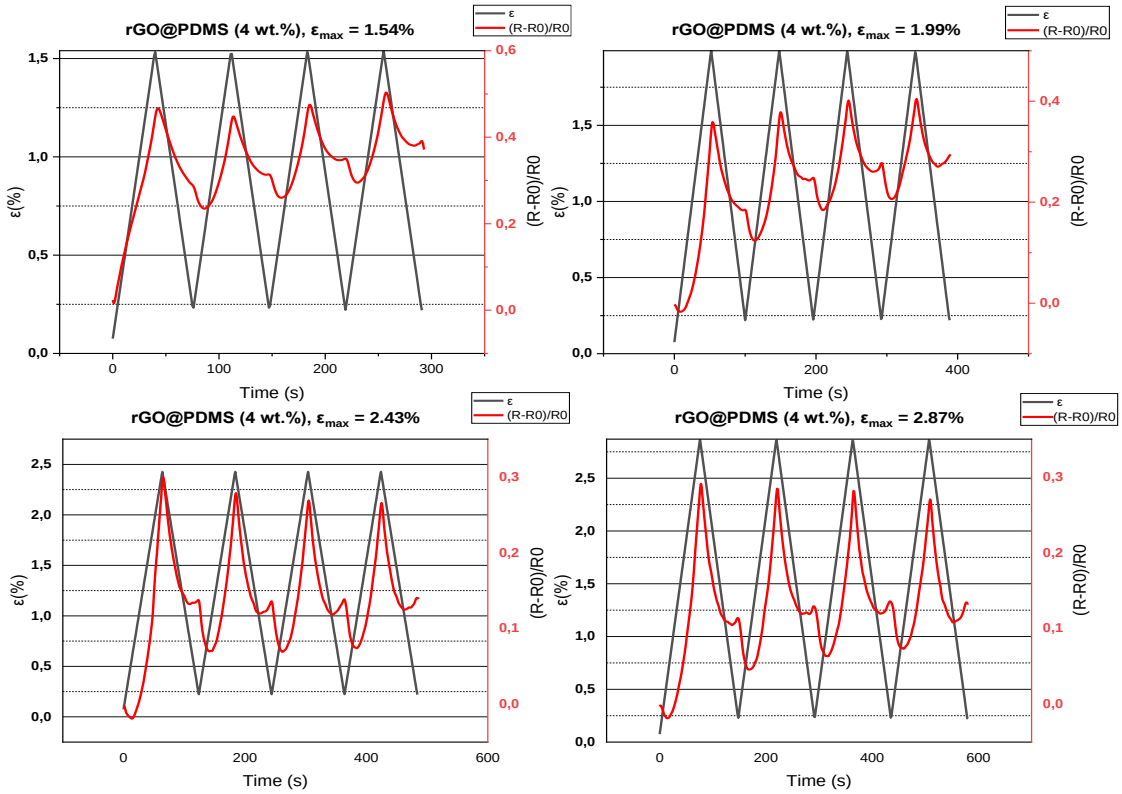

Fig. 64. Piezoresistive behaviour of sample 4A2, for strain rates of 1.54%, 1.99%, 2.34% and 2.87%.

As seen in Figure 64, the sampled electrical signal also shows great linearity. However, now the tendency is a very noticeable rise of relative electrical resistance variation at lower strains, with a gradual reduction of it at higher strains, from one bending cycle to the next. The main explanation in this case is that higher concentrations of rGO interact in a different way with the PDMS matrix, leading to a conductive network that behaves differently at lower and higher strain rates, showing higher variations of relative electrical resistance mainly at the former.

Lastly, samples 5A1, 5A2 and 5A3, produced with a rGO content of 5 wt.%, showed, overall, the lowest recorded average gauge factor, with sample 5A3 achieving a maximum average gauge factor of 9.16, calculated on the first cycle of the lowest deformation. Allied to this, a poorer mechanical performance observed macroscopically and by touch, i.e. highest brittleness and rigidity, as well as the most complicated moulding and demoulding during the manufacturing stages make these samples only useful in zones of the body that experience very low deformations. This can be considered an even graver case of the conductive network negatively influencing the structural integrity of the matrix, leading to the complete loss of the elastomer-like behaviour that PDMS is known for. Therefore, it can be safely assumed that the rGO concentration has, in this case, led to a saturation point. This, allied to lower average gauge factors, are indicators that this group of samples exhibits conductive networks with behaviour already outside of the percolation threshold. Figure 65 shows the graph representing the average gauge factors calculated at the tested strain rates.

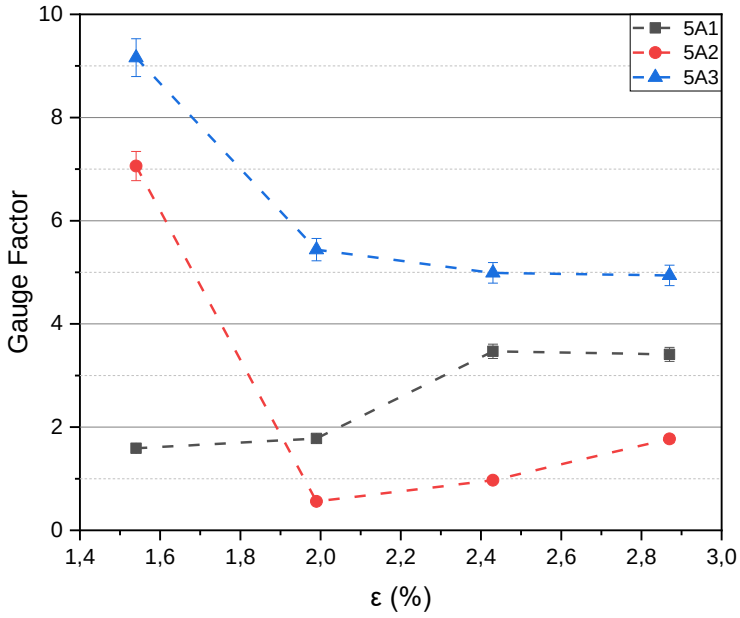

Fig. 65. Average gauge factors calculated for each strain rate, for samples 5A1, 5A2 and 5A3.

Despite this, sample 5A3 showed a somewhat competitive and consistent average gauge factor throughout testing, undoubtedly superior to the other samples and, for these reasons, was

chosen as one of the samples used in the follow-up tests. Moreover, graphs compiling relative electrical resistance variation and strain through time were also constructed, as shown in Figure 66.

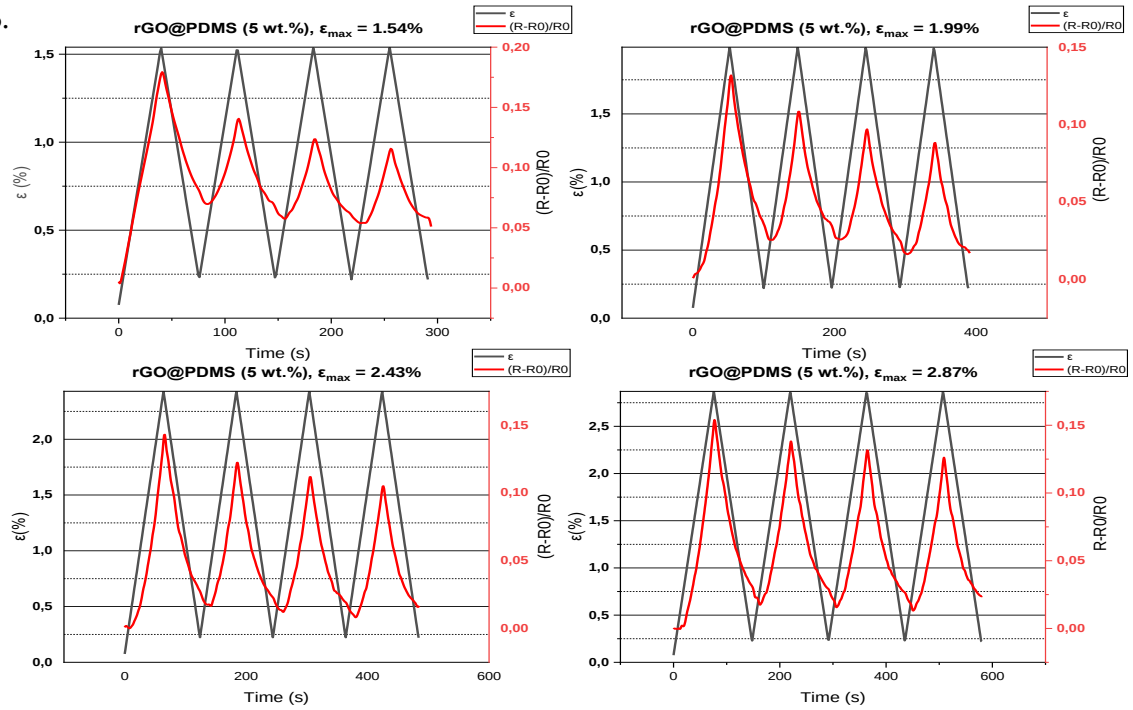

Fig. 66. Piezoresistive behaviour of sample 5A3, for strain rates of 1.54%, 1.99%, 2.34% and 2.87%.

By analysing Figure 66, it can be concluded that the electrical signal is also highly linear, being perfectly synchronized with the applied mechanical deformations. However, the variation of relative electrical resistance reaches considerably lower values, often not reaching 0.10, compared to much higher values of 0.25-0.5 of other samples. Furthermore, despite the mechanical limitations of the film, the gradual reduction of the peak variations is very noticeable at higher strain rates, reflecting a conductive network and piezoresistive performance that is better suited for relatively higher mechanical deformations, with the likely explanation being that a composite with this rGO content already sits outside the percolation threshold, requiring higher strains to achieve consistent relative electrical resistance peaks.

Cyclic Stability Test

Due to many of the samples exhibiting changes in the relative electrical resistance variation throughout the cycles, a new test was made, were sample 3A1 was put through 100 cycles of flexural deformation, with the maximum strain being 1.54%, due to higher values leading to the electrodes breaking off the surface. The aim of this experiment was to observe how the conductive network behaves during longer-term usage, surveilling how it conforms and verifying if eventually a stabilization of the phenomenon occurs. Figure 67 shows a graph representative of the experiment described above.

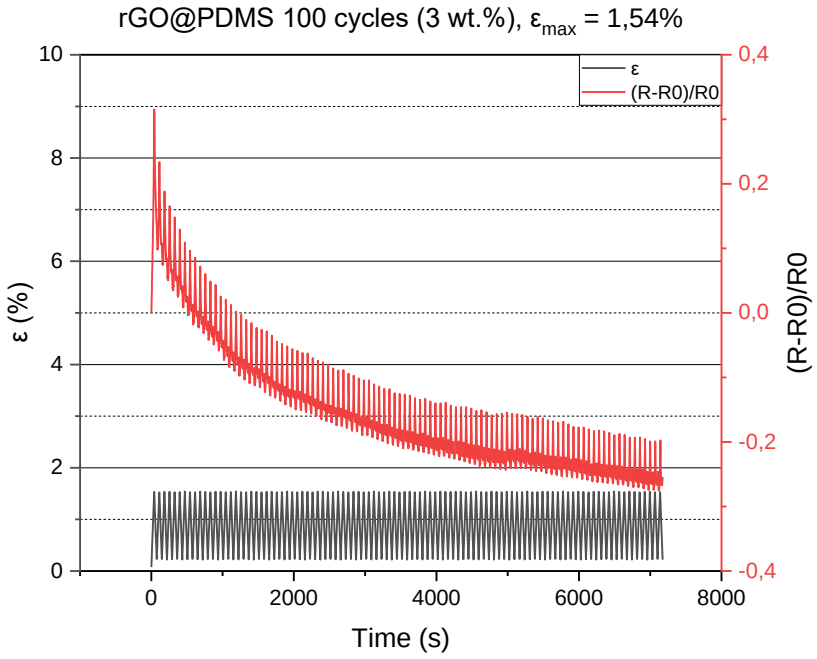

Fig. 67. 100 cycle stability bending test with sample 3A1, compiling both the variation of strain and the relative electrical resistance variation.

By observing the graph it can be concluded that the rGO conductive network is, throughout the experiment, constantly conforming to the mechanical deformation, suffering a pronounced reduction of relative electrical resistance variation in the initial segment of the test, despite maintaining similar amplitude variation each cycle, but also gradually stabilizing during the rest of it (after cycle ≈55), and especially so in the later half, showing that the composite's crystal lattice is able to maintain stable electrical resistance even during sustained mechanical deformation. Thus, it is safe to assume that after a conformation period, the electromechanical behaviour of the composite material stabilizes and the sensor can still function at its full capacity, reflecting a very important characteristic of sensorial systems, which is enduring prolonged periods of usage by the wearer.

Tensile Tests

After all samples were put through 3-point bending tests, samples 3A1, 4A2 and 5A3 were selected to participate in piezoresistive tensile tests, with the aim of observing the electromechanical behaviour of the samples during tensile deformation. In this section, the results to both cyclic tensile tests and tensile deformation until electrical resistance overload will be presented and described.

Beginning with cyclic tensile tests, sample 3A1 was strained up to 40%, while samples 4A2 and 5A3 were strained up to 20%, due to their higher rigidity preventing testing at higher values. Starting with sample 3A1, during testing, this sample displayed the highest average

gauge factor, with a value of 4.894, along with good linearity. However, during the cycles, the variation of relative electrical resistance decreased substantially, especially from the first to the second cycle, most likely a product of the conductive network's conformation. Despite this, its value is still high, denoting good sensitivity.

Passing on to sample 4A2, the calculated average gauge factor was 0.434, due to overall lower values of relative electrical resistance, but showing the best linearity, with some minor interferences at the end of each cycle. This lower average gauge factor could be explained by less straining during the test, but since the mechanical integrity was an important factor during this experiment, nothing could have been done to change this.

Lastly, regarding sample 5A3, it was observed that the piezoresistive behaviour was extremely exacerbated, reaching electrical resistance overload almost instantly when mechanically strained. This could be explained by a less deformable and more brittle PDMS induced by a high rGO content, which may have translated into an accelerated separation of the conductive network's carriers, or the appearance of microfractures at the time of tensile strain application, nullifying conductivity in each cycle. Therefore, no average gauge factor could be calculated, nor could the variation of relative electrical resistance be observed effectively. However, linearity is present, despite the existence of some lag between the mechanical deformation and the electrical response.

Taking this into account, while samples with a rGO content of 3 wt.% and 4 wt.% are suited for applications where tensile deformation is present, samples with a rGO content of 5 wt.% are better suited for applications that only require flexural strain. Figure 68 shows the built strain/relative electrical resistance variation graphs representative of these tests. Something to take into account is that no image processing program, such as ImageJ™, was used to better calculate the strain applied by the universal testing machine, due to the difficulty related to finding the exact moment where the cycles begin and end, which would result in an associated error equal or higher than the one currently present in the below-displayed graphs, built with strain data given by the universal testing machine.

Regarding the tests where the samples were tensile strained until electrical resistance overload was achieved, electrical resistance overload was reached in sample 3A1 at $\varepsilon = 60.06\%$, while overload was achieved in sample 4A2 at $\varepsilon = 24.99\%$. The conclusion that can be drawn from this is that the connections in the rGO's conductive network are lost before the destruction of the sample, acting as a very important indicator of the overall structural health of the composite material. Moreover, after the test stopped and the sample returned to normal, the electrical signal was restored, which means that the conductive network was not damaged irreversibly during the ordeal.

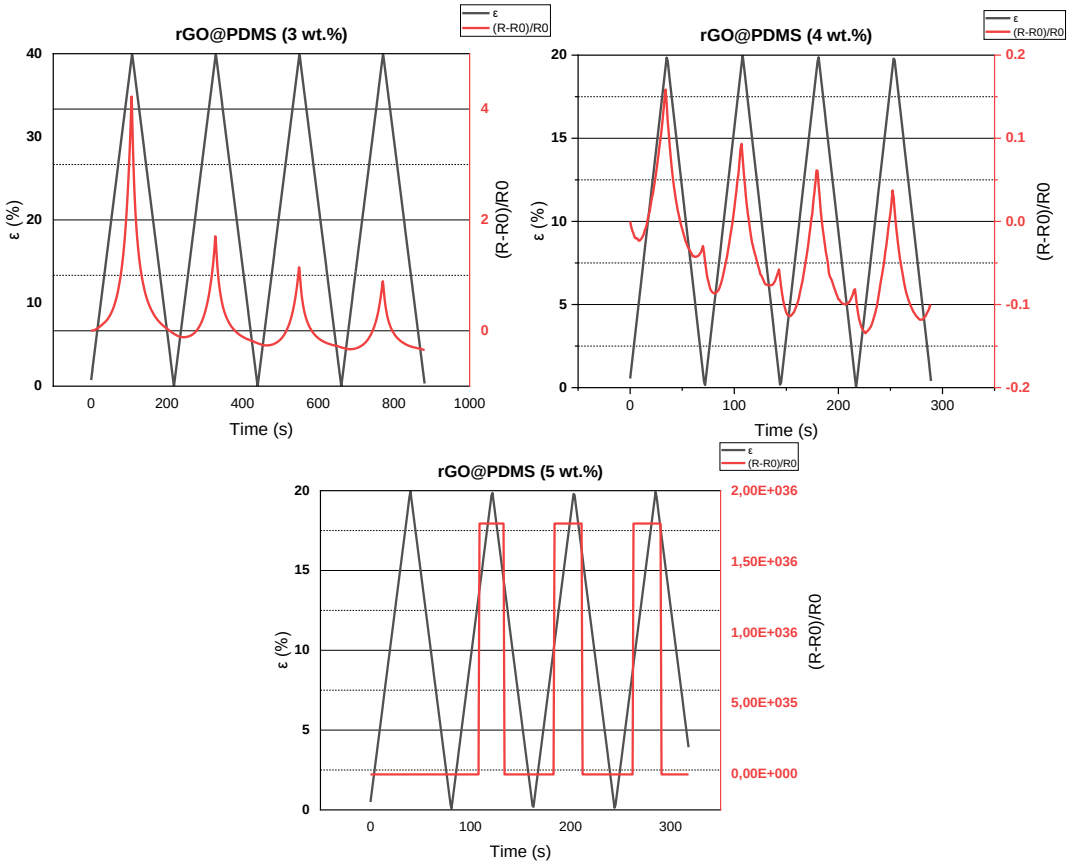

Fig. 68. Piezoresistive behaviour of samples 3A1, 4A2, 5A3, during the cyclic tensile tests, for a maximum tensile strain of 40% and 20%, respectively.

However, regarding sample 5A3, electrical resistance overload was briefly achieved at ε = 5.2%, followed by the signal returning and a second electrical resistance overload at ε = 8.33% leading to the total mechanical failure of the composite material at around ε = 15.1%. This phenomenon can be explained by a possible conformation of the conductive network during the first electrical resistance peak, followed by the irremediable damage suffered by the entire structure and the breakdown of the material in the second peak. Therefore, by looking at this result, it can be assumed that applying enough strain to split the electrical connectors inside the composite is a hazardous condition for the sensor and should not be attempted during prolonged testing or in commercial applications, unless that is the objective of the experiment. Figure 69 shows the strain/relative electrical resistance variation during the above-described test. In the case of this graph, a logarithmic scale was chosen to observe the relative electrical resistance variation to its fullest extent, which tends to infinity, without compromising the visibility of the remaining data.

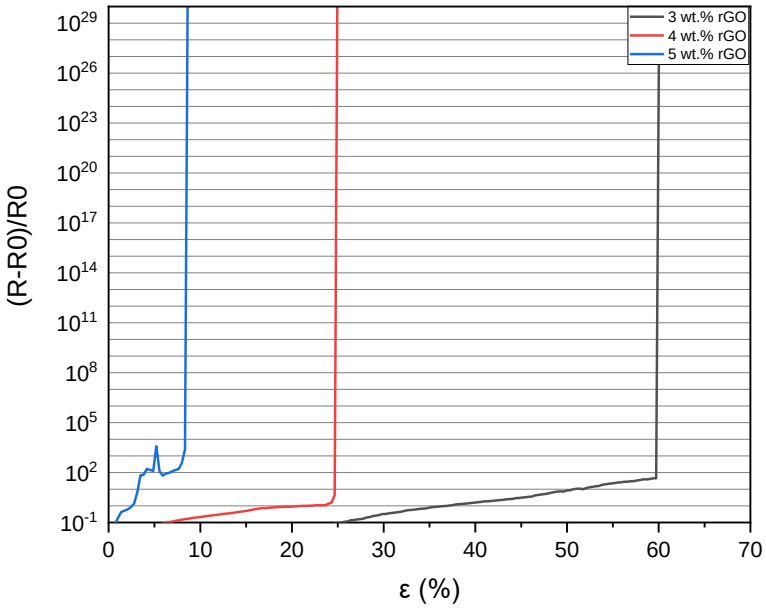

Fig. 69. Strain/Relative electrical resistance variation during the electrical resistance overload tensile test, for samples 3A1, 4A2 and 5A3.

4.3. Mechanical characterisation of rGO@PDMS composites

Moving on to the obtained results in the rGO@PDMS tensile rupture tests, these were grouped in a strain/stress graph, with the best result for each wt.% being chosen to integrate it. In this phase, all samples, 8 of them, were strained until rupture, with their data being used to calculate stress and strain averages and standard deviations, as well as comparing samples between each other.

Starting with the composites produced with 3 wt.% rGO, the sample which achieved the best results was 3A1, with a maximum strain of 141.93% (SD = 19.17%) and a maximum stress of 1.837 MPa (SD = 0.3 MPa), with this group being, by far, the one that reached the highest values. This is likely explained by the lower content of rGO, which allows for piezoresistive behaviour without negatively affecting the mechanical properties of the PDMS matrix, since these are the only samples that resemble flexible films similar to the ones produced with pristine PDMS, a factor that is not witnessed in the other groups. When compared to pristine films cured at the same temperature (120 °C/20 min), this sample exhibits remarkably competitive values of strain and stress, with $\varepsilon \approx 142\%$ being just shy of $\varepsilon \approx 151\%$, and a maximum stress of ≈ 1.84 MPa also sitting very close to the maximum stress of ≈ 1.92 MPa achieved by pristine PDMS samples.

Thus, these samples are suited for physiological signal monitoring on locations of the body that require sensors with high strain capabilities, such as the fingers, elbows, shoulders, etc.

Secondly, regarding samples manufactured with 4 wt.% rGO, the one with the highest performance was 4A2, achieving a maximum strain of 34.74% (SD = 1.47%) and a maximum stress of 0.87 MPa (SD = 0.2 MPa). While these values are much lower than the ones attained by pristine PDMS films, this sample group exhibits very high piezoresistive sensitivity. This can be explained by a higher content of rGO, probably still situated in the percolation threshold, but one that already jeopardizes the morphology of the PDMS's crystal lattice and, consequently, its mechanical performance. Thus, these samples could only be employed in locations of the body that demand lower strain capabilities, such as the neck and throat.

Lastly, when speaking of samples produced with 5 wt.% rGO, 5A2 reached the best outcome of all, with a maximum strain of 30.82% (SD = 1.41%) and a maximum stress of 0.92 MPa (SD = 0.01 MPa). Taking these results into account, also very low when compared to pristine PDMS films, along with the exacerbated responses given during the cyclic tensile tests, it can be concluded that this content of rGO most likely puts the composite outside of the percolation threshold and into the conductor side. Moreover, since it further negatively impacts the mechanical performance of the matrix, this group of samples could only be effectively employed in areas of the body which would not require tensile deformation, only flexural, such as the throat, monitoring deglutition and speech patterns, for example. Figure 70 shows the stress/strain graph of the rGO@PDMS composites during the tensile rupture tests. However, something to bear in mind is that no image processing program, such as ImageJ™, was used in these trials to measure the applied strain, due to this procedure not being applied during the mechanical characterisation of pristine PDMS films and, therefore, providing a possible unfair advantage to these composite films.

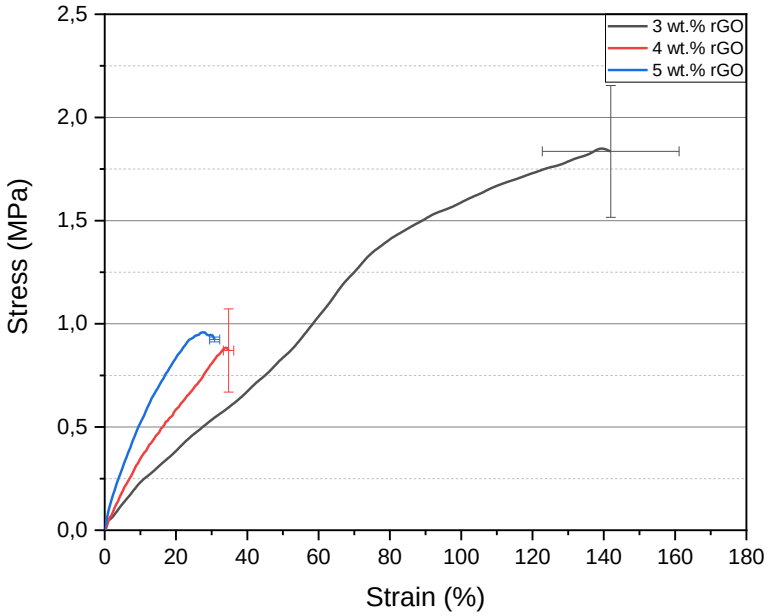

Fig. 70. Strain/Stress graph of the rGO@PDMS composites during the tensile rupture tests, organized by percentage by weight of rGO.

After concluding the mechanical tests, all data was analysed with the objective of calculating the Young's modulus for each of the samples. Once again, the slope of the linear regression in the elastic zone of the composites was calculated. Similarly to pristine PDMS, the elastic zone is located after the curve's first inflection point, which separates the conformation zone from the elastic zone [95]. Table 7 shows the calculated Young's modulus for all the tested configurations.

Table 7. Maximum stress, strain, and calculated Young's modulus for pristine PDMS and composite samples 3A1, 4A2 and 5A2.

Percentage by weight	Maximum Stress (MPa)	Maximum Strain (%)	Young's Modulus (MPa)	R^2
PDMS@120/15	1.92	151	1.05	0.964
3 wt.% (3A1)	1.837	141.93	1.964	0.995
4 wt.% (4A2)	0.87	34.74	2.224	0.999
5 wt.% (5A3)	0.92	30.82	3.084	0.996

After observing the samples' calculated Young's modulus throughout the tensile rupture tests, it can be concluded that the rGO content greatly influences both the electromechanical performance and the product of fabrication, where a rising rGO content is accompanied by rising Young's modulus values. When compared to pristine PDMS films manufactured with the

same characteristics, which had a Young's modulus of 1.05 MPa, a composite with 3 wt.% rGO exhibits a 187% increase of this value, the composite with 4 wt.% rGO had a 211% increase, while the composite with 5 wt.% rGO showed a 293% increase in the Young's modulus. Mainly with the 4 wt.% and 5 wt.% films, this translates into higher rigidity and brittleness when cured, but also greater viscosity throughout the manufacturing process, which hinders a successful final product. Moreover, higher Young's modulus values also mean that the films cannot sustain strain as high as pristine PDMS, which was verified during both cyclic tensile tests and tensile rupture tests.

Taking this into account, it was proven that it is possible to tune the mechanical behaviour of rGO@PDMS composite films by varying the rGO content, as well as its cure temperature and elastomer-crosslinker ratio, depending on the destined application. Thus, this sensor displays immense versatility, where the manufacturing process can be adjusted in accordance with the indicated conformity and comfort.

4.4. Morphological characterisation

With the characterisation by SEM concluded for pristine PDMS and rGO@PDMS composite films, their images were compiled and will be discussed in this section of the work. Starting with the characterisation of the pristine PDMS sample, Figure 71 shows the obtained SEM images at a magnification of ×150 and ×500.

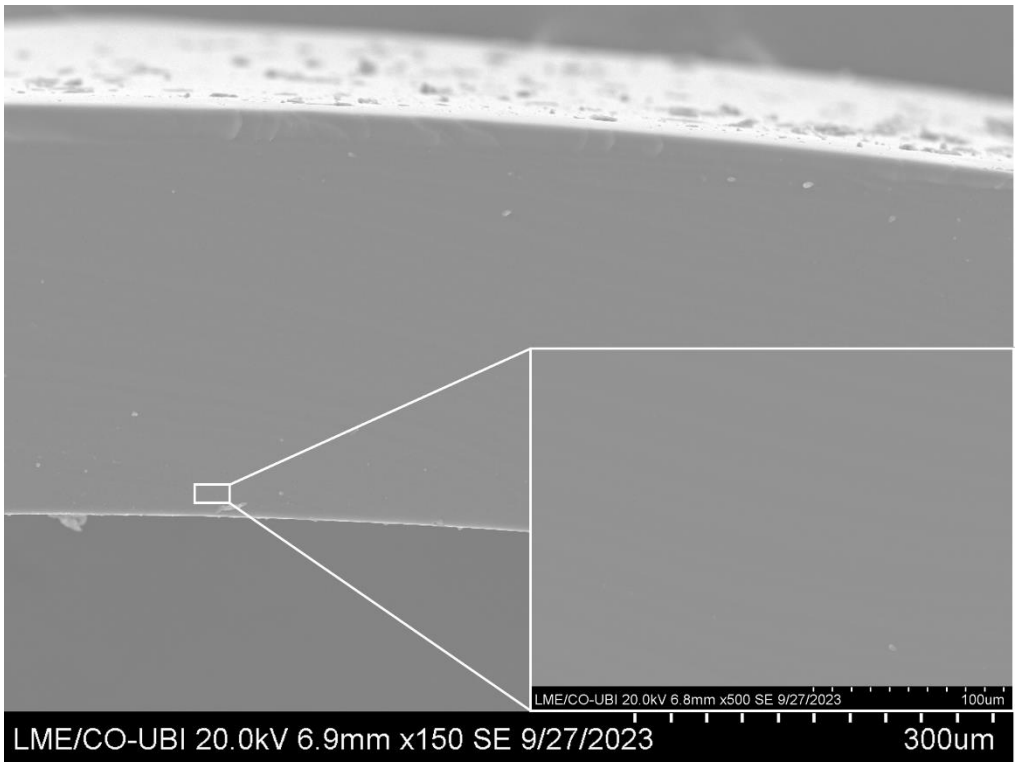

Fig. 71. SEM images of a pristine PDMS film cross-section, at a magnification of ×150 and ×500.

By observing the images, it can be concluded that the microstructure of the chosen matrix did not exhibit visible damage nor the presence of any pores, an indication of the great mechanical elasticity of this material, as well as solid and smooth appearance, as reported by Iqra *et al.* [91] and Wang *et al.* [110]. With this information, it can be assumed that the chosen manufacturing procedures allowed for the production of a matrix that did not show any signs of malformations or weaknesses in its structure, a necessary factor for the good operation of a composite material.

Passing on to the obtained images from the 3 wt.% rGO content sample's microstructure, these are presented in Figure 72 and will be discussed further below.

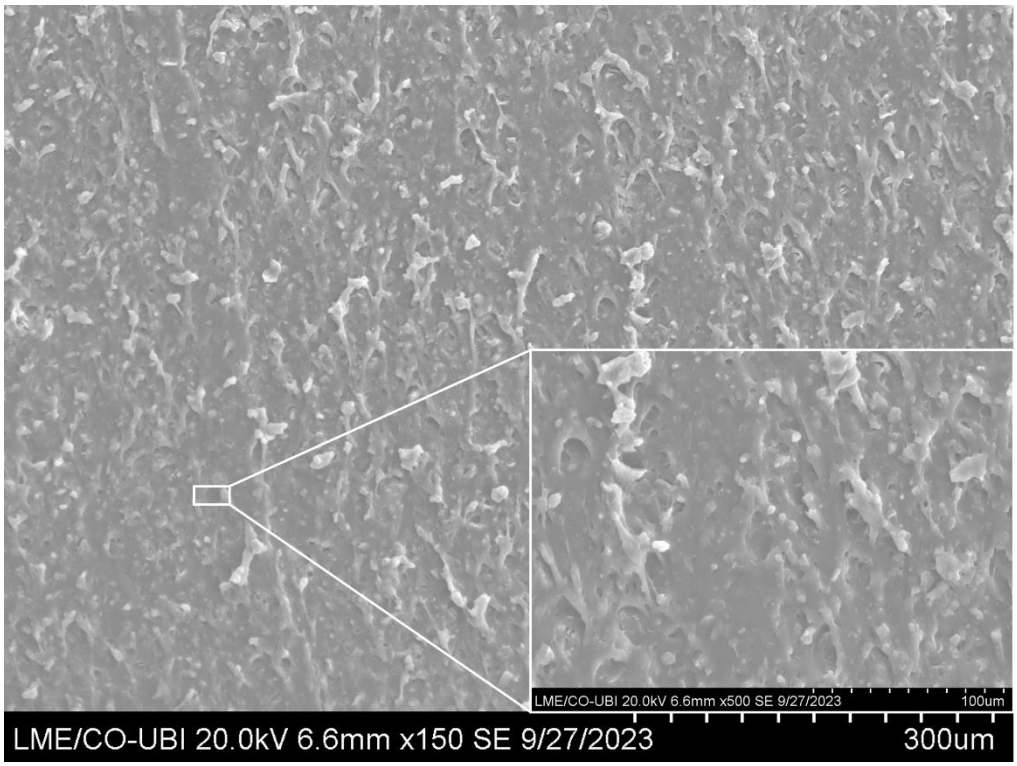

Fig. 72. SEM images of a rGO@PDMS composite with a rGO content of 3 wt.%, at a magnification of ×150 and ×500. Graphene can be identified by the fair-coloured, crumpled, wrinkled, and flaky structures, while the polymer matrix can be identified by the darker, smoother spots.

Contrarily to the smooth microstructure inherent to pristine PDMS, the addition of rGO led to a rougher morphology, but still without the presence of pores. Along these lines, the microstructure of this sample exhibited a crumpled, wrinkled and flaky-like morphology, characteristics that are associated to the addition of this compound and reported in multiple works [91, 110, 111]. This crumpled appearance is also supported by the compound's synthesis approach, since the reduction of GO leads to the loss of many oxygen-containing functional groups, such as hydroxyl (-OH) and carboxyl (-COOH), which causes the loss of binding water between nanosheets and a general loss of volume [111].

Thus, in this cross-section, it was possible to observe the impact that rGO had on the composite's rigidity and internal organization, causing the presence of agglomerate-like structures after the cutting process, a sign of a successful and effective embedding of rGO in the polymer matrix, which in turn translated into a more stable and robust filler [111, 112]. On the other hand, the rGO's dispersion, aided by differences in density and by the production method [110], was most likely uniform, covering the entire visualised area, which explains the good electrical properties inherent to this composite.

To support this, when compared to the other observed composites, the lack of large-sized agglomerates also explains the great resistance variation when mechanical deformation is applied [110]. Thus, the formation of this network could additionally lead to a higher specific superficial area, positively affecting the properties of the composite [113].

Shifting to the obtained images from the 4 wt.% rGO content sample's microstructure, these are presented in Figure 73 and will be discussed below.

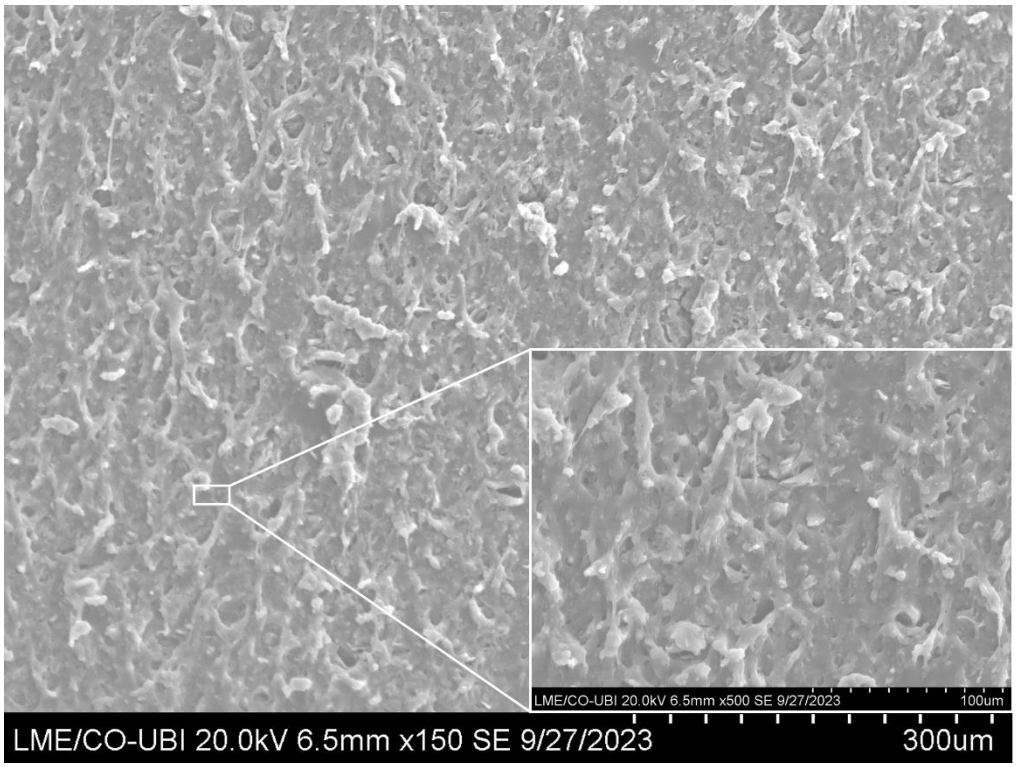

Fig. 73. SEM images of a rGO@PDMS composite with a rGO content of 4 wt.%, at a magnification of ×150 and ×500.

Looking at the taken images of this configuration, it can be stated that much of what was said for the previous configuration samples is still applicable here, namely the filler's dispersion uniformity, as well as its rough appearance, in this case with more crumples and wrinkles, possibly due to the higher degree of rGO nanoparticles agglomeration. Along these lines, since the used rGO concentration was higher, compared with the previous configuration, a larger number of agglomerates are visible, with these having bigger dimensions, explained by

the chemical nature of the filler that promotes the formation of structures with stacked nanoparticles [113].

Nevertheless, the formation of an organized conductive network still took place, which allied to a higher rGO content, led to a composite with the highest recorded sensitivity in this work, an aspect that is proven by this characterisation.

Lastly, carrying on to the obtained images from the 5 wt.% rGO content sample's microstructure, these are presented in Figure 74 and will be discussed next.

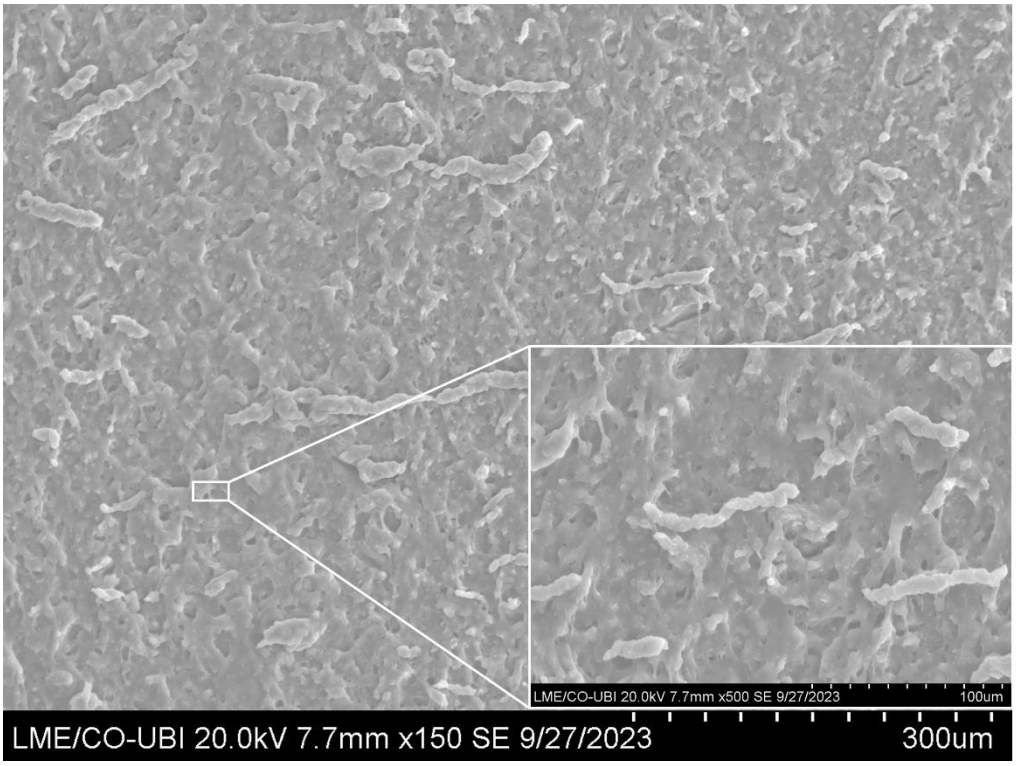

Fig. 74. Scanning Electron Microscope (SEM) images of a rGO@PDMS composite with a rGO content of 5 wt.%, at a magnification of ×150 and ×500.

In the case of this configuration, the obtained SEM images are evidence of the influence that high concentrations of filler have on the composite's microstructure, which significantly altered its mechanical and electrical behaviour, since it is possible to observe the presence of a greater quantity of large-sized agglomerates after the cutting process, the largest of all characterized samples. Furthermore, some pore-like structures are also present in larger quantities, which is possibly induced by agglomerates that were ripped out when the cross-section was being performed.

Thus, by conducting this characterisation process it can be concluded that a direct correlation between the filler concentration in a composite, its microstructure, and its electromechanical properties exists. Associated with this, in this case, despite a conductive network existing, the presence of large agglomerate-like structures proves that the matrix-filler interactions are not ideal, something that is reinforced by previously seen mechanical and

piezoresistive performances, which were subpar when compared with the remaining composite configurations.

4.5. Structural characterisation

After proceeding with the ATR/FTIR structural characterisation of both manufactured pristine PDMS films and rGO@PDMS composite films, the spectra were stacked in a wavenumber/absorbance graph, presented in Figure 75.

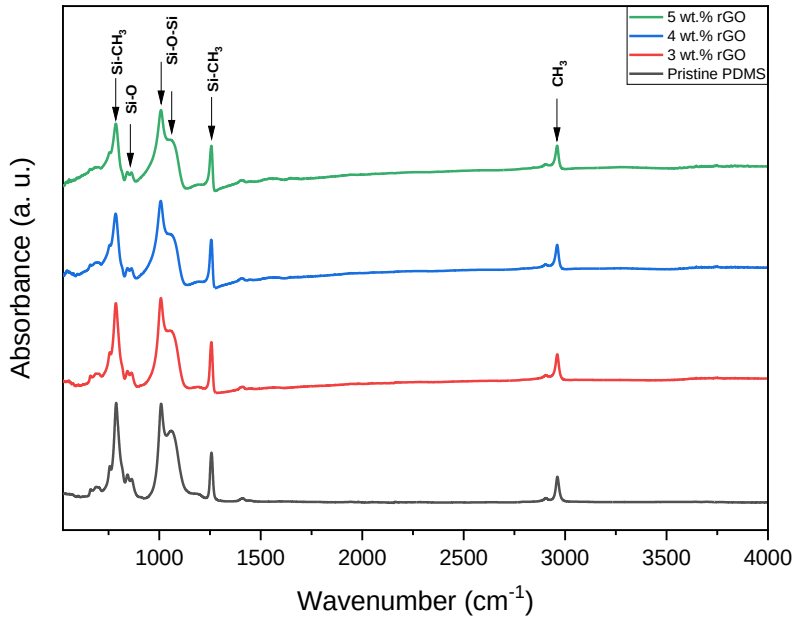

Fig. 75. ATR/FTIR spectra of pristine PDMS and rGO@PDMS composite films. The characteristic peaks have their correspondent functional group identified.

According to several sources [114-116], the PDMS absorbance spectrum exhibits characteristic IR peaks, including a 787 cm^{-1} band of Si-C stretching vibration in $Si-CH_3$, a Si-O stretching vibration in Si-OH at 843 cm^{-1}, double peaks at 1008 cm^{-1} and 1058 cm^{-1}, signalling an asymmetric Si-O-Si stretching vibration, a C-H rocking vibration in $-CH_3$ at 1257 cm^{-1}, and an asymmetric stretching vibration of the $-CH_3$ groups in $Si-CH_3$ at 2961 cm^{-1}.

Despite the morphology of rGO@PDMS spectra exhibiting some changes compared to the pristine PDMS one, such as new peaks at <1000 cm^{-1} and broader peaks in some bands, due to the wavenumber and sheer intensity of the PDMS signature, the characteristic IR peaks of rGO, inherently less intense, are either concealed by the scale of the graph or by certain wavenumbers, whenever they coincide. Nonetheless, it can be observed that these changes in the peaks are related to some loss of purity, but also the creation of new contact points between the matrix and the filler, causing less intense but broader peaks. Thus, to identify functional

group changes introduced by the addition of rGO in the matrix, it was decided to subtract from the composite material spectra the pristine PDMS spectrum, as shown in Figure 76.

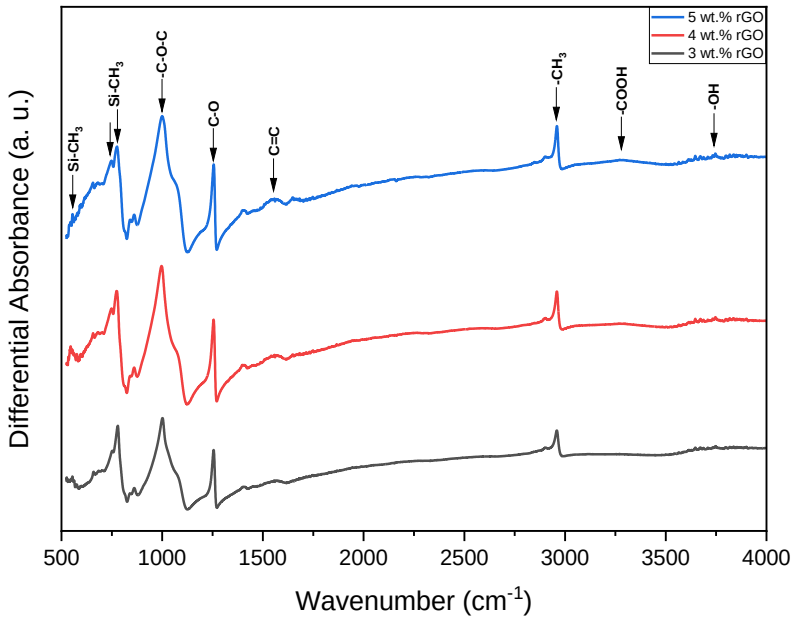

Fig. 76. ATR/FTIR spectra of rGO@PDMS samples, with the pristine PDMS spectrum subtracted. The characteristic peaks have their correspondent functional group identified.

By analysing the graph and cross-referencing several works [117-121], the influence from the new functional groups could be identified, as described in the following paragraph. The peaks at 554 cm^{-1} and 748-775 cm^{-1} could be identified as C-H bending vibrations, the peak at 999 cm^{-1} was caused by C-O-C stretching vibrations from epoxy groups and possible residual -OH groups, a strong peak at 1255 cm^{-1} was caused by C-O stretching of -COOH groups in the material's surface edges, the peak at 1557 cm^{-1}, one of the most characteristic in the rGO spectrum, were caused by the C=C stretching vibrations in the entire structure, signalling the presence of a relatively unchanged and good sp^2 "honeycomb" structure. Moreover, a peak at 2559 cm^{-1} is caused by asymmetric stretching vibrations between C-H in $-CH_2$ groups, while a broad band with a peak at 3271 cm^{-1} is probably caused by -COOH groups forming hydrogen bonds. The last group of has the weakest peaks, with the highest one being at 3746 cm^{-1}, are a consequence of O-H stretching vibrations from -OH groups, along with some water molecules that may have remained from cleaning the device prior to the analysis [120].

With this information, it can be concluded that the rGO used in this work had many of its oxygen-containing functional groups with drastically reduced intensity, a product of the successful reduction of graphene oxide, as seen with the -OH band. Nevertheless, the observed bands signal the presence of epoxy, hydroxyl, and carboxylic groups, as well as a functional hexagonal lattice, as also proven by its electromechanical capabilities. Moreover, the peaks were more pronounced in the sample with 5 wt.% rGO, due to a higher presence of this material. However, the IR signature was still drastically less intense than its GO counterpart, making it

hard for the untrained eye to effectively identify and characterize the structure and functional groups present [118].

Apart from that, something to have in mind is that many factors contribute and influence the IR signature of materials such as rGO, due to the high number of steps that compose its synthesis method, such as the chosen method of reduction and the employed reactants during the process. This leads to variations that can be witnessed from batch to batch, something even more pronounced in novel materials like these, where many synthesis approaches are still currently being investigated and compared.

Nevertheless, it can be concluded that both the matrix and the reinforcement display their characteristic peaks and that they merged into a composite successfully, due to their interaction not leading to unexpected changes in the spectra's morphology.

4.6. Thermal characterisation

With the TGA tests performed on both rGO@PDMS composite films and pristine PDMS films, all data regarding temperature and weight loss for each test were organized, compiled, and stacked in a graph, as seen in Figure 77.

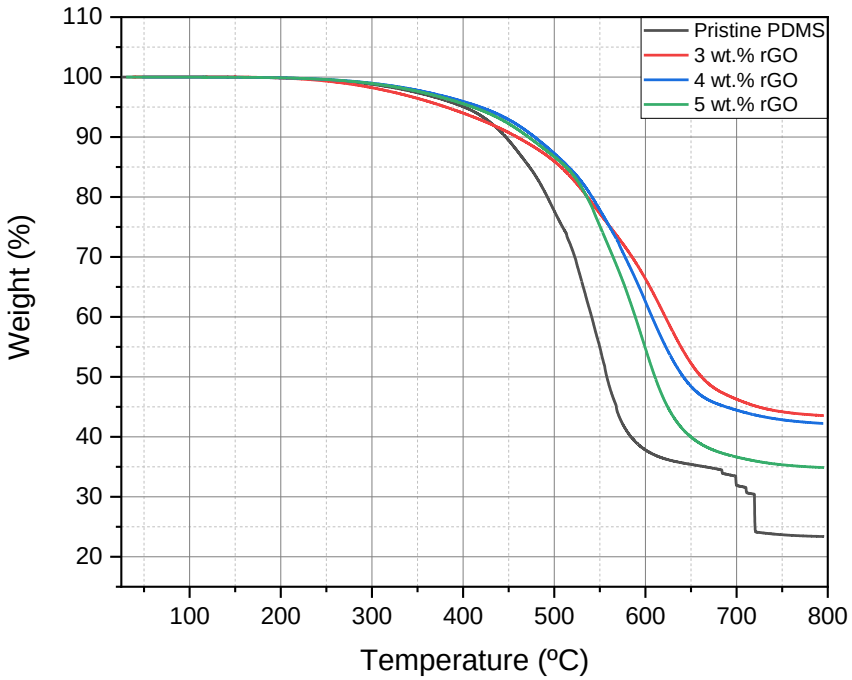

Fig. 77. Thermogravimetric analysis of pristine PDMS films and rGO@PDMS composite films, between ambient temperature and 800 ºC.

Macroscopically speaking, at the end of the tests, the pristine PDMS sample was completely carbonized and torn apart, while composite samples, despite exhibiting significant

thermal degradation and a reduction in size and diameter, maintained their overall shape. This can be explained by the three degradation stages that composite samples went through, compared with the four degradation stages that the pristine PDMS sample did.

As observed in the graph, and similarly reported in other works [122-124], the degradation profile for pristine PDMS started with a slow degradation step at around 250 ºC, attributed to the degradation of small molecules or polymer chains that failed to crosslink with the remaining structure [122]. This was followed by the arrival at the degradation temperature, defined by the temperature in which a 5% mass loss is observed. In the case of the tested sample, this value was 401 ºC, very close to the 410.9 ºC reported by [122] and the 385 ºC by [123].

As the temperature exceeds this point, the degradation rate became more pronounced and the second degradation phase is reached, beginning at around 450 ºC, followed by a significant loss of mass, including 50% mass loss at 557 ºC. With the end of this phase, the curve's slope stabilized and the depolymerization of PDMS began at around 600 ºC, as confirmed by [122-124].

However, when reaching the 700 ºC mark, the sample suffered a sudden loss of mass, as seen multiple times in [125] possibly attributed to the degradation of the last polymer chains and the degradation of the entire structure, with the remaining material, 23.37 % of the original mass, being mainly composed of non-volatile ashes. This could be explained by the depolymerization of PDMS leading to a portion of its chain to evaporate due to high temperatures, with the remaining portion becoming ashes and other non-volatile residues. It should be taken into account that the presence of a filler in the other samples may have postponed the same occurrence for a temperature higher than 800 ºC, a phenomenon that would not be explored due to the temperature limitation of this experiment.

Regarding the composite samples, despite the initial degradation occurring at a similar temperature, the sample with 3 wt.% rGO content was the first to reach its degradation temperature of 380 ºC, followed by the sample with 5 wt.% rGO at 410 ºC and finally the sample with 4 wt.% rGo at 418 ºC. Thus, the presence of rGO did not seem to significantly change the degradation of the samples at this stage.

Afterwards, these three samples also experienced a drastic loss of mass, although at higher temperatures, being observed that the sample with 3 wt.% rGO content lost 50% of its mass at 661 ºC, 4 wt.% at 641 ºC, and 5 wt.% at 610 ºC, a testament to rGO's high thermal stability [126]. Moreover, increments in rGO content led to degradation steps with increasingly steeper slopes, with the 3 wt.% sample having the shallowest slope while the 5 wt.% sample had the steepest. In this stage, both of these factors led to better thermal stability and this could possibly be explained by the creation of more contact points between rGO and PDMS, the extent and overall quality of the filler network in the matrix, especially at a rGO content of 3 wt.%, the chemical bonds in the structure, the amount of filler clusters, and a possible filler saturation at higher concentrations, such as with 4 wt.% and 5 wt.% samples. Hence, the quality of the interactions between the matrix and the filler is one of the main factors behind the displacement

of $T_{5\%}$ and $T_{50\%}$ temperatures, compared to the one that pristine PDMS exhibited [123, 124]. The point of loss of half of the weight always occurred at a temperature higher than that of pristine PDMS.

Lastly, the third stage of the degradation started between 650-675 ºC and was comprised of the stabilization of the curve and the last observed degradation stage for all three samples, where samples with 3 wt.%, 4 wt.%, and 5 wt.% rGO content ended with residues comprising of 43.54%, 42.22%, and 34.87% of the initial mass, respectively. Again, the sample with the best interactions between its matrix and its filler kept the highest amount of residues at the end of the test, a new result that again proves the influence of rGO and deepens the interconnection between all the characterisations made during this dissertation, especially its mechanical and structural aspects, where the quality and quantity of the contact points inside the composite and its overall performance were closely related. Table 8 compiles the major degradation milestones during TGA testing, including the degradation temperature ($T_{5\%}$), the temperature at which loss of mass reached 50% ($T_{50\%}$), and the residue weight.

Table 8. Main thermal degradation, values of pristine PDMS and rGO@PDMS composite samples.

	Pristine PDMS	**3 wt.% rGO**	**4 wt.% rGO**	**5 wt.% rGO**
$T_{5\%}$ (ºC)	401	380	418	410
$T_{50\%}$ (ºC)	557	661	641	610
Residue (wt.%)	23.37	43.54	42.22	34.87

With the TGA tests completed, the correspondent DTA curves were plotted, as seen in Figure 78, to better evaluate the effects of the filler addition on the matrix, since this technique is able to accurately detect endothermic or exothermic transformations in the sample, such as melting, crystallizations, glass transitions, and sublimations, while also making them easier to visualise.

By analysing the graph, it can be observed that the DTA peaks correspond and predict both major degradation steps and other changes in slope of the TGA curves where, for example the sharp loss of mass that begins at ≈ 550 ºC and ends at ≈ 650-670 ºC are accompanied by two endothermic peaks in the DTA curve, shallower in the 3 wt.% rGO sample and sharper in the 4 wt.% and 5 wt.% rGO samples. Moreover, by looking at temperatures lower than 450 ºC, the degradation steps leading to $T_{5\%}$ are more visible in this format, allowing for the observation of how each sample evolves thermally. Thus, these curves indicate that the degradation profile of this compound is mainly done by a two-stage decomposition mechanism in the ≈ 550-670 ºC range (two endothermic peaks), with other minor degradation steps, mainly before the degradation temperature [127]. Additionally, the shallower peaks exhibited by the sample with a rGO content of 3 wt.% also confirms that it has the highest thermal stability of the three and that

the filler concentration and conductive network organization play a major role in the overall properties of the composite.

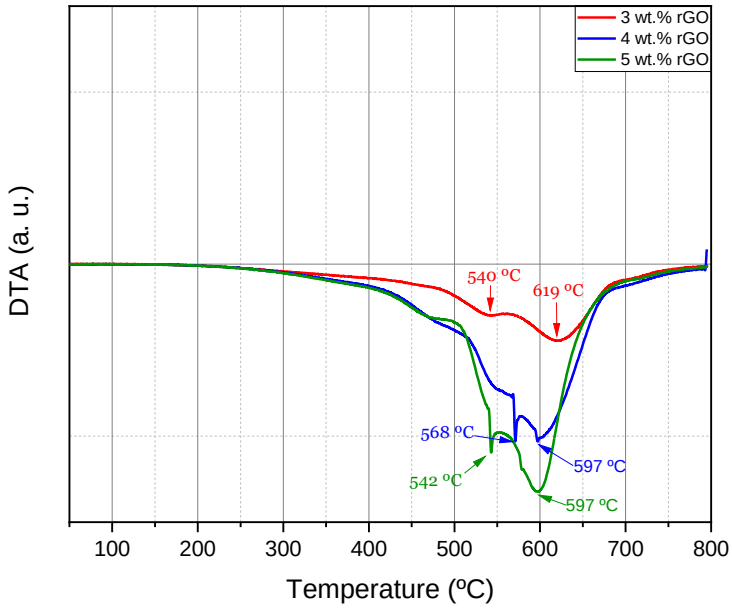

Fig. 78. DTA curves of the characterised rGO@PDMS composites.

4.7. Final remarks

With the characterisation techniques carried out and the results successfully processed and *visualise*d, in this subsection, conclusions regarding the influence of various parameters in the manufacturing process and final performance of the composite will be drawn. These will include how can the mechanical behaviour and piezoresistive performance be influenced, as well as the differences noted between pristine PDMS films and the rGO@PDMS composite throughout the characterisation process, SEM observations, FTIR technique and TGA tests.

Starting with the factors that influence the mechanical performance, curing temperature and elastomer-crosslinker ratio rise as the main ones, since changing the ratios directly influences the maximum stress and strain endured by the film, due to the variation of crosslinker translating into a more or less developed crystal lattice and affecting the overall rigidity. Thus, it can be concluded that a lower elastomer-crosslinker ratio leads to samples with higher Young's modulus, which endure more stress but less strain than others with different configurations. On the other hand, temperature directly impacts curing time, along with the mechanical performance of the samples, by being an active promoter of the crystal lattice's formation and growth along the material. Hence, in this case, it was observed that higher curing temperatures reduce the necessary amount of curing time, significantly accelerating the process, while producing samples with higher rigidity and, therefore, Young's modulus.

Passing on to the parameters that influence the samples' piezoresistive performance, it was concluded that testing velocity is an important factor during the characterisation process,

since higher velocities relate to higher gauge factor values, but also degraded electrical signals sampled by the multimeter. Therefore, a compromise between velocity and signal quality must be achieved in order to obtain the best results possible. Regarding 3-point bending tests, lower tested strain values led to higher gauge factors, while samples with 4 wt.% rGO had the highest sensitivity, followed by 3 wt.% rGO samples and in third place 5 wt.% rGO content samples. On top of that, tested samples exhibited great linearity and no latency in their electrical response, when mechanically deformed. However, when tensile tested, the obtained gauge factors were much lower, with the 3 wt.% rGO samples having the highest value, followed by the 4 wt.% sample. Thus, it can also be concluded that despite the produced samples showing great sensitivity when flexural strain is applied, they lack some performance when tensile strained, since $GF_{flexural} > GF_{tensile}$. Shifting to sample stability, during the cyclic stability test it was observed that the tested sample had the tendency to stabilize its behaviour from the mid-point forward, but a higher number of cycles could be needed to perceive the entire response. Lastly, it was also concluded that samples tend to lose the connections in the conductive network before breaking, when tensile strained. This can be seen by an exponential relative electrical resistance curve when the samples are deformed past their working range, acting as a warning that the structural integrity of the sensor is at risk.

Respecting all the other manufactured samples (0.25 wt.%, 0.5 wt.%, 0.75 wt.%, 1 wt.%, 1.5 wt.%, and 2 wt.%) none of them showed measurable electrical resistances, a sign that no significant conductive network formed inside their structures.

Focusing on the changes induced by the addition of rGO to the PDMS matrix, apart from the obvious difference in appearances between the two, the mechanical performance of the composite was also affected. Despite the values of strain and stress being similar between pristine PDMS and samples with 3 wt.% rGO content, the obtained Young's modulus was almost doubled. Regarding samples with higher rGO content, the mechanical performance was significantly affected, negatively, by the addition of the nanoparticles, due to the profound changes exerted in the composite's structure. Hence, it can be concluded that the addition of rGO leads to a higher Young's modulus, despite contents closer to 3 wt.% still achieving mechanically competitive samples.

With this in mind, a graph comparing the achieved strain and gauge factors of different sensors, manufactured by 9 different teams of researchers, was developed, for the sake of seeing how the produced composites in this work fare in the piezoresistive strain sensor field. Regarding the chosen works, all sensors are piezoresistive, the achieved results were observed while the samples were tensile strained and the conductive materials ranged from CNT [128], rGO [91, 129], ZnO [130], graphene nanoplatelets [131], rGO + sodium carboxymethylcellulose [132], AgNP [133], Au + CNF [134], and CNT + rGO [135]. Despite direct comparisons being hard to make when so many parameters, materials, and configurations are different, the produced sensors, especially sample 3A1, has a similar strain/GF relation to many of the compiled works, reinforcing the tendency that lower strains usually translate into higher gauge factors. However, since the electrodes limited the maximum strain applied to the samples, a

high-strain study of the sample's sensitivity could not be performed, capping, to an extent, the information on how sample 3A1 would compare to sensors with higher strain capabilities, such as the ones produced by [91] and [134]. Figure 79 shows the strain/GF performance comparison graph.

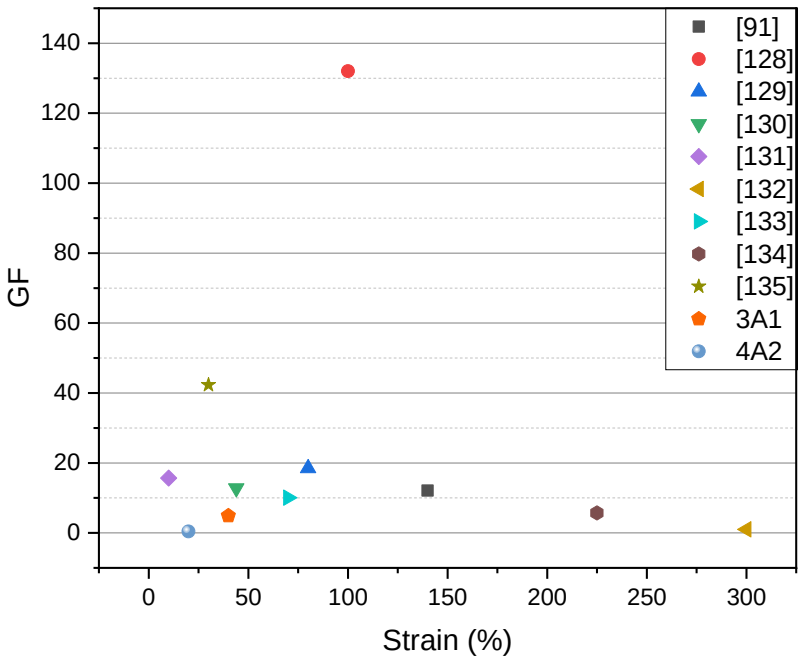

Fig. 79. Strain/gauge factor performance comparison between the best performing samples in this work, 3A1 and 4A2, and other piezoresistive strain sensors in the field.

Shifting towards the materials' thermal properties, it was concluded, by analysing different works in the literature, that the PDMS matrix offers a very wide working range for biomedical applications, since its phase changes at ≈ -40 ºC, signalled by an endothermic peak, where the connections induced by the crosslinker are broken down, and mass loss due to degradation is negligible up to 200ºC and < 2% at 300ºC [136]. Moreover, it is also known that PDMS acts as a thermoset polymer once its pre-polymer liquid-phase is thermally cured and the crosslinking is activated, leading to the rigidity and other mechanical properties not changing with the rise of temperature [137]. Thus, for the scope of this dissertation, thermally characterizing the produced composite by differential scanning calorimetry would not make sense.

On the other hand, it is also known that the addition of carbon-based materials, such as carbon nanofibers, do not broaden nor shift the fusion peak of -40 ºC, indicating that the crystalline structure of the matrix remains the same and that the filler's conductive network does not exhibit any significant bonding with the matrix's, mainly relying on Van der Waals and other weak interactions to interact with the polymer [122].

Regarding the characterisation by TGA, the carried-out tests allowed for first-hand observation of the degradation profile of not only pristine PDMS but also rGO@PDMS composites. Furthermore, it was also possible to better grasp the influence that the addition of fillers has in the thermal stability, as well as the interdependence between points of contact and the matrix-filler interactions with the mechanical and piezoresistive performance, along with the surface's morphology and the microstructure of the composite.

That being said, despite the sample with a rGO content of 3 wt.% exhibiting a lower degradation temperature of 380 ºC, its $T_{50\%}$ was by far the highest, at 661 ºC, denoting its superior thermal stability compared with other samples, an assumption that is supported by a slower degradation rate (shallower slopes in the degradation profile), accompanied by a higher percentage of residues at the end of the PDMS depolymerization, 43,54%, despite having a lower filler concentration. These tests also proved that the composite's properties can be negatively affected if the filler content reaches a saturation point, since the sample with a rGO content of 5 wt.%, as seen in other tests, exhibited an inferior $T_{50\%}$, at 610 ºC, and an overall lower thermal stability, due to a faster degradation rate (steeper slopes) and less residues at the end of the PDMS' depolymerization, 34.87%, despite having the highest concentration of filler.

Lastly, even though it is not very useful for the discussed applications in this dissertation, due to the temperature ranges at which this is applicable, it would be possible to tune the composite's thermal properties by varying the filler content, thanks to the great influence it has on the degradation profile.

Passing on to the ATR/FTIR tests, it was possible to observe that both the matrix and its reinforcement exhibited their characteristic IR peaks in the wavenumber/absorbance curve, an indicator that all expected functional groups were formed and that the produced compounds were successfully manufactured without a loss of intrinsic characteristics. Furthermore, the morphology variations between the peaks of pristine PDMS and the produced composites also emphasise the interaction between both materials, since the composites exhibit peaks with lesser intensity but more width, which can be translated into the creation of contact points between PDMS and rGO, a vital phenomenon for the proper operation of a composite with sensing capabilities such as this.

Lastly, regarding the microstructure's characterisation by SEM, with the images acquisition it was possible to discern significant differences between the pristine matrix and the composites, as well as these between themselves. Additionally, a direct relationship between the filler content and the conductive network general organization exists, along with the formation of agglomerates in the microstructure.

With this taken into account, it was observed that the composite with a rGO content of 3 wt.% exhibited the most uniform dispersion, guaranteeing higher stability to the composite, the configuration with 4 wt.% rGO showed the densest conductive network, which translated into a sensor with the highest recorded sensitivity, while the configuration with 5 wt.% rGO had a microstructure with many agglomerates, which negatively impacted both mechanical and piezoresistive performances.

Chapter 5

Proofs of Concept

5. Proofs of concept

With the characterisation and testing phase concluded, it was decided to develop a proof of concept with the composite material, more specifically, a trial where joint movement and breathing pattern monitoring would be attempted. Therefore, these trials took inspiration from multiple works on the same field, including breathing and deglutition pattern monitoring, foot tapping recognition [138], real-time recording of arterial pulse waves, neck movement monitoring [139], object grasping recognition [140], as well as monitoring the joint movement of fingers [140, 141], elbows and wrists [138, 139]. By reading some commonly employed experiments in strain sensing with piezoresistive and piezoelectric sensors, the following 2 proofs of concept were developed: 1) measuring and monitoring, in real time, the wrist movement of a live volunteer with the support of a newly manufactured rGO@PDMS composite material strain sensor; 2) monitoring, in real time, the breathing patterns of a live volunteer with the support of a newly manufactured rGO@PDMS composite material strain sensor, for a duration of 60 seconds. Thus, in this section, the entire processes will be documented, by describing the entire procedure, explaining why the wrist and chest were chosen over other zones of the body, as well as images of the built setups and movements made by the volunteers.

5.1. First proof of concept

Starting with proof of concept 1), the wrist started off in the relaxed position, fully extended, followed by alternation between this position and a ≈ 65° flexion of the joint, and vice versa, every 20 seconds. By doing 5 cycles of relaxation/flexion, the aim was accurately capturing, in real time, the electrical response of the sensor, and verifying if it could reflect the behaviour of the joint of interest. In order to achieve this, 2 electrodes were prepared by applying silver paste on the sensor's surface, with dimensions of 4 mm × 10 mm and separated by 4mm, as well as 2 copper cables, being each one of them attached to the poles of the Keysight 34461A digital multimeter. Figure 80 shows the built setup for this proof of concept.

By using a box as a mean to support the entire forearm, the volunteer could concentrate on providing the most accurate and consistent movements possible, without feeling fatigue after multiple cycles, factors that would be reflected in the captured electrical signal. On the same note, the rGO@PDMS composite was secured to the volunteer's skin with 2-sided tape, ensuring that the sensor did not move during the trial, while being easily removable after it ended. Moreover, the wrist was chosen over other joints in the body due to its inherently lower range of movement, which translates into lesser applied strain to the sensor. This does not mean that the composite itself could not endure being worn in the fingers or elbow, however, the electrodes would break off due to excessive deformation. Thus, the trial was mainly limited by the maximum strain the electrodes could take, with the fingers, the most common targets for real-

time joint movement monitoring, being out of the equation for this work, something that could not happen if another type of electrode had been employed.

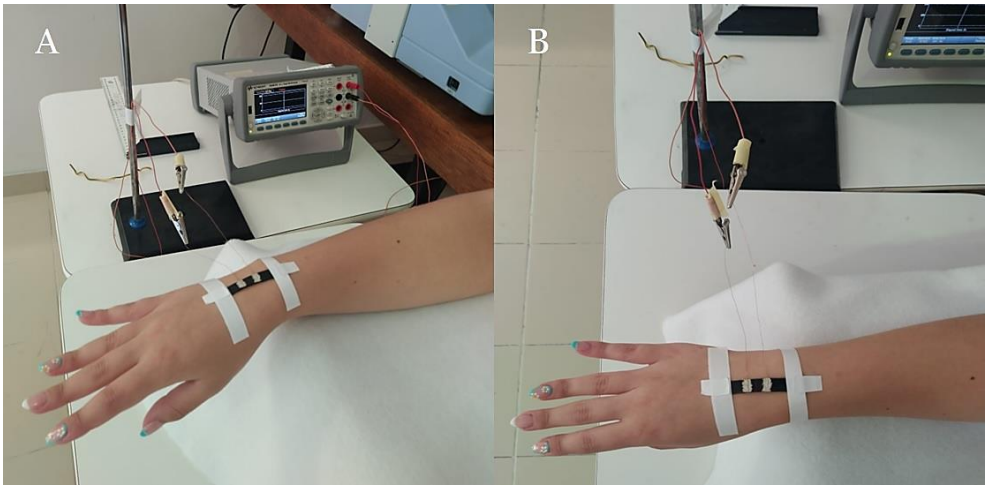

Fig. 80. Prepared setup for the wrist monitoring proof of concept. (A) Panoramic view, with the presence of the Keysight 34461A digital multimeter; (B) Upper view.

Passing on some important parameters for this first proof of concept, the chosen sampling frequency was 2.38 Hz, the wrist did not exhibit any visible or known lesions, and the volunteer was healthy. Furthermore, two samples were chosen for this trial, being taken out from the initial batch of produced samples with a rGO content of 3 wt.% and cured at 120 °C for 20 minutes. Its dimensions were ≈60mm × 10mm, being designated samples 3A4 and 3A5.

Regarding the performance of the samples during the trial, while sample 3A4 showed great piezoresistive behaviour and linearity with the movements performed by the volunteer, sample 3A5, due to a higher thickness and, therefore, rigidity, couldn't follow the movement as well as the former, with the electrodes breaking off during the second cycle. Thus, it is once again proven that in order to achieve the best results possible, it is paramount to manufacture films with low thickness and develop a more efficient way of fitting the electrodes to the sample. Figure 81 shows the developed time/relative electrical resistance variation graph during one of the trials done with sample 3A4, with each ascending peak representing the wrist's ≈ 65° flexion, while the descending peaks represent the full extension of the joint, the designated relaxed position.

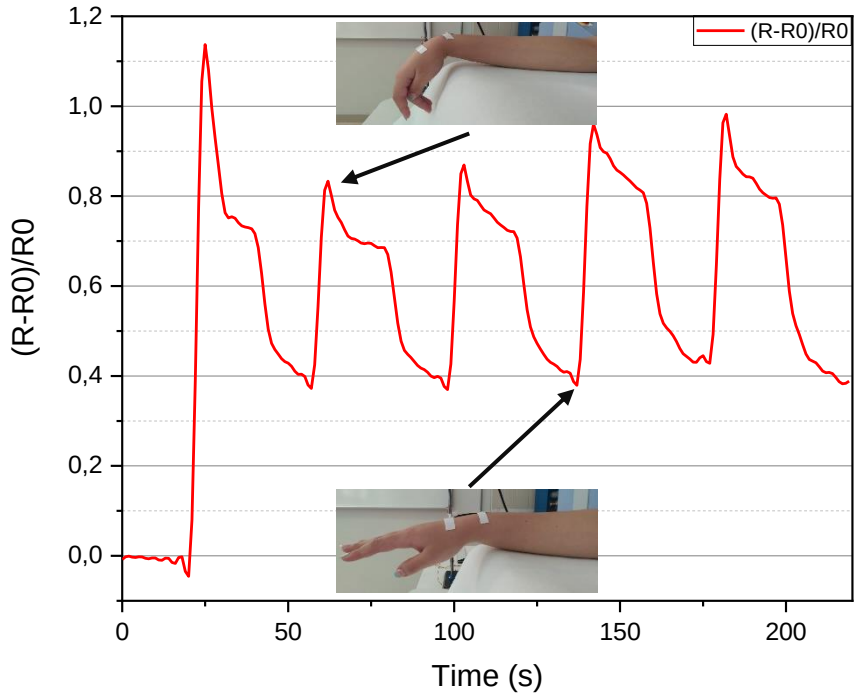

Fig. 81. Time/Relative electrical resistance graph developed for a trial employing rGO@PDMS sample 3A4. Each ascending represents the wrist's ≈65°flexion, while the descending peaks represent the relaxation state.

When analysing the graph, it can be clearly seen that the ascending and descending peaks follow the wrist's flexion and relaxation, respectively, with the ascending peaks being notoriously characterized by an initial apex, followed by the conformation of the conductive network and consequent stabilization of the electrical signal. Since this was the first time sample 3A4 was used post-manufacturing, the first apex, multiple times higher than the others, marked the very first time the conductive network was mechanically deformed, breaking and making new connections all over the structure, a likely explanation for the characteristic morphology of the peak.

Furthermore, the volunteer reported that sample 3A4 was more comfortable to wear on the skin, fruit of lower thickness and similar Young's modulus, as well as higher conformation with it and better adaptability to the performed movements, without feeling mechanical resistance. On the contrary, sample 3A5 was plagued by not only higher weight, due to a higher overall thickness, but also lower comfort while worn on the skin, allied to higher mechanical resistance to movement, attributable to more rigidity and higher Young's modulus. Therefore, it is again proven that the film's thickness is an essential factor related with a good performing and user accepted sensorial system of this kind.

5.2. Second proof of concept

Regarding proof of concept 2), apart from the other works, inspiration for the trial and the used setup was taken from the projects developed by Dihn *et al.* [142], Costa *et al.* [143], and Liu *et al.* [144], which researched and made advancements in respiration sensor designs, breathing pattern recognition and other respiratory rate measurement technologies, respectively.

With this in mind, the volunteer was asked to keep a regular breathing rate while remaining seated, with the arms and legs in a relaxed position and without speaking, during the entirety of the trial, which was decided to take 60 seconds. Thus, movement artifacts and other interferences would hopefully be reduced as much as possible from the sampled signal. Moreover, and similarly to the previous trial, 2 electrodes were placed in the rGO@PDMS 3A4 sample with the same dimensions and separation, while also being connected to the Keysight 34461A digital multimeter. Furthermore, the sample was attached to a cotton belt designed to be adjusted around the volunteer's chest area, without contacting the skin. Figure 82 shows the used setup for this second proof of concept.

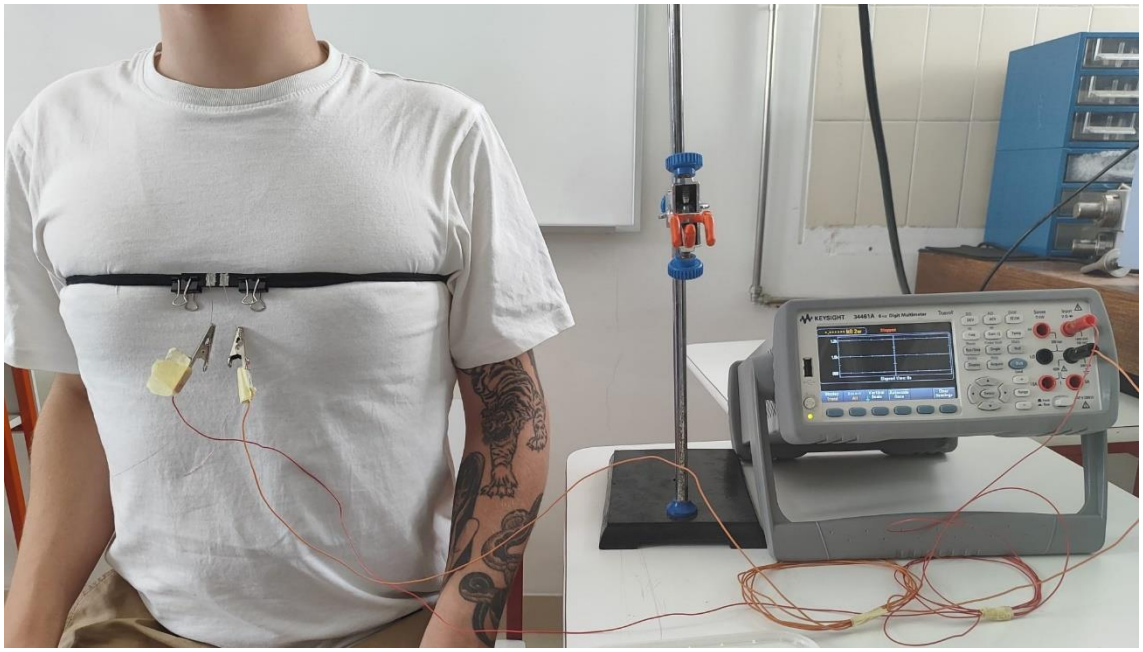

Fig. 82. Setup used during the breathing pattern monitoring trial, part of the proof of concept.

With this setup in place, the volunteer only had to breathe at a constant rate and similar depth, providing the sensor with the best possible data. Regarding the chosen area, monitoring data related with breathing patterns opens the door to monitoring patients with a myriad of respiratory diseases, including asthma, pneumonia, and chronic obstructive pulmonary disease, as well as hypertension, obesity and cardiac arrest [142, 143]. Moreover, other technologies,

related to portable personalized healthcare devices, could provide users with information on real-time medical diagnostics and other figures on complications such as sleep apnea detection, respiratory impedance, speaking detection as a metric of social interaction [143], while the respiration rate, the number of respiration pulses in a minute, is a good indicator of healthy adults, generally lying between 14-18 breaths per minute [142]. Thus, analysing this type of data is a quick way to provide medical experts with an early diagnostic of normal or abnormal respiration.

Taking this into account, the chosen volunteer had no known respiratory complications at the time of the trial, did not exhibit any visible or known injuries and participated in the trial while being healthy. Regarding the signal acquisition, the chosen sampling rate was 2.38 Hz, while the chosen rGO@PDMS sample was, as stated above, sample 3A4, due to its lower thickness allowing for higher tensile rates.

Shifting to the trial itself, sample 3A4 showed great linearity with the breathing movements performed by the volunteer, with enough relative electrical resistance variation to detect every inhalation and exhalation. However, the signal captured by the sensor lacked quality and resolution, exhibiting notorious variation between peaks, mainly in the initial seconds of the trial, despite the breathing depth being relatively the same. This could be attributed to several factors, all of which have influence on the acquired signal, including a low-quality setup, unable to capture the physiological activity to its best ability, the sensor's lower sensitivity to tensile deformation, as observed during the piezoresistive tests, a lack of contact with the skin, which sacrifices the conformation of the sensor and a signal with higher quality, and intrinsic interferences related to the conductive network's rearrangements during the trial.

Despite this, it was decided to apply a percentile filter to the acquired signal, with 2 points of window, no boundary conditions, and a percentile of 67. This led to a signal with less noise and interferences, allowing for the estimation of the breaths per minute - in this specific case, 14- an indicator of an adult with healthy respiratory patterns [142]. Something to take into account, however, is that the use of this filter may compromise the observation of more subtle signal characteristics, due to the saturation of the peaks and the general broadening of the entire curve, overshadowing minor anomalies that may entail a major complication. Thus, different filtering should be employed depending on the desired application, whether counting breaths per duration of time, or observing anomalies and patterns in the breathing pattern. Nevertheless, it can be concluded, without a doubt, that compared to joint movement monitoring, the manufactured sensor exhibits a lower performance in this application, requiring a higher degree of signal filtering, along with a lower signal resolution that may hide vital information in the curves. Nonetheless, it was still possible to count the amount of breathing cycles taken by the volunteer during the 60 seconds (14), completing the challenge proposed by this proof of concept and showing the utility offered by these types of devices in the medical field. Figure 83 shows the developed time/relative electrical resistance variation graph, representative of one of the trials performed during this proof of concept.

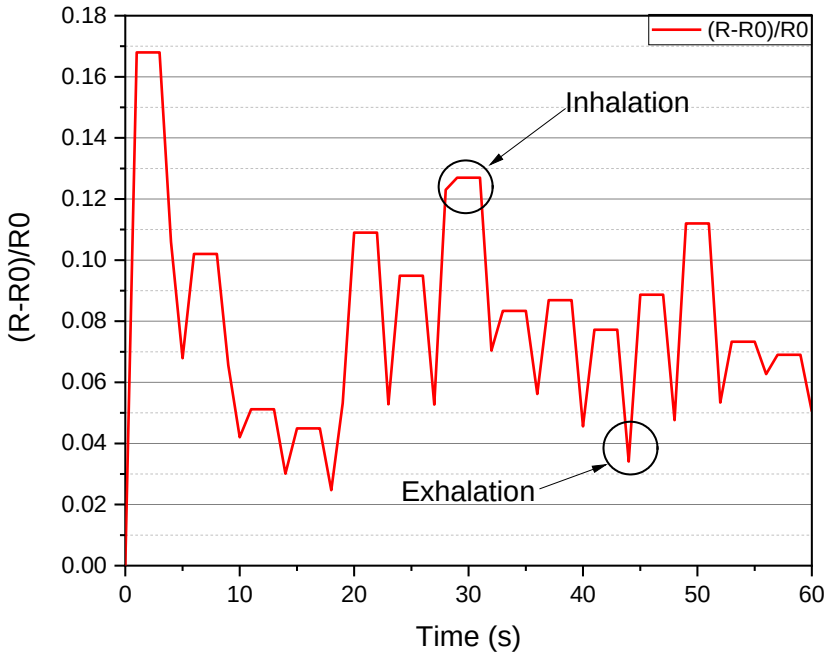

Fig. 83. Time/relative electrical resistance variation graph representative of a breathing pattern monitoring trial, which had the duration of 60 seconds. The signal was filtered with a percentile filter of 2 points of window, no boundary conditions and a percentile of 67. Each peak represents a complete inhalation, with 14 being counted in 1 minute, an indicator of healthy and normal respiration activity, according to Dinh *et al.* [142].

Chapter 6

Conclusions

6. Conclusions

6.1. General Conclusions

Due to all the changes in the economic and demographic landscape in recent years, a longer life expectancy and higher standards of living led people to pursuit new practises and better ways that would give them good health for longer. Thus, today the challenge consists in conceiving a more personalized and optimized healthcare system that answers to these new necessities. With this in mind, flexible sensors able to conform to our bodies' surfaces, along with devices such as prosthetics, are a very important step in this direction.

In this dissertation, in the context of bioengineering, the production of a flexible strain sensor based on the rGO@PDMS composite was proposed, with a discussion and analysis on the relevancy of this technology, as well as how it fits in the current and future markets also being made. Moreover, a long and thorough state-of-the-art was carried out, focusing on fundamental themes surrounding this technology, including flexible sensors themselves, where the needs, operation principles, sought-after properties and most commonly employed sensors were comprehended. Along these lines, there is compiled information on the general considerations of building a sensorial system and their applications, with these being conjugated with the most popular substrates, matrices, conductive reinforcements, geometries, and architectures in the field, currently. Lastly, manufacturing approaches for flexible sensors were also addressed, followed by some case studies and trends developed by research groups in the field.

With a concluded state-of-the-art, a description of the used materials, chosen manufacturing approaches and characterisation techniques of the produced composite was made, together with the obtained results, very insightful information on the piezoresistive and mechanical performance of the sensor, along with all influencing factors. By characterizing the samples and analysing the results, it was observed that the sample which endured the highest stress was 3A1, with 1.837 MPa, the one which endured the least stress was 4A2, with 0.87 MPa, the sample with the highest strain endured was also 3A1, with 141.93%, with sample 5A3 being the one with the lowest endured strain, at a value of 30.82%. Moreover, the sample with the highest recorded Young's modulus was 5A3, with a value of 3.084 MPa, while sample 3A1 exhibited the lowest, with a value of 1.964 MPa. Additionally, regarding the electromechanical characterisation of these samples, in 3-point bending tests, at a strain of 1.54%, sample 3A1 achieved the highest measured average ascendent gauge factor of 14,85, from all 3 wt.% rGO samples, sample 4A2 reached a value of 30.8, also the highest among samples with 4 wt.% rGO, while sample 5A3 reached a value of 9.16. On the other hand, in tensile tests sample 3A1 achieved an average gauge factor of 4.89, at a strain of 40%, sample 4A2 reached 0.43, at a strain of 20%, while sample 5A3's structure suffered irreversible damage during this test, impeding the calculation of the average gauge factor. Moreover, it was also observed during tensile tests that samples always lost their electrical component before its structure collapses, where sample 3A1 endured the most strain (≈ 60%). Lastly, the acquired electrical signals

showed a linear relative electrical resistance variation without any latency, despite the presence of some decay in-between cycles, especially at lower strains.

In the case of other characterisation techniques, the morphological characterisation by SEM revealed that the pristine PDMS' surface was significantly smoother than the rGO@PDMS composites', where a direct relationship between the filler content and the conductive network density, along with the formation of agglomerates, was laid out. Hence, the sample with 3 wt.% rGO content exhibited the most uniform and stable filler dispersion, the sample with 4 wt.% rGO content showed the densest and most sensitive conductive network, although with some agglomerates, while the sample with 5 wt.% rGO content had the conductive network with the highest agglomerate count.

Passing on to the structural characterisation by ATR/FTIR, it was observed that both the matrix and filler exhibited their characteristic IR peaks, displaying the formation of the main functional groups. Furthermore, the interactions between PDMS and rGO were also present, since when compared to pristine PDMS, the composites exhibited less intense but wider peaks, due to the formation of more contact points between both compounds.

Regarding the thermal characterisation by TGA, the main conclusion taken is that the produced composites offer a very wide working range for bioengineering applications, with its endothermic peak at ≈ -40 ºC, signalling a phase transition, and < 2% mass loss at 300 ºC. Additionally, the degradation temperature of composites with 3 wt.% rGO content was 380 ºC, 4 wt.% was 418 ºC, and 5 wt.% was 410 ºC, while the temperature at which 50% mass was lost was 661 ºC in samples with 3 wt.% rGO, 641 ºC for samples with 4 wt.% rGO, and 610 ºC for samples with 5 wt.% rGO. Regarding the remaining residue, 43.54% was left in 3 wt.% rGO samples, 42.22% in 4 wt.% rGO samples, and 34.87% in 5 wt.% rGO samples.

With this in mind, it can be said that samples manufactured with an rGO content of 3 wt.% are indicated for applications that require high strain rates, such as monitoring the movement of joints located in the fingers and elbows, among others, while samples produced with 4 wt.% rGO are better suited for applications such as monitoring the movement of the wrist joint or breathing patterns in the chest. Regarding samples produced with a rGO content of 5 wt.%, due to their higher rigidity, these are better indicated for applications that do not require high tensile strains, only flexural strain, such as measuring deglutition and voice patterns in the throat.

Once all samples were properly characterised, two proofs of concept were elaborated, with the aim of measuring and detecting, in real time, joint movements and breathing patterns on live volunteers. These were executed with 3 wt.% rGO samples, the only ones with both sufficient mechanical performance and sensitivity to endure the flexural and tensile strain inherent to the trials.

Regarding this group of samples, it was noted that their piezoresistive behaviour was linear, showing barely any latency with the applied mechanical deformations, and a very satisfactory sensitivity, while the Young's modulus was similar enough to the human skin to ensure a good conformation and comfort in the volunteer's body surfaces.

However, complications related to a lack of effective electrode deposition methods were the leading limiting factors in this study, since it made it impossible to test the sensor further into its limits due to the electrodes breaking off before reaching this point.

With everything taken into account, the development process of this entire work was crucial to learn more about the current population necessities and trends and, by applying bioengineering expertise, the reached conclusions and results were very positive, taking into account the resources at hand and the available period of time. Furthermore, this was an excellent opportunity to deepen composite-related knowledge, by observing how these advanced materials are structured and how can their potential be applied into society.

Speaking of which, the emergence of this new generation of flexible sensors is a step in the right direction, by aiming to fix the issues of a somewhat antiquated and poorly personalized technology available today, thanks to the possibility of shaping each sensorial device to the needs of its user, adjusting both to body surfaces and prosthetic devices, aiding in the recovery of either body parts or prostheses through monitoring and optimization processes, due to their great potential to mimic the mechanosensitive aspects of the human skin.

6.2. Future Work

With the completion of this dissertation and the fulfilment of the proposed challenges, new questions arise, mainly related with ways to enrich or carry on the current study, harnessing the potential it has, or conceiving entire new approaches, by modifying the manner the device functions.

The first would be devising finer methods related with electrode deposition, including the possibility of altering the entire sensor structure, with integrated electrodes, such as in the developed works by Fu *et al.* [145], Guo *et al.* [146], and Li *et al.* [147] ensuring higher service lives while also enabling superior degrees of mechanical deformation, since it becomes harder to break off the electrodes.

The next approach could be making a more in-depth study of the relation between composite's rGO content and its resistivity, allowing for a better comprehension of the way the conductive network develops, as well as discovering the exact percentage where the percolation threshold is located.

On a similar note, it would be noteworthy to investigate the possibility of manufacturing a hybrid composite material, conjugating silver-based nanomaterials, such as silver nanowires, and rGO, followed by the evaluation of the obtained results and its potential ramifications.

Another possible future endeavour would be observing the influence of dispersants such as 1,4-dioxane in the reduction of defects during the establishment of the conductive network, and how it compares to other candidates.

Shifting towards signal detection and monitoring, a recommended course of action would be scaling up this technology, testing the sensor's performance in new areas of the body,

such as the palm of the hand, larger areas of already tested regions, including more prolonged periods of time.

Lastly, other sensorial elements could be integrated in future studies, either in the form of multiplexed sensors, despite its disadvantages, or creating a network of sensors, each with the ability to detect and monitor different physiological parameters.

Chapter 7

References

References

[1] B. Peng, F. Zhao, J. Ping, e Y. Ying, «Recent Advances in Nanomaterial-Enabled Wearable Sensors: Material Synthesis, Sensor Design, and Personal Health Monitoring», *Small*, vol. 16, n. 44, p. 2002681, nov. 2020, doi: 10.1002/smll.202002681.

[2] H. Luo e B. Gao, «Development of smart wearable sensors for life healthcare», *Engineered Regeneration*, vol. 2, pp. 163–170, 2021, doi: 10.1016/j.engreg.2021.10.001.

[3] U. Pierre Claver e G. Zhao, «Recent Progress in Flexible Pressure Sensors Based Electronic Skin», *Adv. Eng. Mater.*, vol. 23, n. 5, p. 2001187, may 2021, doi: 10.1002/adem.202001187.

[4] F. Khoshmanesh, P. Thurgood, E. Pirogova, S. Nahavandi, e S. Baratchi, «Wearable sensors: At the frontier of personalised health monitoring, smart prosthetics and assistive technologies», *Biosensors and Bioelectronics*, vol. 176, p. 112946, march 2021, doi: 10.1016/j.bios.2020.112946.

[5] M. T. Almansoori, X. Li, e L. Zheng, «A Brief Review on E-skin and its Multifunctional Sensing Applications», *CSM*, vol. 4, n. 1, pp. 3–14, july 2019, doi: 10.2174/2405465804666190313154903.

[6] A. H. Anwer *et al.*, «Recent Advances in Touch Sensors for Flexible Wearable Devices», *Sensors*, vol. 22, n. 12, p. 4460, june 2022, doi: 10.3390/s22124460.

[7] «Wearable Sensors Market Size, Share and Trends forecast to 2022 by Type, Application, Vertical and Geography | MarketsandMarkets™», *MarketsandMarkets*. https://www.marketsandmarkets.com/Market-Reports/wearable-sensor-market-158101489.html (accessed on november 8 2022).

[8] S. Z. Homayounfar e T. L. Andrew, «Wearable Sensors for Monitoring Human Motion: A Review on Mechanisms, Materials, and Challenges», *SLAS Technology*, vol. 25, n. 1, pp. 9–24, feb. 2020, doi: 10.1177/2472630319891128.

[9] M. M. Rodgers, G. Alon, V. M. Pai, e R. S. Conroy, «Wearable technologies for active living and rehabilitation: Current research challenges and future opportunities», *Journal of Rehabilitation and Assistive Technologies Engineering*, vol. 6, p. 205566831983960, jan. 2019, doi: 10.1177/2055668319839607.

[10] R. M. Al-Eidan, H. Al-Khalifa, e A. M. Al-Salman, «A Review of Wrist-Worn Wearable: Sensors, Models, and Challenges», *Journal of Sensors*, vol. 2018, pp. 1–20, dec. 2018, doi: 10.1155/2018/5853917.

[11] S. Nasiri e M. R. Khosravani, «Progress and challenges in fabrication of wearable sensors for health monitoring», *Sensors and Actuators A: Physical*, vol. 312, p. 112105, sept. 2020, doi: 10.1016/j.sna.2020.112105.

[12] H. Liu, L. Wang, G. Lin, e Y. Feng, «Recent progress in the fabrication of flexible materials for wearable sensors», *Biomater. Sci.*, vol. 10, n.º 3, pp. 614–632, 2022, doi: 10.1039/D1BM01136G.

[13] S. M. A. Iqbal, I. Mahgoub, E. Du, M. A. Leavitt, e W. Asghar, «Advances in healthcare wearable devices», *npj Flex Electron*, vol. 5, n.º 1, p. 9, dec. 2021, doi: 10.1038/s41528-021-00107-x.

[14] S. Zhang, S. Li, Z. Xia, and K. Cai, "A review of electronic skin: Soft Electronics and sensors for human health," *Journal of Materials Chemistry B*, vol. 8, no. 5, pp. 852–862, 2020.

[15] F. Xu *et al.*, «Recent Developments for Flexible Pressure Sensors: A Review», *Micromachines*, vol. 9, n.º 11, p. 580, nov. 2018, doi: 10.3390/mi9110580.

[16] M. Xie *et al.*, «Flexible Multifunctional Sensors for Wearable and Robotic Applications», *Adv. Mater. Technol.*, vol. 4, n.º 3, p. 1800626, march 2019, doi: 10.1002/admt.201800626.

[17] H. Lim, H. S. Kim, R. Qazi, Y. Kwon, J. Jeong, e W. Yeo, «Advanced Soft Materials, Sensor Integrations, and Applications of Wearable Flexible Hybrid Electronics in Healthcare, Energy, and Environment», *Adv. Mater.*, vol. 32, n.º 15, p. 1901924, april 2020, doi: 10.1002/adma.201901924.

[18] D. Dias e J. Paulo Silva Cunha, «Wearable Health Devices—Vital Sign Monitoring, Systems and Technologies», *Sensors*, vol. 18, n.º 8, p. 2414, july 2018, doi: 10.3390/s18082414.

[19] Z. Lou, L. Wang, e G. Shen, «Recent Advances in Smart Wearable Sensing Systems», *Adv. Mater. Technol.*, vol. 3, n.º 12, p. 1800444, dec. 2018, doi: 10.1002/admt.201800444.

[20] Y. Huang, X. Fan, S. Chen, e N. Zhao, «Emerging Technologies of Flexible Pressure Sensors: Materials, Modeling, Devices, and Manufacturing», *Adv. Funct. Mater.*, vol. 29, n.º 12, p. 1808509, march 2019, doi: 10.1002/adfm.201808509.

[21] B. Shi, Z. Li, e Y. Fan, «Implantable Energy-Harvesting Devices», *Adv. Mater.*, vol. 30, n.º 44, p. 1801511, nov. 2018, doi: 10.1002/adma.201801511.

[22] O. Parlak, S. T. Keene, A. Marais, V. F. Curto, e A. Salleo, «Molecularly selective nanoporous membrane-based wearable organic electrochemical device for noninvasive cortisol sensing», *Sci. Adv.*, vol. 4, n.º 7, p. eaar2904, july 2018, doi: 10.1126/sciadv.aar2904.

[23] Y. Khan *et al.*, «A flexible organic reflectance oximeter array», *Proc. Natl. Acad. Sci. U.S.A.*, vol. 115, n.º 47, nov. 2018, doi: 10.1073/pnas.1813053115.

[24] R. Chen, X. Xu, D. Yu, C. Xiao, M. Liu, J. Huang, T. Mao, C. Zheng, Z. Wang, and X. Wu, "Highly stretchable and fatigue resistant hydrogels with low Young's modulus as transparent and flexible strain sensors," *Journal of Materials Chemistry C*, vol. 6, no. 41, pp. 11193–11201, 2018.

[25] G. Chen, N. Matsuhisa, Z. Liu, D. Qi, P. Cai, Y. Jiang, C. Wan, Y. Cui, W. R. Leow, Z. Liu, S. Gong, K.-Q. Zhang, Y. Cheng, and X. Chen, "Plasticizing silk protein for on-skin stretchable electrodes," *Advanced Materials*, vol. 30, no. 21, p. 1800129, 2018.

[26] C. L. McDonald, S. Westcott-McCoy, M. R. Weaver, J. Haagsma, e D. Kartin, «Global prevalence of traumatic non-fatal limb amputation», *Prosthetics & Orthotics International*, vol. 45, n.º 2, pp. 105–114, april 2021, doi: 10.1177/0309364620972258.

[27] Z. Wang, L. Zhang, J. Liu, H. Jiang, and C. Li, "Flexible hemispheric microarrays of highly pressure-sensitive sensors based on breath figure method," *Nanoscale*, vol. 10, no. 22, pp. 10691–10698, 2018.

[28] M. D. Dickey, «Stretchable and Soft Electronics using Liquid Metals», *Adv. Mater.*, vol. 29, n.º 27, p. 1606425, july 2017, doi: 10.1002/adma.201606425.

[29] Y. Yu *et al.*, «Biofuel-powered soft electronic skin with multiplexed and wireless sensing for human-machine interfaces», *Sci. Robot.*, vol. 5, n.º 41, p. eaaz7946, april 2020, doi: 10.1126/scirobotics.aaz7946.

[30] Q. Hua *et al.*, «Skin-inspired highly stretchable and conformable matrix networks for multifunctional sensing», *Nat Commun*, vol. 9, n.º 1, p. 244, dec. 2018, doi: 10.1038/s41467-017-02685-9.

[31] W. Zhou, S. Yao, H. Wang, Q. Du, Y. Ma, e Y. Zhu, «Gas-Permeable, Ultrathin, Stretchable Epidermal Electronics with Porous Electrodes», *ACS Nano*, vol. 14, n.º 5, pp. 5798–5805, may 2020, doi: 10.1021/acsnano.0c00906.

[32] A. Sharma, Mohd. Z. Ansari, e C. Cho, «Ultrasensitive flexible wearable pressure/strain sensors: Parameters, materials, mechanisms and applications», *Sensors and Actuators A: Physical*, vol. 347, p. 113934, nov. 2022, doi: 10.1016/j.sna.2022.113934.

[33] Z. Ismail, W. F. W Idris, e A. H. Abdullah, «Graphene-based temperature, humidity, and strain sensor: A review on progress, characterisation, and potential applications during Covid-19 pandemic», *Sensors International*, vol. 3, p. 100183, 2022, doi: 10.1016/j.sintl.2022.100183.

[34] Y. Gao, L. Yu, J. C. Yeo, e C. T. Lim, «Flexible Hybrid Sensors for Health Monitoring: Materials and Mechanisms to Render Wearability», *Adv. Mater.*, vol. 32, n.º 15, p. 1902133, april 2020, doi: 10.1002/adma.201902133.

[35] D. Barmpakos e G. Kaltsas, «A Review on Humidity, Temperature and Strain Printed Sensors—Current Trends and Future Perspectives», *Sensors*, vol. 21, n.º 3, p. 739, jan. 2021, doi: 10.3390/s21030739.

[36] M. Chung, G. Fortunato, e N. Radacsi, «Wearable flexible sweat sensors for healthcare monitoring: a review», *J. R. Soc. Interface.*, vol. 16, n.º 159, p. 20190217, oct. 2019, doi: 10.1098/rsif.2019.0217.

[37] A. M. V. Mohan, V. Rajendran, R. K. Mishra, e M. Jayaraman, «Recent advances and perspectives in sweat based wearable electrochemical sensors», *TrAC Trends in Analytical Chemistry*, vol. 131, p. 116024, oct. 2020, doi: 10.1016/j.trac.2020.116024.

[38] L. Wang, Z. Lou, K. Jiang, and G. Shen, "Bio-multifunctional Smart wearable sensors for medical devices," *Advanced Intelligent Systems*, vol. 1, no. 5, p. 1900040, 2019.

[39] B. Dai, C. Gao, e Y. Xie, «Flexible wearable devices for intelligent health monitoring», *VIEW*, vol. 3, n.º 5, p. 20220027, nov. 2022, doi: 10.1002/VIW.20220027.

[40] B. Arman Kuzubasoglu e S. Kursun Bahadir, «Flexible temperature sensors: A review», *Sensors and Actuators A: Physical*, vol. 315, p. 112282, nov. 2020, doi: 10.1016/j.sna.2020.112282.

[41] Z. Ma, T. Fei, e T. Zhang, «An overview: Sensors for low humidity detection», *Sensors and Actuators B: Chemical*, vol. 376, p. 133039, feb. 2023, doi: 10.1016/j.snb.2022.133039.

[42] X. Gong, K. Huang, Y.-H. Wu, e X.-S. Zhang, «Recent progress on screen-printed flexible sensors for human health monitoring», *Sensors and Actuators A: Physical*, vol. 345, p. 113821, out. 2022, doi: 10.1016/j.sna.2022.113821.

[43] Bijender e A. Kumar, «Recent progress in the fabrication and applications of flexible capacitive and resistive pressure sensors», *Sensors and Actuators A: Physical*, vol. 344, p. 113770, sept. 2022, doi: 10.1016/j.sna.2022.113770.

[44] T. Beduk *et al.*, «Smartphone-Based Multiplexed Biosensing Tools for Health Monitoring», *Biosensors*, vol. 12, n.º 8, p. 583, july 2022, doi: 10.3390/bios12080583.

[45] K. Xu, Y. Lu, e K. Takei, «Multifunctional Skin-Inspired Flexible Sensor Systems for Wearable Electronics», *Adv. Mater. Technol.*, vol. 4, n.º 3, p. 1800628, march 2019, doi: 10.1002/admt.201800628.

[46] Y. Gu *et al.*, «Mini Review on Flexible and Wearable Electronics for Monitoring Human Health Information», *Nanoscale Res Lett*, vol. 14, n.º 1, p. 263, dec. 2019, doi: 10.1186/s11671-019-3084-x.

[47] Y. Su *et al.*, «Printable, Highly Sensitive Flexible Temperature Sensors for Human Body Temperature Monitoring: A Review», *Nanoscale Res Lett*, vol. 15, n.º 1, p. 200, dec. 2020, doi: 10.1186/s11671-020-03428-4.

[48] C. Liu *et al.*, «3D Printing Technologies for Flexible Tactile Sensors toward Wearable Electronics and Electronic Skin», *Polymers*, vol. 10, n.º 6, p. 629, june 2018, doi: 10.3390/polym10060629.

[49] M. Cheng *et al.*, «A review of flexible force sensors for human health monitoring», *Journal of Advanced Research*, vol. 26, pp. 53–68, nov. 2020, doi: 10.1016/j.jare.2020.07.001.

[50] K. K. Yeung, T. Huang, Y. Hua, K. Zhang, M. M. F. Yuen, e Z. Gao, «Recent Advances in Electrochemical Sensors for Wearable Sweat Monitoring: A Review», *IEEE Sensors J.*, vol. 21, n.º 13, pp. 14522–14539, july 2021, doi: 10.1109/JSEN.2021.3074311.

[51] A. H. Abdul Razak, A. Zayegh, R. K. Begg, and Y. Wahab, "Foot plantar pressure measurement system: A Review," *Sensors*, vol. 12, no. 7, pp. 9884–9912, 2012.

[52] A.-C. Bunea *et al.*, «E-Skin: The Dawn of a New Era of On-Body Monitoring Systems», *Micromachines*, vol. 12, n.º 9, p. 1091, sept. 2021, doi: 10.3390/mi12091091.

[53] C. García Núñez, L. Manjakkal, e R. Dahiya, «Energy autonomous electronic skin», *npj Flex Electron*, vol. 3, n.º 1, p. 1, jan. 2019, doi: 10.1038/s41528-018-0045-x.

[54] K. Senthil Kumar, P.-Y. Chen, e H. Ren, «A Review of Printable Flexible and Stretchable Tactile Sensors», *Research*, vol. 2019, pp. 1–32, nov. 2019, doi: 10.34133/2019/3018568.

[55] M. Ha, S. Lim, e H. Ko, «Wearable and flexible sensors for user-interactive health-monitoring devices», *J. Mater. Chem. B*, vol. 6, n.º 24, pp. 4043–4064, 2018, doi: 10.1039/C8TB01063C.

[56] W. Gao, H. Ota, D. Kiriya, K. Takei, e A. Javey, «Flexible Electronics toward Wearable Sensing», *Acc. Chem. Res.*, vol. 52, n.º 3, pp. 523–533, march 2019, doi: 10.1021/acs.accounts.8b00500.

[57] L. Duan, D. R. D'hooge, e L. Cardon, «Recent progress on flexible and stretchable piezoresistive strain sensors: From design to application», *Progress in Materials Science*, vol. 114, p. 100617, oct. 2020, doi: 10.1016/j.pmatsci.2019.100617.

[58] A. Sharma, Mohd. Z. Ansari, e C. Cho, «Ultrasensitive flexible wearable pressure/strain sensors: Parameters, materials, mechanisms and applications», *Sensors and Actuators A: Physical*, vol. 347, p. 113934, nov. 2022, doi: 10.1016/j.sna.2022.113934.

[59] S. M. Yun *et al.*, «Recent Advances in Wearable Devices for Non-Invasive Sensing», *Applied Sciences*, vol. 11, n.º 3, p. 1235, jan. 2021, doi: 10.3390/app11031235.

[60] J. Li, L. Fang, B. Sun, X. Li, e S. H. Kang, «Review—Recent Progress in Flexible and Stretchable Piezoresistive Sensors and Their Applications», *J. Electrochem. Soc.*, vol. 167, n.º 3, p. 037561, jan. 2020, doi: 10.1149/1945-7111/ab6828.

[61] N. Afsarimanesh, A. Nag, S. Sarkar, G. S. Sabet, T. Han, e S. C. Mukhopadhyay, «A review on fabrication, characterisation and implementation of wearable strain sensors», *Sensors and Actuators A: Physical*, vol. 315, p. 112355, nov. 2020, doi: 10.1016/j.sna.2020.112355.

[62] T. Yan, Z. Wang, e Z.-J. Pan, «Flexible strain sensors fabricated using carbon-based nanomaterials: A review», *Current Opinion in Solid State and Materials Science*, vol. 22, n.º 6, pp. 213–228, dec. 2018, doi: 10.1016/j.cossms.2018.11.001.

[63] M. J. Yee *et al.*, «Carbon nanomaterials based films for strain sensing application—A review», *Nano-Structures & Nano-Objects*, vol. 18, p. 100312, apr. 2019, doi: 10.1016/j.nanoso.2019.100312.

[64] K. Shrivas, A. Ghosale, P. K. Bajpai, T. Kant, K. Dewangan, e R. Shankar, «Advances in flexible electronics and electrochemical sensors using conducting nanomaterials: A review», *Microchemical Journal*, vol. 156, p. 104944, july 2020, doi: 10.1016/j.microc.2020.104944.

[65] J. X. Lin *et al.*, «Micro/nanoarrays and their applications in flexible sensors: A review», *Materials Today Nano*, vol. 19, p. 100224, aug. 2022, doi: 10.1016/j.mtnano.2022.100224.

[66] Y. Ben-Shimon e A. Ya'akobovitz, «Flexible and bio-compatible temperature sensors based on carbon nanotube composites», *Measurement*, vol. 172, p. 108889, feb. 2021, doi: 10.1016/j.measurement.2020.108889.

[67] R. Chen, T. Luo, D. Geng, Z. Shen, e W. Zhou, «Facile fabrication of a fast-response flexible temperature sensor via laser reduced graphene oxide for contactless human-machine interface», *Carbon*, vol. 187, pp. 35–46, feb. 2022, doi: 10.1016/j.carbon.2021.10.064.

[68] G. Zhu *et al.*, «Highly flexible TPU/SWCNTs composite-based temperature sensors with linear negative temperature coefficient effect and photo-thermal effect», *Composites Science and Technology*, vol. 217, p. 109133, jan. 2022, doi: 10.1016/j.compscitech.2021.109133.

[69] N. Wang, «Flexible temperature sensor based on RGO/CNTs@PBT melting blown nonwoven fabric», *Sensors and Actuators*, 2022.

[70] Y. Geng, «A high-sensitive wearable sensor based on conductive polymer composites for body temperature monitoring», *Composites Part A*, 2022.

[71] H. Zhao, Z. Wang, Y. Li, e M. Yang, «Single-sided and integrated polyaniline/poly(vinylidene fluoride) flexible membrane with micro/nanostructures as breathable, nontoxic and fast response wearable humidity sensor», *Journal of Colloid and Interface Science*, vol. 607, pp. 367–377, feb. 2022, doi: 10.1016/j.jcis.2021.08.214.

[72] A. Yoshida *et al.*, «Printed, all-carbon-based flexible humidity sensor using a cellulose nanofiber/graphene nanoplatelet composite», *Carbon Trends*, vol. 7, p. 100166, apr. 2022, doi: 10.1016/j.cartre.2022.100166.

[73] Y. Guo, H. Xi, Z. Gu, M. Li, X. Li, e D. Gao, «A self-powered PVA-based flexible humidity sensor with humidity-related voltage output for multifunctional applications», *Colloids and Surfaces A: Physicochemical and Engineering Aspects*, vol. 658, p. 130700, feb. 2023, doi: 10.1016/j.colsurfa.2022.130700.

[74] T. Liang, W. Hou, J. Ji, e Y. Huang, «Wrinkled reduced graphene oxide humidity sensor with fast response/recovery and flexibility for respiratory monitoring», *Sensors and Actuators A: Physical*, vol. 350, p. 114104, feb. 2023, doi: 10.1016/j.sna.2022.114104.

[75] B. Li, Q. Tian, H. Su, X. Wang, T. Wang, e D. Zhang, «High sensitivity portable capacitive humidity sensor based on In2O3 nanocubes-decorated GO nanosheets and its wearable application in respiration detection», *Sensors and Actuators B: Chemical*, vol. 299, p. 126973, nov. 2019, doi: 10.1016/j.snb.2019.126973.

[76] J. Du *et al.*, «Optimized CNT-PDMS Flexible Composite for Attachable Health-Care Device», *Sensors*, vol. 20, n.º 16, p. 4523, aug. 2020, doi: 10.3390/s20164523.

[77] Y. He, L. Zhao, J. Zhang, L. Liu, H. Liu, e L. Liu, «A breathable, sensitive and wearable piezoresistive sensor based on hierarchical micro-porous PU@CNT films for long-term health monitoring», *Composites Science and Technology*, vol. 200, p. 108419, nov. 2020, doi: 10.1016/j.compscitech.2020.108419.

[78] X. Wang *et al.*, «PDMS-based conductive elastomeric composite with 3D reduced graphene oxide conductive network for flexible strain sensor», *Composites Part A: Applied Science and Manufacturing*, vol. 161, p. 107113, oct. 2022, doi: 10.1016/j.compositesa.2022.107113.

[79] B. Herren, V. Webster, E. Davidson, M. C. Saha, M. C. Altan, e Y. Liu, «PDMS Sponges with Embedded Carbon Nanotubes as Piezoresistive Sensors for Human Motion Detection», *Nanomaterials*, vol. 11, n.º 7, p. 1740, july 2021, doi: 10.3390/nano11071740.

[80] C. Mu *et al.*, «Flexible strain/pressure sensor with good sensitivity and broad detection range by coupling PDMS and carbon nanocapsules», *Journal of Alloys and Compounds*, vol. 918, p. 165696, oct. 2022, doi: 10.1016/j.jallcom.2022.165696.

[81] O. Parlak, S. T. Keene, A. Marais, V. F. Curto, e A. Salleo, «Molecularly selective nanoporous membrane-based wearable organic electrochemical device for noninvasive cortisol sensing», *Sci. Adv.*, vol. 4, n.º 7, p. eaar2904, july 2018, doi: 10.1126/sciadv.aar2904.

[82] M. E. Payne, A. Zamarayeva, V. I. Pister, N. A. D. Yamamoto, e A. C. Arias, «Printed, Flexible Lactate Sensors: Design Considerations Before Performing On-Body Measurements», *Sci Rep*, vol. 9, n.º 1, p. 13720, sept. 2019, doi: 10.1038/s41598-019-49689-7.

[83] M. C. Hartel, D. Lee, P. S. Weiss, J. Wang, e J. Kim, «Resettable sweat-powered wearable electrochromic biosensor», *Biosensors and Bioelectronics*, vol. 215, p. 114565, nov. 2022, doi: 10.1016/j.bios.2022.114565.

[84] L. Zheng, Y. Liu, e C. Zhang, «A sample-to-answer, wearable cloth-based electrochemical sensor (WCECS) for point-of-care detection of glucose in sweat», *Sensors and Actuators B: Chemical*, vol. 343, p. 130131, sept. 2021, doi: 10.1016/j.snb.2021.130131.

[85] Z. Xu *et al.*, «A conducting polymer PEDOT:PSS hydrogel based wearable sensor for accurate uric acid detection in human sweat», *Sensors and Actuators B: Chemical*, vol. 348, p. 130674, dec. 2021, doi: 10.1016/j.snb.2021.130674.

[86] A. Turco, A. G. Monteduro, F. Montagna, E. Primiceri, M. Frigione, e G. Maruccio, «The effect of synthetic conditions on piezoresistive properties of ultrasensitive carbon nanotube/PDMS 3D composites», *Polymer*, vol. 264, p. 125534, jan. 2023, doi: 10.1016/j.polymer.2022.125534.

[87] Z. Qiao, A. Wei, K. Wang, N. Luo, e Z. Liu, «Study of flexible piezoresistive sensors based on the hierarchical porous structure CNT /PDMS composite materials», *Journal of Alloys and Compounds*, vol. 917, p. 165503, oct. 2022, doi: 10.1016/j.jallcom.2022.165503.

[88] G. Rajitha e R. K. Dash, «Optically transparent and high dielectric constant reduced graphene oxide (RGO)-PDMS based flexible composite for wearable and flexible sensors», *Sensors and Actuators A: Physical*, vol. 277, pp. 26–34, july 2018, doi: 10.1016/j.sna.2018.04.040.

[89] Dow Chemical Company," SYLGARD™ 184 Silicone Elastomer",11-3184-01 C, 2017 (accessed July 11th,2023).

[90] P. Lv *et al.*, «Ultrathin encapsulated rGO strain sensor for gesture recognition», *Microelectronic Engineering*, vol. 259, p. 111779, april 2022, doi: 10.1016/j.mee.2022.111779.

[91] M. Iqra, F. Anwar, R. Jan, e M. A. Mohammad, «A flexible piezoresistive strain sensor based on laser scribed graphene oxide on polydimethylsiloxane», *Sci Rep*, vol. 12, n.º 1, p. 4882, mar. 2022, doi: 10.1038/s41598-022-08801-0.

[92] J. Yuan *et al.*, «Graphene liquid crystal retarded percolation for new high-k materials», *Nat Commun*, vol. 6, n.º 1, p. 8700, nov. 2015, doi: 10.1038/ncomms9700.

[93] N. Abid *et al.*, «Synthesis of nanomaterials using various top-down and bottom-up approaches, influencing factors, advantages, and disadvantages: A review», *Advances in Colloid and Interface Science*, vol. 300, p. 102597, feb. 2022, doi: 10.1016/j.cis.2021.102597.

[94] D. Gupta, V. Chauhan, e R. Kumar, «Sputter deposition of 2D MoS2 thin films -A critical review from a surface and structural perspective», *Inorganic Chemistry Communications*, vol. 144, p. 109848, oct. 2022, doi: 10.1016/j.inoche.2022.109848.

[95] W. D. Callister, "Propriedades Mecânicas dos Materiais," in *Ciência e Engenharia de Materiais: Uma introdução*, Rio de Janeiro: LTC, 2013, pp. 154–161

[96] Standard Test Method for Tensile Properties of Thin Plastic Sheeting, ASTM D882-10, ASTM International, West Conshohocken, 2010.

[97] A. S. Fiorillo, C. D. Critello, e S. A. Pullano, «Theory, technology and applications of piezoresistive sensors: A review», *Sensors and Actuators A: Physical*, vol. 281, pp. 156–175, oct. 2018, doi: 10.1016/j.sna.2018.07.006.

[98] Z. Raheem, *Standard Test Methods for Flexural Properties of Unreinforced and Reinforced Plastics and Electrical Insulating Materials 1*. 2019.

[99] J. Rydz, A. Šišková, e A. Andicsová Eckstein, «Scanning Electron Microscopy and Atomic Force Microscopy: Topographic and Dynamical Surface Studies of Blends, Composites, and Hybrid Functional Materials for Sustainable Future», *Advances in Materials Science and Engineering*, vol. 2019, pp. 1–16, july 2019, doi: 10.1155/2019/6871785.

[100] A. Mohammed e A. Abdullah, «SCANNING ELECTRON MICROSCOPY (SEM): A REVIEW».

[101] A. Sala *et al.*, «Biofluid diagnostics by FTIR spectroscopy: A platform technology for cancer detection», *Cancer Letters*, vol. 477, pp. 122–130, may. 2020, doi: 10.1016/j.canlet.2020.02.020.

[102] H. Tiernan, B. Byrne, e S. G. Kazarian, «ATR-FTIR spectroscopy and spectroscopic imaging for the analysis of biopharmaceuticals», *Spectrochimica Acta Part A: Molecular and Biomolecular Spectroscopy*, vol. 241, p. 118636, nov. 2020, doi: 10.1016/j.saa.2020.118636.

[103] M. Asim *et al.*, «Thermal stability of natural fibers and their polymer composites», *Iran Polym J*, vol. 29, n.º 7, pp. 625–648, july 2020, doi: 10.1007/s13726-020-00824-6.

[104] N. Saadatkhah *et al.*, «Experimental methods in chemical engineering: Thermogravimetric analysis—TGA», *Can J Chem Eng*, vol. 98, n.º 1, pp. 34–43, jan. 2020, doi: 10.1002/cjce.23673.

[105] R. Kumar, A. Ganguly, e R. Purohit, «Thermogravimetric analysis of natural fiber reinforced hybrid composites – A review», *Materials Today: Proceedings*, p. S221478532304275X, aug. 2023, doi: 10.1016/j.matpr.2023.08.025.

[106] J. Drzeżdżon, D. Jacewicz, A. Sielicka, e L. Chmurzyński, «Characterisation of polymers based on differential scanning calorimetry based techniques», *TrAC Trends in Analytical Chemistry*, vol. 110, pp. 51–56, jan. 2019, doi: 10.1016/j.trac.2018.10.037.

[107] T. Bardelli, C. Marano, e F. Briatico Vangosa, «Influence of curing thermal history on cross-linking degree of a polydimethylsiloxane: Swelling and mechanical analyses», *Express Polym. Lett.*, vol. 16, n.º 9, pp. 924–932, 2022, doi: 10.3144/expresspolymlett.2022.67.

[108] I. D. Johnston, D. K. McCluskey, C. K. L. Tan, e M. C. Tracey, «Mechanical characterisation of bulk Sylgard 184 for microfluidics and microengineering», *J. Micromech. Microeng.*, vol. 24, n.º 3, p. 035017, march 2014, doi: 10.1088/0960-1317/24/3/035017.

[109] Z. Zeng, S. I. Seyed Shahabadi, B. Che, Y. Zhang, C. Zhao, e X. Lu, «Highly stretchable, sensitive strain sensors with a wide linear sensing region based on compressed anisotropic graphene foam/polymer nanocomposites», *Nanoscale*, vol. 9, n.º 44, pp. 17396–17404, 2017, doi: 10.1039/C7NR05106A.

[110] X. Wang *et al.*, «Polydimethylsiloxane Composite Sponge Decorated with Graphene/Carbon Nanotube via Polydopamine for Multifunctional Applications», *ACS Appl. Polym. Mater.*, vol. 5, n.º 8, pp. 6022–6033, aug. 2023, doi: 10.1021/acsapm.3c00718.

[111] J. Xu, L. Zhang, X. Lai, X. Zeng, e H. Li, «Wearable RGO/MXene Piezoresistive Pressure Sensors with Hierarchical Microspines for Detecting Human Motion», *ACS Appl. Mater. Interfaces*, vol. 14, n.º 23, pp. 27262–27273, june 2022, doi: 10.1021/acsami.2c06574.

[112] Z. Kang *et al.*, «Piezo-Resistive Flexible Pressure Sensor by Blade-Coating Graphene–Silver Nanosheet–Polymer Nanocomposite», *Nanomaterials*, vol. 13, n.º 1, p. 4, dec. 2022, doi: 10.3390/nano13010004.

[113] C. He *et al.*, «Electrochemically Active Phosphotungstic Acid Assisted Prevention of Graphene Restacking for High-Capacitance Supercapacitors», *Energy & Environ Materials*, vol. 1, n.º 2, pp. 88–95, june 2018, doi: 10.1002/eem2.12007.

[114] L. M. Johnson *et al.*, «Elastomeric microparticles for acoustic mediated bioseparations», *J Nanobiotechnol*, vol. 11, n.º 1, p. 22, dec. 2013, doi: 10.1186/1477-3155-11-22.

[115] M. Tagaya e M. Nakagawa, «Incorporation of Decanethiol-Passivated Gold Nanoparticles into Cross-Linked Poly(Dimethylsiloxane) Films», *Smart Materials Research*, vol. 2011, pp. 1–7, dec. 2011, doi: 10.1155/2011/390273.

[116] S. Hamouni, O. Arous, D. Abdessemed, G. Nezzal, e B. Van Der Bruggen, «Alcohol and Alkane Organic Extraction Using Pervaporation Process», *Macromolecular Symposia*, vol. 386, n.º 1, p. 1800247, aug. 2019, doi: 10.1002/masy.201800247.

[117] R. Ikram, B. M. Jan, e W. Ahmad, «An overview of industrial scalable production of graphene oxide and analytical approaches for synthesis and characterisation», *Journal of Materials Research and Technology*, vol. 9, n.º 5, pp. 11587–11610, sept. 2020, doi: 10.1016/j.jmrt.2020.08.050.

[118] M. Strankowski, D. Włodarczyk, Ł. Piszczyk, e J. Strankowska, «Polyurethane Nanocomposites Containing Reduced Graphene Oxide, FTIR, Raman, and XRD Studies», *Journal of Spectroscopy*, vol. 2016, pp. 1–6, 2016, doi: 10.1155/2016/7520741.

[119] M. Namvari, L. Du, e F. J. Stadler, «Graphene oxide-based silsesquioxane-crosslinked networks – synthesis and rheological behaviour», *RSC Adv.*, vol. 7, n.º 35, pp. 21531–21540, 2017, doi: 10.1039/C7RA02764H.

[120] R. A. Rochman, S. Wahyuningsih, A. H. Ramelan, e Q. A. Hanif, «Preparation of nitrogen and sulphur Co-doped reduced graphene oxide (rGO-NS) using N and S heteroatom of thiourea», *IOP Conf. Ser.: Mater. Sci. Eng.*, vol. 509, p. 012119, may 2019, doi: 10.1088/1757-899X/509/1/012119.

[121] C. Monteserín *et al.*, «Effects of Graphene Oxide and Chemically-Reduced Graphene Oxide on the Dynamic Mechanical Properties of Epoxy Amine Composites», *Polymers*, vol. 9, n.º 12, p. 449, sept. 2017, doi: 10.3390/polym9090449.

[122] N. S. Gupta, K.-S. Lee, e A. Labouriau, «Tuning Thermal and Mechanical Properties of Polydimethylsiloxane with Carbon Fibers», Polymers, vol. 13, n.º 7, p. 1141, april 2021, doi: 10.3390/polym13071141.

[123] D. E. Kherroub e T. Boulaouche, «Maghnite: novel inorganic reinforcement for single-step synthesis of PDMS nanocomposites with improved thermal, mechanical and textural properties», *Res Chem Intermed*, vol. 46, n.º 12, pp. 5199–5217, dec. 2020, doi: 10.1007/s11164-020-04257-x.

[124] A. Berkem, A. Capoglu, T. Nugay, E. Sancaktar, e I. Anac, «Self-Healable Supramolecular Vanadium Pentoxide Reinforced Polydimethylsiloxane-Graft-Polyurethane Composites», *Polymers*, vol. 11, n.º 1, p. 41, dec. 2018, doi: 10.3390/polym11010041.

[125] A. Łapińska *et al.*, «Influence of the filler distribution on PDMS-graphene based nanocomposites selected properties», *Sci Rep*, vol. 12, n.º 1, p. 19038, nov. 2022, doi: 10.1038/s41598-022-23735-3.

[126] N. P. D. Ngidi, M. A. Ollengo, e V. O. Nyamori, «Effect of Doping Temperatures and Nitrogen Precursors on the Physicochemical, Optical, and Electrical Conductivity Properties of Nitrogen-Doped Reduced Graphene Oxide», *Materials*, vol. 12, n.º 20, p. 3376, oct. 2019, doi: 10.3390/ma12203376.

[127] X. Gao, H. Liu, H. Wei, J. Zheng, e G. Huang, «Effect of incompletely condensed tri-silanol-phenyl-POSS on the thermal stability of silicone rubber», *Polym. Bull.*, vol. 76, n.º 6, pp. 2835–2850, june 2019, doi: 10.1007/s00289-018-2499-3.

[128] L. Liu *et al.*, «Highly stretchable, sensitive and wide linear responsive fabric-based strain sensors with a self-segregated carbon nanotube (CNT)/Polydimethylsiloxane (PDMS) coating», *Progress in Natural Science: Materials International*, vol. 32, n.º 1, pp. 34–42, feb. 2022, doi: 10.1016/j.pnsc.2021.10.012.

[129] J. Ma, P. Wang, H. Chen, S. Bao, W. Chen, e H. Lu, «Highly Sensitive and Large-Range Strain Sensor with a Self-Compensated Two-Order Structure for Human Motion Detection», *ACS Appl. Mater. Interfaces*, vol. 11, n.º 8, pp. 8527–8536, feb. 2019, doi: 10.1021/acsami.8b20902.

[130] S. Sun *et al.*, «A wearable strain sensor based on the ZnO/graphene nanoplatelets nanocomposite with large linear working range», *J Mater Sci*, vol. 54, n.º 9, pp. 7048–7061, may 2019, doi: 10.1007/s10853-019-03354-6.

[131] H. M. Soe, A. M. Asrulnizam, M. Atsunori, e M. Mariatti, «Flexibility and sensitivity of graphene nanoplatelets-polydimethylsiloxane strain sensor», apresentado na 3RD INTERNATIONAL POSTGRADUATE CONFERENCE ON MATERIALS, MINERALS & POLYMER (MAMIP) 2019, Penang, Malaysia, 2020, p. 020033. doi: 10.1063/5.0015765.

[132] L. Wu, Y. Hu, P. Tang, H. Wang, e Y. Bin, «High stretchable, pH-sensitive and self-adhesive rGO/CMCNa/PAA composite conductive hydrogel with good strain-sensing performance», *Composites Communications*, vol. 24, p. 100669, april 2021, doi: 10.1016/j.coco.2021.100669.

[133] H. M. Soe, A. Abd Manaf, A. Matsuda, e M. Jaafar, «Performance of a silver nanoparticles-based polydimethylsiloxane composite strain sensor produced using different fabrication methods», *Sensors and Actuators A: Physical*, vol. 329, p. 112793, oct. 2021, doi: 10.1016/j.sna.2021.112793.

[134] M. Vahdani *et al.*, «Highly stretchable strain sensors based on gold thin film reinforced with carbon nanofibers», *Smart Materials in Manufacturing*, vol. 1, p. 100016, 2023, doi: 10.1016/j.smmf.2023.100016.

[135] X. Zhang *et al.*, «High-performance flexible strain sensors based on biaxially stretched conductive polymer composites with carbon nanotubes immobilized on reduced graphene oxide», *Composites Part A: Applied Science and Manufacturing*, vol. 151, p. 106665, dec. 2021, doi: 10.1016/j.compositesa.2021.106665.

[136] J. A. Smith *et al.*, «Polydimethylsiloxane and poly(ether) ether ketone functionally graded composites for biomedical applications», *Journal of the Mechanical Behaviour of Biomedical Materials*, vol. 93, pp. 130–142, may 2019, doi: 10.1016/j.jmbbm.2019.02.012.

[137] J. H. Lee *et al.*, «Rapid mould-free fabrication of long functional PDMS fibers», NPG Asia Mater, vol. 14, n.º 1, p. 13, dec. 2022, doi: 10.1038/s41427-022-00359-7.

[138] C. Yu *et al.*, «High-performance multifunctional piezoresistive/piezoelectric pressure sensor with thermochromic function for wearable monitoring», Chemical Engineering Journal, vol. 459, p. 141648, march 2023, doi: 10.1016/j.cej.2023.141648.

[139] X. Zhang *et al.*, «Breathable and Wearable Strain Sensors Based on Synergistic Conductive Carbon Nanotubes/Cotton Fabrics for Multi-directional Motion Detection», ACS Appl. Mater. Interfaces, vol. 14, n.º 22, pp. 25753–25762, june 2022, doi: 10.1021/acsami.2c04790.

[140] P. Yang *et al.*, «Highly Stretchable and Sensitive Flexible Strain Sensor Based on Fe NWs/Graphene/PEDOT:PSS with a Porous Structure», IJMS, vol. 23, n.º 16, p. 8895, aug. 2022, doi: 10.3390/ijms23168895.

[141] Y.-G. Kim, J.-H. Song, S. Hong, e S.-H. Ahn, «Piezoelectric strain sensor with high sensitivity and high stretchability based on kirigami design cutting», npj Flex Electron, vol. 6, n.º 1, p. 52, june 2022, doi: 10.1038/s41528-022-00186-4.

[142] T. Dinh, T. Nguyen, H.-P. Phan, N.-T. Nguyen, D. V. Dao, e J. Bell, «Stretchable respiration sensors: Advanced designs and multifunctional platforms for wearable physiological monitoring», Biosensors and Bioelectronics, vol. 166, p. 112460, oct. 2020, doi: 10.1016/j.bios.2020.112460.

[143] T. Daiana Da Costa, M. De Fatima Fernandes Vara, C. Santos Cristino, T. Zoraski Zanella, G. Nunes Nogueira Neto, e P. Nohama, «Breathing Monitoring and Pattern Recognition with Wearable Sensors», em Wearable Devices - the Big Wave of Innovation, N. Nasiri, Ed., IntechOpen, 2019. doi: 10.5772/intechopen.85460.

[144] H. Liu, J. Allen, D. Zheng, e F. Chen, «Recent development of respiratory rate measurement technologies», Physiol. Meas., vol. 40, n.º 7, p. 07TR01, july 2019, doi: 10.1088/1361-6579/ab299e.

[145] R. Fu, X. Zhao, X. Zhang, e Z. Su, «Design strategies and applications of wearable piezoresistive strain sensors with dimensionality-based conductive network structures», Chemical Engineering Journal, vol. 454, p. 140467, feb. 2023, doi: 10.1016/j.cej.2022.140467.

[146] X. Guo *et al.*, «Human touch sensation-inspired, ultrawide-sensing-range, and high-robustness flexible piezoresistive sensor based on CB/MXene/SR/fiber nanocomposites for wearable electronics», Composite Structures, vol. 321, p. 117329, oct. 2023, doi: 10.1016/j.compstruct.2023.117329.

[147] Y. Li *et al.*, «Hybrid strategy of graphene/ carbon nanotube hierarchical networks for highly sensitive», Scientific Reports, 2021, doi: 10.1038/s41598-021-00307-5.